ALGENOL

Production of Biocrude in an Advanced Photobioreactor-Based Biorefinery

October 1, 2016 – March 31, 2020

Final Report

ACKNOWLEDGEMENT:
This material is based upon work supported by the U.S. Department of Energy's Office of Energy Efficiency and Renewable Energy (EERE) under the Bioenergy Technologies Office Award Number DE-EE0007690.

Project Title:	Production of Biocrude in an Advanced Photobioreactor-Based Biorefinery
Award number:	DE-EE0007690
Recipient:	Algenol Biotech LLC, 16121 Lee Rd, Fort Myers, FL 33912
Principal Investigators:	Drs. Ronald Chance (ron.chance@algenol.com) and Paul Roessler (paul.roessler@algenol.com), 239-498-2000
Business Contact:	James Pecenka (james.pecenka@algenol.com), 239-498-2000
Project Partners:	National Renewable Energy Laboratory (NREL), Georgia Institute of Technology (GIT), Reliance Industries Limited (RIL), Arizona State University (ASU)
Report Date:	April 23, 2020
Project Period:	October 1, 2016 – March 31, 2020

Table of Contents

Introduction

This report describes the results and conclusions of research and development activities conducted by Algenol Biotech LLC, the National Renewable Energy Laboratory (NREL), Reliance Industries Limited (RIL), Georgia Institute of Technology (GIT), and Arizona State University (ASU) in a project entitled "Production of Biocrude in an Advanced Photobioreactor-Based Biorefinery." This project was funded through the U.S. Department of Energy (DOE) Office of Energy Efficiency and Renewable Energy (EERE), and more specifically through the Bioenergy Technologies Office (BETO) Advanced Algal Systems Program under Funding Opportunity "Advancements in Algal Biomass Yield, Phase 2 (ABY2)" (Award Number DE-EE0007690).

The research performed in this project addressed several key focus areas of the ABY2 program as well as the overall BETO and Advanced Algal Systems Program goals. The stated overall ABY2 goal was to develop technologies that are likely to succeed in producing 3,700 gallons of algal biofuel intermediate (BFI) (or equivalent dry weight basis) per acre per year on an annualized average basis through multiple batch campaigns or on a semi-continuous or continuous basis, in an outdoor test environment by 2020. To achieve this target, the ABY2 FOA specified three Priority Areas, indicated verbatim below:

> *Priority Area 1* - Strain/Productivity Improvement: This priority area is targeted at applied research that will accelerate the development of promising algal strains and cultivation techniques that will result in increased algal biomass productivity in outdoor cultivation environments relevant to commercial scales (60,000 liters, open pond system).
>
> *Priority Area 2* - Improvements in Pre-processing Technologies: This priority area is targeted at applied research and engineering to build and operate innovative harvesting, dewatering, and intermediate processing (e.g., extraction) unit operations that can be integrated at scale with biomass production (i.e., support appropriate volumetric flow-through); can be operated efficiently so that the energy expended does not exceed 10% of the energy content contained in the biofuel intermediate; and are low cost (both CAPEX and OPEX) to scale.
>
> *Priority Area 3* - Integration of Cultivation with Pre-processing Technologies: This priority area is targeted at ensuring that the integrated system is capable of meeting target yields and can be scaled and operated to produce cost-competitive fuels and products.

Each of these Priority Areas were addressed in this project, which is reflected in the key project objectives:

1) Achieve a biofuel intermediate (BFI) productivity of >4,000 gal-BFI/acre-yr on an annualized basis (using a combination of strain development and cultivation engineering advances).
2) Pilot energy efficient innovations in biomass harvesting, dewatering, and hydrothermal Liquefaction (HTL) to deliver an energy expenditure <10% of the energy content in BFI and an overall >60% carbon footprint reduction compared to fossil sources.
3) Deliver a comprehensive techno-economic analysis (TEA) that firmly identifies limiting factors for commercial viability for a photobioreactor (PBR)-based biofuel product, a detailed comparison of BFI production in PBR *vs* open pond systems, and a biofuel market entry strategy that includes a high-value co-product.

There were three phases in this project:

Phase 1: DOE Validation Phase

Phase 2: Improve overall performance with a combination of strain development, operational optimizations, and PBR engineering approaches

Phase 3: Develop downstream processing unit operations and performance assessment of advanced strains in commercially relevant cultivation systems and environments. In addition, operate a PBR Block (4,000 - 20,000 L) using the advanced strain with enhanced yield, dewatering and HTL traits integrated with energy efficient downstream processing, with a goal of stable operation and characterization of the final BFI product.

Formal entry into Phases 2 and 3 required the successful outcome of a major milestone (Go/No-Go decision) at the end of the preceding phase. Those milestones were achieved, enabling completion of the project. The phases of the project were broken down into eight interconnected tasks, as listed below:

Tasks	**Task Description**
Phase 1 – Project Validation	
Task 1: DOE project validation	Review data and recommend project
Phase 2 – Improve biofuel intermediate (BFI) yield	
Task 2: Strain development to improve productivity and processing	Identify genetic strategies and then engineer strains with improved productivity, dewatering, and HTL-based BFI yield and quality followed by evaluation in indoor and outdoor PBRs.
Task 3: Improved productivity through operational and engineering approaches	Improve productivity through culture management and PBR light capturing properties.
Task 4: Intermediate scale process validation	Develop TEA and LCA models for 2,000 acre facility and demonstrate combined strain, operation, and PBR engineering at PDU.
Phase 3 – Pilot and improve efficiency of unit operations	
Task 5: Iterative strain and process optimization	Build on Phase 2 strain development and outdoor PBR studies to make incremental strain advancements in biomass productivity, dewatering traits, and HTL BFI yield and quality.
Task 6: Operation and biomass harvest at scale	Build out 4,000-20,000 L PBR system at Algenol's IBR and operate the system with new strains. Harvests support downstream processing studies (Task 7). Determine *Cyanobacterium* sp. and *Arthrospira* productivity in PBR and open pond systems.

Task 7: Downstream processing optimization	Detailed pilot scale heat and material balance (HMB) and optimization studies with dewatering systems, HTL, and co-product processing units.
Task 8: Integrated operation and commercial assessment	Operate 4,000-20,000 L Block with commercial strain integrated with downstream processing units to determine final system yield and HMB. Use data to validate TEA and LCA models to project commercial viability of 2,000 acre algae BFI facility.

These tasks were conducted in an integrated fashion, with the results of early tasks providing information and guidance for the later tasks. Strain development work was performed by Algenol and NREL researchers, cultivation studies were conducted by Algenol, RIL, and ASU (AzCATI), HTL-related work was carried out by RIL and NREL, and co-product (phycocyanin) development was accomplished by Algenol. GIT worked with Algenol engineers to develop Techno-Economic Analyses (TEA) and Life Cycle Assessments (LCA) based on data generated in this project. A Gantt chart showing the timing of the project tasks is shown in Figure I-1.

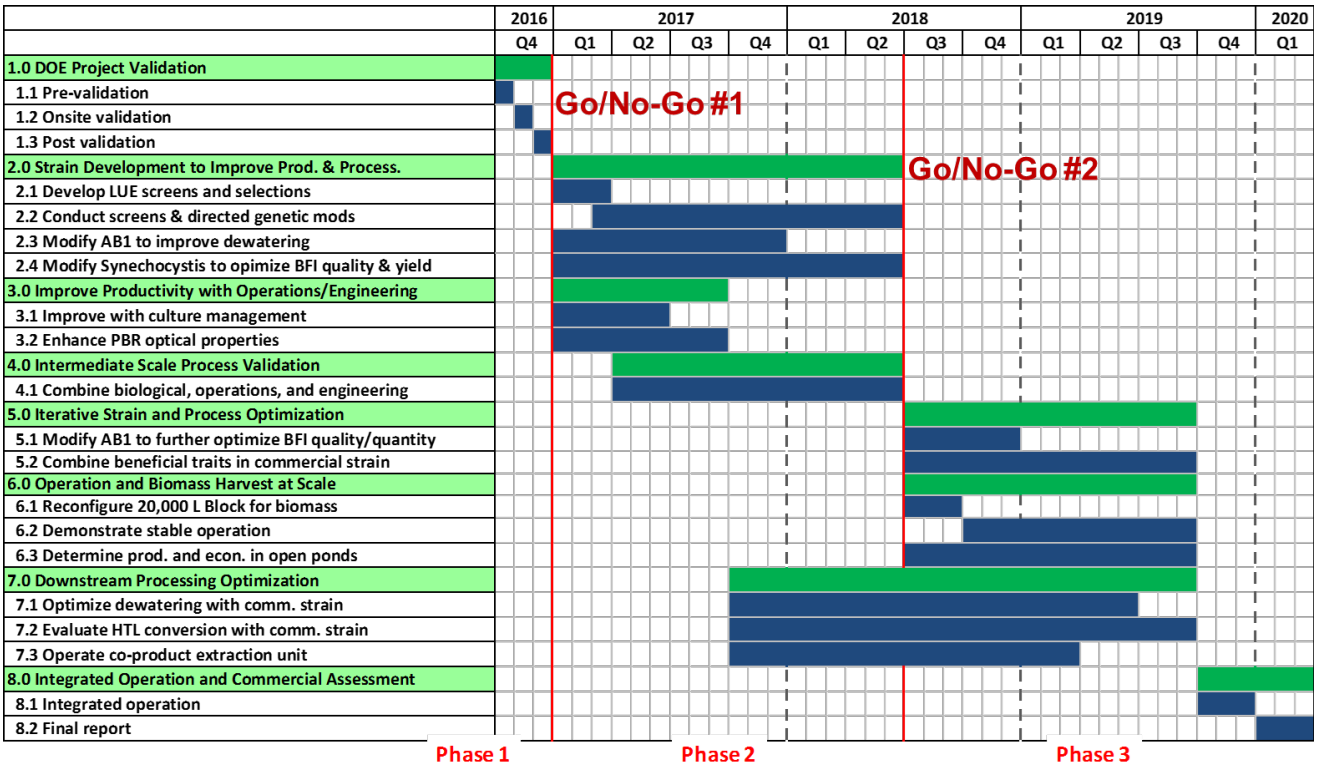

Figure I-1. Gantt chart indicating the proposed timing for the various project tasks.

Algenol has conducted algal biofuels research since its founding in 2006, with a primary focus on ethanol production in recombinant cyanobacteria. In the course of this R&D program, Algenol has developed many proprietary technologies, including various recombinant DNA methods for strain development, cultivation practices for enhanced productivity and contamination control, PBR

design and associated upstream systems, downstream product recovery procedures, and various models for site-specific productivity, techno-economics, and life cycle assessments. Although originally used for ethanol production, most of these technologies are directly relevant for algal biomass-based biocrude (BFI) production as well, and have been highly leveraged in this project. Further background on these technologies are provided in the relevant sections of this report.

Project Partners

National Renewable Energy Laboratory (NREL)
Georgia Institute of Technology (GIT)
Reliance Industries Limited (RIL)
Arizona State University (ASU)/Arizona Center for Algae Technology and Innovation, (AzCATI)

Abbreviations and Acronyms

aPC – allophycocyanin
ATP – adenosine triphosphate
BFI – biofuel Intermediate
CBB – Calvin Benson Bassham cycle
CE – Carbon Engineering
CHG – Catalytic Hydrothermal Gasification
CHP – combined heat and power
CDW – cell dry weight
CIP – clean-in-place
CO_2 – carbon dioxide
cPC – c-phycocyanin
CUE – carbon (CO_2) use efficiency
DAC – direct air capture
DNA – deoxyribonucleic acid
DOC – dissolved organic carbon
DOE – Department of Energy
DW – dry weight
EPS – exopolysaccharides
FACS – fluorescence-activated cell sorting
FBPase – fructose-1,6-bisphosphatase
FDA – Food and Drug Administration
FGD – flue gas desulfurization
FGPC – food grade phycocyanin
FPP – field processing pad
FTE – full time equivalent (employee)
GC – gas chromatography
GHG – greenhouse gas
GPM – gallons per minute

GRAS – generally recognized as safe (FDA designation)
HHV – high heating value
HMB – heat and material balance
HTL – hydrothermal liquefaction
HTS – high throughput system
IBR – integrated biorefinery
LCA – life cycle assessment
LMH – liters per m^2 per hour
LOA – linear alpha olefins
LSS – liquid solid separator
LUE – light utilization efficiency
MC – moisture content
mcl-LOA – medium chain length linear alpha olefins
mcl-PHA – medium chain length polyhydroxyalkanoates
mt – metric tons (tonnes)
NADPH – nicotinamide adenine dinucleotide phosphate
NGCC – natural gas combined cycle
NREL – National Renewable Energy Laboratory
OEM – original equipment manufacturer
ORF – open reading frame
PAR – photosynthetically active radiation
PBR – photobioreactor
PC – phycocyanin
PDU – process development unit
PE – polyethylene
PET – photosynthetic electron transport
PHA – polyhydroxyalkanoate
PHB – polyhydroxybutyrate
PLC – programmable logic controller
PSI – photosystem I
PSII – photosystem II
psig – pounds per square inch gauge
R&D – research and development
RIL – Reliance Industries Limited
RNA – ribonucleic acid
RO – reverse osmosis
Rubisco – ribulose-bisphosphate carboxylase/oxygenase
SLPM – standard liters per minute
sOD – standard optical density (measured at 750 nm)
SOP – standard operating procedure
TAG – triacylglycerol

TEA – techno-economic analysis
TFF – tangential flow filtration
TGA – thermal gravimetric analysis
TOC – total organic carbon
UV – ultraviolet radiation

Executive Summary

This algal biofuels project, funded by the U.S. Department of Energy's Bioenergy Technologies Office (BETO) Advanced Algal Systems Program under Funding Opportunity "Advancements in Algal Biomass Yield, Phase 2 (ABY2), brought together four partners with complementary and overlapping skill sets. Algenol, the lead organization, provided expertise in strain development, engineering, photobioreactor (PBR) development and manufacturing, techno-economic analysis (TEA), and outdoor algae cultivation. Reliance Industries Limited (RIL) provided engineering, hydrothermal liquefaction (HTL)-based conversion of biomass to biofuel intermediate (BFI, or biocrude), outdoor cultivation (open pond and PBR), and extensive knowledge in refining and fuels. The National Renewable Energy Laboratory (NREL) was focused on strain development, HTL, and chemical analysis of biomass and BFI. The Georgia Institute of Technology (GIT) provided process engineering, TEA, and life cycle assessment (LCA). In addition, Arizona State University (ASU) was a subcontractor for pond cultivations in support of pond *vs* PBR comparative studies. These skill areas were merged to advance the state of the art in algal production and biofuel processing *via* achievement of the following three objectives, all directly aligned with the Priority Areas defined in the ABY2 program:

1. Achieve a biofuel intermediate (BFI) productivity of >4,000 gal-BFI/acre-yr on an annualized basis.
2. Pilot energy efficient innovations in biomass harvesting, dewatering, and hydrothermal liquefaction to deliver an energy expenditure <10% of the energy content in biofuel intermediates and an overall >60% carbon footprint reduction compared to fossil sources.
3. Deliver a comprehensive technical-economic analysis (TEA) that firmly identifies limiting factors for commercial viability for a photobioreactor (PBR)-based biofuel product, a detailed comparison of biofuel intermediates production in PBR *vs* open pond systems, and a biofuel market entry strategy that includes a high-value co-product.

Objective 1 was achieved largely through discovery of a new cyanobacterial strain and development of a semi-continuous production process for PBR-based cultivation. Numerous strain development strategies, utilizing both recombinant and non-recombinant methods, were attempted in order to increase the light utilization efficiency (LUE) and enhance dewatering effectiveness for Algenol's primary production strain, *Cyanobacterium* sp. AB1. In the end, however, it was the discovery of a new wild type strain, *Cyanobacterium* sp. AB1166 that provided the largest advantages. This strain is similar to AB1, but exhibits ~10% higher biomass productivity as well as superior viscometric properties that enable more efficient harvesting. Coupling this strain with optimized semi-continuous operation during cultivation yielded an 80% improvement in biomass productivity over our baseline batch cultivation procedure for AB1. These results, combined with HTL results from RIL and NREL, yield a BFI productivity of 4,100 gal/acre-yr, meeting our objective and exceeding the DOE's ABY2 program target of 3,700 gal/acre-yr.

Objective 2 involved two related elements, energy efficiency for biomass recovery and conversion to biocrude, and the carbon footprint for the overall process. The 10% energy efficiency target for pre-processing steps was an ambitious goal, as we noted in the original proposal. We made good progress towards that goal. With a biomass processing model that included both HTL and catalytic hydrothermal gasification (CHG) of the aqueous phase HTL output, improved dewatering, enhanced CO_2 utilization, and nutrient recycle, we were able to achieve about 20% overall energy efficiency (with respect to BFI energy content) and about 10% energy efficiency when only considering the pre-processing energy expenditures (harvesting and dewatering). The latter achievement meets the DOE target delineated in ABY2 Priority Area 2. At those energy efficiency levels, we were able to show that a >60% carbon footprint reduction relative to fossil fuels was achievable for a number of CO_2 sourcing options.

The TEA efforts associated with Objective 3 provided detailed guidance for cost reduction opportunities in PBR-based biorefineries. As stated above, experimental results for biomass productivity (27 g/m^2-d, annualized for Fort Myers climate conditions) and HTL yield predict BFI productivity of 4,100 gal BFI/acre-yr. That productivity in our TEA model yields a BFI production cost of about $450/bbl of biocrude. Considering an estimated upper limit of 40 g/m^2-d biomass productivity and a catalytic HTL yield of 60% (achieved under laboratory conditions by RIL), the TEA result is about $100/bbl for biocrude. These cost estimates are based on biomass production systems using PBR technology that has been demonstrated under commercially relevant conditions at Algenol, i.e., without a requirement for achieving unmet stretch targets for biomass production costs. Sensitivity analyses are reported to identify opportunities for improvements. CAPEX is a major contributor to the biocrude cost; the PBR cost is a major contributor to CAPEX and remains a major opportunity for cost reduction.

The TEA effort also included examination for the co-production of phycocyanin (PC), a natural blue colorant used in foods and beverages. Extraction of PC was demonstrated for AB1 and also for a second cyanobacterial strain, *Arthrospira platensis* (AB2293), commonly referred to as spirulina. PC extraction for AB2293 is much easier than AB1 due to its weaker cell wall. Also, harvesting of AB2293 is much more efficient due to its filamentous morphology. Thus, co-product work focused on this *Arthrospira* strain. An extraction process was designed, built, and tested. The PC product from this pilot facility was extensively tested against commercial products from various suppliers and found to meet required quality specifications. PC production plants at various scales were designed and subjected to TEA analysis. Overall, PC production from a PBR-based outdoor facility was shown to be competitive, from both a product quality and cost perspective, with existing production from open pond systems. PC is not a rational co-product for biofuel production because of the small market size in comparison to fuels, and was therefore considered primarily to advance the PBR-based algal production platform and support the economics and financing prospects for initial biofuel production facilities. The only co-products considered that would potentially have a production scale comparable to fuels were protein for food and feed, and biofertilizer for land reclamation and other agricultural applications. The overall conclusion from this work is that biofuel production from algae must stand on its own economically. High value products such as PC can help pave the way by enabling smaller, profitable operations that demonstrate operability of biomass production technology and mitigate the risks associated with biofuel investments.

The project included R&D aimed at comparing biomass production from open ponds *vs* PBRs. All partners participated in that effort. Both RIL and ASU carried out pond production experiments with AB1, but both were largely unsuccessful due to protozoan predation issues. This result was not unexpected as the small cell size and culture parameters for AB1 (e.g., neutral pH) invite competition and predation by numerous organisms. ASU also conducted experiments on *Arthrospira platensis*, a species that is readily grown commercially in open ponds due in large part to the high pH and alkalinity cultivation conditions that suppress predation. The ASU experiments were successful and consistent with our productivity modeling efforts which yielded an annualized productivity ratio of approximately 3:1 for PBRs *vs* ponds. A similar PBR:pond productivity ratio was also observed for AB1. This productivity advantage for PBR systems is sufficient to make PBR cultivation fully competitive with open pond cultivation from both an economic and a life cycle perspective.

Major Accomplishments

- Quantified BFI (biocrude) production potential *via* extensive outdoor biomass production combined with hydrothermal liquefaction testing, demonstrating BFI productivity of 4,100 gal BFI/acre-yr, exceeding BETO's ABY2 goal
- Produced a step change in biomass productivity by developing and deploying a semi-continuous production system for PBR-based outdoor deployments at scales up to 24,000 L
- Identified and characterized a cyanobacterial strain (*Cyanobacterium* sp. AB1166) with improved productivity and enhanced viscometric properties that results in more efficient harvesting
- Produced a cyanobacterial strain (*Synechocystis* sp.) with a reduced glycogen content that exhibited 15% higher BFI yield upon hydrothermal liquefaction of biomass
- Demonstrated *via* a combination of state-of-the-art productivity modeling, quantitative outdoor experimentation, and detailed techno-economic modeling that PBR-based cultivation is fully competitive with open pond cultivation of cyanobacteria
- Determined that the carbon footprint for biofuels produced from a PBR-based algal biorefinery was at least 60% lower than for petroleum-derived gasoline
- Fully explored a high-value co-product opportunity for PBR-based production, including both upstream and downstream plant design
- Broad dissemination of scientific results from the project via over 25 presentations at universities and scientific conferences, five publications submitted to peer-review journals, and one patent application

Acknowledgements

Numerous talented people in many locations conducted the research described in this report. The efforts of these dedicated researchers, along with supporting administrative personnel, are gratefully acknowledged. The PIs would also like to acknowledge the following individuals who helped directly with the drafting of this report: Algenol - William Porubsky, Yanhui Yuan, Laura Belicka, Jonathan Chin, Paul Hill, Lisa Pickell, Josée Bouchard, Kim Anderson, Monica Brown, Lucas Eastham, Matthew Anderson, and Lanny Miller; GIT - Valerie Thomas, Matthew Realff, Ankush Karemore, and Pratham Arora; RIL - Makarand Phadke, Rajaram Ghadge, and Ramesh Bhujade; NREL - Jianping Yu, Tao Dong, and Phil Pienkos; ASU - John McGowen.

Task 1 – DOE project validation

Task 1 Objective

The objective of the first phase of the project (Task 1) was to provide an initial validation of the project proposal, ending with a Go/No-Go decision for the full project within three months of the start date.

Task 1 Activities

Pre-validation: A Validation Kickoff Meeting was held *via* teleconference on Sept 8, 2016 with Algenol and the DOE Validation Team. A series of questions and requests for specific information was subsequently provided to Algenol by the Validation Team in advance of the onsite validation meeting; the requested information was provided in written form to the team on Oct 13. The Project Team provided current performance data for the base organism (*Cyanobacterium* sp. AB1) in PBR systems, current unit operation metrics, Standard Operating Procedures, and the initial process TEA to the DOE Validation Team. The onsite meeting was scheduled for Nov 2-3, 2016.

Onsite validation: The onsite validation meeting was held on Nov 2 in Fort Myers, FL at Algenol's headquarters. A tour of Algenol's facility was provided, followed by detailed presentations to discuss project objectives, performance metrics, and to answer any additional questions from the Validation Team. Some discussion about ways to improve the Technical-Financial Table occurred. NREL also hosted the Validation Team at a later date and reviewed their project plans.

Post-validation: Requested revisions to the TechFin table were made and provided to the Validation Team on Nov 15. The Validation Team report was completed and provided to the Program Technical Manager in December. Based on the analysis, a "Go" decision was made to continue the project.

Task 1 Milestones

Subtask Topic	Milestone Number	Milestone Description	Milestone Verification Process	End Quarter
Pre-validation	M1.1	Tech/financial data and initial performance metrics disclosed	DOE Validation Team reviews data and schedules onsite meeting	1
Outcome: **Completed.** Technical and financial data and performance metrics disclosed to DOE Validation Team. Onsite meeting scheduled for November 2-3, 2016.				
Onsite validation	M1.2	Project aligned with BETO goals and tracking process agreed upon	Project Team revises tech/fin data and submits to DOE for report preparation	1
Outcome: **Completed.** DOE Validation Team and Project Team met on November 2-3, 2016 and worked together to align project activities and milestones with BETO goals. Tech/Fin table revised and submitted to DOE Validation Team.				
Post-validation	M1.3	Validation team completes report	Validation team delivers report to DOE Program Technology Manager	1

Outcome: **Completed.** Validation Team delivered report to the DOE Program Technology Manager.				
Go/No-Go Decision Point	Go/No-Go #1	DOE validation review complete and Project approved to continue	DOE Validation Team determines if process metrics support technical readiness and submits a report to DOE. Technology Manager and Project Team release remaining scope and funding.	1
Outcome: **Passed.** "Go" decision made to continue project.				

Task 2 – Strain development to improve productivity and processing

Task 2 Objective

The overall objective of Task 2 was to improve the economics of generating high quality biofuel intermediate (BFI, also referred to as biocrude or bio-oil) *via* the development of more productive algal strains, ideally coupled to an improved biomass composition that is well suited for conversion to BFI *via* hydrothermal liquefaction (HTL). An additional objective was to improve harvesting economics by creating algal strains that could be dewatered more efficiently.

Expected outcome: Strains improved for productivity, downstream processing and higher HTL-based BFI yield and quality.

Task 2 Activities

Overall biomass productivity plays a major role in determining the economics of algal BFI manufacturing, from both CAPEX and OPEX perspectives. Improving the HTL conversion yield of biomass to BFI also improves overall economics, and producing a BFI with a lower nitrogen content (e.g., lower amines and N-heterocyclic molecules) reduces BFI cleanup costs and increases market acceptance. In addition, cost and energy savings in biomass recovery processes are likely possible through reducing the viscosity of cultures. Each of these areas was addressed in part by innovative algal (cyanobacterial) strain development strategies designed to 1) improve the efficiency of light capture and conversion of CO_2 to biomass, 2) increase the levels of cellular compounds that are preferred HTL substrates, and 3) minimize the production of extracellular compounds that increase culture viscosity. Work conducted toward these objectives was carried out by scientists at Algenol's Fort Myers and Berlin laboratories and at NREL. Algenol scientists focused their strain development research on strains of the genus *Cyanobacterium*, including the strain AB1, an excellent and well characterized production strain for which an extensive set of genetic tools and knowledge has been established over many years through Algenol's ethanol program. NREL scientists focused their efforts on the globally recognized model organism *Synechocystis* PCC 6803, for which a great deal of knowledge and expertise has been gained. It is anticipated that NREL's strain modification strategies and results with *Synechocystis* should be directly translatable to Algenol's *Cyanobacterium* sp. commercial production strains.

Improved Biomass Productivity

Strain development efforts to improve biomass productivity were focused on improving the light utilization efficiency (LUE) of cyanobacteria, mainly by minimizing cell acclimation effects observed in dense cultures that result in reduced photosynthetic rates. Algenol's Productivity

Model suggested that biomass productivity could be increased by 50% or more if we could eliminate acclimation in cell cultures through a combination of strain improvement and optimized culture management. Parallel approaches using both recombinant and non-recombinant means were attempted to overcome these acclimation effects, and were directed at modifications of both the light and dark reactions of photosynthesis as well as associated regulatory networks.

Non-recombinant ("Non-targeted") Approaches for Improving Productivity

Non-recombinant approaches involved the use of various screens and selections to identify improved strain variants with higher productivity in dense cultures, presumably by reducing light acclimation effects. An advantage of non-recombinant (non-targeted) approaches is that they can identify improved strains without *a priori* knowledge of the mechanisms involved. And yet, with today's genome sequencing technologies, it is possible to sequence the genome of an improved (e.g., non-acclimating) strain generated by "classical" (screening and selection) methods and compare the sequence with the parental strain in order to identify the genetic basis of the improvement. This knowledge can then allow scientists to make the same genetic change in a "targeted" manner through recombinant methods to new strains. This is particularly important in that strains identified in selection and screening programs may have accumulated additional, non-beneficial mutations, especially if the parental strain was subjected to chemical or UV mutagenesis in order to generate genetic variability in the screening population. The ability to make targeted genetic changes is also crucial for being able to combine or "stack" additional beneficial traits.

<u>FACS-based screening to identify strain variants that don't acclimate to low light</u>

In natural environments, phototrophs must respond to rapidly changing conditions including flux in irradiance from below to above photosynthetic light saturation. However, these natural survival strategies benefiting the cell come at the cost of optimal productivity for the population. Safe, yet efficient, light utilization was clearly a key evolutionary trait impacting the fitness of a phototrophic cell. Low-light acclimated cyanobacterial cells have more pigment and can harvest more energy per cell per unit of irradiance. Under low light, this trait helps cells to more closely match the output from the light harvesting reactions to the total photosynthetic and biosynthetic capacity of the cell. However, while advantageous when competing for low light, enhanced light harvesting capacity can result in over-saturation of the reaction centers when light levels are high, creating a need to dissipate excess energy (e.g., as heat) at lower irradiances than a high-light acclimated cell. While evolutionarily advantageous to a single cell, the total population is disadvantaged by conversion of light energy into waste heat instead of conversion of CO_2 into fixed carbon (i.e., biomass).

It was considered possible that pigment reduction alone may improve biomass productivity in Algenol's outdoor VIPER photobioreactors (PBRs). However, photosynthetic activity declines during batch cultivation in these systems because high culture density leads to self-shading and acclimation to the resulting low average light environment. Under these conditions, energy losses may occur as cells experience high irradiances at the surface of the PBRs. In contrast, a cell with lower pigment levels lacks the same capacity for light reaction activity (NADPH and ATP production) needed to fully satisfy the enzymatic (dark) reactions of photosynthesis. In a dense, reduced pigment mutant culture, light penetrates more deeply, increasing the photic zone and allowing for productive light capture by more cells. However, pigment reduction alone can

disadvantage a dense algal culture during periods of the day with light levels below the light saturation point, which is indicated by the photosynthetic parameter E_k. This portion of the day would be extended in a strain with an enhanced E_k.

The phenotypic traits of a high-light acclimated cell are the result of far more than just pigment reduction. The acclimation response is a globally regulated remodeling of cellular structure and metabolism for enhanced photosynthetic activity and growth. Strategies differ greatly among phototrophs, and even between different cyanobacteria. Remodeling processes that may occur include regulation of the abundance and ratios of light harvesting pigments, reaction center proteins, electron transport components, CO_2 import and fixation enzymes, and electron acceptor capacity to support higher carbon fixation rates (Derks et al. 2015). The manifestation of high light acclimation also likely involves regulation of general cellular metabolism to maximize growth. These long term acclimation responses are likely to be regulated at the genetic level as well as in response to signaling and direct regulation by cellular redox, ATP levels, and metabolite (product/reactants) pools.

The complexity of the global response to the light environment has so far complicated attempts to engineer a substantially more productive microbial phototroph by simple pigment reduction or by the modified activity of individual enzymes. However, locked-in high light (LIHLA) regulators of global transcriptional regulation have been identified in the eustigmatophyte *Nannochloropsis gaditana* (Bailey *et al*., 2014). A similar regulator of the light acclimation response in cyanobacteria has not been described to date, however. If such a form of regulation does exist, the underlying control of various desirable traits observed in a high-light acclimated cell could potentially be elucidated by a mutant screen. Such a deregulated mutant, which would demonstrate many of the hypothetical beneficial modifications as orchestrated in a high light induced cell, could also serve as a biological chassis for further genetic modification. Sub-regulated photosynthetic traits such as pigment stoichiometry, photosystem abundance and balance, mechanisms of non-photochemical quenching, carbon concentrating mechanisms and more can be further adjusted upon this globally-deregulated platform to support the highest photosynthetic efficiency possible in commercial production systems.

In order to identify mutant *Cyanobacterium* sp. strains that were “locked in” to the high light-acclimated state, populations of cells were allowed to acclimate to high light conditions, and then transferred to low light conditions. After an appropriate amount of time, the populations were then passed through a Fluorescence-Activated Cell Sorter (FACS) in a high throughput manner. This FACS-based enrichment for low chlorophyll fluorescence from a population of low light-acclimated cells, followed by down-selection for combined low pigment and enhanced P_{max}, was anticipated to potentially result in the isolation of mutants with constitutive traits similar to the high light-acclimated wild type. Under conditions resulting in low light acclimation of the wild type, desired mutants would have reduced chlorophyll, reduced NPQ, higher qP, higher E_k, and higher P_{max} per unit chlorophyll. Since it is likely that this screen would also pick up mutants that are simply defective in pigment biosynthesis or similar deleterious lesions, it was important to have a secondary assay to deselect unproductive mutants and focus on those that have low pigment levels but retain a high P_{max} and consequently remain highly productive.

Prior to the initiation of the ABY2 project, Algenol had already made progress in developing a FACS-based screen for light acclimation mutants of ethanologenic cells. For the ABY2 biomass

project, protocols were developed that identified and isolated both low chlorophyll mutants as well as mutants with altered ratios of phycocyanin to chlorophyll, which can also be a measure of the light acclimation state. To increase genetic diversity of AB1 populations used for screening, libraries of mutant cells were created using several different methods, including UV and chemical mutagenesis (EMS). In other cases, random transposon insertion libraries (total of ~45,000 independent mutants) were created in which various, presumably random genes were inactivated by the introduction of the Tn5 transposon containing an antibiotic resistance marker.

Hundreds of thousands of cells could be sorted based on selected criteria onto agar plates or individual wells of multi-well plates in a short period of time. A typical graph of chlorophyll fluorescence *vs* forward scatter (which is correlated with cell size) is shown in Figure 2-1. However, it became apparent relatively quickly that a robust method for secondary screening would be necessary before it would be possible to narrow down the number of selected variants in order to isolate strains that were truly more productive than the parental strain.

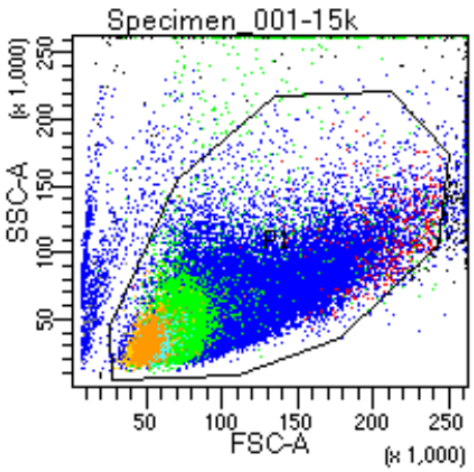

Figure 2-1. Representative FACS output indicating chlorophyll fluorescence per cell (measured as relative SSC-A level) and cell size (measured as forward scatter, or FSC-A). For primary screening of cells locked into a high light (low chlorophyll) state with potential higher photosynthetic rates under low light environments (such as occurs at a high culture density), a window can be selected to sort out and recover cells that exhibit low chlorophyll fluorescence not attributed to small cell size.

Several different approaches were taken to develop medium-throughput secondary screens, which were all designed to measure photosynthetic activity in one form or another. The primary approach receiving the most attention is outlined below:

Growth / pH assay as secondary screen: Work was performed to develop a mid-throughput growth and CO_2 fixation-based secondary screen of FACS-sorted cells using 96-deepwell plates incubated in a CO_2-enriched, illuminated chamber on a rotary shaker (Figure 2-2). Significant effort was put into plate location and orientation, along with other means to eliminate edge effects, in order to achieve consistent and reproducible growth of control cells, but such consistency proved difficult to achieve. The method evolved to using the deepwell growth plates with periodic, adjustable dilution of the individual wells to achieve a consistent stage of growth and light adaptation across the different clones (wells) and to then use these cultures in a plate-based CO_2

fixation assay that measured CO_2 uptake of cells based on concomitant pH shifts that altered the color absorbance of a pH-responsive dye included in each well (Figure 2-3). Unfortunately, these secondary screens were not found to be as robust and reproducible as necessary to have confidence for finding significantly improved strains. Further work on this approach was therefore halted.

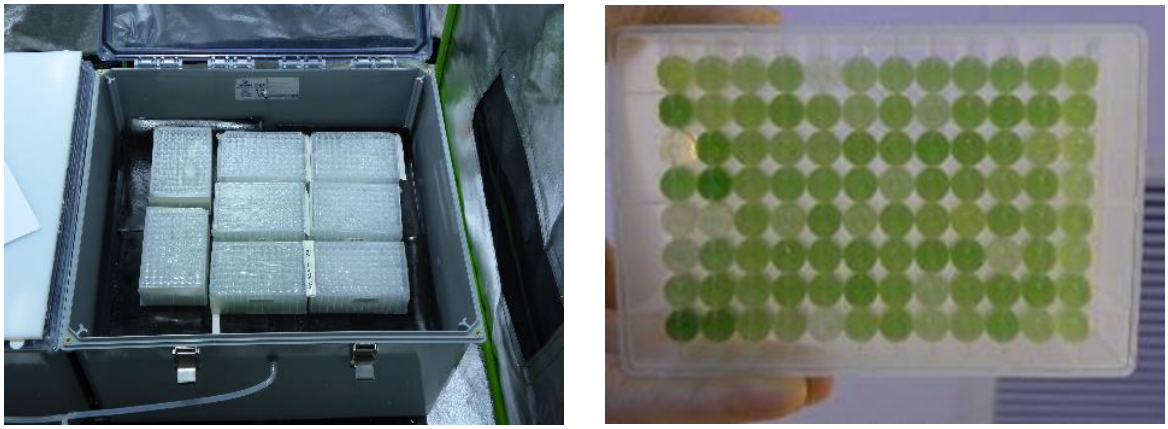

Figure 2-2. 96-deepwell plate system used for screening primary hits from FACS screening procedure (left). Deepwell plate indicating growth of different isolates (right).

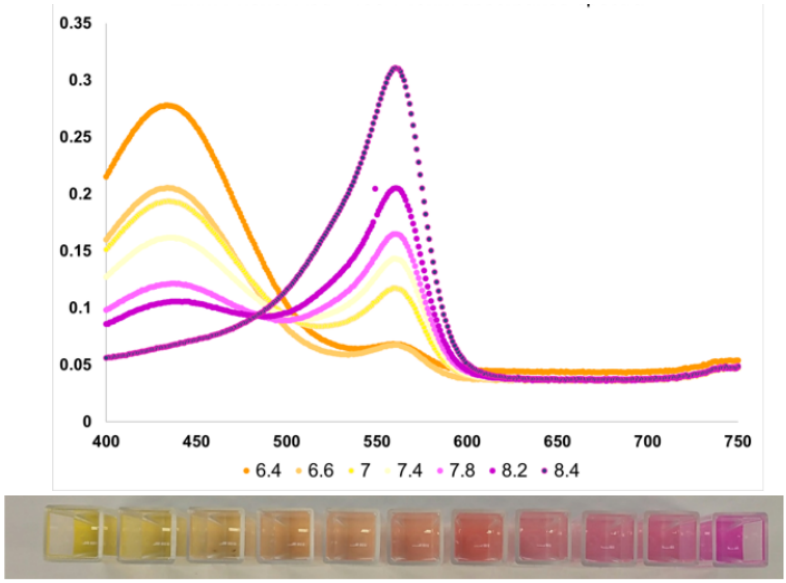

Figure 2-3. Color shift assay using phenol red designed to indicate different rates of photosynthesis (CO_2 uptake) for individual isolates.

Continuous cultivation to identify faster growing strain variants:

In an alternative non-targeted approach, scientists at Algenol's Berlin R&D Facility spent time developing and successfully utilizing turbidostat PBRs (i.e., continuous cultivations) to select for strains with higher growth rates in dense cultures, which reflects higher LUE. In one case,

continuous cultivation experiments were used to determine if there were wild-type strains in Algenol's collection within the genus *Cyanobacterium* that are similar to AB1 (and therefore possibly amenable to the genetic tools similar to those developed for AB1), but that had higher inherent productivity than AB1. (Note that shortly before the initiation of the ABY2 project, one such strain had already been identified that exhibited 15-20% higher biomass productivity than AB1 in the lab under typical growth conditions; this strain was referred to as AB1111.) After inoculating the continuous culture with 40 additional *Cyanobacterium* sp. strains, three additional candidates were identified after several weeks of cultivation that exhibited similar growth properties as AB1111. However, none of those strains showed a significant advantage over AB1111, re-confirming AB1111 as a well- suited production strain worth further study.

This continuous cultivation selection system was also applied to libraries of mutant AB1 cells, including the transposon insertional inactivation ("knockout") libraries described above. At various points in the continuous cultivations, small aliquots of the culture were transferred onto agar plates to isolate independent clones. Colonies that grew well on plates were transferred to individual wells in a high throughput growth system (HTS) similar to that described above. Over five hundred isolates were screened in this manner; the top eleven of the strains that appeared to grow most rapidly based on several criteria are shown in Figure 2-4. Four of these strains were further tested in laboratory PBRs (LvPBRs) (Figure 2-5). Despite initial promising results seen in the HTS screen, increases in productivity were rather minor in these LvPBR growth studies.

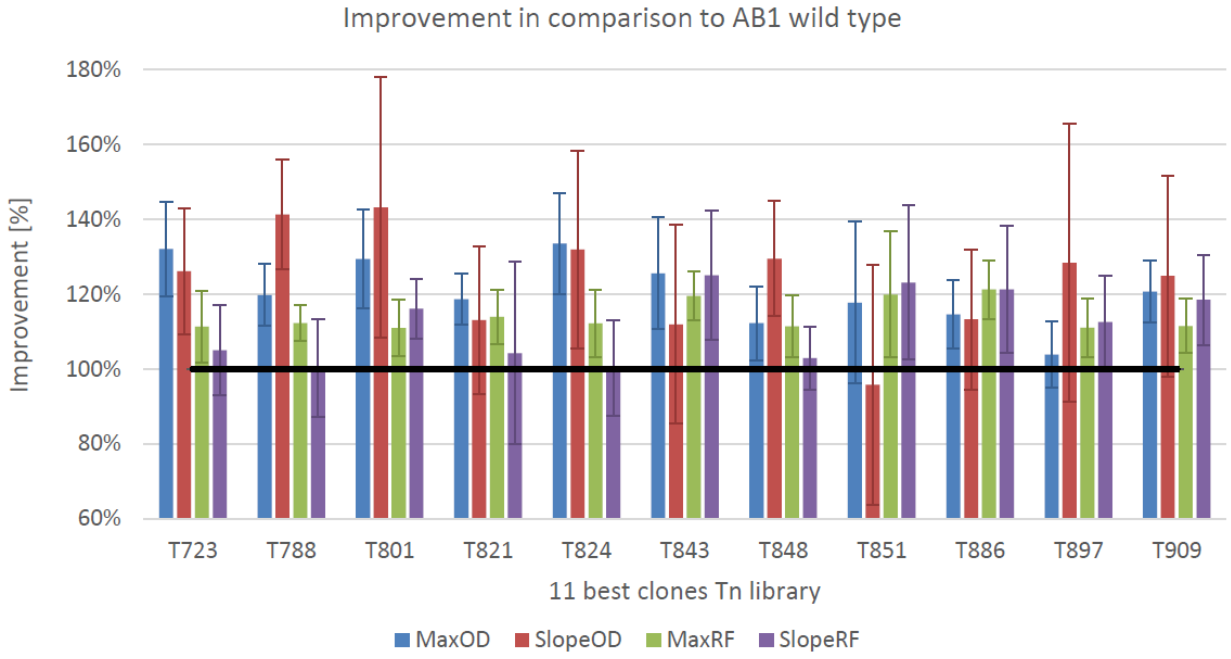

Figure 2-4. Best apparent isolates obtained by the HTS system used to screen transposon insertional mutagenesis libraries grown in long-term (~100-day) continuous cultivations. Values were normalized to 100% of the wild-type references in the deep well plates. Blue bars indicate the maximal OD_{750}, red bars indicate maximal OD_{750} slope, green bars indicate maximal red fluorescence and the violet bars indicate maximal red fluorescence slope values of the strains including standard deviations of the four replicates. The dark blue line indicates the wild-type values (set to 100%).

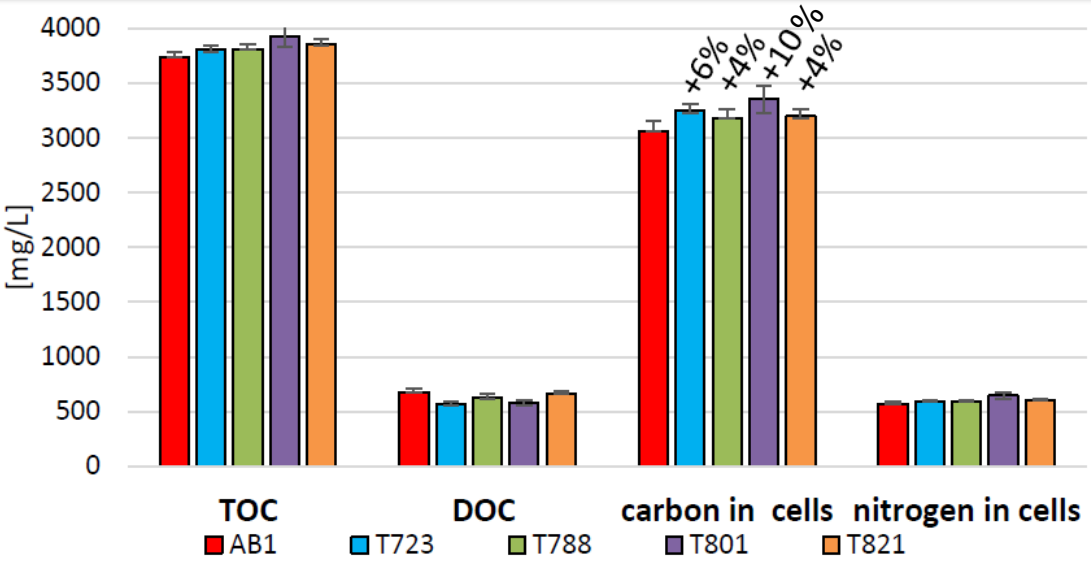

Figure 2-5. TOC, DOC, TOC-DOC (= "carbon in cells"), and TN data for T723 (blue bars), T788 (green bars), T801 (violet bars), and T821 (orange bars) in comparison to AB1 wild-type (red bars). Sum of all measurements of the four batches (mean values and standard deviations of two biological replicates of all four batches) are shown.

In addition, a library of mutant AB1 cells was created by a "knock-in" approach by introduction of a plasmid library carrying random AB1 genome fragments (3-8 kb fragment library) flanked by metal- and nitrogen-inducible promoters. This allowed for overexpression of random native AB1 genes in the library. Photographs of plates/colonies were taken periodically to identify faster growing colonies, according to the methods described by Patel et al. (2016). Approximately 50 of the isolates that appeared to be growing most rapidly were then tested for growth rates in 20-mL vials and the five strains that looked the most promising were then grown in semi-continuous cultivations in "mini-LvPBRs" (200-250 mL volume). Again, despite the significant efforts involved, these candidates did not exhibit faster growth rates than wild type AB1111 (see below). Therefore, this and related screening projects were all ultimately discontinued.

Transcriptomics, bioinformatics analysis, and genetic tool development:

Due to the realization that AB1111 held the most promise of the *Cyanobacterium* strains and derivatives examined to date, it was decided to put effort into developing genetic tools for this strain and to understand more about the strain's genetic composition and regulation. Various "omics" technologies were applied toward this end, some of which were supported in part by the ABY2 program. The results of these analyses are described below.

Global transcriptional analysis (RNAseq) experiments and associated bioinformatics studies were conducted with strain AB1111 in order to identify constitutive and inducible native promoters and to define their sequence boundaries. This information and resulting genetic tools will be useful for making targeted genetic changes to this strain. Initial analysis of global expression patterns of AB1111 identified 2,270 genes that were found to be differentially expressed to a significant extent under one or more conditions. Nitrate and copper inducible promoters were identified which had

the highest levels of induced expression (the strongest), those that had the lowest levels of basal expression (the tightest), and those that delivered a mix of tight basal level control and high induced expression. Three copper regulated promoters and one nitrate regulated promoter identified in this study were amplified using PCR and tested for basal and induced expression levels in AB1166 by the use of reporter gene (Table 2-1).

Table 2-1. Top copper-inducible promoters identified in RNAseq experiments with AB1111.

Promoter	Annotation	Notes
Porf01460	Metal-binding protein	Low basal expression
Porf11330	Plastocyanin	High basal expression
Porf01450	Photosystem I subunit	in same operon as 1460
Porf01540	Type 3 multicopper oxidase	High, but noisy

Additional studies were conducted to identify the transcriptional start sites of the identified genes in AB1111. This work involved the use of terminator 5′-phosphate-dependent exonuclease (TEX)-based dRNAseq analysis using a custom algorithm which examines both +TEX and –TEX treated samples, as based on Thomason *et al.* (2014). In this manner, the transcriptional start sites of many RNA species found within AB1111 were identified. Altogether, 2673 transcriptional start sites associated with a total possible 4,096 open reading frames (ORFs) in the AB1111 genome were identified. These transcriptional start sites give both a way to identify the precise location of promoters and also to allow the identification of non-translated RNA species such as small RNAs (sRNAs), which often have regulatory functions in the cell.

To identify both translated and non-translated species of RNA, a custom program called RNAseg was used to identify Transcriptional Units (TUs) from the +/- TEX RNAseq data. Initially, over 14,000 TUs were identified using this algorithm, which was higher than expected based on identified ORFs. Custom software was written to combine and filter the TUs obtained in this step, resulting in a more reasonable number.

The RNA-seq reads from experiments in AB1111 and AB1 were mapped to TUs identified as described above and the top differentially expressed non-coding RNAs were identified and characterized. The characterization involved analysis using the GLASSgo software algorithm from the Freiburg RNA Tools suite (http://rna.informatik.uni-freiburg.de). This tool looks for full length homologs of the RNA sequence across related organisms (cyanobacteria) and returns a multiple alignment of these homologous sequences for further evaluation. Hits with sufficient homology were further characterized using the CopraRNA algorithm to determine potential interactions between promoters and small RNAs as well as RNAFold to determine the secondary structure of the potential regulatory sRNAs. In this manner, several potential regulatory sRNAs were identified for further study.

Algenol scientists were interested in examining the role of sRNAs in regulating cellular processes that impact photosynthetic carbon fixation, growth rate, biomass composition, *etc.*, with the eventual goal of manipulating these sRNAs through genetic engineering to improve overall biofuel production rates. Several potential regulatory sRNAs which were identified from experiments in AB1111 and AB1 were further analyzed to prioritize the list for follow-up analysis. An algorithm was devised to rank the potential sRNAs based on a variety of factors. These factors included:

the similarity of the sRNA with known sRNAs from other cyanobacterial species as determined by BLAST sequence analysis; the conservation of the sRNA sequence compared to other cyanobacterial genomes as determined by the GLASSGo algorithm; the potential of the sRNA to bind to multiple promoters within the AB1 or AB1111 genomes as determined by the CopraRNA algorithm; the presence of sRNA-like secondary structural features as determined by the RNAFold algorithm; and the differential expression of the sRNA under various conditions. In this manner, the six most highly ranked sRNAs (see Figure 2-6) were identified and deemed worthy of further analysis, but time and financial constraints required a postponement of this analysis.

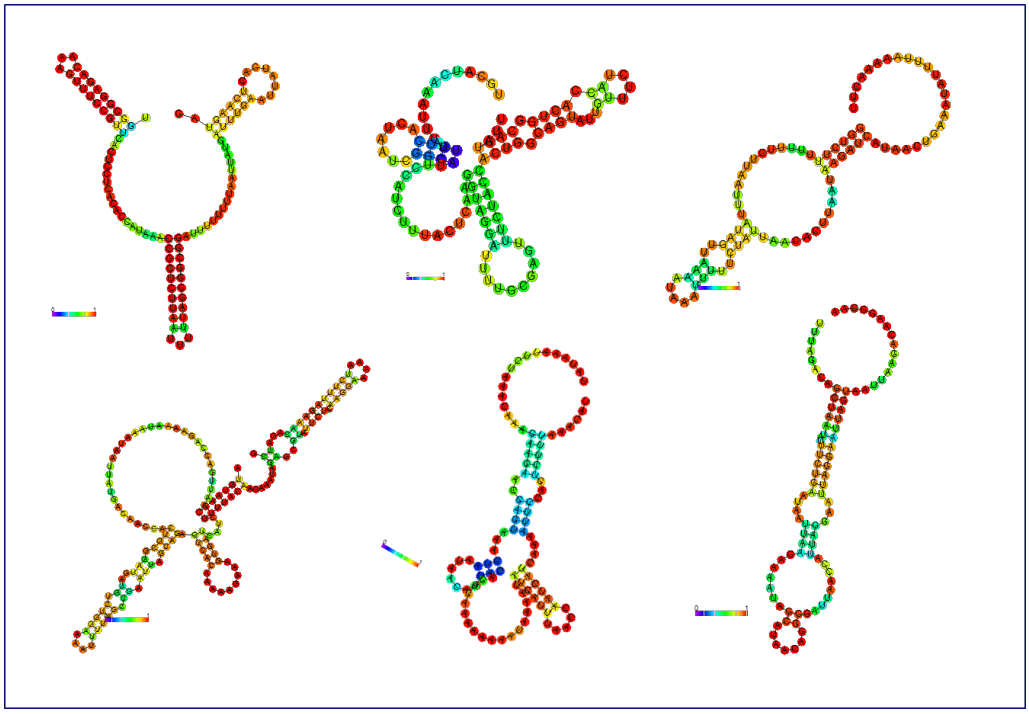

Figure 2-6. Structures of six different potential sRNAs identified in AB1111.

Recombinant ("Targeted") Approaches for Improving Productivity:

Numerous targeted genetic modifications have been made to AB1 and AB1111 (or more specifically a variant of AB1111 referred to as AB1166 that for unknown reasons can be transformed with higher efficiency) with the intent of improving productivity. Some of these activities were supported in part by the DOE ABY2 program, and included overexpression of metabolic enzymes involved in carbon fixation and altered expression of various regulatory proteins. In addition, attempts were made to lower the expression of light-harvesting photosynthetic pigments, proteins, and complexes such as phycocyanin (PC), chlorophyll, and photosystem I as a means of increasing light availability to dense cultures.

Carbon fixation and metabolism

Previous experimentation done within Algenol's ethanol research program had led to the discovery that inactivation or deletion of the native AB1 regulatory gene *orf0997* (*kai*C) resulted in an increase in productivity, and therefore higher light utilization efficiency. For the ABY2 program, we have expanded these studies to non-ethanologenic strains. AB1:Δ*orf0997* (strain AB0952) and two derivatives of AB0952, one overexpressing the inorganic carbon transporter *orf32660* (*bic*A) (strain AB1168) and the other overexpressing both *orf32660* and the Rubisco operon (strain AB1169). These strains were grown in LvPBRs in the lab under semi-continuous cultivation for 40 days. Different dilution modes were compared (daily dilutions initially, followed by dilutions every two or three days). Unfortunately, under the given cultivation conditions, AB1168 and AB1169 exhibited no further improvement over the parental Δ*orf0997* strain (AB0952) (Figures 2-7 and 2-8). In addition, a *kai*C knockout was produced in AB1166 (strain AB1118), but there was less than a 10% increase in biomass productivity.

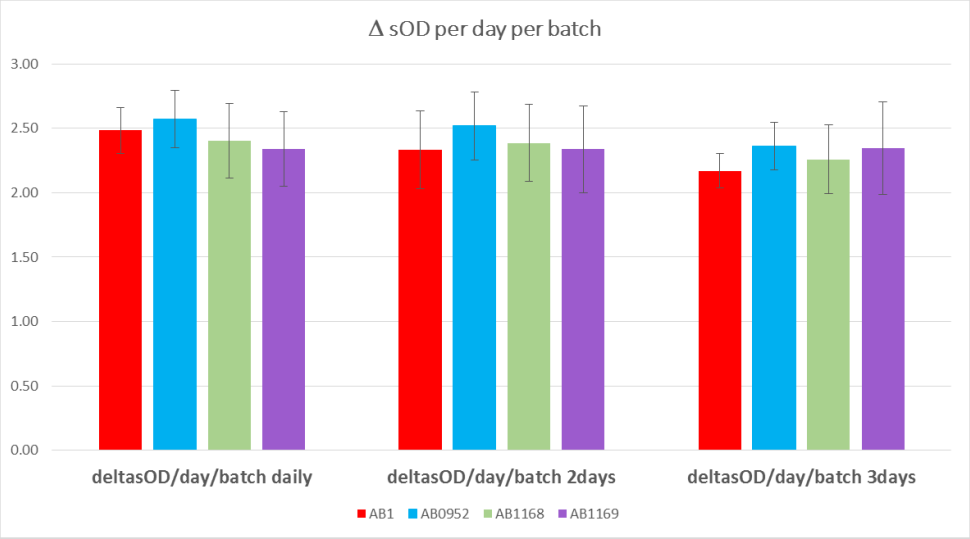

Figure 2-.7. Growth of AB1 wild-type and derivative strains in semi-continuous cultivations with dilutions every 1, 2, or 3 days. Strains are modified as follows: 1) AB0952 has an inactivated kaiC gene; 2) AB1168 has an inactivated kaiC gene and overexpresses the bicA gene; 3) AB1169 has an inactivated kaiC gene and overexpresses both the bicA gene and the rbcLXS (Rubisco) operon. Growth is measured as the change in sOD_{750} per day. (sOD_{750} refers to a standardized optical density at 750 nm.)

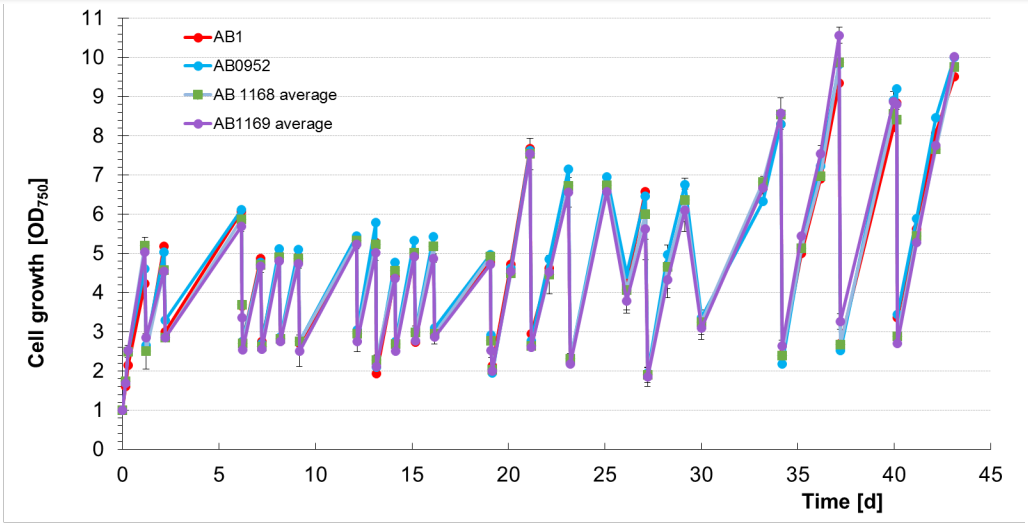

Figure 2-8. Growth of AB1 wild-type and derivative strains in semi-continuous cultivations with dilutions every 1, 2, or 3 days. Strains are modified as follows: 1) AB0952 has an inactivated kaiC gene; 2) AB1168 has an inactivated kaiC gene and overexpresses the bicA gene; 3) AB1169 has an inactivated kaiC gene and overexpresses both the bicA gene and the rbcLXS (Rubisco) operon. Growth is measured as the change in sOD_{750} per day.

Strains overexpressing certain enzymes involved in the Calvin-Benson-Bassham (CBB) Cycle were also tested for higher productivity and light utilization efficiency compared to wild type AB1. AB1-based strains overexpressing three different native or heterologous CBB Cycle enzymes were evaluated in semi-continuous laboratory LvPBR systems with daily dilutions over a two-week cultivation period. In initial tests, strains overexpressing transketolase (*tkl*) (strain AB1192) and fructose-1,6-bisphosphatase (FBPase) (*glp*X) (strain AB1190) exhibited marginally higher biomass productivities (8% and 11%, respectively) compared to the control strain. In addition to these strains, AB1193 was created that overexpressed the native *tkl* gene along with a heterologous gene from the plant *Arabidopsis* that encoded sedoheptulose-bis-phosphatase (SBPase), which had been reported to increase photosynthesis and productivity in tobacco and other plants (Lefebvre *et al*., 2005). AB1193 failed to show an improvement in biomass productivity compared to the parental strain, however.

Since some positive results were obtained in overexpressing *glp*X (FBPase) in AB1, the same genetic change was made to AB1166, resulting in strain AB1315. Despite the fact that there was a 3-4x increase in the FBPase activity for this strain (Figure 2-9), as measured by an adaptation of the method of Tamoi et al. (1999), no increase in biomass productivity was observed. In fact, in this same experiment, the previously observed increase in biomass productivity noted for the strain AB1190 (*glp*X-overexpressing AB1 derivative) also was not observed, indicating that this approach doesn't appear robust (Figure 2-10).

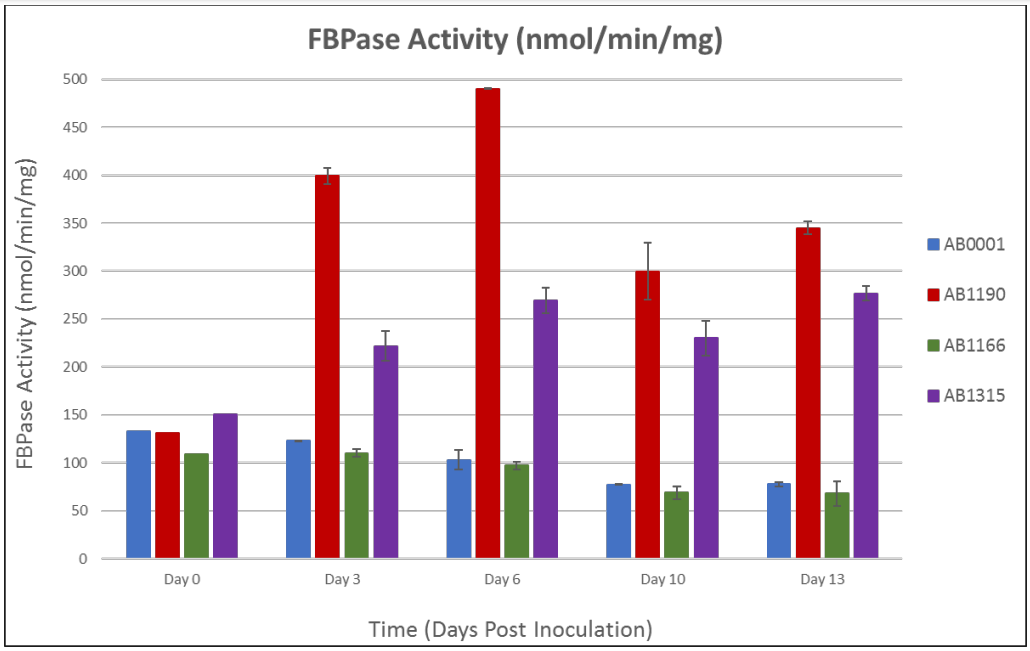

Figure 2-9. Activity of FBPase in glpX-overexpression derivatives of AB1 and AB1166 (strains AB1190 and AB1315, respectively) compared to the parental wild-type strains.

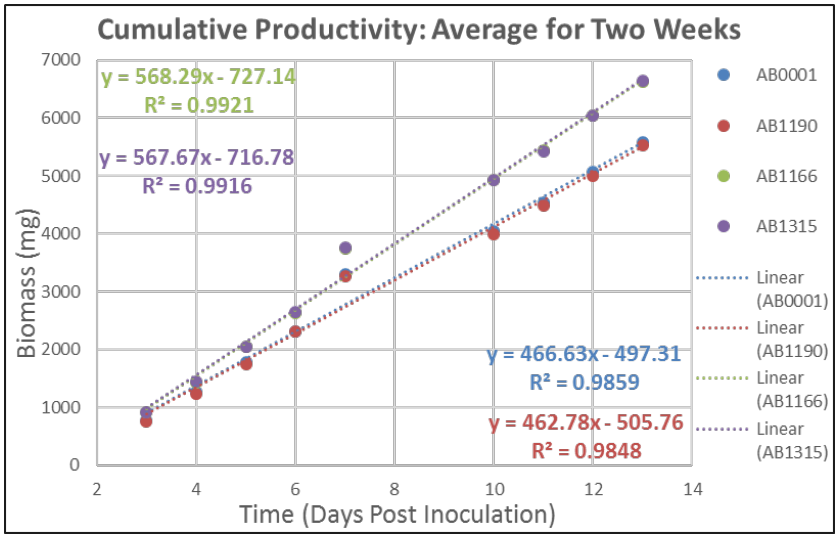

Figure 2-10. Biomass productivity in glpX-overexpression derivatives of AB1 and AB1166 (strains AB1190 and AB1315, respectively) compared to the parental wild-type strains.

Due to the complicated interplay of multiple cellular systems and pathways in defining overall growth rates and biomass formation and composition, Algenol scientists investigated the possibility that altering the levels of certain regulatory proteins known to impact several aspects of carbon metabolism could potentially lead to increase photosynthesis rates and biomass accumulation. Toward this end, AB1-based strains were produced in which two related transcription factors (regulatory proteins) involved in carbon metabolism (*orf30270*, annotated as

*cyAbr*B1 and *orf38080*, annotated as *cyAbr*B2) were overexpressed, either individually or together in an operon. These strains were evaluated in lab-scale LvPBRs using daily dilutions in semi-continuous operation (Figure 2-11). Overexpression of both of these regulatory proteins together (strain AB1176) resulted in stagnation of growth, however. Overexpression of one of the regulatory proteins alone (*orf38080;* strain AB1178) resulted in lower biomass productivity than AB1. However, overexpression of the other regulatory protein alone (*orf30270;* strain AB1177) resulted in a slight (~10%) increase in biomass productivity compared to AB1.

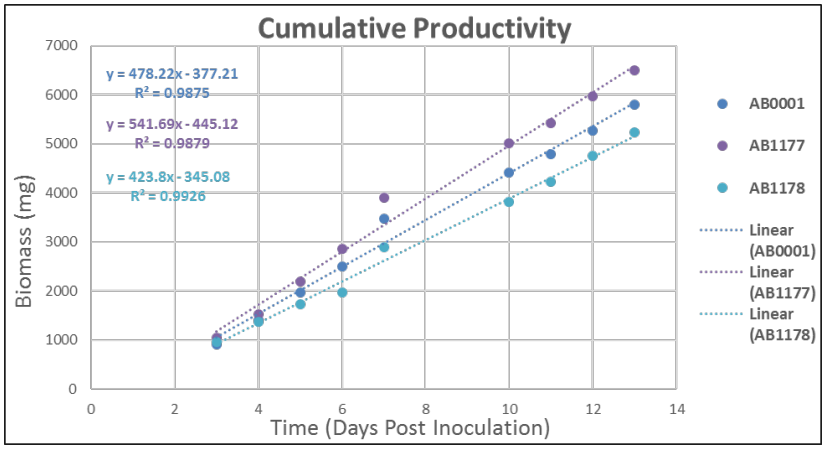

Figure 2-11. Biomass accumulation over time in semi-continuous cultivations for wild-type AB1 and derivatives overexpressing the regulatory proteins encoded by cyAbrB1 (strain AB1177) and cyAbrB2 (strain AB1178).

Pigment reduction

As described above, reductions in the levels of photosynthetic pigments can provide several advantages, including deeper penetration of light into cultures and a better balance between light harvested and actual photosynthetic light utilization. Derivative strains of AB1166 with reduced levels of phycocyanin (PC) and chlorophyll pigmentation were created by targeted means. PC reduction was accomplished by lowering the expression level of the *cpc*BA operon to different extents by swapping the native *cpc*BA promoter with promoters that transcriptomic experiments had revealed a converse response to low light levels compared to the native *cpc*BA promoter (i.e., two variants of the *rbc*L promoter and a variant of the *opr*B promoter). Strains containing these new constructs had PC contents that were 70% to 90% of the AB1166 wild-type strain (Figure 2-12). Growth, as measured by an increase in sOD_{750}, was slightly reduced for these strains while actual dry weight production was slightly enhanced (5-10%) at the end of 7-day indoor batch cultivations. Associated Total Organic Carbon (TOC) and Total Nitrogen (TN) measurements indicated that strains with lower PC levels exhibited an elevated C/N ratio (+10%), likely due to a lower overall protein content of the cells; this would be expected to positively influence quality and quantity of the HTL yield in these AB1166 low PC derivatives. In another approach, an additional strain (AB1259) derived from AB1166 had ~30% lower chlorophyll levels as a result of knocking out the *ycf*37 gene, which is involved in Photosystem I assembly (Figure 2-12). In a 3-week semi-continuous cultivation in laboratory PBRs in the Algenol's Berlin lab, AB1259 exhibited higher biomass productivity than wild-type AB1166, with a 10-15% improvement based on dry weight or cellular organic carbon content. A double mutant with both low chlorophyll content and reduced

PC levels was also created in AB1166 (strain AB1278). This strain also had higher biomass productivity (15-20% higher than AB1166), observable both as enhanced dry weight and cellular organic carbon accumulation. Unfortunately, when cultivation experiments with AB1278 were repeated in Fort Myers labs using site well water and semi-continuous cultivation conditions similar to those used in outdoor cultivations, the magnitude of the increase was less pronounced.

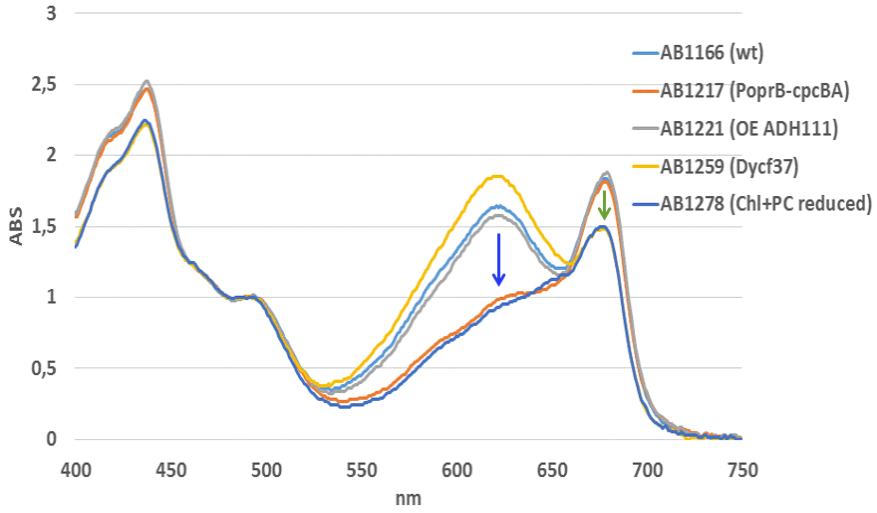

Figure 2-12. Absorption spectra of AB1166 wild-type cells and derivatives reduced in phycocyanin (AB1259), chlorophyll (AB1221), or both of these photosynthetic pigments (AB1278).

In another approach, attempts were made to replace a Photosystem I gene (*psaA*) in AB1166 with a mutated version that could potentially provide an enhancement in LUE (replacement of a conserved leucine at consensus sequence position 722 in the PsaA protein with threonine). This strategy was based on a report by Santabarbara (2010) indicating potentially beneficial changes in the inter-quinone electron transfer dynamics for such mutants. Unfortunately, the cells were not healthy and it wasn't possible to fully replace the native gene due to the negative phenotype associated with the expression of this mutated gene. This line of research was therefore abandoned.

All in all, strain development efforts to improve biomass productivity had limited success. In a number of cases, a strain that showed an increase in productivity in indoor batch cultivations ended up not showing an improvement when the cells were grown with semi-continuous operations under more commercially-relevant conditions. Several engineered strains derived from AB1 exhibited ~10-15% higher productivity even under semi-continuous cultivation, but these strains (along with multiple other *Cyanobacterium* sp. strains from Algenol's culture collection) didn't exceed the productivities that were observed with native strain AB1166. It is quite possible that AB1166 and other top strains are naturally so productive that it is not realistic to be able to increase their productivity with what we know today.

Improved Processing (more efficient harvesting and dewatering)

Significant cost savings would result from identifying or creating strains that could be harvested and dewatered with less energy and lower handling costs. One the disadvantages of Algenol's primary production strain, *Cyanobacterium* sp. AB1, is that cultures become quite viscous over time. This viscosity interferes with efficient harvesting of cells, whether done by centrifugation or filtration. It was believed that reducing culture viscosity would significantly improve harvesting efficiency and therefore reduce energy utilization and overall cost of the harvesting and dewatering process. It was also realistic to expect that reduced culture viscosity would result in better culture mixing, allowing more rapid distribution and homogenization of nutrients and gases.

A major factor leading to culture viscosity in algal cultures is the presence of exopolysaccharides (EPS) secreted by the production strain. Algenol scientists therefore conducted research to reduce the viscosity of cultures by deleting genes involved in EPS production. During the course of Algenol's ethanologenic strain development program, a bioinformatics analysis of the AB1 genome revealed a number of possible genes potentially encoding enzymes or transporters involved in EPS production, based on sequence comparisons with known EPS genes identified in reports by Jittawuttipoka et al. (2013) and Pereira et al. (2013). Insertional inactivations of ten of these genes were attempted in AB1, but only two of the knockouts yielded transformants that were able to be fully segregated, including: (1) AB1:Δ*orf_3817* (strain AB0377), in which a weak homolog of the *Synechococcus* PCC 6803 *gum*C / *Cyanothece* CCY0110 *wzc* gene was inactivated; and (2) AB1:Δ*orf_1052* (strain AB0388), involving a knockout of a homolog of the *Synechococcus* PCC 6803 *gum*B / *Cyanothece* CCY0110 *wza* gene.

Although AB0377- and AB0388-based strains had been previously studied for effects on ethanol production, these strains had not been evaluated for the effects on biomass production in the absence of ethanol production. Ethanologenic derivatives of AB0388 exhibited a ~30% decrease in viscosity (measured with a Brookfield DV2T viscometer at a shear rate of 1.223 s^{-1}), while AB0377 cultures showed no measurable viscosity at this shear rate. Another strain (AB1161) contained a knockout of the *orf_1052* EPS gene as well as a knockout of the *orf_3817* (*ccm*R) gene involved in regulating inorganic carbon uptake. In ethanologenic strains, knocking out the *ccm*R gene resulted in an increase in ethanol and biomass productivity, but led to higher viscosity, potentially due to an increase in EPS production. For the ABY2 program, these three strains (AB0377, AB0388, and AB1161) were evaluated for biomass productivity in comparison to AB1 wild type and AB0948 (AB1:Δ*ccm*R) control strains, but didn't show an improvement. AB0377 clearly demonstrated very low viscosities when compared to AB1, but had the lowest biomass productivity, due to the fact that the culture quickly settled out of suspension in early stages of the culture.

Since cultures of AB0377 showed no measurable increase in viscosity as the culture grew, but exhibited an undesirable settling phenotype, it was considered possible that a partial knockdown in the expression of the *orf_3817* gene might lead to a reduction in viscosity without the settling issue. Several strains were generated that enabled an inducible knockdown based on antisense sRNA expression. Two of the constructs used different sRNA backbones that were linked to the copper-inducible P*orf_0316* promoter, but the resulting strains (AB1062, AB1063, AB1124, and AB1125) exhibited too much expression even in the absence of induction, so additional strains

(AB1126 and AB1127) were created that used the tighter P*orf_0221* promoter driving expression of the anti-*orf_3817* sRNA.

Strains that were generated to have lower exopolysaccharide (EPS) levels via inducible antisense knockdown of a gene involved in EPS production were grown in bubbling bottles to determine if the knockdown resulted in decreased gene expression. For this cultivation, two strains were inoculated into bubbling bottles and allowed to grow for two days before the knock-down was induced with the addition of copper, followed by an additional bolus of copper after sampling on day 4. Samples for quantitative RT-PCR (qRT-PCR) analysis of gene expression were taken prior to induction, as well as after each induction (copper addition), to determine the effect of the inducible knockdown on gene expression. Results of this experiment demonstrated that within 24 hours of the first copper dose, the expression of AB1_orf3817 decreased after inoculation, regardless of whether copper was added or not (Figure 2-13). After copper addition, the fold change did not decrease further, suggesting that the induction of the antisense knockdown was likely not strong enough to impact the gene expression. Because of these results, the strains were not evaluated further in LvPBRs.

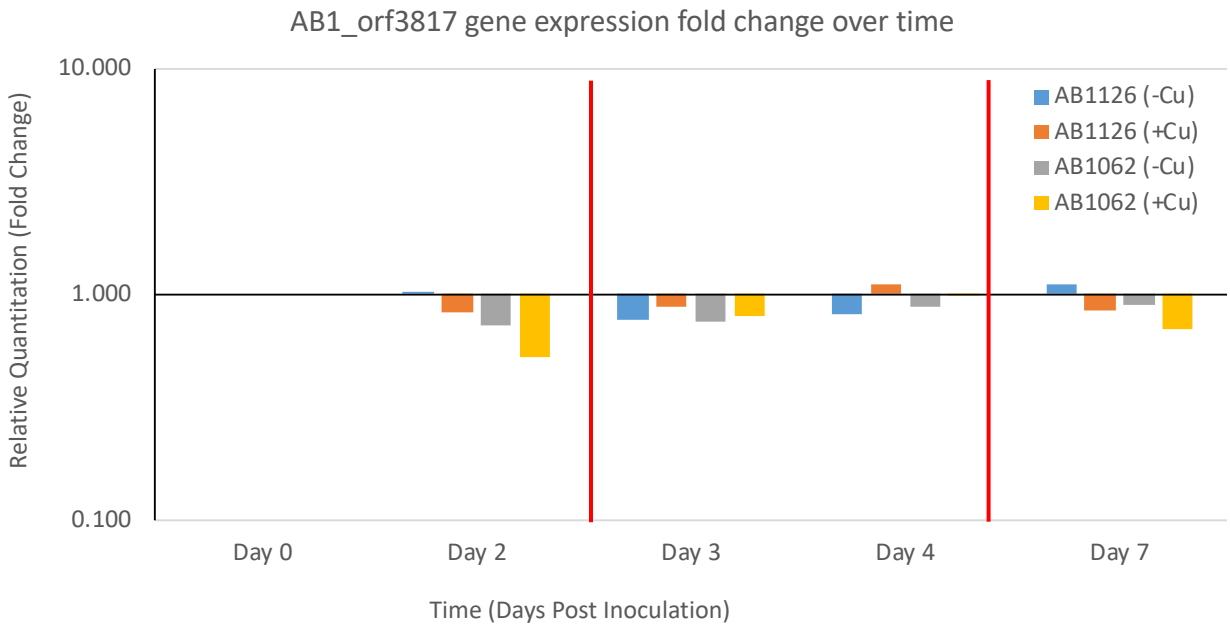

Figure 2-13. Fold change in gene expression of AB1_orf3817 after induction of antisense knockdown in strains AB1126 and AB1062. Fold change was calculated by comparing the expression of AB1_orf3817 at each time point with the expression level on day 0. Red lines on the graph represent induction by addition of copper.

While work was underway on creating and characterizing EPS-deficient mutants of AB1, Algenol scientists were gaining a better understanding of the attributes of AB1111 and AB1166. Both of these strains were reported to demonstrate more efficient harvesting when compared to AB1. An LvPBR evaluation of AB1166 and AB1 using semi-continuous operation was undertaken to better quantify any decrease in viscosity of AB1166 compared to AB1. There was a difference of ~40% in the dissolved organic carbon (DOC) produced by the two strains, with AB1166 producing less

DOC than AB1 (Figure 2-14); previous studies had indicated that the bulk of the DOC in the cultures was EPS.

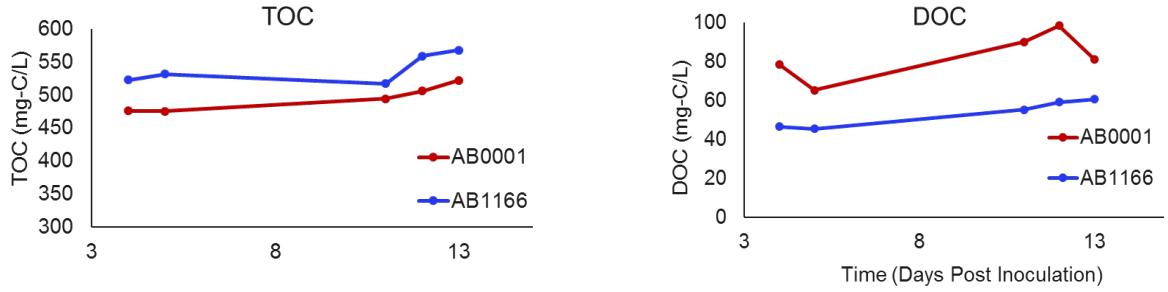

Figure 2-14. Organic Carbon in AB1 and AB1166 semi-continuous cultures before and after centrifugation. Left: Total organic carbon in culture medium. Right: Dissolved organic carbon remaining in supernatant fluid after centrifugation at 7,000xg for 10 minutes.

Figure 2-15 provides a good visual representation of how AB1166 cells can be separated from culture medium more quickly than AB1 cells. Upon sitting undisturbed on a benchtop for up to 71 hours, it is clear that the AB1166 cells settle out of the medium much more quickly than AB1 cells. This behavior is also manifest in centrifugation efficiency trials, in which about 90% of the organic carbon in an AB1 culture was pelleted after centrifugation for 2 minutes at 10,000 x g (simulating commercial-scale continuous centrifugation), while for AB1166, about 97% of the carbon was removed from the supernatant under the same conditions, indicating that more efficient removal of cellular material was achieved via centrifugation for AB1166 compared with AB1. It is reasonable to assume that this enhanced recovery is due to the lower viscosity of AB1166 cultures, which was confirmed by the use of a Brookfield DV2T viscometer. When measured at a shear rate of 73.38 s^{-1}, the viscosity of AB1 cultures was on average 2.4 cP, whereas for AB1166 cultures it was 1.1 cP, demonstrating a decrease of >50% in measurable viscosity for AB1166 compared to AB1.

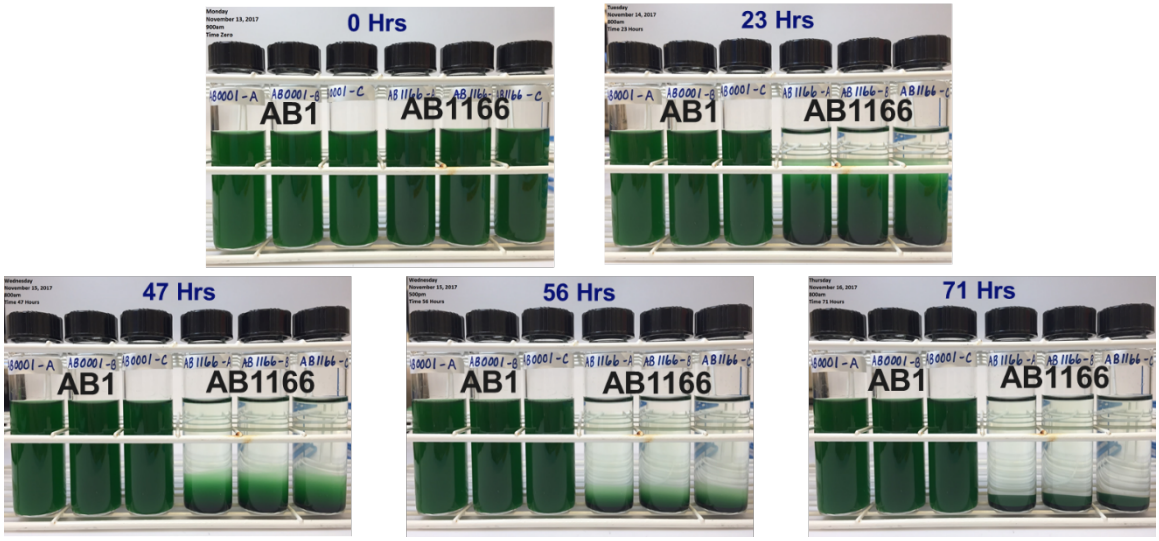

Figure 2-15. Photographs of AB1 and AB1166 cultures allowed to sit undisturbed on a benchtop after various periods of time.

As strain AB1166 was shown to exhibit both higher biomass productivity and >50% reduced viscosity compared to AB1, which met the milestone criteria for an improved strain, further efforts to reduce the viscosity of AB1 cultures were stopped and resources directed to other activities in the ABY2 program. Additional information on the viscosity and harvesting differences between AB1 and AB1166 grown in outdoor cultivations can be found in the Task 4 section of this report, which describes the results of the Milestone 4.1 experiment.

Enhanced HTL-Based BFI Yield and Quality

The overarching hypothesis for the work conducted at NREL in support of this project is that variations in cyanobacterial biomass composition are expected to have significant impact on the yield and quality of Biofuel Intermediate (BFI, or bio-oil) generated through hydrothermal liquefaction. The goal is to generate *Synechocystis* strains with optimized biomass composition that leads to higher BFI yield and quality. The knowledge will then be transferred to AB1 or another commercial production strain. As a first step, bench scale HTL was conducted on samples of cyanobacterial biomass altered by the additional inclusion of various materials typically used by cyanobacteria as storage compounds as well as by testing strains known to vary in biochemical composition.

Bench-scale HTL process

Bench-scale HTL reactors were made with 316 stainless steel with 4 in length of 0.5 in O.D. tube with a wall thickness of 0.065 in. A cap was placed on one end, and the other end was fitted with an 18 in. length of 1/8 in. O.D. tube, with a wall thickness of 0.028 in., connected to a high-pressure valve. In a typical experiment 5 mL of biomass slurry (20 wt% DCW) were loaded into a reactor. The slurry loading was selected such that 95% of the reactor volume was occupied by liquid at reaction conditions. The air in the headspace of the reactor was replaced with helium by repeated cycles of evacuation and charging with helium. 140 psi of helium was retained to serve as an internal standard for the quantification of gas yields.

HTL reactions were carried out by placing the reactors vertically in a fluidized sand bath, and the temperature was maintained at 300 °C for 30 min. After the reaction, the reactors were removed from the sand bath and immersed in a cold-water bath for about 30 min to quench the reaction. The reactors were placed in ambient temperature for up to 3 hours to allow the liquid and gas phase to equilibrate. The gas phase was collected into gas bags for analysis. The gas bags were directly hooked up to and analyzed by an Agilent 490 micro-GC with Molecular Sieve 5A, PoraPLOT Q, CP-Sil 5CB, and CP-Wax 52CB columns for He, N_2, H_2, CO, CO_2, and C_1-C_4 hydrocarbons.

HTL product recovery

The mixture in the reactor was transferred to a separatory funnel and the reactor was rinsed with dichloromethane (DCM) and deionized (DI) water to transfer all the material into the separatory funnel. The funnel was shaken vigorously to extract bio-oil into the DCM phase. Then the phases were allowed to separate under gravity for analysis. The DCM and aqueous phase were

sequentially filtered to remove biochar. The obtained DCM phase was transferred into a 10 mL volumetric flask to make up to 10 mL using DCM. One microliter of DCM phase was injected into a GC for analysis. Then an aliquot of DCM phase was transferred into a pre-weighed tube. The DCM was evaporated under a nitrogen stream for 2 hours. Then the bio-oil was evaporated in a vacuum oven under 40 °C for 2 hours to get a gravimetric yield. An aliquot of aqueous phase was freeze-dried to get the dry weight for aqueous phase yield. The general HTL product recovery scheme is illustrated in Figure 2-16.

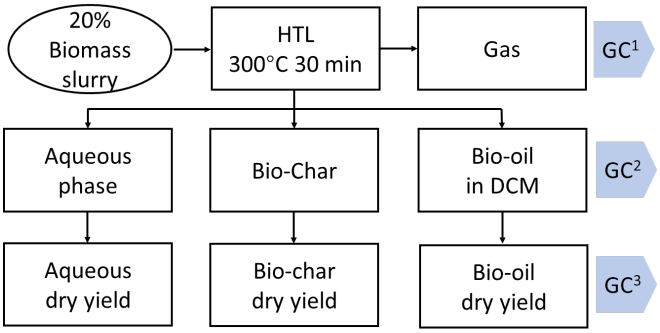

Figure 2-16. Bench scale HTL experiment setting up (The gas phase was analyzed by GC[1]; the bio-oil in DCM was analyzed by GC[2]; after DCM evaporation the bio-oil was analyzed by GC[3].)

The yield of bio-oil was quantified by a gravimetric method. The boiling point distribution was analyzed by thermal gravimetric analysis (TGA) and GC. Elemental analysis was performed to quantify the C, H, N and S in order to calculate the theoretical high heating value (HHV). Bio-oil with a low boiling point distribution and high energy density (i.e., HHV) is usually preferred. Lower nitrogen and sulfur contents are also favored for easier downstream catalytic upgrading.

Identification of existing strains with variations in the amount of glycogen, PHB, and cyanophycin

NREL has assembled a collection of hundreds of *Synechocystis* strains, with mutations that affect various aspects of photosynthesis and carbon/nitrogen metabolism. Some of the strains affect biomass composition and were further studied in this project, as shown in Table 2-2.

Table 2-2. Synechocystis mutant strain list identification of medium chain length polyhydroxyalkanoates (mcl-PHA) as a possible way to improve HTL yield and quality.

Strain	Mutation	Reference
Wild-type	none	Carrieri *et al.,* 2012
Δ*glgC*	Deletion of *glgC* thus blocking glycogen synthesis	Carrieri *et al.,* 2012
Δ*glgC*_P*psbA*::*glgC*	*glgC* put-back under psbA promoter; lower glycogen content *vs* WT	Carrieri *et al.,* 2012
Δ*glgC*_P*petE*::*glgC*	*glgC* put-back under *petE* promoter; lower glycogen content *vs* WT	Carrieri *et al.,* 2012
WT_P*psbA*::*glgC*	*glgC* overexpression under *psbA* promoter; potentially higher glycogen content *vs* WT	Unpublished

Δ*phaAB*	Deletion of *phaAB* thus blocking PHB synthesis	Unpublished
Δ*cphA*	Deletion of *cphA* thus blocking cyanophycin synthesis	Unpublished

At the inception of this project, the prevailing wisdom was that lipids such as triacylglycerol (TAG) contribute favorably to HTL BFI formation. A natural storage lipid in some cyanobacteria, including *Synechocystis* PCC 6803, is polyhydroxybutyrate (PHB). Thus it was thought that a cyanobacterial biomass enriched in PHB might be a preferred HTL feedstock. However, the NREL team questioned this assumption based on thermal degradation chemistry.

The PHB can be depolymerized to form short chain carboxylic acids, such as crotonic acid, which are hydrophilic and miscible with water and therefore cannot contribute to bio-oil yield. Thus, PHB might not be converted into bio-oil due to the short chain building monomers. This potential technical gap was identified at the beginning of this project and it was proposed that polyhydroxyalkanoates (PHA) with medium chain length monomers (*mcl*-PHA) might be promising compounds that can increase the bio-oil yield, because the medium chain carboxylic acids and their derivatives derived *via* HTL can be hydrophobic, easily migrating into the bio-oil phase. Thus, addition of triacylglycerol (TAG), PHB and *mcl*-PHA into wild type *Synechocystis* PCC 6803 biomass for HTL was tested in order to identify the effect of these compounds on BFI yield.

Unfortunately, there is no commercially available *mcl*-PHA. In order to obtain the necessary material, we grew the bacterial species *Pseudomonas putida,* which is known for its capacity to accumulate high amounts of *mcl*-PHA when grown on glucose or other carbon sources under nitrogen deficient conditions. We fed the *P. putida* with glucose while limiting the nitrogen supply. The PHA content reached 8.6% cell dry weight (CDW) at the end of the fermentation, with 3-hydroxydecanoic acid as the dominant monomer. The *mcl*-PHA was then extracted and used in the bench scale HTL doping study.

Doping the wild type biomass with different lipid compounds demonstrated that TAG and *mcl*-PHA significantly increased the bio-oil yields, while doping with PHB reduced the bio-oil yield. Doping PHB into the biomass led to a considerable amount of gas production after HTL. The dominant gas compounds were equal amounts of propylene and carbon dioxide, which are believed to be produced via PHB depolymerization, isomerization and decarboxylation. Thus, PHB was confirmed as a poor HTL feedstock.

The addition of *mcl*-PHA indeed increased the bio-oil yields (Figure 2-17) and HHV content from *Synechocystis* biomass, indicating a positive effect of *mcl*-PHA on bio-oil production. In the initial experiments, DCM was used to dissolve the viscous bio-oil for efficient removal from the reactor, followed by solvent evaporation to get the gravimetric yield. To capture the oil-soluble volatile compounds, bio-oil was directly injected into GC-MS before DCM evaporation. As anticipated, considerable amounts of volatile compounds were identified in the bio-oil before DCM evaporation. A detailed analysis showed that the major volatile compounds were 1-heptene, 1-nonene and 2-nonene. These compounds were also detected in the bio-oil that was produced from pure *mcl*-PHA before solvent evaporation, thus were considered thermal degradation

products from *mcl*-PHA. The results showed that about 35-45% of *mcl*-PHA were converted into α-olefins, which is a value-added co-product that can be used for either biofuel or biomaterials.

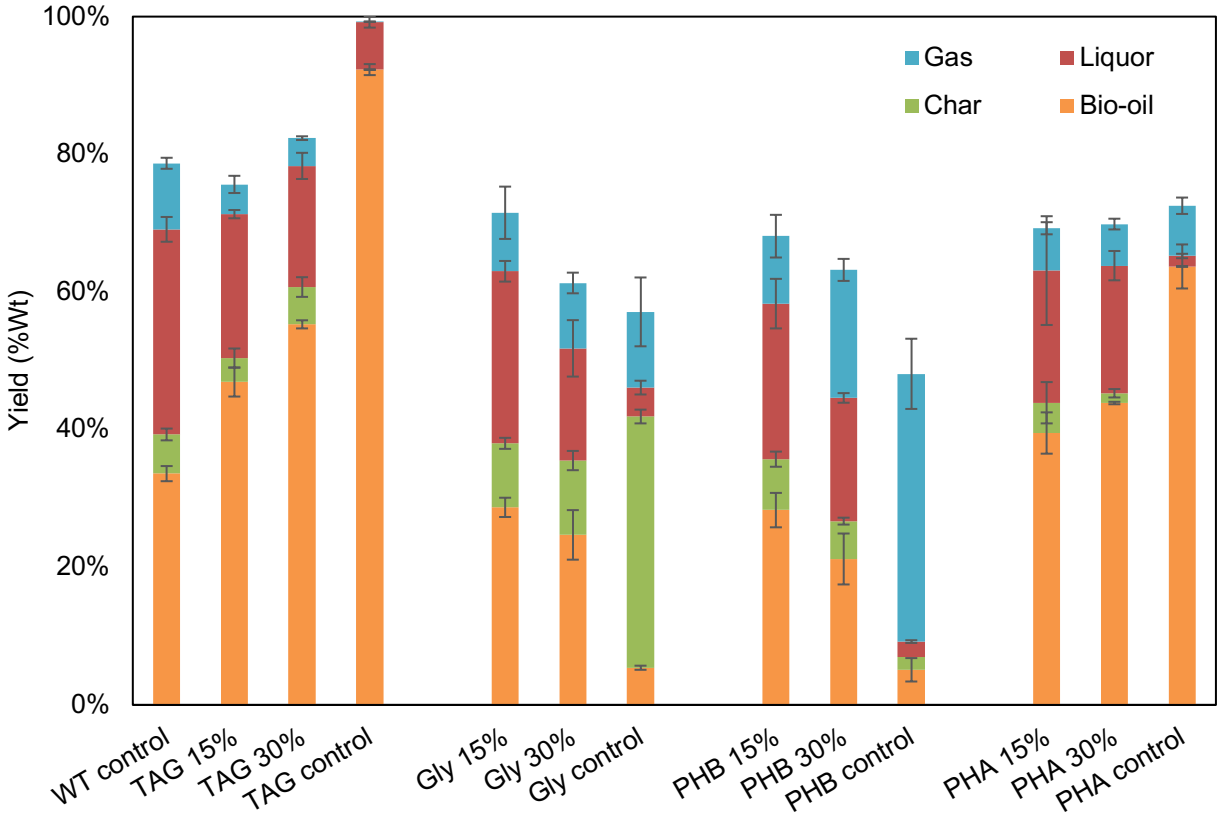

Figure 2-17. HTL results of WT Synechocystis biomass doped with different model compounds

Due to their terminal functionality, linear α-olefins (LAO) are extremely versatile and valuable precursors for producing many commodity chemicals. Medium chain-length LAO (*mcl*-LAO) are of particular interest because they can be used as "drop-in" fuels that are compatible with the existing engine systems and transportation infrastructure. The propylene can be directly used as a "drop-in" fuel or can be converted into butanol for fuel blending. Thus, energy-dense olefins (propylene and *mcl*-olefins) have been included in our overall BFI yield. As shown in Figure 2-18, even though the co-production of propylene contributed to 5.9% and 9.3% of BFI yields with 15% and 30% of doped PHB, the total BFI yield was lower at higher doping of PHB. Doping of biomass with15% *mcl*-PHA increased bio-oil yield from 33.6% in the control biomass to 39.5% and co-produced 2.3% of *mcl*-LAO, leading to a total 41.8% BFI yield. Doping of 30% *mcl*-PHA resulted in a total BFI yield of 49.6% (43.7% bio-oil yield and additional 5.9% of *mcl*-olefin yield). This result shows that producing *mcl*-PHA in biomass has great potential to boost the biofuel yield.

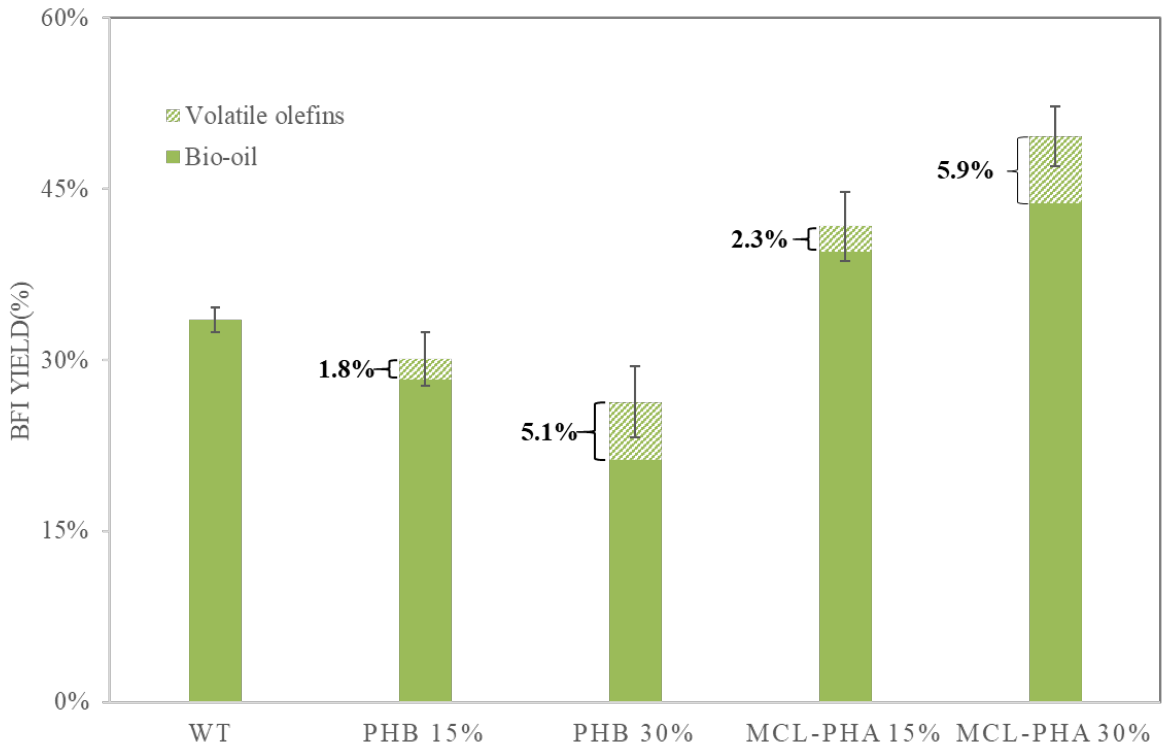

Figure 2-18. Overall BFI yield from algal biomass doped with PHB and mcl-PHA. Volatile olefins are volatile hydrocarbons that were removed during solvent evaporation.

Attempts to introduce and express mcl-PHA genes in Synechocystis

A metabolic pathway was designed, as shown in Figure 2-19, including three genes from *Pseudomonas putida* KT2440, i.e., *phaG* (Uniprot locus PP_1408), *acl* (PP_0763) and *phaC1* (PP_5003). These three genes have each been codon optimized and synthesized by GenScript (Piscataway, NJ). However, we encountered many obstacles in the synthesis of these genes in *E.coli* by Genscript, and the subsequent in-house cloning and transformation, in various configurations, into *Synechocystis* PCC 6803 at NREL. We were not able to detect mcl-PHA from the engineered *Synechocystis* strains. Similar difficulties were also observed with transformation into AB1 at Algenol. It is likely that heterologous expression of these genes caused a metabolic imbalance in *E. coli* and in the two cyanobacteria strains. We were unfortunately not able to perform further troubleshooting and fine tuning of gene expression levels within this project.

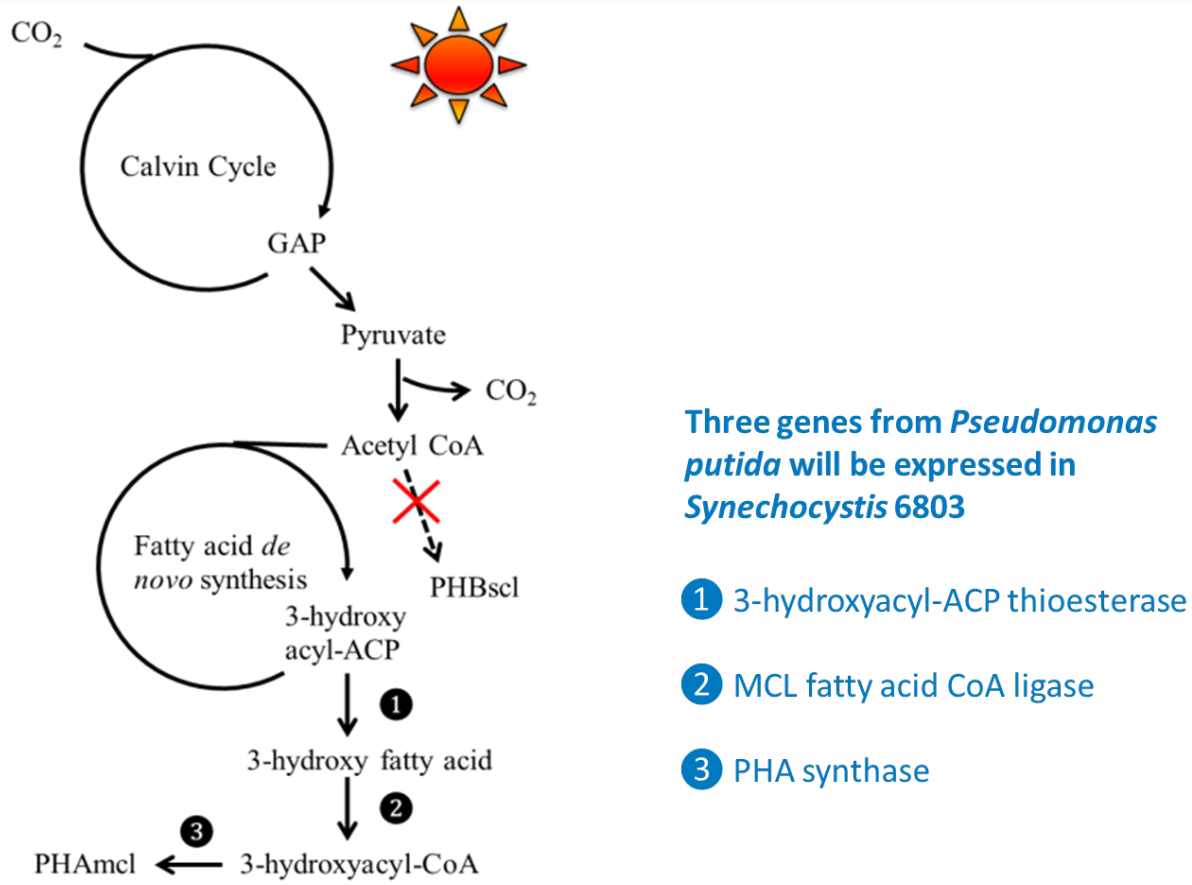

Figure 2-19. Designed pathway for the biosynthesis of mcl-PHA in cyanobacteria.

We observed mcl-PHA accumulation in *E. coli* as a cloning host. In one of the DNA configurations, all three genes were expressed from a single construct as shown in Figure 2-20. Plasmid pBE116 was constructed that includes an arabinose-inducible promoter upstream of the three genes. The mcl-PHA product was found in the *E. coli* strain that harbors this plasmid. Upon induction of the expression of the mcl-PHA synthesis genes by adding 1 mM L-arabinose into the culture medium, mcl-PHA was seen under microscope by Nile Red fluorescence staining (Figure 2-20), and its content reached 19.5% of dry cell weight after over-night cultivation, as evidenced by GC-MS and GC-FID (Figure 2-21). The mcl-PHA composition is similar to that from naturally-occurring *Pseudomonas putida* KT2440. These results verified the function of the three genes in a heterologous host, and may be the basis for future work on mcl-PHA production for energy or for renewable plastics.

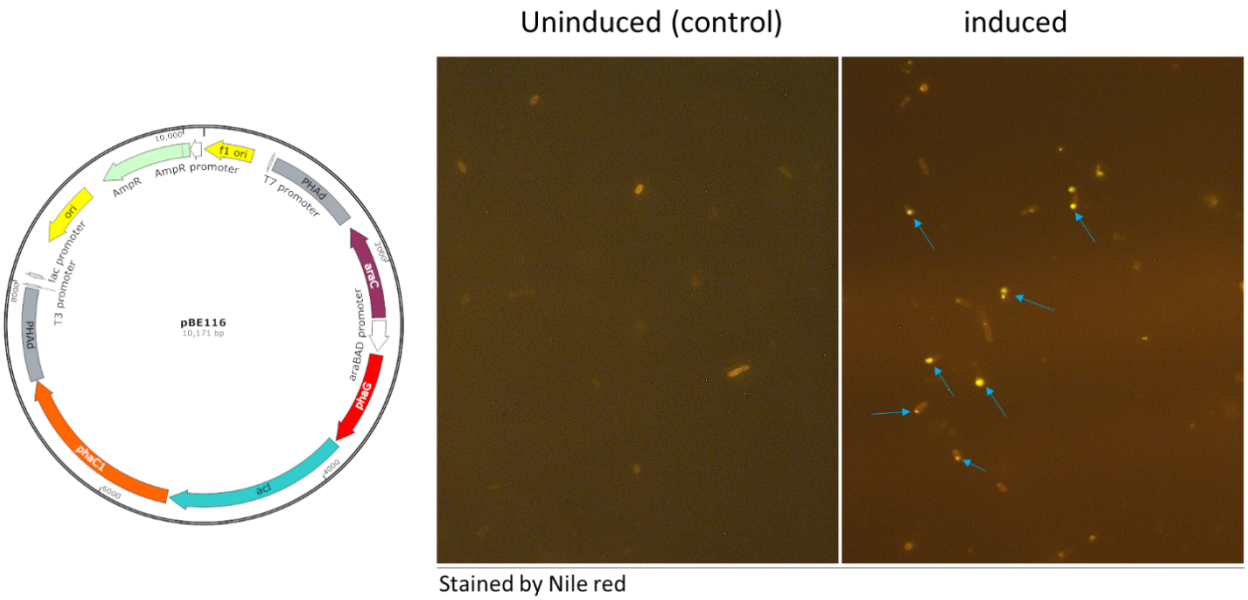

Figure 2-20. Fluorescent staining of mcl-PHA in E. coli Top10/pBE116.

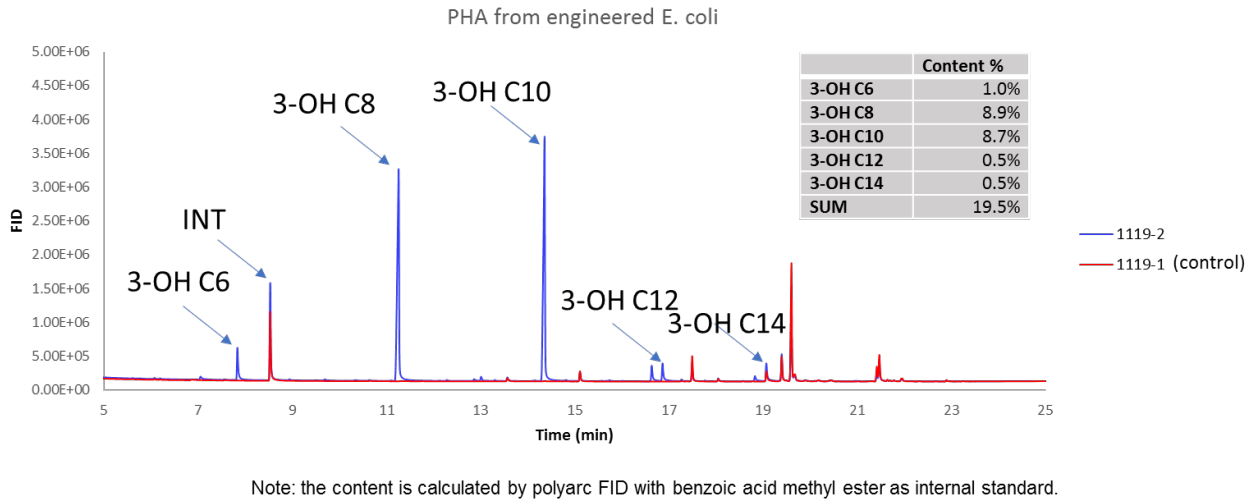

Figure 2-21. Determination of mcl-PHA content and composition from E. coli Top10/pBE116.

Task 2 Summary

- Multiple approaches were taken to increase the light utilization efficiency, and therefore biomass productivity, of *Cyanobacterium* sp. AB1, including both targeted (recombinant) and non-targeted (screening/selection) strategies. Although several of the approaches yielded strains with 10-15% higher productivity under batch growth conditions, the advantages were largely lost under the preferred semi-continuous cultivation conditions.
- Genetic modifications were made to the exopolysaccharide synthesis/transport system of AB1 that reduced culture viscosity significantly, although cells settled out of solution more rapidly than desired, so an antisense RNA knockdown strategy was attempted.

- A wild-type *Cyanobacterium* sp. strain (AB1166) was identified in Algenol's proprietary culture collection that exhibited ~10% higher productivity than AB1 under batch and semi-continuous cultivation and also had 50% lower viscosity, facilitating dewatering processes.
- HTL experiments at NREL with *Synechocystis* sp. PCC 6803 biomass supplemented with various biochemicals indicated that medium chain length polyhydroxyalkanoates (mcl-PHA) were able to increase the yield of BFI produced. Attempts were made to introduce mcl-PHA genes from *Pseudomonas putida* into *Synechococcus*, but these attempts were not successful, suggesting that expression of the genes let to detrimental metabolic imbalances. Attempts to express these genes in *Cyanobacterium* sp. were likewise unsuccessful.

Task 2 Milestones

Subtask Topic	Milestone Number	Milestone Description	Milestone Verification Process	End Quarter
Develop screens and selections	M2.1	Screens and selections to improve LUE determined	Algenol develops screens, assays, vectors, libraries, and growth conditions to identify AB1 variants with enhanced LUE	2
Outcome: **Completed.** High throughput screening procedures were successfully developed, but this approach was discontinued due to difficulties in establishing robust secondary screens. Protocols for selection of high-LUE strains in turbidostats were successfully established and transposon insertion mutant libraries were created to enable selection of high-LUE strains in this system. In addition, Photosynthesis-Irradiance curves for determining photosynthetic parameters relevant to assessing LUE (i.e., P_{max} and E_k) were established in Algenol's labs, as was the ability to assess LUE in controlled indoor PBR cultivations.				
Enhance strain productivity	M2.2	AB1 derivative created with >10% higher productivity	Lab and outdoor experiments verify productivity increase in enhanced strain	6
Outcome: **Completed.** This milestone was achieved by identifying *Cyanobacterium* sp. AB1111 (and derivative AB1166) as a more highly productive strain, routinely exhibiting >10% higher productivity than AB1 under a variety of cultivation conditions. In addition, strain AB1278, which has lower photosynthetic pigment content, has been shown to have >10% productivity than AB1.				
Enhance strain dewatering efficiency	M2.3	AB1 derivative created with >50% reduction in viscosity at harvest density	Lab and outdoor experiments confirm viscosity decrease	5
Outcome: **Completed.** Effectively achieved through identification of *Cyanobacterium* sp. AB1111 (and derivative AB1166) as an AB1-like strain with a >50% reduction in viscosity. This strain was demonstrated to be harvestable *via* centrifugation at higher efficiency, reducing energy consumption by about 30% compared to AB1 when using centrifugation as the dewatering technology.				
Increase strain HTL yield & quality	M2.4	*Synechocystis* strain created with 8% higher HTL BFI yield (C-basis) ~~and 7% less N in BFI~~	Bench scale chemical analysis confirms improved BFI yield and quality compared to wild type *Synechocystis*	6
Outcome: **Completed.** A 17% increase in BFI yield using biomass from a glycogen-deficient *glgC* knockout *Synechocystis* strain, meeting the first part of this milestone. The specified reduction in the BFI nitrogen content was not achieved with this strain, however; subsequent discussions with the DOE resulted in eliminating this second part of the milestone. The *glgC* knockout strain is not robust, however, and grows poorly. A potential solution is a knock-down mutant with a lower level of glycogen; this approach was pursued in Task 5.				

Section References

Bailey, S., Mccarren, J., Lieberman, S.L., Meuser, J.E., Romano, A.E., Yee, D., Soriaga, L., Brown, R.C., Weissman, J.C., Prince, R.C. and Nielsen, R.D. 2014. Algal mutants having a locked-in high light acclimated phenotype. WIPO Patent Application WO2014089533A2.

Carrieri, D., Paddock, T., Maness, P.C., Seibert, M. and Yu, J. 2012. Photo-catalytic conversion of carbon dioxide to organic acids by a recombinant cyanobacterium incapable of glycogen storage. *Energy & Environmental Science* 5:.9457-9461.

Derks, A., Schaven, K. and Bruce, D. 2015. Diverse mechanisms for photoprotection in photosynthesis. Dynamic regulation of photosystem II excitation in response to rapid environmental change. *Biochimica Biophysica. Acta* 1847:468-485.

Jittawuttipoka, T., Planchon, M., Spalla, O., Benzerara, K., Guyot, F., Cassier-Chauvat, C., and Chauvat, F. 2013. Multidisciplinary Evidences that *Synechocystis* PCC 6803 Exopolysaccharides Operate in the Cell Sedimentation and Protection against Salt and Metal Stress. *PLoS One.* 8(2): e55564.

Lefebvre, S., Lawson, T., Fryer, M., Zakhleniuk, O., Lloyd, J. and Raines, C.A. 2005. Increased sedoheptulose-1, 7-bisphosphatase activity in transgenic tobacco plants stimulates photosynthesis and growth from an early stage in development. *Plant Physiology* 138:451-460.

Patel, V. K., Maji, D., Pandey, S. S., Rout, P. K., Sundaram, S. and Kalra, A. 2016. Rapid budding EMS mutants of *Synechocystis* PCC 6803 producing carbohydrate or lipid enriched biomass. *Algal Research* 16:*36*–45.

Pereira, S., Mota, R., Santos, C., De Philippis, R. and Tamagnini, P. 2013. Assembly and Export of Extracellular Polymeric Substances (EPS) in Cyanobacteria: A Phylogenomic Approach. In F. Chauvat and C. Cassier-Chauvat (Eds.), *Advances in Botanical Research* 65:235-279.

Santabarbara, S., Reifschneider, K., Jasaitis, A., Gu, F., Agostini, G., Carbonera, D., Rappaport, F. and Redding, K.E. 2010. Interquinone electron transfer in photosystem I as evidenced by altering the hydrogen bond strength to the phylloquinone(s). *The Journal of Physical Chemistry B*, 114:9300-9312.

Tamoi, M., Takeda, T. and Shigeoka, S. 1999. Functional analysis of fructose-1,6-bisphosphatase isomerase (fbp-I and fbp-II gene production) in cyanobacteria. *Plant Cell Physiology* 40:257-261.

Thomason, M., Bischler, T., Eisenbart, S., Förstner, K., Zhang, A., Herbig, A., Nieselt, K., Sharma, C. and Storz, G. 2015. Global transcriptional start site mapping using differential RNA sequencing reveals novel antisense RNAs in *Escherichia coli*. *Journal of Bacteriology* 197:18-28.

Task 3 – Improved productivity through operational and engineering approaches

Task 3 Objective

The primary objective of Task 3 was to improve biomass productivity and economics with improved cultivation operations, including PBR design, culture management, and optimization of nutrient and CO_2 supply procedures, and to validate these in outdoor operations. A subsequent objective was to use the results of these studies to formulate best practices for Task 4, which was focused on demonstration of a significant (30%) improvement in productivity at an intermediate scale.

Expected Outcome: Stable outdoor operation with improved yield and product quality

Task 3 Activities

A number of experiments were performed at lab and outdoor scales with *Cyanobacterium* sp. strains AB1, AB1111/AB1166, and *Arthrospira platensis* strain AB2293 to investigate operational and engineering changes that could lead to improved productivity. The parameters investigated spanned the full range of cultivation variables that control biomass production, including nutrient composition and feeding strategy, light availability, gas delivery and utilization, cultivation mode, and contamination control.

Light Availability through Spacing and Operational Density

Previous cultivation and Techno-Economic Analysis (TEA) studies for ethanol production (Figure 3-1) was leveraged to identify the optimal PBR spacing for biomass productivity and economics for AB1 and related strains. Additional work performed in association with this project focused on optimizing spacing for co-product production from *Arthrospira,* leveraging the adaptability of the VIPER PBR system for optimization of multiple products, as the optimal spacing for a high value co-product will not be the same as for biomass to produce a biofuel intermediate. The spacing for biomass production from AB1 and other *Cyanobacterium* sp. strains was very consistent with that expected from previous studies with ethanologenic organisms, leading to a recommendation of deployment at a culture height to PBR spacing (H:S) ratio of 2.4:1. Because phycocyanin (the main co-product from the *Arthrospira* strain also employed in the ABY2 project) is an accessory pigment used for photosynthetic light harvesting, the concentration of phycocyanin (PC) increases as the average light experienced by the culture decreases. This suggested a closer spacing at an H:S ratio of 4:1 to 4.4:1 for PC production. It is also the case that a closer spacing is generally favored for high value products such as PC, where higher CAPEX can be justified.

As an additional “dial” for altering light availability, operational cell (optical) density for semi-continuous cultivation was also explored for optimization of biomass and co-product productivity. This is demonstrated in Figure 3-2, where a lower operational cell density (leading to higher average light experienced by the culture) led to higher biomass productivity, while a higher operational cell density resulted in an overall higher food grade phycocyanin (FGPC) content (Figure 3-2; more details on the definition of FGPC can be found in the Task 7 section). Clearly, it is important to adjust the light availability to algal cultures in a strain- and product-specific manner to optimize the desired output.

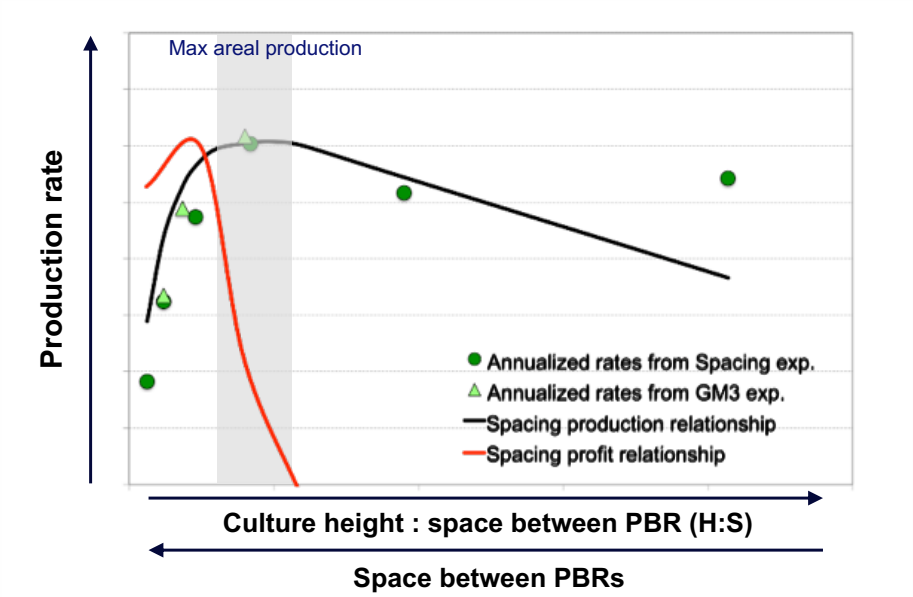

Figure 3-1. General relationship between productivity and PBR spacing, demonstrating increasing productivity with increasing average light (right to left in the graph), as controlled by wider distances between PBR panels, up to an inflection point where productivity decreases due to poor light distribution (the limit being a horizontal or pond result approaching zero H:S). CAPEX, and to a lesser degree OPEX, increases right to left in the figure, resulting in a lower "profit" peak than the productivity peak. These results were generated for ethanol production, but a similar result is expected for biomass production, leading to high H:S for high value products and low H:S for fuels.

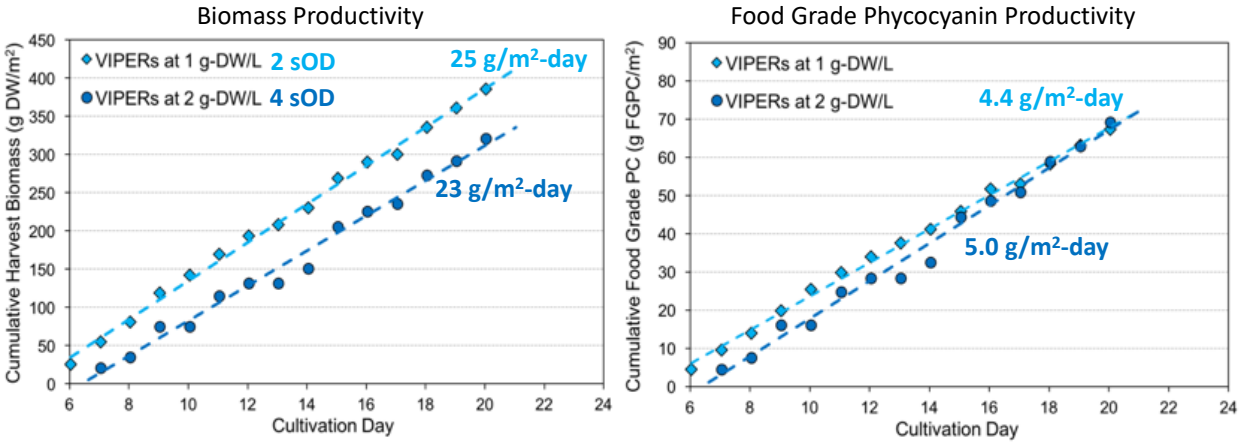

Figure 3-2. Biomass productivity (left) and food grade phycocyanin (FGPC) productivity (right) for Arthrospira platensis cultivations at average operational densities of 2 and 4 sOD.

Nutrient Composition and Use Efficiency

Nutrient optimization played a large role in the research for Task 3, as changes to nutrient sources and feeding strategies could significantly impact productivity and economics, as well as aid in

contamination control. As the largest component of the cultivation medium for most strains, nitrogen was the primary focus.

Early in the program, impacts to productivity resulting from the use of urea and ammonium were investigated, as these reduced sources of nitrogen are less expensive than nitrate. Lab-scale cultivations confirmed that use of urea as the sole nitrogen source resulted in comparable productivity to nitrate-grown cultures for AB1, and cultivations of AB1111 indicated that growth rate and dry weight productivity was 17 and 20% higher, respectively, when cultures were given urea relative to controls grown on nitrate only, using concentrations that provided equimolar levels of N. Early work testing ammonium chloride as a nitrogen source for AB1 led to challenges with pH control; however, work to expand the use of ammonium continued for *Arthrospira* cultivation with greater success, due in part to the large buffering capacity of the high-bicarbonate cultivation medium for *Arthrospira*. At the LvPBR scale (1.2 L), ammonium bicarbonate, ammonium nitrate, and ammonium chloride were tested as N-sources for *Arthrospira platensis* strain AB2293 grown under semi-continuous cultivation conditions and compared to nitrate controls with a 1.5 mM total N per day feeding strategy. When dosed with any of the ammonium sources, AB2293 exhibited a 25-30% boost in biomass productivity (Figure 3-3). As a further benefit, phycocyanin (PC) content was also found to be, on average, 22% higher for cultures fed ammonium relative to nitrate, leading to an approximate 55% increase in overall FGPC productivity compared to controls. Therefore, the use of ammonium enables a boost to productivity along with a cost reduction relative to nitrate.

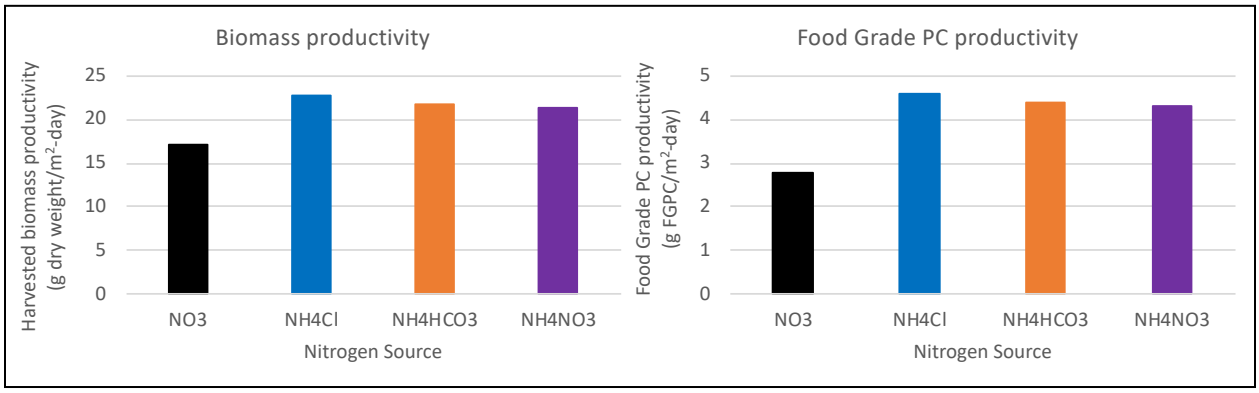

Figure 3-3. Harvested biomass productivity (left) and FGPC productivity (right) averaged over the semi-continuous operation portion (days 7-30) of the experiment comparing nitrogen source compounds provided at a rate of 1.5 mM total N per day.

Together with work to optimize the nitrogen source for cyanobacterial production strains, efforts to improve nutrient use efficiency were undertaken by exploring medium recycle operations. The majority of efforts here focused on *Arthrospira* due to the comparative ease of harvesting and dewatering this filamentous strain compared to AB1 and other *Cyanobacterium* sp. strains; however, lessons learned are translatable to *Cyanobacterium* sp., allowing for strain-specific nutrient demands. Early efforts with full nutrient recycling at the laboratory scale demonstrated that periodic general nutrient refreshes (additions) (approximately every 14-21 days) were necessary to maintain high levels of productivity. Furthermore, recharging with nitrogen through daily feeding was also needed to sustain N-replete conditions under medium recycling. Similar to the observations in the nitrogen source experiments discussed above, ammonium feeding, even

in medium recycling, resulted in higher productivity (~10%) and higher FGPC productivity (~20%) compared to nitrate feeding (Figure 3-4). FGPC is defined based on optical absorbance of a solution of the extracted PC product in a standard buffer medium and corresponds to a protein-rich product that is about 30 wt% PC. The concentration of PC in the whole cell biomass is typically 10%, composed of approximately 7% c-phycocyanin (cPC) and 3% allophycocyanin (aPC) (MacColl, 2004).

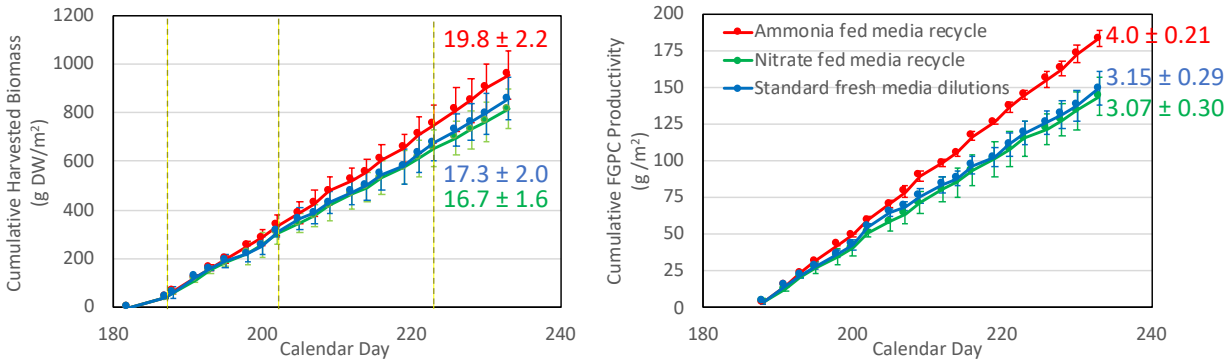

Figure 3-4. Impact of medium recycle on cultivation of Arthrospira platensis AB2293. Cumulative harvested biomass versus time (left) and cumulative food grade phycocyanin (FGPC) production versus time (right) during a lab-scale (LvPBR) medium recycling experiment. For the controls, 100% of the dilution volume was replaced with fresh medium at each dilution. For the recycling treatments, at each dilution, 90% of the previously used culture medium after cell removal was recycled back into the cultivation vessel, and treatments were fed either 1.5 mM nitrate (green data series) or ammonium (red data series) to maintain replete conditions. For this experiment, semi-continuous operations commenced at an sOD >2, and the cultures typically grew to 3.0 – 3.5 sOD before being diluted back to 2.0 sOD (i.e., approximately 1/3 of the whole 1.2 L culture volume was replaced during dilutions). On calendar days 187, 202, and 223, a full medium refresh was performed for the recycling treatments, where 100% of the dilution volume was replaced with fresh medium. The color-coded values reported in the figures indicate estimated biomass productivity in g/m²-d (left) and FGPC productivity in g FGPC/m²-d (right) calculated as the slope of the plotted lines.

Nutrient recycling experiments progressed from lab-scale to the outdoor Process Development Unit (PDU), where the focus shifted to stability of operations and optimization of N-feeding strategies to meet the increased demand outdoors during high growth periods. Lab-scale projections are for average annual conditions; actual outdoor cultivations can therefore result in higher and/or lower nutrient demand, depending on weather conditions and seasonality. For one of the early medium recycling trials at the PDU scale, nutrient consumption was reduced by more than 80% relative to the control cultures for some of the cultivation medium components (Table 3-1). While this experiment utilized nitrate, even larger cost-cutting gains would be expected through implementation of ammonium or urea feeding.

Table 3-1. Daily nutrient consumption and % reduction achieved by medium recycling for an Arthrospira AB2293 cultivation at the PDU. Quantities represent average (n=2) nutrient mass (g) added per day to a 350 L cultivation system.

	System Consumption		
	Control	Recycle	Reduction
Nutrient	g added per day	g added per day	%
$NaHCO_3$	726.7	122.4	83.2
$NaNO_3$	216.3	160.7	25.7
K_2SO_4	86.5	14.6	83.2
NaCl	86.5	14.6	83.2
$K_2HPO_4 \bullet 3H_2O$	57.1	22.9	59.9
$MgSO_4 \bullet 7H_2O$	17.3	16.1	7.0
$CaCl_2 \bullet 2H_2O$	3.5	0.6	83.2

Medium recycling was also implemented for *Arthrospira* AB2293 cultivations at the larger DEMO scale, which encompassed a total footprint area of 371.5 m^2 with a cultivation volume of 26,400 L. In-line harvesting with a Russell-Finex centrifugal screen-based liquid solid separator (LSS, see more detailed description in later sections) resulted in >96% of the recovered liquid medium (filtrate) being returned to the cultivation field. Trials with both nitrate and ammonium feeding were conducted, resulting in average reductions of ~75% for water, bicarbonate, and phosphate at scale and an approximate 36% reduction in nitrogen usage. Medium recycling also led to lower biomass loss, as *Arthrospira* cells that passed through the dewatering LSS filter during harvest were returned to the cultivation field with the recycled medium instead of lost to waste. Furthermore, medium recycling led to improved CO_2 use efficiency, in that lower daily bicarbonate additions resulted in less CO_2 off-gassing to waste. Along with these noted benefits to medium recycling, a potential disadvantage of the operation was discovered at DEMO scale, however. Small contaminants, such as the microalga *Chlorella* (~3-5 µm), were able to pass through the dewatering filter and return to the field with the recycled culture medium. If not otherwise mitigated, the recycling process could lead to concentration of these contaminants over time. This observation resulted in additional media optimizations geared toward reaching and maintaining a higher pH as a means to mitigate contamination during medium recycling.

CO_2 Delivery and Improvements in Carbon Use Efficiency

CO_2 delivery algorithms developed for production of ethanol by AB1 have been leveraged for biomass production with AB1-derived and other *Cyanobacterium* sp. strains. These delivery methods rely on inputs of photosynthetically active radiation (PAR, 400-700 nm), temperature, and culture density to predict CO_2 demand using Algenol's productivity model. This type of algorithm improves carbon use efficiency (CUE), as CO_2 addition is tightly regulated based on real-time demand. Cost savings and reliability can also be improved because instead of monitoring culture pH, which would require significant, capital-intensive instrumentation at scale, the concentration of CO_2 in the PBR headspace, as measured in the exhaust gas, is used as the process variable for proportional-integral-derivative (PID) control of CO_2 delivery based on the demand calculated from the model. This allows for a reduction in the amount of instrumentation necessary in the culture liquid phase, as a single CO_2 probe in the common exhaust header

(manifold) for a block of PBRs can be used, and improves delivery efficiency to support high productivity based on real-time weather conditions. These CO_2 delivery methods have been used for all *AB1-like* (*Cyanobacterium* sp.) cultivations at the PDU, which serve as the base case.

In addition to advanced, on-demand CO_2 delivery algorithms, gas recycling is an additional means of improving CO_2 use efficiency. Previous lab-scale work for production of ethanol demonstrated >85% CUE for AB1-derived strains using gas recycle operations, with no impact on productivity. Following this, lab-scale cultivations in LvPBRs under full gas recycle were performed to understand the impact of the resulting elevated, photosynthetically-produced O_2 on *Arthrospira* AB2293 productivity and to quantify CUE under two venting scenarios (i.e., venting only when O_2 levels reach 150% or 250% air saturation (31.5% and 53% O_2, respectively)) and compared to the standard full (constant) venting operation (Figure 3-5). This experiment demonstrated that AB2293 was tolerant of elevated O_2 concentrations, with no observed differences in biomass productivity or PC content for the gas recycle treatments. Carbon use efficiencies exceeding 90% were realized at the laboratory scale under gas recycle mode, a dramatic increase compared to standard operation (Figure 3-5). Even without gas recycling, the high alkalinity of the cultivation medium and the high operational pH (9.8) for *Arthrospira* AB2293 improves carbon use efficiency, reducing the need for gas recycling from an economic perspective (Figure 3-6). During DEMO Campaign 6, which included high pH (9.8) and medium recycling for the *entire* campaign, a 33-day average biomass productivity of 26.9 g/m^2-d was realized. Expected productivity during this time period, modeled based largely with validations using data under non-recycle and lower pH (9.2) conditions, ranged from approximately 25-30 g/m^2-d, suggesting negligible impact on productivity from medium recycling and the higher pH set-point. As an added benefit, the higher pH reduced contaminant *Chlorella* populations.

Treatment	Ave. daily CUE (%) (active & passive vent)	Productivity (g DW m^{-2} day^{-1})
Control, constant vent	24.6 % (+/- 2.4)	18.0
Gas recycle, 150% O_2 vent	94.9 % (+/- 1.5)	17.0
Gas recycle, 250% O_2 vent	98.5 % (+/- 0.2)	17.7

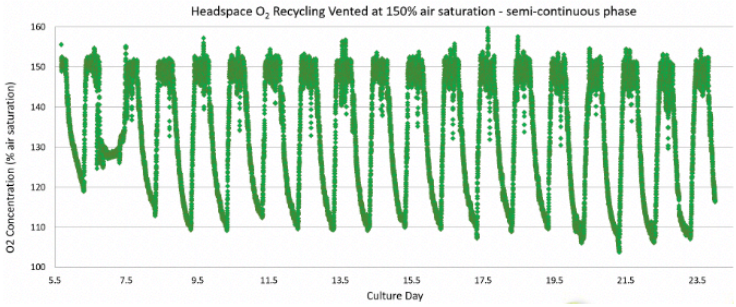

Figure 3-5. Photograph of lab-scale system for gas recycle experiment with Arthrospira AB2293 (left) and average daily carbon use efficiency (CUE) and biomass productivity for a standard control versus O_2 concentration vent setpoints (i.e., 150% and 250% of air saturation levels) (table right). Headspace O_2 vs time (graph right) for the gas recycle, 150% O_2 vent treatment.

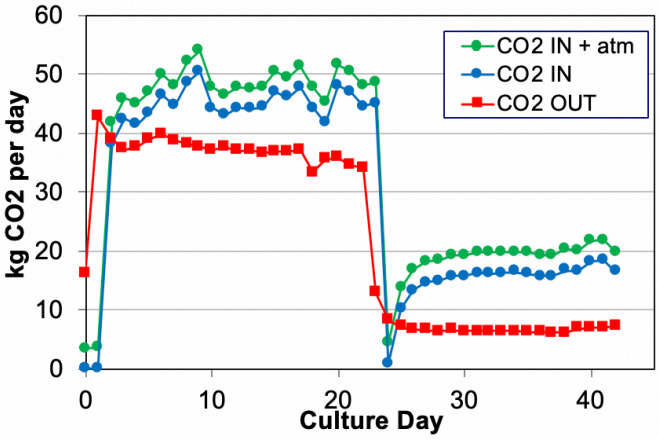

Condition	CO_2 headspace set point (ppm)	Ave. CO_2 input (kg/d)	% reduction
pH 9.2	7500	41.0	64%
pH 9.7	1500	15.0	
Air	400	3.5	

Campaign	Media Recycle	Culture pH	Ave. CUE	Productivity for 33-day Batch
4	No	9.2	20.2 (± 4.4)	17.2
5	Yes	9.2	24.1 (± 4.8)	18.8
5	Yes	9.8	67.0 (± 1.4)	
6	Yes	9.8	65.5 (± 2.1)	26.9

Figure 3-6. Inputs and outputs of CO_2 to DEMO Campaign No. 5 during cultivation of Arthrospira AB2293 in semi-continuous mode (left). As shown in the top table on the right, during the first 21 days of cultivation, the CO_2 headspace concentration was set to 7500 ppm, resulting in a pH of approximately 9.2. On day 22, the headspace concentration was decreased to 1500 ppm, resulting in an average culture pH of approximately 9.7. This change resulted in a 64% reduction in carbon inputs to the system, and translated to an increase in average carbon use efficiency from 24.1 ± 4.8 % during the first portion of the cultivation to 67.0 ±1.4 % during the latter portion of the cultivation. During Campaign 6, the full implementation of medium recycling and a higher pH setpoint showed no negative impacts on productivity, as discussed above. Productivity units are g/m^2-d.

Cultivation Mode

The relationship between productivity and operation mode was thoroughly investigated for AB1 and other *Cyanobacterium* sp. strains; *Arthrospira* work leveraged these results and focused largely on optimizing operational density during semi-continuous cultivation. Multiple experiments in turbidostat (indoors) and semi-continuous (indoors and outdoors) modes for AB1 and AB1 derivatives have been conducted and the results are consistent with expectations described in Algenol's ABY2 proposal as well as with historical indoor data taken in a turbidostat mode for AB1 for other purposes. Indoor semi-continuous cultivations were conducted for AB1 and AB1111 (and AB1166), using different sOD (standard optical density at 750 nm) set points that reflect average Florida outdoor light and temperature conditions. The AB1 results were consistent with expectations, yielding predicted, annualized outdoor productivities for Fort Myers in the 17-27 g/m^2-d range for AB1 (Figure 3-7), demonstrating optimal productivity when cultures were maintained between 2 and 4 sOD. The AB1 results were validated in two outdoor experiments in Florida that were compared on an annualized basis using the Algenol Productivity Model for

biomass production. One experiment with AB1 involved manual daily dilution to a nominal target sOD of 2. The second experiment (also using AB1) was conducted with Algenol's newly designed semi-continuous automated system, again with a nominal target of 2 sOD post-dilution. Both showed productivities in the 20-25 g/m^2-d range, in good agreement with the indoor results (Figure 3-8; also see Task 4.1 section).

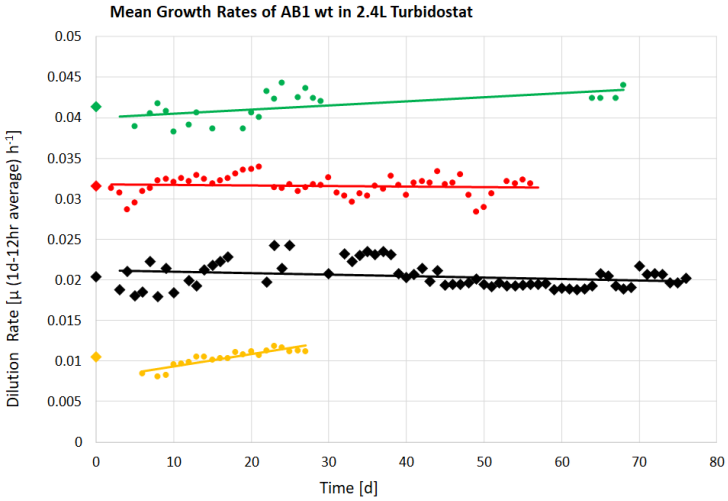

sOD	Growth Rate (sOD per day)	Predicted 4:1 spacing Outdoor Productivity (g AFDW/m^2-d)
2	1	22.8
3	1.15	27.4
4	1	22.8
5.5	0.7	17.1

Figure 3-7. Dilution rates versus time for long-term turbidostat experiments conducted for strain AB1 at a light level representative of outdoor 4:1 spacing (PBR height to distance between PBRs, = 230 μmol photons/m^2-s). Average daily growth rates ranged from 0.7 sOD per day for the highest density culture (5.5 sOD) to a maximum of 1.15 sOD per day for the culture operated at a density of 3 sOD.

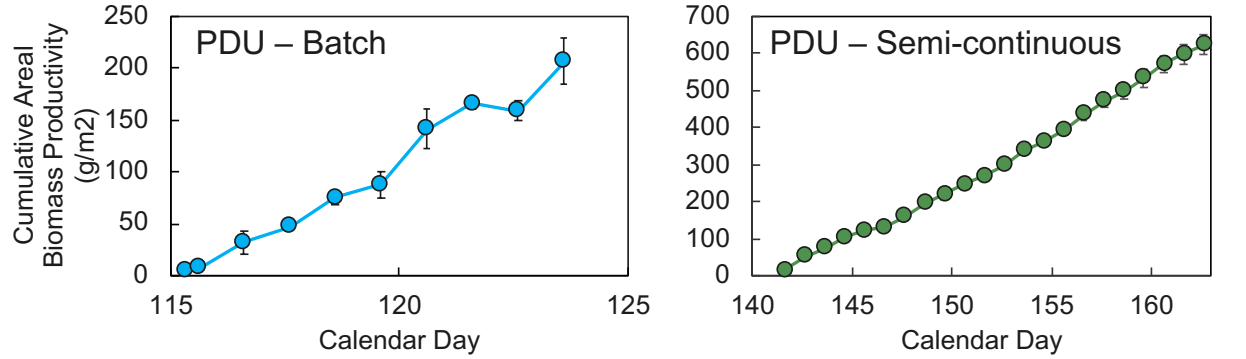

Strain	Operation Mode	Location	Operational Density (sOD)	Annualized productivity (g-AFDW/m^2-d)
AB1	Batch	PDU	0.1 – 16	15.5
AB1	Semi-continuous	PDU	2 – 4.5	24.2
AB1	Turbidostat	Lab	3	23.3*

*Lab cultivation was operated using average annual conditions for PBRs arranged in a 2.4:1 (H:S) ratio (230 μE m^{-2} day^{-1}).

Figure 3-8. Cumulative biomass versus time for batch (left) and semi-continuous (right) cultivation of AB1 outdoors at the PDU in April (batch) and May (semi-continuous) 2018. Annualized productivities for these cultivations show significant improvement in productivity for semi-continuous operation and closely match laboratory cultivations (see table).

Enhanced Light Distribution and Optical Properties of Vertical "VIPER" PBRs

This task involved development of strategies for producing a more uniform light distribution across the surface of the PBRs. We have already demonstrated (in the previous DOE-funded IBR project) that covering the ground with low transmission white plastic produces an approximate 10% yield improvement for ethanologenic strains. As an added benefit, this film serves as a means for weed control, maintaining a high reflectivity compared to native sandy soils where weeds proliferate. We expected similar results for biomass only production from AB1 and utilized white ground cover as the base case for testing in all outdoor experiments for this project. In addition, we have also manufactured PBRs with white plastic films of varying transmission in order to improve light distribution. Unfortunately, significant productivity improvements with this film were not realized, due primarily to increased reflective losses to the sky. More complicated modifications to the PBRs for enhanced light distributions were considered but not attempted due to predicted negative impacts on PBR cost.

Recommended Best Cultivation Practices

The objective of Task 3 was to explore operational and engineering approaches for improved productivity, with the overarching goal of delivering best cultivation practices in order to reach milestones involved in intermediate scale process validation (Task 4). The best practices for biomass production by AB1 and similar *Cyanobacterium* sp. strains as well as *Arthrospira* AB2293 are summarized below (Tables 3-2 and 3-3, respectively).

Table 3-2. Summary of best cultivation practices determined in Task 3 for AB1-like Cyanobacterium sp. strains for improved productivity.

Parameter	Description
Medium composition and strategy	NO_3-free marine BG-11 with 7 mM urea
Cultivation mode	Semi-continuous
Operational density	Dilution target of 2 sOD (~0.6 g/L)
Spacing	H:S = 2.4:1 (16" on-center PBR spacing)
CO_2 delivery	PAR-OD modeled demand with headspace CO_2 measurement
Other infrastructure	White plastic groundcover

Table 3-3. Summary of best cultivation practices determined in Task 3 for Arthrospira AB2293 for improved productivity.

Parameter	Description
Medium composition and strategy	Zarrouk's medium formulation (200 mM HCO_3 for high alkalinity) with ammonium feeding; Medium recycling with ~20% refresh over ~14 days
Cultivation mode	Semi-continuous
Operational density	Dilution target of 2 sOD (~1 g/L)
Spacing	H:S = 4:1 (10" on-center PBR spacing)
CO_2 delivery	Headspace CO_2 with 1500 ppm daytime set-point to maintain culture pH ~9.8
Other infrastructure	White plastic groundcover

Task 3 Summary

- Experiments confirmed that a 2.4:1 culture height: PBR spacing (H:S) ratio is appropriate for *Cyanobacterium* sp. AB1 for biomass production in order to optimize the balance between biomass productivity and economic return. For the high value co-product phycocyanin from *Arthrospira platensis*, the optimal H:S ratio was determined to be ~4:1.
- Significant improvements in biomass productivity were achieved using semi-continuous cultivation *vs* batch cultivation. At a light intensity of 350 μmol photons/m^2-sec (equivalent to an H:S spacing of 2.4:1), productivity was maximal for *Cyanobacterium* sp. AB1 and AB1166 when the culture density was maintained between 2 and 4 sOD_{750}.
- Growth experiments with various nitrogen sources indicated that urea enabled higher and more cost-efficient biomass production for *Cyanobacterium* sp. AB1166 compared to nitrate, and that ammonium was preferred for *Arthrospira*.
- Medium recycling was shown to be an effective, cost-saving cultivation strategy, especially when growing *Arthrospira*. Periodic nutrient refreshes (including daily N feeding) were necessary to obtain maximal productivity.
- Carbon use efficiency (CUE) was significantly improved to >95% by employing CO_2-containing gas recycling coupled to periodic venting to maintain non-inhibitory O_2 levels in the culture. For *Arthrospira* cultures growing at high pH (9.8), CUE was >65% even in the absence of gas recycling due to the large inorganic carbon buffering capacity of the medium.
- "Best cultivation practices" were recorded for outdoor growth of both *Cyanobacterium* sp. and *Arthrospira platensis.*

Task 3 Milestones

Subtask Topic	Milestone Number	Milestone Description	Milestone Verification Process	End Quarter
Operation optimization	M3.1	Stable outdoor operation with >10% productivity increase achieved	Algenol PDU demonstrates outdoor yield increase, writes AB1 operation best practices and delivers to 4.1 team	3

Outcome: **Completed.** Milestone achieved for three strains in outdoor operations, due in large part to the implementation of semi-continuous outdoor operation. Increases on the order of 30% were achieved and reproduced several times for *Cyanobacterium* and *Arthrospira*.				
Enhance PBR light capture	M3.2	>10% biomass productivity increase in new PBR prototypes achieved	Algenol's 4.1 team receives manufactured advanced PBRs for operational testing	4
Outcome: **Partially completed.** Though we made numerous improvements in the PBR area related to cost and integrity, and some yield increases due to better uniformity of mixing (e.g., improved diffuser design), we have not produced a new PBR design enabling better light utilization consistent with a >10% biomass increase. Given that we have achieved much greater improvements via operational changes (semi-continuous operation) and strain improvements, we opted to not pursue this approach any further, absent a new, cost effective idea.				

Task 4 – Intermediate scale process validation

Task 4 Objective

The main objective of Task 4 was to demonstrate improved overall performance using a combination of strain development, operational optimizations, and PBR engineering approaches. Incorporated in this task was a milestone experiment (Milestone 4.1) designed to demonstrate a 30% greater biomass yield with an improved strain compared to base strain (*Cyanobacterium* sp. AB1) grown under baseline conditions (batch cultivation in the PBR system in use at the initiation of the project. The results of the milestone experiment were used to inform a Go/No-Go decision required for continuation of the project.

Expected Outcome: 30% greater biomass yield compared to baseline strain and cultivation system and procedures

Task 4 Activities

Combine Biological, Operation, and Engineering Advances

This task was largely focused on combining the best cultivation practices and engineering advances identified in Task 3 with the improved strain identified in Task 2 to demonstrate a 30% increase in biomass productivity compared to baseline conditions. Thus, the results of the "Milestone 4.1" results are the primary emphasis of this section. Other aspects of this task (i.e., pre-operation assessment of AB1 in small open ponds, LCA and TEA model development, BFI and co-product quality) are described in other sections of this report.

The Milestone 4.1 experiment was conducted at the Process Development Unit (PDU) in Q2 CY2018. The experiment was conducted using the automated airlift platform, which was designed and built in Fall 2016 to serve as a semi-automatic platform for cultivations requiring daily dilutions. The infrastructure and human-machine interface (HMI) software were designed in house. There are six airlift units in the platform, each of which consists of three interconnected VIPER v3.4 PBRs, in mirrored sets of two in order to allow replicate cultures (Figure 4-1). Each airlift holds approximately 324 L of culture. The faces of the PBRs were oriented east-west at a 2.4:1 height to spacing ratio (Figure 4-1, Table 4-1), with one PBR containing green dye at each end of the airlift units to prevent end effects associated with having greater illumination. White reflective film covered the ground under the PBR field to improve light use efficiency.

Figure 4-1. Automated airlift system showing the six 3-PBR units. Each set of airlifts is flanked by a dye bag at the east and west end, with one dye bag separating the duplicate airlifts.

The improved yield strain AB1166 (*Cyanobacterium* sp.) is a re-isolated single clone of AB1111. In addition to having a lower viscosity and a higher biomass production potential than AB1, AB1166 also exhibits much higher conjugation efficiencies compared to its parent strain AB1111, thereby facilitating strain engineering efforts. In a previous indoor LvPBR experiment, a 10-15% increase in biomass productivity was observed for AB1166 compared to AB1. The lower viscosity characteristic of AB1166 is a quality that could help improve the efficiency of the biomass dewatering process.

Table 4-1. Description of experimental parameters.

Treatments	AB1 in batch mode; AB1166 and AB1 in semi-continuous mode
Inoculation date	AB1 batch: Apr 24th, 2018; AB1/AB1166 semi-continuous: May 18th 2018
Culture medium	BG11 with 7 mM urea as a nitrogen source
PBR type	VIPER 3.4
Airlift type	Two 3-PBR airlift units per treatment
Diffuser type	Laser-perforated diffuser improving system uniformity (14 SLPM/PBR)
CO_2 delivery	PAR-OD algorithm-based CO_2 delivery
Spacing	2.4:1 Height:Spacing (16” between PBR centerpoints)
Orientation	East-West
Operation mode	Semi-continuous, Target dilution to sOD = 2 (~0.6 g/L)
White plastic under airlifts	To reflect light diffusely to improve light utilization efficiency (LUE)

On April 24th, 2018, four of the six cultivation units were inoculated with the base strain AB1 with the intent of cultivating two units in batch mode and two units in semi-continuous mode. The two

other units were inoculated with the improved yield strain AB1166 with the intent of cultivating them in semi-continuous mode. Due to a mechanical issue with the nutrient delivery pump used for the daily dilutions of AB1 and AB1166, these semi-continuous treatments were terminated early. Since the mechanical issue did not impact the AB1 batch cultivation, the batch was completed as initially intended. After repairing the nutrient delivery pump and cleaning the cultivation system, the semi-continuous treatments with AB1 and AB1166 were reset on May 18th, 2018. (Table 4-2).

Table 4-2. Treatment summary including orientation and target density post-dilution.

Treatment	Strain/Operation mode	Replication	Target OD after dilution	Cultivation timing
1	AB1 Batch Mode	2 airlifts	N/A	Apr 2018
2	AB1 Semi-Continuous	2 airlifts	2 (~0.6 g/L)	May – Jun 2018
3	AB1166 Semi-Continuous	2 airlifts	2 (~0.6 g/L)	May – Jun 2018

The average daily insolation was 43% and 9% above the Fort Myers annual average (i.e., 36 mol photons/m^2-d) for the April and May/June cultivations, respectively (Figure. 4-2A,B). The average culture temperature was very similar between the two cultivation periods, with an average of 26.0 ± 1.1°C and 27.3 ± 2.2°C for the April and May/June cultivations, respectively (Figure 4-2C,D). In batch mode, the AB1 culture reached >4.6 g/L (or 15.7 OD) in 10 days (Figure 4-2E). In semi-continuous mode, the cultures were diluted daily for 21 consecutive days and the density was maintained between 0.6 and 1.7 g/L (2.0 – 4.8 sOD), thereby reducing the effects of self-shading and keeping the cells in the more photosynthetically optimal range of the growth curve for improved productivity (Figure 4-2F). Figure 4-3 presents the cumulative areal biomass productivity for AB1 and AB1166 in semi-continuous cultivation mode. To account for the differences in insolation during the different cultivation periods, the biomass harvest productivity was annualized (Table 4-3). Overall, AB1 produced 15.5 g/m^2-d in batch mode thereby confirming the baseline productivity established in the original proposal. In semi-continuous mode, AB1 produced 24.2 g/m^2-d, a 61% increase compared to the AB1 baseline of 15 g/m^2-d. AB1166 produced 26.8 g/m^2-d in semi-continuous mode, which corresponds to a 79**%** increase compared to the AB1 baseline rate of 15 g/m^2-d and a 10% increase compared to AB1 in semi-continuous mode (Table 4-3).

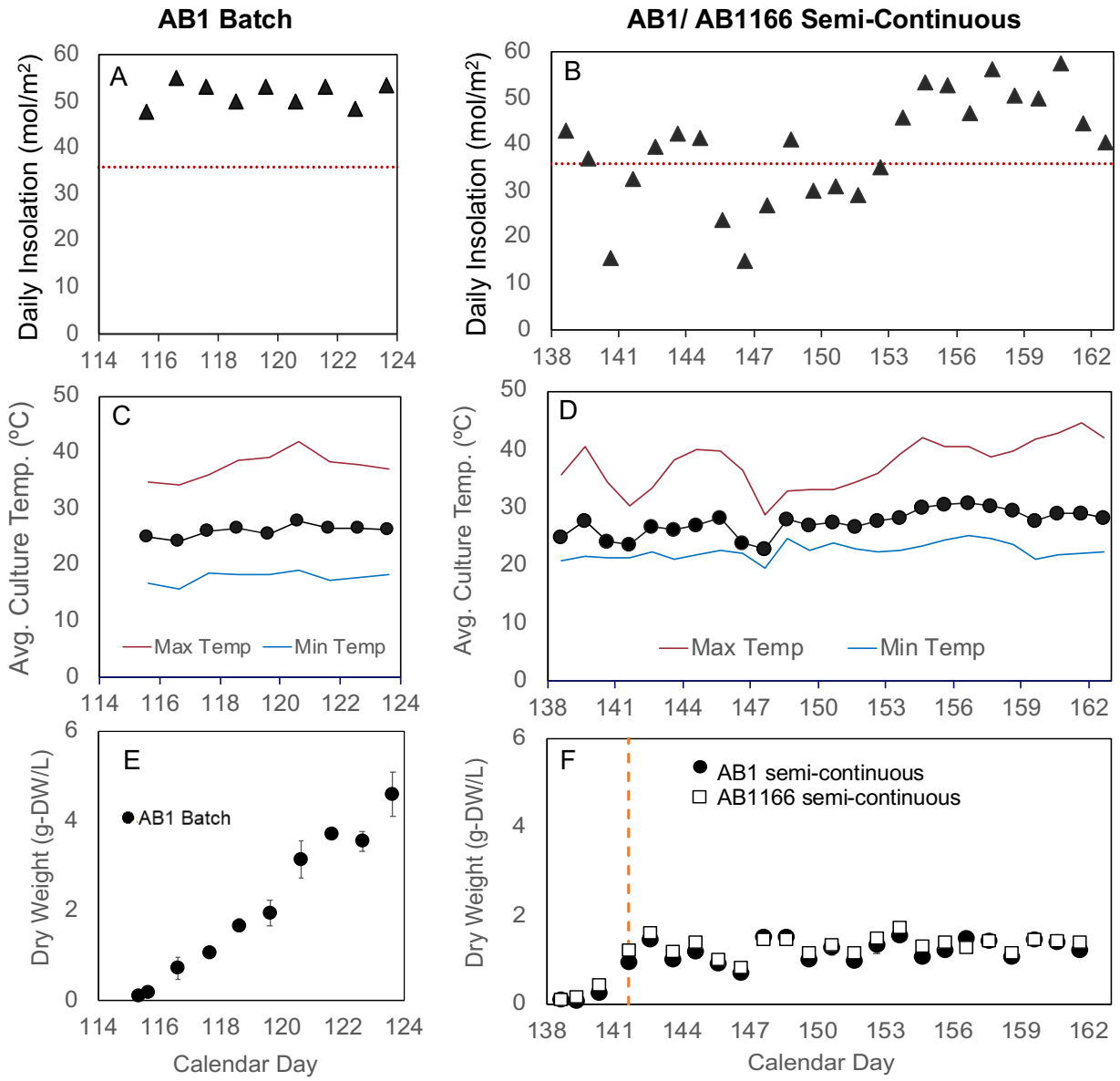

Figure 4-2. A-B) Daily mean ambient temperature and insolation for AB1 in batch mode and AB1/AB1166 in semi-continuous cultivation mode, C-D) Daily maximum, minimum, and mean culture temperature for AB1 in batch mode and AB1/AB1166 in semi-continuous cultivation mode, E-F) Culture dry weight for AB1 in batch mode and AB1/AB1166 in semi-continuous cultivation mode. Calendar days 114 and 138 correspond to April 24th and May 18th 2018, respectively.

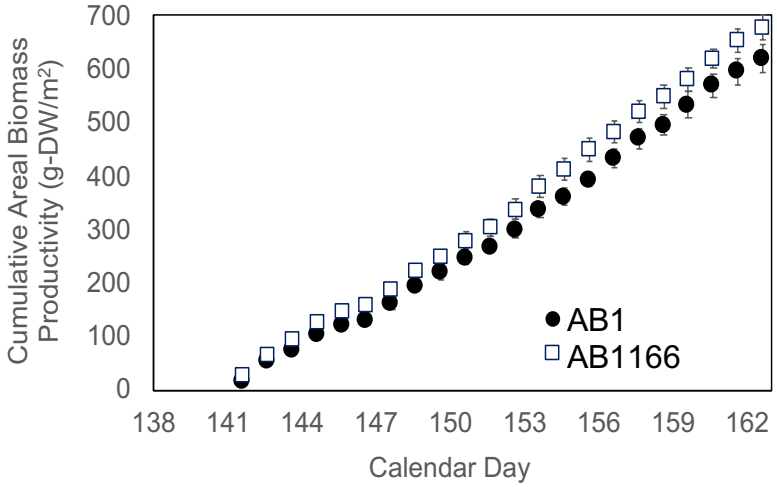

Figure 4-3. Cumulative areal biomass productivity for AB1 and AB1166 in semi-continuous cultivation mode.

Table 4-3. Harvest annualized productivity rates for AB1 in batch and in semi-continuous cultivation mode as well as for AB1166 in semi-continuous mode. The right column shows the % difference from the 15 g/m^2-d baseline for AB1 in batch mode.

	Harvest Annualized Productivity (g/m^2-d)	% increase compared to original baseline
AB1 Batch Mode	15.5	3%
AB1 Semi-Continuous	24.2	61%
AB1166 Semi-Continuous	26.8	79%

During semi-continuous cultivation, cultures of AB1 and AB1166 were centrifuged in the laboratory using conditions comparable to a commercial continuous centrifuge, and the supernatant was analyzed for total organic carbon (TOC). The supernatant TOC for AB1166 was 38% lower than that of the AB1 samples, indicating fewer cells (and potentially less dissolved organic carbon) left in suspension in the supernatant and a better separation efficiency (Figure 4-4). Based on these results, it is reasonable to assume that AB1166 would show an increased separation efficiency compared to that of AB1. The limited viscosity data collected during this cultivation (using a Brookfield DV2T viscometer) also supports this statement. At a shear rate of 73.38 s^{-1} (torque >10%), the viscosity determined for AB1166 was 1.2 cP, more than 45% lower than that of AB1 (viscosity of 2.2 cP). Dissolved organic carbon (DOC) measured during the semi-continuous cultivation showed that AB1166 produced ~18% less DOC than AB1 (Figure 4-5). It is hypothesized that AB1166 releases less EPS in the culture medium than AB1 as it maintains a bigger EPS capsule around the cells (Figure 4-4C) and that EPS is an important contributor to the DOC pool. Cultures of both AB1 and AB1166 show dramatic shear thinning behavior that is attributable to the network of released EPS connecting individual cells. Viscosity is still high, especially at low shear rates, even in the absence of cells. In the absence of released EPS, specific viscosities are essentially zero.

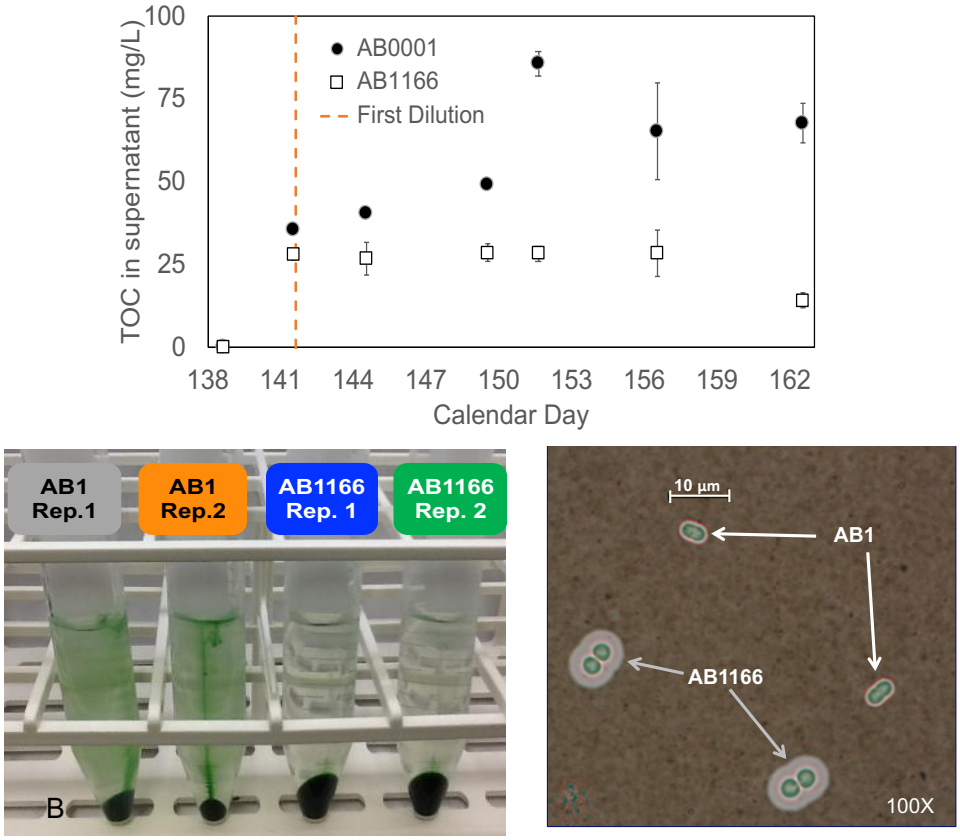

Figure 4-4. A) Total organic carbon (TOC) detected in supernatant of culture samples centrifuged at 10,000xg for 2 minutes. Lower TOC values were expected in the samples with lower viscosity since more carbon would be present in the pellet. B) Pictures of AB1 and AB1166 after centrifugation. Samples with AB1166 present a tighter pellet and clearer supernatant, suggesting a less viscous culture that is easier to separate from the culture medium. C) Micrographs of capsule staining of AB1 and AB1166 at 100X. Overall, AB1166 cells appear slightly larger than AB1 cells and had a much larger EPS capsule around the cells.

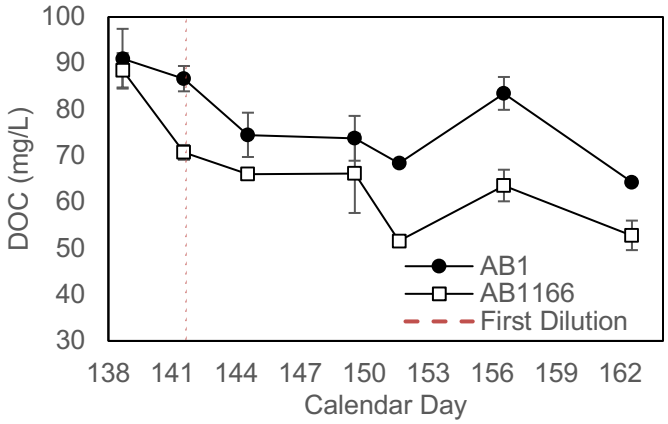

Figure 4-5. Dissolved organic carbon (DOC) detected during the semi-continuous cultivation of AB1 and AB1166.

At the end of cultivation, 20 L of AB1 culture was saved for dewatering *via* centrifugation and approximately 10 g-DW equivalent biomass at 20% solids was shipped to the National Renewable Energy Laboratory for compositional analysis and bench-scale HTL conversion, using the conditions indicated in the Task 2 section. The results are provided in Tables 4-4 to 4-6, including a comparison with model strain *Synechocystis* PCC 6803.

Table 4-4. Composition of Cyanobacterium sp. AB1 biomass

Sample	Ash	FAME	Protein	Carbohydrates
AB1	11.3%	5.0%	41.0%	13.8%

Table 4-5. HTL results from Cyanobacterium sp. AB1 and Synechocystis PCC 6803 biomass

Sample	*Bio-oil %	Liquor	Bio-char	Gas
AB1	34.7 ± 0.7	30.6 ± 0.6	9.8 ± 0.8	2.8 ± 2.0
6803	33.6 ± 1.1	29.8 ± 1.8	5.7 ± 0.9	9.6 ± 2.5

t

Table 4-6. The CHN content and High Heating Value (HHV) of HTL-produced bio-oil from Cyanobacterium sp. AB1 and Synechocystis PCC 6803 biomass

Sample	Nitrogen %	Carbon %	Hydrogen %	Oxygen %	HHV (MJ/kg)
AB1	8.0	73.0	9.1	9.9	35.9
6803	7.9	72.7	9.6	9.9	36.4

Task 4 Summary

- Overall, the results obtained with the Milestone 4.1 experiment successfully met the Go/No-Go #2 decision point criteria which read: >30% biomass productivity increase with a combination of improved yield strain, culture operations, and PBR design; no LCA or TEA showstoppers. There were no issues identified with the LCA or TEA, and clearly no showstoppers in those areas, as discussed further in Task 8.
- *Cyanobacterium* sp. AB1 achieved a biomass productivity of 24.2 g/m^2-d in semi-continuous mode, a 61% improvement over the AB1 baseline stated in the proposal (batch cultivation).
- Enhanced strain *Cyanobacterium* sp. AB1166 achieved a biomass productivity of 26.8 g/m^2-d which is greater than the task end target of 26 g/m^2-d in semi-continuous mode, and which represents a 79% improvement over the AB1 baseline.
- A 10% improved productivity with AB1166 compared to AB1 was demonstrated in semi-continuous mode.
- AB1166 culture was less viscous and was shown to be easier to dewater than AB1.
- DOE 4.1 milestone achieved per Go/No-Go meeting held at Algenol in July 2018.

Task 4 Milestones

Subtask Topic	Milestone Number	Milestone Description	Milestone Verification Process	End Quarter
Combine Biol/Op/Eng approaches	M4.1	Stable outdoor operation with 30% greater biomass productivity compared to AB1 and previous PBR design	Algenol PDU team verifies productivity potential compared to control in outdoor 300 L scale PBR experiment; Algenol/ GIT has delivered full TEA/LCA version	7
Outcome: **Completed.** The combination of a more productive strain, improved cultivation operations, and PBR system improvements resulted in a 79% increase in productivity in outdoor 324-L airlift cultivation units. TEA and LCA modeling did not indicate any showstoppers.				
Go/No-Go Decision Point	Go/No-Go #2	Improved yield strain, culture operations and PBR design with combined result of >30% biomass productivity increase; no LCA or TEA related showstoppers	Project Team delivers higher yielding strain, operational enhancements, PBR spacing, and advanced PBR to Algenol IBR; TEA team verifies economic benefits with realized yield increases	7
Outcome: **Passed** (“Go” decision made)				

Task 5 – Iterative strain and process optimization

Task 5 Objective

The primary objective of this task was to combine advances in strain development with enhanced cultivation protocols in an iterative fashion. Beneficial traits discovered by the strain development teams at NREL (using the model organism *Synechocystis* PCC 6803) or Algenol would be incorporated to the extent possible in one of Algenol’s commercial cyanobacterial strains, followed by outdoor testing at the PDU in Fort Myers, FL.

Expected Outcome: Advance strains based on field trial feedback and combine best traits into high performance strain

Task 5 Activities

As described in the Task 2 section, attempts to express heterologous genes encoding the mcl-PHA pathway in cyanobacteria (either *Synechocystis* PCC 6803 or *Cyanobacterium* sp.) were not successful, suggesting that the expression of one or more of the genes was detrimental to the health of the cells, possibly due to metabolic imbalances that were created. Two alternative approaches to improve BFI yield and quality were attempted in this task, one involving a partial reduction in glycogen levels (using *Synechocystis* PCC 6803 as a model organism) and another in which nitrogen-rich pigments (i.e., phycocyanin and chlorophyll) were lowered in the advanced strain *Cyanobacterium* sp. AB1166. These approaches are described below.

Knockdown of glycogen biosynthesis in Synechocystis

NREL researchers demonstrated that cyanobacterial biomass composition has a substantial impact on HTL-based BFI yield. Glycogen is the major carbon storage compound in cyanobacteria, and it has a negative impact on BFI yield. While the glycogen knockout mutant Δ*glgC* produced a favorable no-glycogen biomass composition, which led to higher BFI yield (Table 5-1), the strain was not as robust as the wild type strain under diurnal growth conditions, making it a poor choice for outdoor cultivation. Consequently, mutants with a range of *glgC* expression levels were used to determine whether a low-glycogen mutant might display an increased BFI yield without compromised growth characteristics under diurnal conditions.

Wild type *Synechocystis* PCC 6803 was compared with a glucose-1-phosphate adenyltransferase mutant (Δ*glgC*) that lacks glycogen and previously displayed a 17% increase in BFI yield, and a Δ*glgC* mutant with a *PpsbA* promoter driving *glgC* expression that displays a 34% reduction in daily glycogen accumulation. The growth rate of each strain was assessed in a 2-L PBR under a 12 h day (600 µmol photons/m^2-s):12 h night cycle supplemented with 5% CO_2. Growth was characterized by OD_{730} over 10 days. The Δ*glgC* strain displayed a 3-day lag phase relative to wild type and the complemented Δ*glgC* line (*ΔglgC_PpsbA::glgC*) upon PBR inoculation, and was prone to culture crashes (6/9 PBRs inoculated crashed before the 4th day; Figure 5-1A). Exponential growth rates were similar between wild type (0.323 ± .003 d^{-1}), the Δ*glgC* strain (0.312 ± .004 day^{-1}), and the *ΔglgC_PpsbA::glgC* strain (0.354 ± .024 d^{-1}). *In situ* PSII efficiency (Fv/Fm) measured at the end of each light period was found to be identical between wild type and the complemented Δ*glgC* mutant (*ΔglgC_PpsbA::glgC*) with significant reductions observed in the Δ*glgC* mutant, indicating photoinhibition (Figure 5-1B). Energy charge ([ATP]/[ATP]+[ADP]) was quantified during the night between the 4th and 5th days to investigate the role of glycogen catabolism in maintaining nighttime ATP levels. We observed increased energy charge, and consequently [ATP] concentrations in the Δ*glgC* mutant and the complemented Δ*glgC* line (*ΔglgC_PpsbA::glgC*; Figure 5-1C). This indicates an alternative mechanism for ATP generation in the Δ*glgC* mutant.

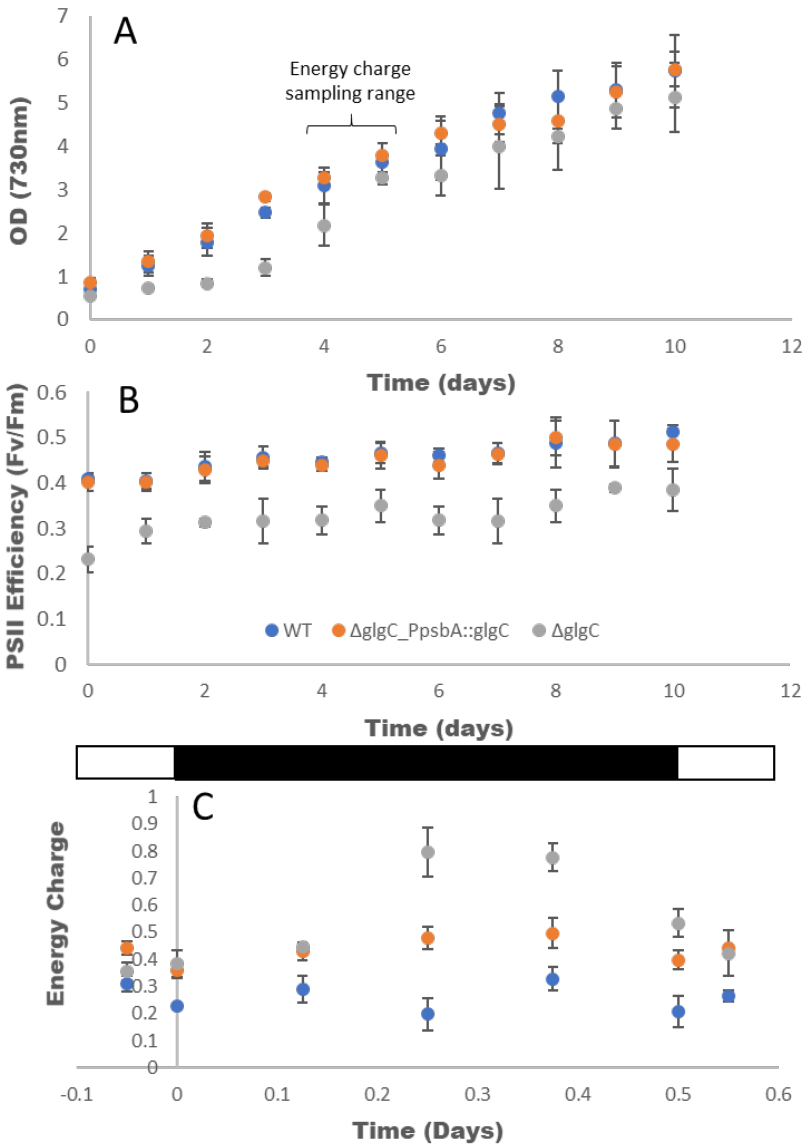

Figure 5-1. Growth and physiology of WT, the ΔglgC mutant and the complemented ΔglgC line (ΔglgC_PpsbA::glgC) (A) Optical density (OD_{730}) of cultures during 10 days of growth. (B) In situ PSII efficiency measured at dusk during PBR growth. (C) Night time energy charge ([ATP]/[ATP]+[ADP]).

To test if *Synechocystis glgC* down regulation improves BFI yield, we grew *ΔglgC_PpsbA::glgC* and *ΔglgC_PpetE::glgC* strains in 30 L bags under conditions used previously to characterize the BFI yields of wild type and *ΔglgC* strains (500 µmol photons/m^2-s; Dong *et al,* manuscript in preparation). Under these conditions, *ΔglgC_PpetE::glgC* failed to grow, and eventually bleached due to apparent light stress. Biomass slurry from the *ΔglgC_PpsbA::glgC* strain was processed using a bench-scale HTL tube reactor as described above in the Task 2 section. The contents in the reactors were extracted with DCM for BFI recovery. Biochar was filtered from the aqueous phase. The filtered aqueous phase was lyophilized to obtain the dry weight for yield calculations.

As shown in Table 5-1, the BFI yield from *ΔglgC_PpetE::glgC* biomass was 38.6%, which represented a 15% increase relative to the wild type biomass.

Table 5-1. HTL results of wild type and glycogen mutant biomass

Strain	BFI** (%)	biochar (%)	aqueous (%)	gas (%)
wild type	33.60 ± 1.10	5.70 ± 0.90	29.80 ± 1.80	9.60 ± 0.80
ΔglgC	39.40 ± 1.00	5.20 ± 0.40	34.80 ± 3.70	11.40 ± 7.30
ΔglgC_PpsbA::glgC	38.65 ± 0.77	5.36 ± 1.27	26.47 ± 2.15	

*The ash content in the biomass was 4.1%.

**BFI yield was based on AFDW.

Unfortunately, these results were generated near the end of the project, and there was not sufficient time to translate the results into a commercially-relevant strain such as *Cyanobacterium* sp. AB1 or AB1166, Future studies will look at this possibility. However, as described earlier, Algenol scientists did produce several strains derived from *Cyanobacterium* sp. AB1166 that had reduced photosynthetic pigment levels. One of these strains, AB1278, was completely void of c-phycocyanin and had lower levels of chlorophyll a. In batch cultures, this strain exhibited 10-15% higher productivity than AB1166; the increase was primarily due to continued growth in the latter stages of the culture, presumably because of enhanced light penetration into the optically dense cultures. In semi-continuous cultivations maintained at lower cell density levels, this advantage was lost. Nonetheless, because phycocyanin and chlorophyll are high in nitrogen, it was decided to subject AB1278 biomass through HTL to determine whether the quality of the resulting BFI was improve. Therefore, a sample of dewatered AB1278 was provided to NREL for conversion in their lab-scale HTL units. The HTL yields were found to be slightly lower than those for AB1 and AB1166, but the large ash content of the sample (42%) may have a deleterious effect on the measurements.

Task 5 Summary

- A strain of *Synechocystis* sp. was produced by replacing the native *glgC* gene with a version driven by the weaker *psbA* promoter, resulting in a 34% reduction in glycogen content. This strain had growth characteristics similar to the wild type parental strain (PCC 6803).
- HTL of the new mutant strain indicated a BFI yield of nearly 39%, representing a 15% increase relative to the wild type strain.
- HTL results with a reduced pigment derivative of *Cyanobacterium* sp. AB1166 (=AB1278) did not reveal an enhanced BFI yield, although results were difficult to interpret due to a high salt load in the biomass sample.

Task 5 Milestones

Subtask Topic	Milestone Number	Milestone Description	Milestone Verification Process	End Quarter
Enhance strain HTL product	M5.1	~~*Synechocystis* strain created with 22% higher HTL BFI yield~~	Chemical analysis confirms improved BFI yield compared to	9

		~~(C-basis) and 18% less N in BFI~~ *Synechocystis* strain demonstrated with un-compromised diurnal growth and 10-15% higher HTL BFI yield (C-basis) compared to wild type (WT)	wild type *Synechocystis*; ready to transfer technology to AB1	
Outcome: **Completed.** The BFI yield from the biomass of a Δ*glgC*_P*psbA::glgC Synechocystis* strain was 38.6%, which represented a 15% increase compared to the wild type strain. The growth rate of this strain was similar to that of the wild type strain. (Note that the original milestone was changed with DOE approval after it was deemed unfeasible to reach the original milestone despite repeated efforts.)				
Combine traits	M5.2	Commercial *Cyanobacterium* sp. based strain with combined traits created	Strain performance verified at PDU	12
Outcome: **Partially completed**. There was not sufficient time to transfer the glycogen knockdown trait to *Cyanobacterium* sp. by the end of the research phase of this project. As an alternative, Algenol researchers created a derivative of the enhanced biomass/reduced viscosity strain *Cyanobacterium* sp. AB1166 which has lower phycocyanin and chlorophyll levels and grows slightly faster than the wild type parental strain in batch cultures; this strain is referred to as AB1278. HTL results with this strain were compromised due to a high ratio of inorganic/organic matter (presumably due to high salt levels since the saline medium of the supplied biomass was too high and the sample had to be lyophilized to reach the required solids level).				

Task 6 – Operation and biomass harvest at scale

Task 6 Objective

The main objective of this task was to demonstrate cultivation and biomass harvest operations at a scale that is suitable for generating data useful for commercial scale techno-economic and life cycle assessments and preliminary plant design.

Expected Outcome: Production yield potential in PBR systems and open ponds; harvest biomass for downstream processing studies

Task 6 Activities

Engineering Package

The Integrated Process Demonstration (DEMO) system is an integrated, full process pilot-scale demonstration of *Arthrospira platensis* cultivation in a commercial airlift PBR system that also includes biomass harvest, phycocyanin (PC) extraction, concentration and drying. The DEMO system serves as a platform to evaluate scale-up risk of unit operations and integrated operation of cultivation with downstream processing. The DEMO system was used to validate designs and confirm processes and operating procedures for *Arthrospira* cultivation and downstream extraction of phycocyanin to support Algenol's commercial engineering package. It is expected that much of the knowledge and information gained from operation of the DEMO system with *Arthrospira* will translate directly to production of other cyanobacteria (including *Cyanobacterium* sp.) for biomass-based BFI production. Most of the R&D costs associated with the DEMO system

were funded outside the ABY2 program, but results are included here to provide a more thorough understanding of how the work also supported the goals of the ABY2 program.

Task 6.1 highlighted the major design components of the DEMO system, as well as significant departures from previous plant designs developed at Algenol. The engineering package was subdivided into numeric areas for organizational reference. A rendering of the general arrangement is shown in Figure 6-1. The areas listed below will be addressed in this section.

1. Photobioreactor (PBR)
2. Area 100 - Inoculum Field
3. Area 200 - Production Block
4. Area 600 - Nutrients
5. Area 700 - Clean in Place (CIP)
6. Area 800 - Gas Management
7. Area 300 - First Stage Dewatering
8. System Commissioning

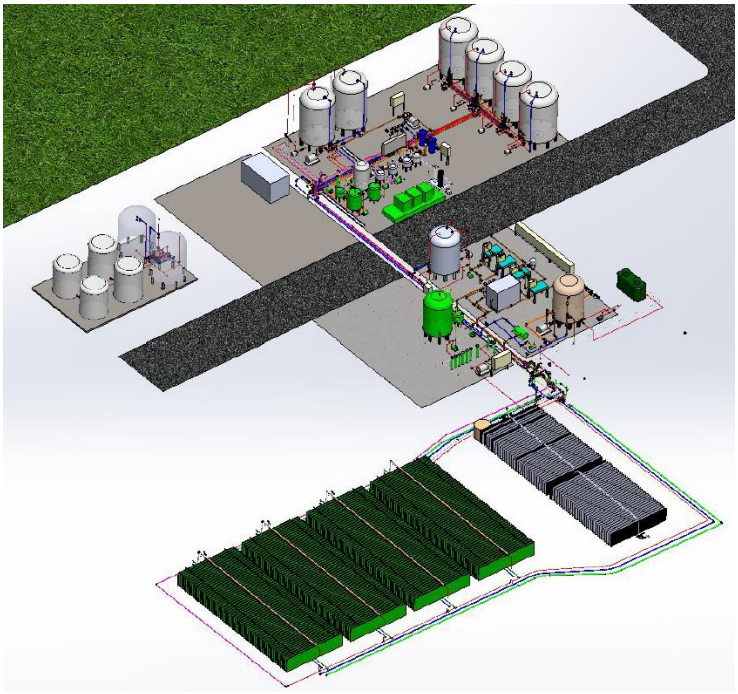

Figure 6-1. DEMO System general arrangement rendering.

Photobioreactor (PBR)

The PBRs deployed at DEMO are VIPER 3.4s. A diagram of the VIPER 3.4 is shown in Figure 6-2. The VIPER 3.4 is a 20-foot long flat panel PBR with dot welds throughout the surface. It has a cultivation height of 40 inches, average cultivation thickness of 1 inch, and volume of approximately 110 L. Air is delivered through a laser perforated tube diffuser with holes every 2" on center. Both the PBR design and film type were updated from previous installations.

PBRs were constructed with a custom polyethylene based multi-layer film with UV protection elements.

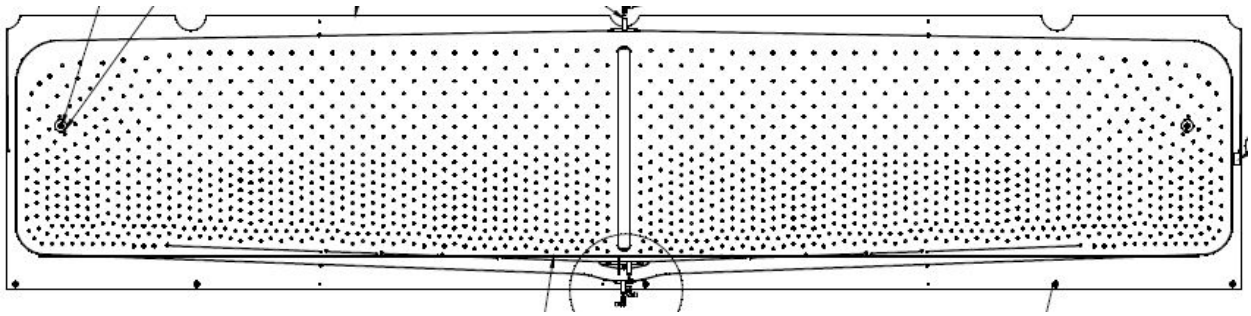

Figure 6-2. VIPER 3.4 Diagram

Area 100 - Inoculum Field

The Inoculum Field consisted of a 64-PBR airlift system, with an approximate volume of 6,600 L. In Figure 6-1, it is represented by the longer gray PBR row, offset from the production field. The system was designed with isolation valves between 1, 4, and 16 PBRs to allow for significant inoculum grow up to take place within the outdoor field. The culture grew up in batch mode to the required density before being passively 'cascaded' to subsequent PBRs by opening isolation valves. Each cascade interval was a 4-fold culture dilution, which required much less initial 'seed' culture prior to field transfer. When all 64 PBRs were at sufficient sOD, the inoculum was transferred to the Area 200 Production Block.

Both the inoculum field and production block required cooling systems for cultivation *of Arthrospira platensis*. A sprinkler system was installed to deliver fresh water spray across the outer surface of the PBRs. Liquid sprayers were activated automatically when culture temperature reached a user-defined set point. Table 6-1 highlights additional major design elements of the Inoculum Field and Production Block.

Table 6-1. Comparison summary between Areas 100 and 200

Design and Demonstration Features	Area 100	Area 200
Cultivate spirulina in a connected 60 PBR airlift	X	X
Cascade inoculation	X	
Cooling system	X	X
White film on ground	X	X
Production for PC sample extraction	X	X
3 post structure	X	X
Connect (4) 60 PBR airlifts into a single isolation unit		X
Medium recycle		X
Automated harvest and dewatered medium return		X
Automated nutrient injection		X
Gas recycle		X
Buried and sloped manifold pipes		X

Area 200 - Production Block

The Production Block consisted of four rows of 60 PBRs for a total of 240 interconnected PBRs and a volume of approximately 26,400 L. There were no isolation valves between the four units, so they were all intended to be inoculated, cultivated, harvested, and cleaned together as a single block. This type of interconnection is a key demonstration for a large-scale commercial design, reducing capital and operational costs associated with isolation valves. In Figure 6-1, the production block is represented by the four green rows of PBRs. PBRs were set at 4.0:1 to 4.4:1 culture height to space ratio (depending on fill volume/culture height), resulting in 10" on center positioning. PBR faces were oriented with large, flat sides in the North/South directions. PBRs were supported with a 3-post structure made of galvanized steel. The structure was anchored with 10" diameter concrete footings. White plastic was installed on the ground surface for three reasons: light reflection for higher productivity, controlling weed growth that can damage PBRs, and managing rain runoff to avoid channeling effects around the structure.

A significant design element at the DEMO production block was the culture circulation method. Rather than an airlift, culture was circulated by a pump in a turnover loop. The turnover pump was a progressing cavity, positive displacement pump with an ultralow-shear rate of 150 s^{-1} to avoid damaging cells. Turnover flow rate was set at 227 LPM (60 GPM), equating to ~0.95 LPM/PBR. This flow rate resulted in the entire culture entering the pump and being redistributed back to the field, or culture "turnover", approximately every 2 hours. The liquid distribution network was designed to ensure even mixing throughout the system, defined as a tolerance within ±10% of the target flow rate. This was accomplished with buried and sloped manifold pipes delivering fluid to and from both sides of each header. Manifold installation and header configuration is shown in Figure 6-3.

Harvest of the production block was designed for full automation. A user-defined flow rate was entered in the control screen, and an automated 3-way valve was positioned to harvest. Volume was logged with a flow meter, and the valve switched back to cultivation position when the harvest volume was reached.

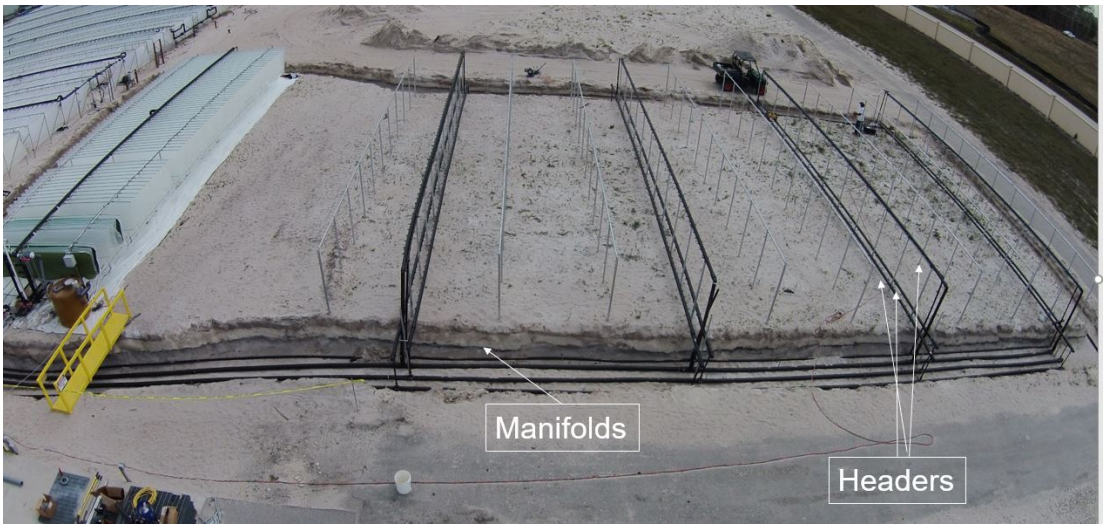

Figure 6-3. DEMO Manifold and Header Construction

Area 600 - Nutrients

Area 600 was designed for nutrient batches to be prepared in an automated system. The nutrient system consisted of five mixing tanks, one for each nutrient stock. Phosphorus and nitrogen were mixed together in a 150-gal tank with a paddle mixer for bulk solid handling. The solution was then transferred and stored in a 1,000-gal tank. Bicarbonate was mixed in a 200-gal tank with a paddle mixer for bulk solid handling and stored in a 2800-gal holding tank. Trace Metals, calcium, and magnesium salts were mixed and stored in individual 40-gal tanks. All nutrient stocks were prepared in reverse osmosis (RO)-treated fresh water.

Nutrients were added *via* metering pumps to allow for individual concentrations based on media variations. A user input at the HMI allowed for automated volumetric addition of individual stocks to create a desired finished medium composition. Each stock was recirculated prior to delivery to homogenize fluid, then added to the Volume-In tank (excluding trace metals). Finished medium was then filtered through an ultrafiltration (UF) skid prior to field delivery. Trace metals were filtered through a dedicated filter and slipstream injected into the medium delivery line.

Area 700 - Clean in Place (CIP)

The CIP system was designed to prepare and deliver sodium hydroxide with bleach, sulfuric acid, and 0.2 micron filtered final rinse water. CIP fluids are sent to the inoculum field, production block, tanks, and filter housings. The system was designed to be primarily manual, with no PLC automation of valves for drain or fill operations. Area 100 tanks were capable of full fill and soaking. Areas 200 and 600 used tank sprayers to reduce the required volume of CIP fluids. The RO water supply tank, UF supply tank, volume-in tank, and flex tank were also equipped with ball sprayers for the same purpose. The system was capable of recycling CIP fluids through filters, or sending them directly to the wastewater system for treatment.

Area 800 - Gas Management

Air supply for the field was delivered with Tuthill rotary lobe blowers. Blowers were selected and sized to deliver sufficient air volumes at low pressure requirements (<10 psi). The air flow rate was set to 14 SLPM per PBR, but could be adjusted in the control system by user input. An aftercooler and water knockout were installed to remove moisture from ambient air prior to filtration. Numerous low-point drains were also installed to remove residual liquid. A back-up compressed air supply was connected to the system to continue air flow to the field in the event of blower problems.

CO_2 was held in a large tank and was delivered to the PBRs via mass flow controllers. . CO_2 supply to the PBRs was controlled by headspace concentration, and set to 0.75% during the day and, 0.1% at night. Software allowed for adjustment to different set points, if needed. All gas entering the field was passed through 0.2 micron pore size filters.

The gas system was designed to run in a vent mode and a gas-recycle mode. During vent mode, gas passively exited the system through a pressure relief valve set at 4” water column pressure. During gas recycle the system was configured to return gas to the blower for re-entry back to the

field. The purpose of designing gas recycle was to maximize the CO_2 transfer into the culture, thereby decreasing the total volume of CO_2 required. The system could not operate in gas recycle for 100% of the time due to numerous process variables, so the control system was designed to enter venting mode based on numerous inputs. During recycle, the control system would change to vent mode at either a high back pressure set point, a high culture temperature set point, or a high oxygen headspace setpoint. Recycle and vent flows were controlled through proportional valves configured with concurrent PID loops.

The gas system field lines were designed to remove liquid from the gas delivery and gas return piping. The system was designed to be floodable with CIP fluids for full liquid contact and soaking time. Sloped manifolds and a low-point sump drain allowed for liquid removal from the system after CIP. The low-point sump and sloped manifolds were also designed to manage foam removal from the system during cultivation.

Area 300 - First Stage Dewatering

First stage dewatering was designed to remove a portion of concentrated solids from the field during cultivation, while returning the medium back to the PBRs for reuse. The dewatering was accomplished using a Russel Finex Liquid Solid Separator (LSS), which is very effective for application to filamentous strains, such as *Arthrospira*. It was installed on an elevated platform, to allow the turnover pump pressure to feed the unit, but return medium and biomass harvest *via* gravity flow. The installed unit is shown in Figure 6-4.

Figure 6-4. Russel Finex Liquid Solid Separator Installed on Platform at DEMO

The LSS was designed to concentrate field solids from 1-2.2 g/L to 60-90 g/L, with a minimum capture efficiency of 90%. Culture could enter the LSS at a 30-60 GPM flow rate. During daily harvests, medium (filtrate) was recycled back to the field. During full harvests, medium was sent to waste. The LSS control was fully automated for harvest operations. Users entered a harvest

amount, and flow was directed to the LSS with automated valves and logged with a flow meter. After the selected volume was removed, the valves would reposition for turnover mode. The control system would also direct medium filtrate flow back to the field or to the waste system, based on user input.

System Commissioning

Systems were commissioned at the DEMO unit following an installation qualification, operation qualification, process qualification paradigm. Installation qualification (IQ) is the process of inspecting, verifying, and recording that all physical equipment, tankage, and piping was properly installed according to the manufacturer's specifications and design intent. IQ was performed by the engineering, electrical, and controls teams.

Operation qualification (OQ) is the process of inspecting, verifying, and recording that all equipment, tankage, and piping functions as intended within the specified operating ranges. OQ was led by the controls team, with engineering, electrical, and operations teams in a support role. OQ was generally referred to as "water tests". It involved checking all flow paths and connections for leaks and verifying pump flow rates. The control system was fully tested during OQ, including: on/off local controls, sensor/transmitter function, safety stops, software, HMI function, and all other system automation and control functions. The DEMO system also had a function to capture data from field sensors, log, and report output. Data acquisition functionality was also tested during the OQ process. The final step of the OQ process is finalizing the detailed SOPs and checklists used to operate the system.

After completing the IQ and OQ activities, the system was handed over to begin plant operations. Process qualification (PQ) involved the use of live cultures to test the system as a whole, under operational conditions. PQ involves understanding and documenting performance over a period of time. Unexpected results or system problems were documented and investigated through the Root Cause Analysis (RCA) process. During PQ, operators could also propose equipment or process changes to improve or optimize system performance. Design or process changes were proposed, evaluated, and documented through the Management of Change process.

DEMO Results

The DEMO unit was constructed to gain operational experience with the current iteration of Algenol's commercial production system and for production of phycocyanin (PC), a natural blue colorant from the cyanobacterium *Arthrospira platensis* (also referred to as Spirulina). The DEMO Pilot Plant, diagrammed in Figure 6-5, was operated over a 17 month period with the overarching goal of building a PBR-based cultivation platform and PC extraction and purification process to demonstrate scaled operations envisioned at a commercial plant. More specifically, the project aimed to de-risk, validate and optimize commercial engineering designs and operational procedures with the following targeted objectives:

- Operate cultivation system for >120 days
- Demonstrate integration of semi-continuous operation of the cultivation system with downstream batch PC extraction and purification process
- Demonstrate process stability with respect to cultivation and productivity

- Determine system performance and relevant material balances on both unit and integrated system basis
- Produce food grade PC samples for business development

In addition, the DEMO system was used as a platform to i) develop training and operational checklists, ii) develop system maintenance procedures and requirements, iii) evaluate equipment performance, capital and operational costs, and iv) validate control parameters.

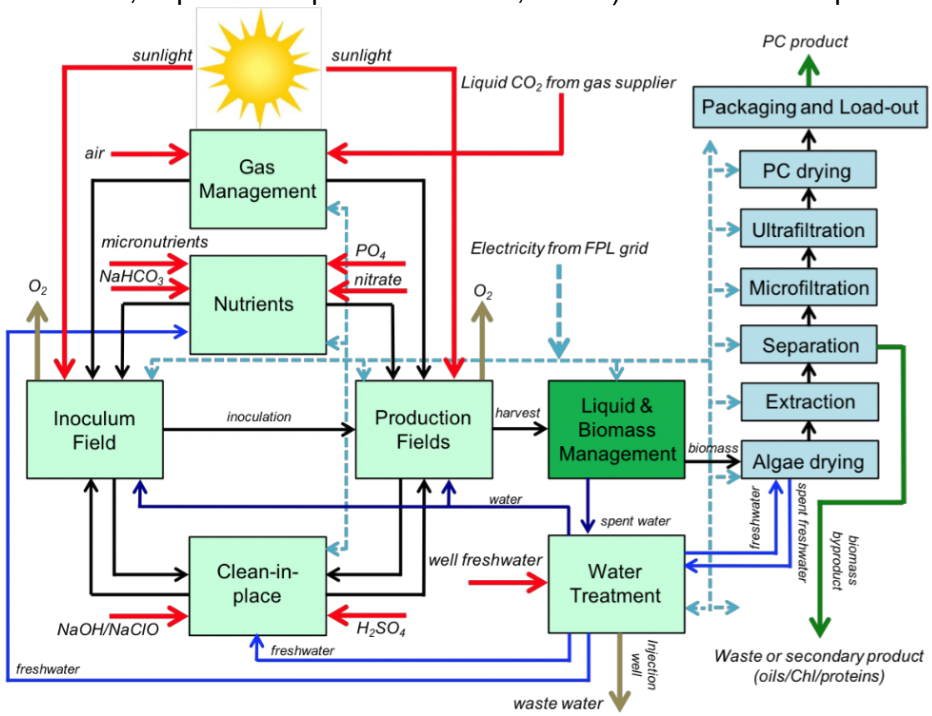

Figure 6-5. Generalized process flow diagram of the Algenol PC Plant carried out at the Integrated DEMO unit. Light green shading indicates algal cultivation and upstream areas; Dark green shading indicates biomass harvest, rinsing and dewatering; and Light blue shading indicates PC extraction and purification steps. Arrows indicate inputs and outputs.

Cultivation and Dewatering

Arthrospira platensis (strain AB2293) was cultivated in the DEMO system from March 2017 through August 2018. In total, the field was operated for 474 days (Inoculum Array and/or Production Field), which equated to 88% of DEMO duration. The DEMO cultivation field included the Inoculum Array (Area 100) and Production Block (Area 200) with integrated biomass harvesting capabilities through the liquid solid separator (LSS) at first-stage dewatering (Area 300). *Arthrospira* was cultivated in Zarrouk's medium with RO water base, following the established recommended cultivation conditions and PBR parameters (Table 6-2).

i) Inoculum Array (Area 100)

The Inoculum Array consisted of a 64-PBR airlift unit where typically 1-4 PBRs were initially inoculated at a target inoculation density of 0.6 sOD. The culture grew up in batch mode to ≥ 2.4

sOD before being passively 'cascaded' to subsequent PBRs by opening isolation valves. Each cascade interval was a ~4-fold culture dilution (i.e., 1 PBR to 4, 4 PBRs to 16, 16 PBRs to 64), until all 64 PBRs were inoculated. When all 64 PBRs were at the desired density, the Production Block was inoculated. Since ~25% of the culture was to remain in the Inoculum Array post-inoculation, the culture was scaled to a higher density (≥ 3.5 sOD) at the final 64 PBR stage. The scale-up process typically took 12-14 days to complete.

Table 6-2: Standard cultivation conditions and PBR parameters for the DEMO Inoculum Array (Area 100) and Production Block (Area 200)

Parameter	Description
Cultivation Platform Area 100	64 integrated PBRs, circulated by 2 airlift columns
Cultivation Platform Area 200	240 integrated PBRs, circulated by pump through turnover loop
PBR Type	VIPER 3.4
Plastic	Clear polyethylene
Diffuser	Laser perforated tubing
PBR Spacing	4:1
PBR Orientation	N-S
Gas Sterilization	0.2 µm filter
Medium	RO water base, Zarrouk's nutrient medium
Medium Sterilization	0.04 µm UF skid
Supplemental Nutrients	2 mM daily nitrate dose during medium recycle
Cultivation Operations Area 100	Batch grow-up with 4-fold dilutions every 3-4 days
Cultivation Operations Area 200	Semi-continuous, daily morning dilutions, baseline density = 1.35 g/L (2.7 sOD)
Turnover pump speed Area 200	60 GPM (227 LPM) during cultivation 30 GPM (113.5 LPM) during harvest through LSS
PBR cooling set point	35°C

The Inoculum Array was inoculated a total of 11 times, starting March 3, 2017 and was used to inoculate nine production campaigns. Contaminants, including *Chlorella* (both in suspension and biofilms) were routinely observed during scale-up.

ii) Production Block (Area 200)

The Production Block consisted of four rows of 60 reactors for a total of 240 interconnected PBRs, where culture was circulated by a pump in a turnover loop at 227 LPM (60 GPM), equating to ~0.95 LPM/PBR. Total system turnover time was approximately 2 hours. The target inoculation density of the field was 0.6 sOD from the Inoculum Array (a 4- fold culture dilution). Once inoculated, the culture grew up in batch mode until the culture density reached > 2.7 sOD (1.35 g-/L), upon which semi-continuous operation with daily dilutions began. The grow-up period typically took 3 – 4 days. Culture was harvested daily before sunrise to bring the culture density back down to the targeted 2.7 sOD baseline. An exception was Campaign 2, which was cultivated at a higher baseline density of 4 sOD (2 g/L) (see campaign details below).

The Production Block ran a total of nine campaigns, starting April 13, 2017. In total, the Production

Block was under cultivation for 396 days and CIP for 74 days. Some periods of CIP were prolonged due to extenuating circumstances (e.g., Hurricane Irma) or repeated when CIP metrics failed to meet criteria. The base-case campaign length was 72 days; 69 days cultivation and 3 days CIP, however productivity was most stable over the first four weeks and therefore the last four campaigns were intentionally run for 36 days; consisting of 33 days for cultivation and 3 days for CIP.

Productivity Summary

The primary key performance metric for DEMO operations was PC productivity. The food grade phycocyanin[1] (FGPC) target was ≥ 5.0 g-FGPC/m^2-d, which represents the annual average, and was expected to vary with season. The main drivers of FGPC productivity were:

- Biomass productivity (daily growth)
- Phycocyanin content of the cells at harvest
- Biomass harvest efficiency (through LSS)
- Overall PC yield
- PC purity

One combination of the above productivity drivers that resulted in 5.0 g-FGPC/m^2-d, and served as the baseline targets for DEMO, was as follows;

- Biomass productivity = 20.1 g/m^2-d
- PC content = 12.0% by weight (g-PC/g-DW)
- Harvest efficiency = 95% biomass retained at harvest (assumed constant)
- Overall PC yield = 65% (assumed constant)
- PC Purity (E1% $_{620nm}$ = 18; quality spec for food grade PC & aPC/cPC mass ratio = 0.45) = 29.84% by weight (g-PC/g-FGPC) (assumed constant)

Figures 6-6 through 6-8 show average weekly biomass productivity, PC content, and calculated FGPC production for each campaign over the duration of DEMO operations, respectively. Productivity from week-to-week within a campaign varied, with some campaigns remaining generally on or near target, especially over the first four weeks and given seasonality, and others

[1] Food Grade PC (FGPC) is an industry standard composition comprising PC and a diluent. The diluent consists of other colorless protein components from the original *Arthrospira* biomass plus one of several common additives (trehalose dehydrate, dextrin, and other sugars). The definition for FGPC is based on optical absorption specified as E1% = 18, where E1% is the optical density at 620 nm for a 1 wt% solution in water. 620 nm is the peak absorption for cPC. A typical PC sample contains about 70% cPC and 30% aPC as the majority pigments. The peak aPC absorption is at about 650 nm, and appears as a shoulder on the PC spectrum peaking at about 620nm. (MacColl, 2004; see Task 8 reference section). The relative content of cPC and aPC determines the "color" of the sample; the 70-30 ratio cited above is close to the optimum and provides a deep blue color comparable to the synthetic blue dyes that FGPC is designed to replace. Algenol routinely produced FGPC that met all the specifications for the commercial product and was well received by potential users. FGPC is typically about 25-30% PC. PC is typically 10% of the DW biomass, but varies with temperature and irradiance (See Appendix X).

showing declining productivity as the weeks progressed (causes for which are detailed in campaign descriptions below). At times productivity exceeded targets, for instance Campaign 6, where average FGPC was >6.0 g-FGPC/m^2-d.

The overall average biomass productivity for full campaign lengths was 18.0 g/m^2-d (non-annualized), with an average PC concentration of 11.9% (Table 6-3). Assuming 33-day campaign lengths, the average biomass productivity and %PC content increased to 19.7 g/m^2-d (non-annualized) and 12.2%, respectively. Given these and the assumed values above, the overall average FGPC productivity at DEMO over 17 months was 4.4 g-FGPC/m^2-d considering full campaign lengths, and 5.0 g-FGPC/m^2-d assuming 33-day campaign lengths, thus achieving the desired target.

Since the Production Block operated for over a year, valuable experience was gained cultivating *Arthrospira* in all seasons and weather experienced in southwest Florida. Peak biomass production was observed during spring (April-May) when PAR was highest (Figure 6-6), and average culture temperatures were moderate (Figure 6-9). May 2018 was unusually overcast and rainy, which impacted campaign 7 biomass production. Productivity was lowest during the winter months with overall lower PAR and cooler temperatures; i.e., minimum culture temperatures dipped down to ~5°C on several occasions (Figure 6-9). The average daily integrated PAR over DEMO duration was 39.5 mol photons/m^2-d (average yearly integrated PAR was 36 mol photons/m^2-d).

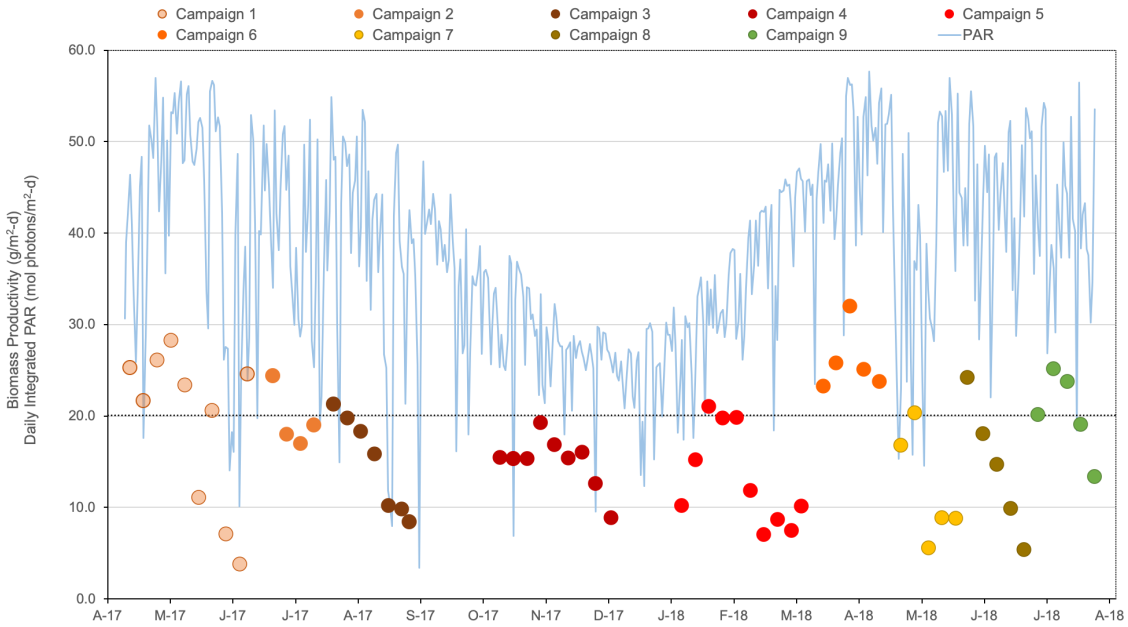

Figure 6-6. Average biomass productivity (g/m^2-d) from the Production Block (Area 200) over the full length of each campaign during DEMO operations from April 2017 to August 2018. Each data point represents the average daily productivity over 7 days. Data do not include full harvests, however average productivity during batch grow-up is plotted. Also plotted is the daily integrated irradiation (PAR) (mol photon/m^2-d), and the harvest productivity target of 20.1 g/m^2-d for reference (horizontal dashed line). Hurricane Irma passed through Fort Myers on Sept 10, 2017 (extreme low PAR), and May 2018 was unusually rainy and overcast; such weather conditions are not typically seen until June.

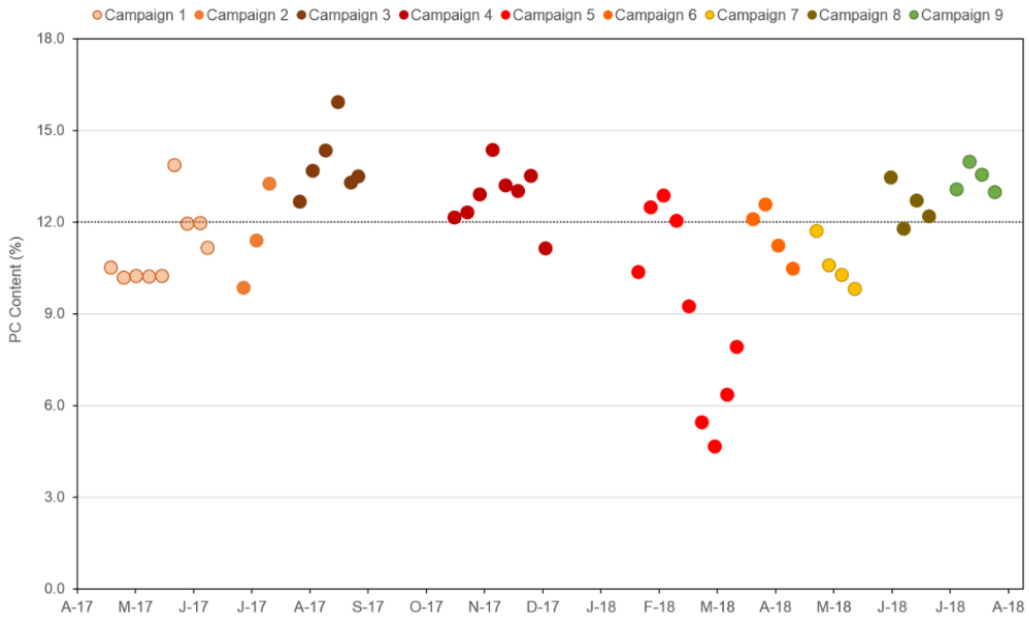

Figure 6-7. Average weekly %PC content (g-PC/g-DW) of Arthrospira cells at harvest from the Production Block (Area 200) over the full length of each campaign during DEMO runs from April 2017 to August 2018. Each data point represents the average PC content over 7 days. Also plotted is the PC content target of 12% for reference (horizontal dashed line). Average PC content during grow up is not plotted.

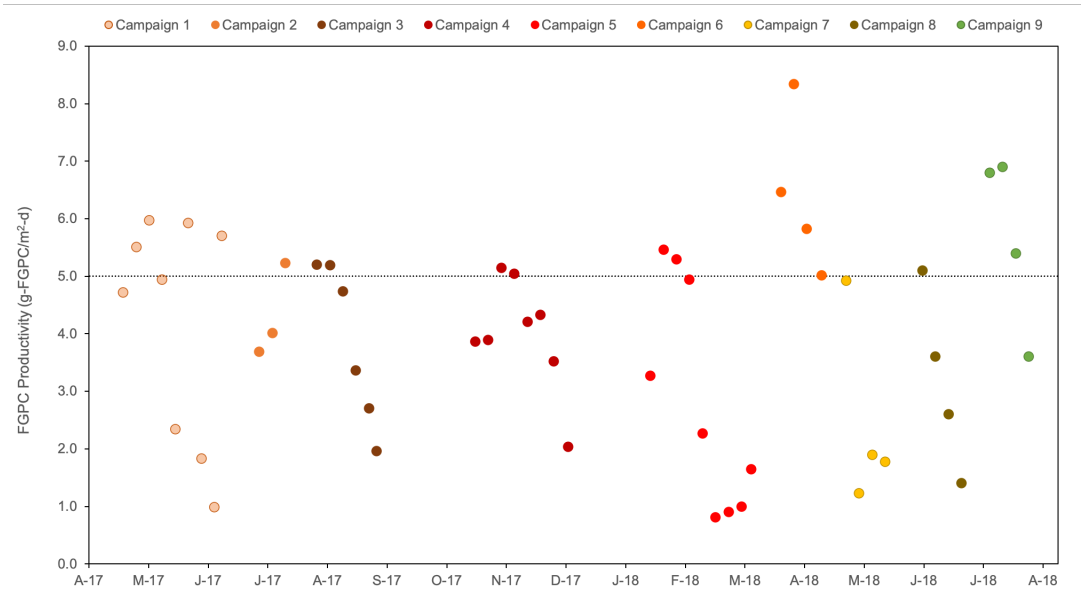

Figure 6-8. Average daily FGPC productivity (g-FGPC/m^2-d) from the Production Block (Area 200) over the full length of each campaign during DEMO runs from April 2017 to August 2018. Each data point represents the average productivity over 7 days. Also plotted is the harvest production target of 5.0 g-FGPC/m^2-d for reference (horizontal dashed line). Average productivity during grow up and final full harvest are not plotted.

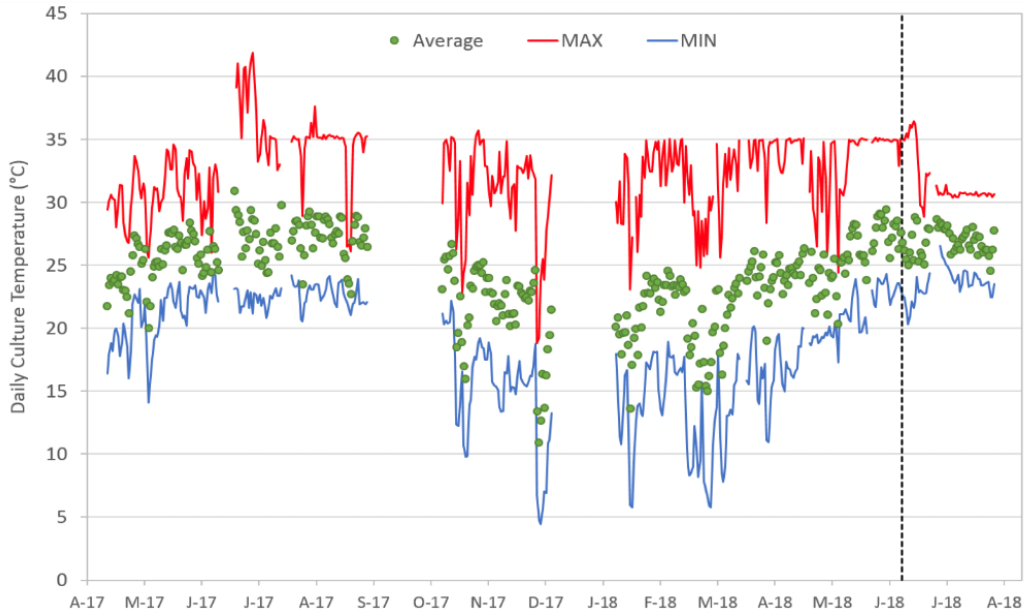

Figure 6-9. Daily culture temperature (°C) from the Production Block (Area 200) over the full length of each campaign during DEMO runs from April 2017 to August 2018. Plotted are the average, maximum and minimum culture temperatures experienced daily. Dashed vertical line represents monitoring switch from external probe (taped to PBR exterior) to internal probe in turnover loop. Maximum temperature set point before cooling sprinklers were activated was 35°C for all campaigns except for Campaign 9 (Jul-Aug 2018), which used 30°C as the set point.

Table 6-3: Total production and average productivity, PC and environmental parameters from 17 months of DEMO production field (Area 200) operations for full and 33-day campaign lengths. Productivity values are not annualized.

		Full length campaigns	**33-day campaigns**
Cultivation days	Total days	396	297
Biomass production	Total kg-DW	2529	2105
Biomass productivity	Average g/m^2-d	18.0	19.7
Average PC content	Average %	11.9	12.2
FGPC production	Total kg-FGPC	521	374
FGPC productivity	Average g-FGPC/m^2-d	**4.4**	**5.0**
Average culture temperature	Average °C	25.0	25.2
Average daily insolation (PAR)	Average mol photons/m^2-day	39.5	39.6

Table 6-4. Total production, productivity, PC and environmental values from the DEMO production field (Area 200) for each campaign over full campaign lengths (top) and 33-day campaign lengths (bottom), including final harvests. [1]Campaigns 5-8 were run in medium recycle, and Campaigns 6-9 were intentionally run for 33 days. Productivity values are not annualized.

Full Campaigns		1	2	3	4	5[1]
Season		spring	summer	summer	fall	winter
Duration		63-d	26-d	43-d	62-d	70-d
Biomass production	kg-DW	429	201	240	351	343
Biomass productivity	g/m^2-d	18.4	21.1	15.2	15.4	13.3
Average PC content	%	11.1	11.9	13.9	12.8	9.6
FGPC productivity	g-FGPC /m^2-d	4.2	5.2	4.4	4.1	2.6
Minimum culture temperature	°C	11.7	20.8	20.5	4.4	5.8
Average daily insolation (PAR)	mol photons/m^2-day	42.5	40.5	38.9	28.0	35.7

33-day Campaigns		1	2	3	4	5[1]	6[1]	7[1]	8[1]	9
Season		spring	summer	summer	fall	winter	spring	spring	summer	summer
Duration		33-d	26-d	33-d	33-d	33-d	33-d	33-d	33-d	33-d
Biomass production	kg-DW	294	201	207	208	230	325	181	192	267
Biomass productivity	g/m^2-d	24.3	21.1	17.1	17.2	18.8	26.9	14.8	15.7	21.8
Average PC content	%	10.3	11.9	14.1	13.0	12.0	12.1	11.0	12.5	13.2
FGPC productivity	g-FGPC m^2-d	5.2	5.2	5.0	4.6	4.7	6.4	3.4	4.1	6.0
Minimum culture temperature	°C	12.0	20.8	20.5	9.8	5.8	10.9	15.9	20.3	21.3
Average daily insolation (PAR)	mol photons/m^2-day	45.5	40.5	39.8	29.4	31.4	48.7	37.9	42.3	41.0

Campaign and Cultivation Summary

Several cultivation strategies aimed at reducing operational costs were implemented successfully, including medium recycle, refined-grade nitrate use, intentional N-depletion by campaign end, and increasing culture pH (eliminating the requirement for gas recycle and mitigating *Chlorella* contamination). Other strategies tested, however, had detrimental or inconclusive outcomes, such as decreased airflow rates, higher baseline density, gas recycle, and ammonium dosing. Some of these changes were made synchronously, making it difficult to assess individual impacts, and/or unrelated culture issues were concurrently observed when implemented.

Below are summaries of several selected campaigns which highlight deviations from standard cultivation recommendations along with and notable observations (refer to Figures 6-6 through 6-9 and Table 6-4).

Campaign 4: Oct 17-Dec 18, 2017 (62 days)
After Hurricane Irma, new v3.4 VIPER PBRs were deployed in the field. Productivity was stable and near target for most of this campaign, with a decline observed in the final week 7. *Chlorella* was detected on day 49 of cultivation. During this campaign and going forward, culture was harvested using the LSS. Area 100 (cultivated in semi-continuous mode) and a smaller scale outdoor cultivation at the PDU (CTP1.2) were run concurrently as comparisons to determine whether system flow and/or drain and fill rates impacted productivity due to issues associated with culture homogenization at scale. Overall, productivities were very similar for each of these systems (<10% difference), indicating that system flow rates in the Production Field were enough to sustain homogeneity and achieve expected productivity.

Campaign 5: Jan 22-April 2, 2018 (70 days)
Cultivation started at pH 9.2 but was increased to 9.8 on culture day 22. The pH change did not impact *Arthrospira* productivity, however the suspended *Chlorella* population declined (Figure 6-10). Medium recycle was implemented successfully from the first harvest, where the LSS-clarified medium was returned to the field. Under medium recycle, a 2 mM nitrate dose was delivered daily over 2 hours (field turnover time). The daily N-dose was given to keep baseline nitrate concentrations at ~12 mM. A rapid depletion of Fe was observed under medium recycle, and therefore two bolus doses of Fe/EDTA were given 9 days apart (starting culture day 29); some cell breakage was observed, potentially due to an imbalance between EDTA and Fe levels.

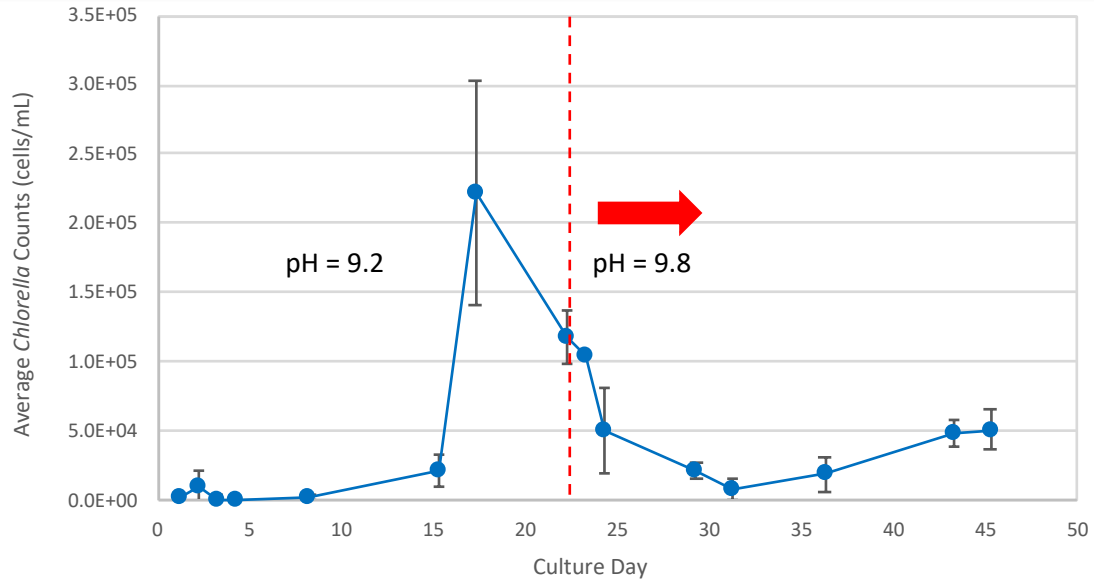

Figure 6-10. Average (± SD) cell counts of suspended Chlorella during Campaign 5; initially at a culture pH of 9.2, and after the shift to a higher pH baseline of 9.8 on cultivation day 22.

Campaign 6: April 5-May 8, 2018 (33 days)

This was the first campaign intentionally run for 33 days, all under medium recycle. Additional studies regarding Fe levels suggested that under high pH, all unchelated Fe added precipitated out of solution and was likely unavailable to the cells. Despite low Fe, productivity was stable and above target for the duration of the campaign. Refined-grade nitrate was used in Zarrouk's and for N-dosing during this and all subsequent campaigns with no impact on productivity. Intentional nitrate depletion by the end of the 33-day campaign was targeted to mitigate nitrogen loss to the waste stream by stopping supplemental N-dosing four days prior to full harvest.

Campaign 7: May 10-June 12, 2018 (33 days)

Daily supplemental nitrate dosing during medium recycle was replaced with ammonium chloride (technical grade). Using ammonium has a 3-fold potential benefit:

i) Nutrient cost reduction
ii) Boost in *Arthrospira* productivity (observed in the lab)
iii) Combined beneficial impact of ammonium and high pH to reduce *Chlorella* contamination

Starting at the first harvest, a 2 mM ammonium dose was added to the field on a daily basis. Interestingly, while ammonium was quickly consumed, urea accumulated in the culture, presumably due to bacterial utilization (Figure 6-11).

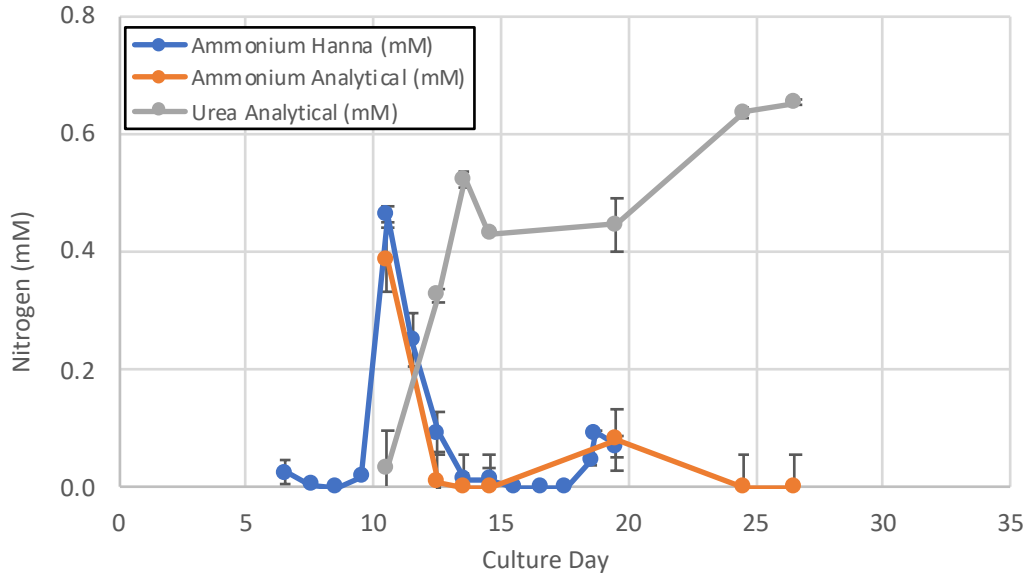

Figure 6-11. Average ammonium and urea measurements (mM ± SD) in the Production Field during Campaign 7. The 'Ammonium Hanna' measurement was a hand-held meter used to obtain real-time measurements from the field to make the daily dose/no-dose call, which closely matched analytical wet lab results.

Campaign 9: July 20-August 22, 2018 (33 days)

Due to excessive clumping observed in Campaigns 7 and 8, which were also conducted during the summer, Campaign 9 tested the hypothesis that warmer culture temperatures promoted EPS production and clump formation, namely in areas that were not well mixed (i.e., distal edges, drain channels). Therefore, cooling was initiated at a maximum culture temperature of 30°C to mitigate localized 'hot spots', and ultimately clump formation. This was compared to concurrently run controls in Area 100 and the PDU (see Figure 6-12). CO_2 delivery to the production field was controlled by culture pH set to 9.8 (*vs* headspace concentration as used previously), which worked well to maintain culture pH. Overall, Campaign 9 achieved target productivities through all but the final week, when a ~30% decline was observed due to the development of a *Chlorella* biofilm.

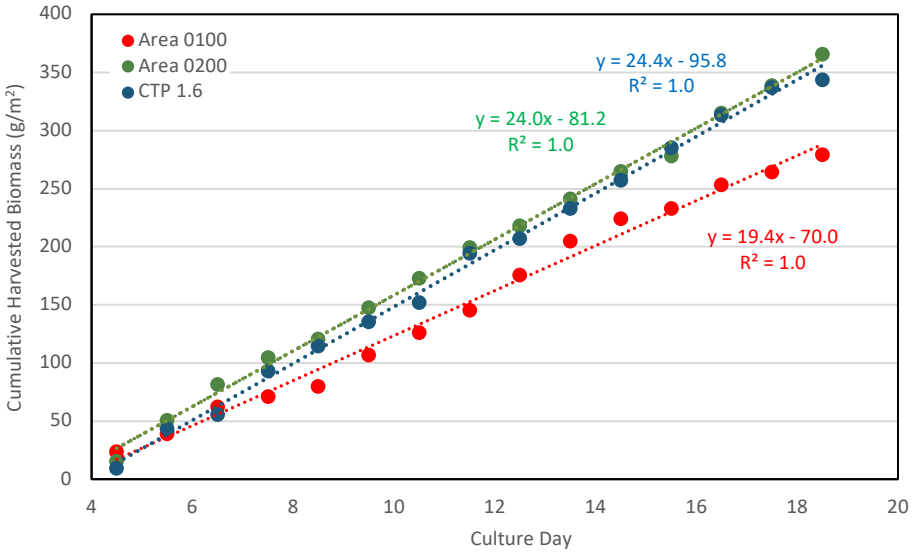

Figure 6-12. Cumulative biomass production for Area 200 (Campaign 9) cooled at 30°C, and the controls, Area 100 and the PDU ("CTP1.6"), which were cooled at 35°C. Average daily biomass productivity (g/m^2-d) is indicated by the slopes of the lines. After 2 weeks, no visible culture clumping was observed in any of the platforms. A Chlorella biofilm had started to form in Area 100 during the first week, confounding temperature-based comparisons with that platform. Note that the PDU CTP1.6 run started 2 weeks after Areas 100 and 200, however PAR and temperature conditions were similar during these different times

Successful implementation of medium recycle and higher culture pH were significant DEMO achievements, offering considerable benefits associated with reducing operational and resource costs and improving cultivation conditions. Advantages of performing medium recycle included:

i) Significantly smaller volume of fresh medium was required. Since >96% of the filtrate was returned to the field (see below), much less water and nutrients were needed for daily top off (Table 6-5)
ii) Significantly less operational time required for making medium/nutrient stocks and for daily top off operation
iii) No significant change in culture volume/height in the PBRs; keeping light and CO_2 headspace control conditions more consistent through harvest
iv) Minimal biomass losses; *Arthrospira* cells that did pass through the LSS filter during harvest were returned to the field and not lost to waste
v) Improved CO_2 use efficiency; less bicarbonate added daily resulting in less off-gassing waste and lower CO_2 cost

A disadvantage to medium recycle, however, was the potential for contaminant concentration over time. For instance, small contaminants such as *Chlorella* (3-5 µm) passed through the LSS and were returned to the field.

Operating at a higher pH had the following advantages:

i) Mitigation of *Chlorella* contamination; when pH was increased during cultivation (i.e., from 9.2 to 9.8), the suspended *Chlorella* population decreased (Figure 6-10)
ii) Less CO_2 used on a daily basis; in conjunction with medium recycle, CO_2 use efficiency increased up to 3-fold by shifting the pH to 9.8 (Table 6-6). Efficiencies were lowest at pH 9.2, with no medium recycle (~25%) and highest at pH 9.8 with medium recycle

(~65%). During Campaign 9, CO_2 injection was controlled by culture pH, which in non-medium recycle had a carbon (CO_2) use efficiency of 38%. Using this control strategy under medium recycle may improve efficiencies further (i.e., >65%).

A disadvantage to higher pH was the likelihood for metal-oxide precipitation, which may render metals, including Fe, unavailable to the cells, thereby impacting productivity and/or pigment concentrations.

Table 6-5. Average daily amount and % reduction of water and major macronutrients required during non-medium recycle (Campaign 4) and medium recycle (Campaign 5) over a 33-day campaign length. The listed nitrate value accounts for daily 2 mM supplemental dose during medium recycle.

Resource	Campaign 4 (No medium recycle)	Campaign 5 (Medium recycle)	% Reduction
Water (L/day)	4044	1024	74.7
Bicarbonate (kg/day)	67.9	17.2	
Phosphate (kg/day)	2.0	0.52	
Nitrate (kg/day)	10.1	6.5	35.9

*Table 6-6. Carbon use efficiency for each campaign during semi-continuous cultivation. CO_2 inputs included injected + atmospheric; measured CO_2 outputs included injected, atmospheric and bicarbonate off-gassing. Campaign 9 CO_2 delivery was controlled by culture pH rather than headspace CO_2 concentrations, which was used for all other campaigns. *Continuous pH monitoring was implemented by installing a pH probe into the turnover loop for Campaigns 6 through 9, thus the average culture pH during semi-continuous operation is given. Previously, daily pH spot checks were taken once per day pre-dilution.*

Campaign	Season	Target pH	Average culture pH	Medium Recycle?	Carbon (CO_2) use efficiency (%)	Notes
Campaign 1	Spring	9.2	--	No	25.9	Average up to day 25 (when airflow decreased)
Campaign 2	Summer	9.2	--	No	28.6	Higher density culture (4 sOD), average of full campaign (26 days)
Campaign 3	Summer	9.2	--	No	26.9	Average over 33 days
Campaign 4	Fall	9.2	--	No	21.0	Average over 33 days
Campaign 5	Winter	9.2	--	Yes	25.6	Average over 13 days
		9.8	--		67.0	Average over 16 days
Campaign 6*	Spring	9.8	9.83	Yes	65.0	Average of full campaign (33 days)
Campaign 7*	Spring	9.8	9.75	Yes	56.7	Culture clumping and poor productivity, average of full campaign (33 days)
Campaign 8*	Summer	9.8	9.75	Yes	58.0	Average over 10 days
				No	31.7	Average over 16 days (culture clumping and poor productivity)
Campaign 9*	summer	9.8	9.73	No	38.4	CO_2 delivery controlled by culture pH, average of full campaign (33 days)

iii) Culture Harvest (Area 300)

Biomass harvest and dewatering was performed on a daily basis. The expectations from the harvesting and dewatering systems were to deliver intact biomass with high solids content and no PC loss. As described above, there were two dewatering stages performed to concentrate biomass into sludge. The first stage of dewatering occurred in the field at harvest with the integration of the Russell-Finex liquid solid separator (LSS), a centrifugal filtration technology, to harvest and concentrate biomass from the field during 1st stage dewatering. For daily and full system harvests, culture was diverted through the LSS where the cell-free medium filtrate was then either discarded or looped back to the field during medium recycle mode. The second stage of dewatering employed vacuum filtration indoors. Full details on dewatering and additional downstream processes are provided in Section 7.2.

Pond operations at RIL and ASU (AzCATI) facilities

A series of pond experiments for *Cyanobacterium* sp. AB1 were attempted at RIL in India and at ASU (AzCATI). Both are described in detail in Appendix 2. In both locations, the experiments were plagued by predators. Only one experiment showed a modest amount of success. That experiment is described in more detail in the productivity modeling portion of the Task 8 discussion. The *Arthrospira platensis* UTEX1926 strain chosen for pond experiments at ASU performed as expected for Mesa, AZ in Aug/Sept 2019, with an average productivity of ~9 g/m^2-d. By way of comparison to other cultivation trials being conducted at the AzCATI site during this time period, sustained productivities for a number of strains were observed to be in excess of 25 g/m^2-d in June/July/Aug, with their benchmark summer strain UTEX393 (*Acutodesmus obliquus)* showing a sustained 30 g/m^2-d for the month of July and a summer average of 25.4 g/m^2-d for all of June/July/Aug. The ASU *Arthrospira* results are discussed in more detail in the Task 8 section and ASU's full final report is available in Appendix 2.

Task 6 Summary

- An integrated process demonstration (DEMO) system was designed that consisted of a 64-PBR (6,600 L) cascading inoculum field coupled to a production field comprising an interconnected block of 240 PBRs (26,400 L). Culture medium was circulated in the production field by means of a turnover pump. An inline centrifugal screening apparatus (liquid solid separator) enabled biomass harvesting with return (recycle) of clarified medium to the production field. CO_2-enriched air supply was controlled by an algorithm that took into account modeled growth rates coupled to real time weather conditions; CO_2 supply could be run in pass through or recycle modes.
- The DEMO system was commissioned and used to grow and harvest *Arthrospira platensis* for biomass and phycocyanin production. The average biomass productivity over nine 33-day runs throughout the year was 19.7 g/m^2-d.
- Medium recycle was successfully implemented in the DEM system, which resulted in a much better understanding of the benefits and constraints of medium recycling. Substantial reductions of water and nutrient use were realized, and calculations for daily nitrogen requirements were refined.

- Experience was gained with the use of an in-line Russell Finex Liquid Solid Separator, highlighting some of the benefits of using filamentous strains such as *Arthrospira* for algal biomass production.
- RIL and ASU (AzCATI) made multiple attempts to grow *Cyanobacterium* sp. AB1 in open ponds, but had little success due to significant predation by various protozoans. AzCATI was able to grow *Arthrospira platensis*, obtaining an average summer productivity of ~9 g/m^2-d. More details are provided in the Task 8 section.

Task 6 Milestones

Subtask Topic	Milestone Number	Milestone Description	Milestone Verification Process	End Quarter
Reconfigure 4,000-20,000 L Block	M6.1	4,000-20,000 L PBR Block commissioned	Algenol completes 4,000-20,000 L Block and certifies ready for operation studies in 6.2	8
Outcome: **Completed**. The construction and commissioning of 6,400-L and 24,000-L interconnected PBR blocks was completed.				
Operate 4,000-20,000 L Block	M6.2	Stable biomass operation with *Cyanobacterium* sp. and *Arthrospira*; harvests with advanced yield, dewatering and HTL stains	Algenol confirms yield estimates at scale and produces biomass for dewatering and HTL unit studies	12
Outcome: **Completed.** Over a year of operation at the 24,000 L scale was completed for *Arthrospira* biomass, demonstrating the scalability of the semi-continuous operation platform, a key innovation coming out of this project. The biomass productivity results generated from these operations were described in a presentation made at the Algal Biomass Summit in October 2018. Excellent agreement between the Algenol Productivity Model (based on small scale laboratory experiments) and this extensive outdoor biomass productivity data base was observed. A PBR system consisting of 55 VIPER 3.4 PBRs (~6,000 L), was inoculated with *Cyanobacterium* sp. AB1166 on several occasions in summer 2019. The experimental biomass productivity with semi-continuous operation was 22.5 g/m^2-d (annualized rate of 25 g/m^2-d), which is in good agreement with expectations from earlier outdoor experiments. Two batch runs were also conducted, resulting in an annualized rate of ~18 g/m^2-d, confirming at larger scale a ~40% higher biomass productivity in semi-continuous operation compared to batch operation.				
Operate RIL and ATP3 raceways	M6.3	Open pond raceway operated with *Cyanobacterium* sp. and *Arthrospira* and yield, CAPEX, OPEX determined	Algenol receives written report from RIL and ATP^3 on *Cyanobacterium* sp. and *Arthrospira* performance in open pond raceways	12
Outcome: **Completed**. RIL attempted multiple pond growth experiments with *Cyanobacterium* sp. AB1, but the cultures were routinely taken over by protozoan predators, so reliable growth measurements could not be obtained. ASU (AzCATI, ATP^3) successfully grew both *Cyanobacterium* sp. AB1 and *Arthrospira* in their small ponds and obtained growth data, but the growth of AB1 was again subject to severe predation for many of the runs. Reports were received from both partners and are included in Appendix 2.				

Task 7 – Downstream processing optimization

Task 7 Objective

The objectives of this task were to: 1) compare and optimize dewatering systems, namely centrifugation and membrane filtration, for commercial *Cyanobacterium* sp. strains (i.e., AB1166);

2) evaluate procedures for conversion of algal biomass to BFI *via* HTL; and 3) develop and operate a phycocyanin extraction process for co-product generation.

Expected outcome: Unit operation specifications, unit heat and material balances, and BFI quantity and quality

Task 7 Activities

Optimize Dewatering Systems at IBR with Advanced Strains

During Phase 3 of the project, advanced strain *Cyanobacterium* sp. AB1166 was cultivated outdoors at large scale, which provided feedstock for optimization of downstream operations. Investigated technologies included centrifugation and tangential flow filtration (TFF). The accomplishments and learnings from these experiments are summarized below.

Centrifuge optimization

The commercial-scale continuous centrifuge used in these experiments was an SC-35 model from GEA/Westfalia. For the purpose of Task 7, centrifuge feed flow rate, bowl ejection intervals, and number of passes through the centrifuge were varied to determine separation efficiency and power draw. The focus of the task was to minimize the power draw while maintaining a high separation efficiency.

Separation efficiency

For the purposes of this document, separation efficiency is defined as the amount of biomass present in the centrate stream subtracted from the amount of biomass present in the feed stream divided by the biomass present in the feed stream (Equation 7-1).

$$Separation\ Efficiency\ (\%) = \frac{Biomass_{Feed} - Biomass_{Centrate}}{Biomass_{Feed}}$$

Equation 7-1: Separation efficiency.

Although adjusting the feed flow rate and the ejection interval affected the separation efficiency, it was found that incoming biomass concentration, represented by sOD, also played a role. As shown in Table 7-1, at a given flowrate, assuming an equivalent incoming feed sOD, by decreasing the discharge rate (i.e., more frequent bowl ejections), the separation efficiency increased. For the most part, by increasing the flow rate and maintaining an equivalent discharge rate, the separation efficiency decreased. Furthermore, as the incoming sOD increased, there was a decrease in separation efficiency. These data, taken as a whole, suggest that the centrifuge is able to process a set amount of biomass in the bowl; if the centrifuge processes excess biomass, the separation efficiency drops. Anecdotal observations also hint that the bowl ejections performed were not sufficient to clear the majority of collected biomass in the centrifuge. Although bowl ejections were able to clarify the centrate line once biomass was observed, biomass was always observed in the centrate line again prior to the next bowl ejection.

Table 7-1: Separation efficiency and sludge solids content of different test runs. Test Runs with a '' indicate that the centrifuge parameters were repeated. Table is organized based on increasing flowrate, decreasing discharge rate, and decreasing incoming sOD (in that order).*

Test Run #/Pass	Flowrate (GPM)	Discharge rate (min)	Incoming sOD	Separation Efficiency (%)	Sludge Solids Content (%)
1 / 1st Pass	5	30	2.60	59.7%	7.93%
5 / 1st Pass	5	10	2.86	93.2%	7.60%
9 / 1st Pass	7.5	15	2.01	74.6%	6.68%
9 / 2nd Pass	7.5	15	0.72	99.9%	5.83%
7 / 1st Pass	7.5	10	1.78	99.6%	7.75%
4 / 1st Pass	10	10	2.37	78.1%	7.49%
4 / 2nd Pass	10	10	0.98	97.2%	6.13%
6 / 1st Pass	10	7.5	2.75	81.9%	8.91%
8 / 1st Pass	10	5	3.35	59.6%	7.64%
8* / 1st Pass	10	5	3.04	75.1%	8.46%
1 / 2nd Pass	10	2.5	1.07	99.8%	5.94%
2 / 2nd Pass	12.5	10	0.97	99.0%	8.34%
8* / 2nd Pass	12.5	10	0.28	99.9%	4.88%
2 / 1st Pass	12.5	5	2.75	53.1%	7.89%
11 / 1st Pass	15	3.5	2.50	99.4%	8.08%
11* / 1st Pass	15	3.5	2.13	99.5%	7.64%
12 / 1st Pass	20	2	2.23	99.5%	6.54%
12* / 1st Pass	20	2	2.21	99.2%	5.15%

The overall goal of the experiment was to achieve a separation efficiency >95% of the incoming biomass feed. The data suggest that under a given flowrate a separation efficiency of > 99% should be possible by varying the discharge rate. Achieving this efficiency becomes more difficult if the incoming sOD is too high, and conversely becomes easier if the incoming sOD is decreased (i.e., feed solution is diluted). As the discharge rate decreases, more ejections would be needed to process a given volume of harvest. If the same amount of biomass is in the feed, having more ejections would only serve to dilute the discharged solids, assuming the same volume is discharged every ejection.

Solids Content

At the end of each test run pass, a 'Small Partial' and 'Large Partial' discharge was performed on the centrifuge to clear out any remaining biomass within the centrifuge bowl. The 'Large Partial' discharge usually resulted in a more "watery" discharge compared to a 'Small Partial' discharge. However, in the interest of time, the SOP was written to perform 'Small Partial' and 'Large Partial' rather than multiple 'Small Partial' discharges. As such, the solids content collected from the optimization study may not be indicative of what could be achieved by the centrifuge.

There does not appear to be a correlation between any of the measured parameters and the solids content of the different runs (Table 7.1).

An additional overall goal of this task was to try to achieve a target of ~20% (w/w) solids content. Unfortunately, with the parameters that were tested, this does not appear to be achievable using the centrifuge technology tested only. In order to discharge the biomass within the centrifuge

bowl, some amount of water is necessary to dislodge and flush the biomass out of the centrifuge. Although there were a few settings on the centrifuge that were adjusted to try to minimize this amount of water (namely the "Pre Fill Time" setting of the 'Small Partial Preset' and 'Hood Spray' valve), this was not enough to achieve the desired target. By increasing the "Pre Fill Time" the overall volume ejected by the centrifuge, per discharge, would decrease, it likely would also affect the separation efficiency. Due to the limited time/resources, this parameter was not adjusted during the optimization trials. Likely the solids content could be improved slightly by adjusting this value, but unlikely to the degree necessary to achieve a 20% w/w solids content.

Power Draw

The overall power draw (kV·A) during these experiments was calculated from the data recorded by a Fluke Power Logger. Because the centrifuge ran on a 3-phase power supply, three different currents and voltages were recorded. For the purpose of this experiment, the voltage and current used for calculation was the average of the three different values. The average voltage and current were then multiplied by √(3) to account for the 3-phase power supply (Equation 7-2).

$$kV \cdot A = Voltage_{average} \times Current_{average} \times \sqrt{3}$$

Equation 7-2: Power calculation.

Because the Fluke Power Logger captures the voltage and current every 5 seconds, the power draw of each ejection interval is also captured. For the purposes of this experiment, the power reported is the average of the current draw peaks of each ejection interval, and therefore represents the entirety of the operational process. Note that only current and voltage during the actual process was used to calculate the average voltage and current (see yellow box in Figure 7-1), no power draw of the start-up/shut-down is factored into the presented power data because in commercial operations the centrifuges would be running most of the time.

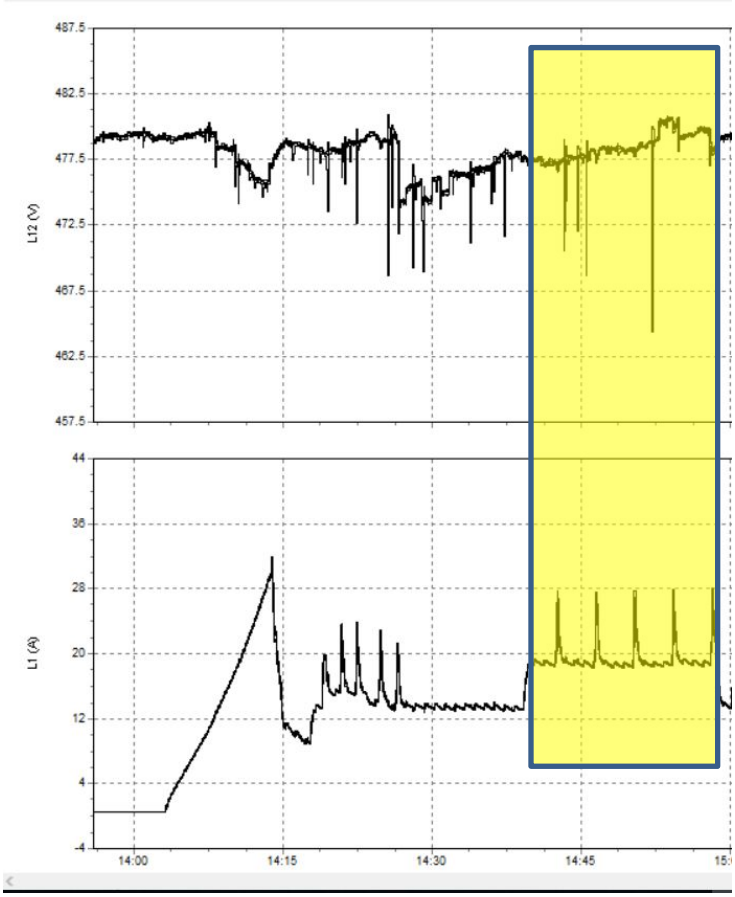

Figure 7-1: Example data from Fluke 1735 Data Logger. Area highlighted in yellow represents the actual centrifugation separation process and data used to calculate the power draw for the process.

The ejection interval does play a role in the amount of power used for the process; as the ejection interval decreases (i.e., more frequent ejections), the power draw is higher. However, it was noted that flow rate plays a larger role in determining the overall power draw compared to the ejection interval. Because of this, the power and energy (power x time to process) are presented based on a given flowrate (Figure 7-2). From the data, there appears to be a correlation between the flow rate and the power draw; as the flow rate increases so does the power draw. What this does not take into consideration is the time and the volume that was processed. To more accurately compare the different flow rates, the power was multiplied by the time of processing (to get energy) and then divided by the volume that was processed to get a 'specific' energy at a given flow rate. From the data, the energy used to process a set volume of product (i.e., 'per liter') decreases as the flow rate increases (Figure 7-2).

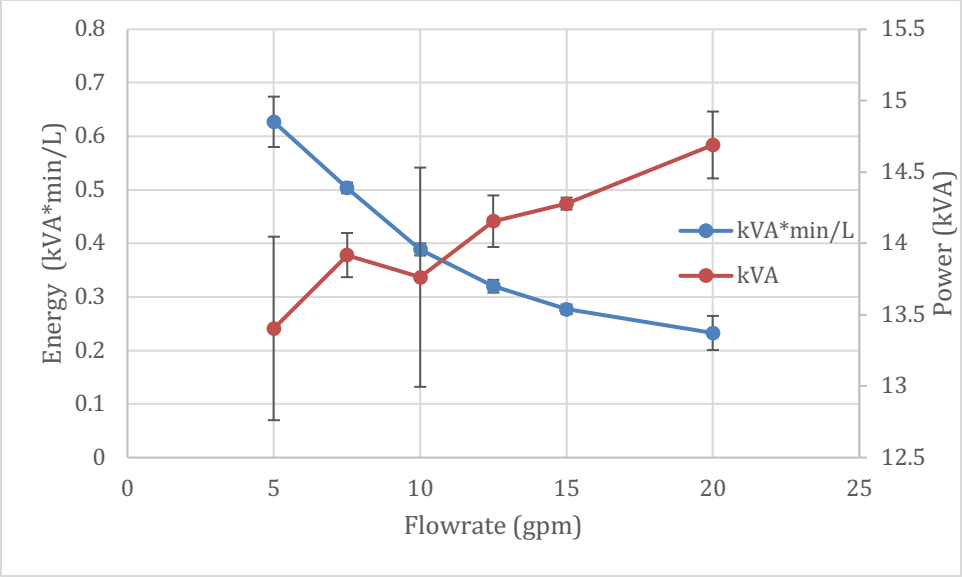

Figure 7-2: Power and energy draw per a given flow rate. The flowrate and discharge intervals used can be found in Tables 7-1 and 7-2.

An important goal of these experiments was to achieve a separation efficiency >95% of the incoming biomass feed while minimizing power draw. The data suggest that under a given flow rate a separation efficiency of > 99% should be possible by varying the discharge rate. Achieving this efficiency becomes more difficult if the incoming sOD is too high, and conversely, becomes easier if the incoming sOD is decreased (i.e., feed solution is diluted). The only restriction is the centrifuge's ability to perform a discharge; from manufacturer's recommendation, the discharge interval should not be faster than 1 minute to allow the centrifuge to reset itself before the next discharge. At the onset of the experiment, it was thought that potentially two passes at a high flow rate could be more energy efficient than a single pass at a slower flow rate. However, the data collected in this study suggest that doubling the flow rate does not halve the energy, though it is close, but by decreasing the ejection interval, a high separation efficiency was able to be achieved. Single pass energy demands could now be compared rather than trying to compare single pass runs to multiple pass runs. From an energy perspective, it is beneficial to go as fast as possible (assuming all other things are equal, i.e., separation efficiency can be achieved while keeping solids content comparable). It should be noted that the energy draw calculated for this experiment only includes the processing energy draw of the centrifuge under continuous running conditions.

Conclusions and Recommendations:

Because this task was focused primarily on improving energy efficiency, processing culture in a single pass was the goal. This likely caused the solids content to be lower than desirable. During process optimization, the solids content of the sludge never got above 9% (w/w). There are a few parameters that potentially could have been changed to help increase the solids content. Most notably, not performing a large ejection at the very end of the run, which typically diluted the sludge, should be considered. A large ejection was performed in order to ensure that all of the biomass was removed from the centrifuge prior to processing the next run. This could be improved by using several (e.g., two) small ejections instead; the difference is that a small ejection

yields ~1.4-1.8 kg of sludge (assuming sufficient content in the centrifuge bowl), whereas the large ejection yields >6 kg of sludge. Another process change would be to sacrifice energy efficiency to improve solids content. Likely, centrifugation technology, at least with the disk-stack centrifuge that was tested, is not able to achieve the target of a 20% w/w solids content in the sludge. Because there was minimal difference in solids content when using different flow rates or different ejection intervals at a given flow rate, solids content was the last parameter to try to target (i.e., target high separation efficiency and energy efficiency were prioritized).

In the end, it is recommended to continue processing using a 20 GPM feed flow rate and a 2 minute small partial ejection interval, if the culture conditions are similar to those used for the optimization study (i.e., culture growing ~1 sOD/d, feed culture ~2.0-2.5 sOD). This still allowed for a sufficient separation efficiency (>99%) with a single pass while minimizing the energy required for processing.

Tangential flow filtration

Permeate water flux of different membranes

One aspect of this project was to compare the energy requirements and efficiency of cell harvesting using membrane filtration *versus* centrifugation. To determine the intrinsic flux and membrane resistance of different microfiltration/ultrafiltration (MF/UF) membranes, pure water fluxes of the membranes were measured at different inlet pressures from 15 to 40 psig (Figure 7-3). The membranes used were: Regenerated Cellulose (RC) with a 100 kDa nominal molecular weight cutoff (MWCO), Polyethersulfone (PES) 150 kDa MWCO, and PES 0.1 µm MWCO; all with a 0.1 m^2 surface area. The filtration unit used was a ConSep II 3000 Membrane Module from Techverse. The results indicate that the water flux rate was proportional and increased with inlet pressure for each membrane, as shown in Figure 7-3. The initial water flux was measured before each experimental run and after CIP treatments to serve as a baseline to help the operator recognize the occurrence of membrane fouling after every experimental and CIP run. Since the PES-0.1 µm membrane has a much higher porosity/cutoff than the RC-100 kDa and PES-150 kDa membranes, PES-0.1 µm exhibited the highest flux rate (from 700 to 1600 L/m^2-h, or LMH), whereas the RC-100 kDa membrane showed the lowest flux at the same inlet pressure. For the RC-100 kDa and PES-150 kDa membranes, the flux rates were comparable and ranged from 200 to 800 LMH. At the standard operating pressure of 35 psig, the water flux of the PES-0.1 µm membrane was about 2.5 times that of the RC-100 kDa and PES-150 kDa membranes.

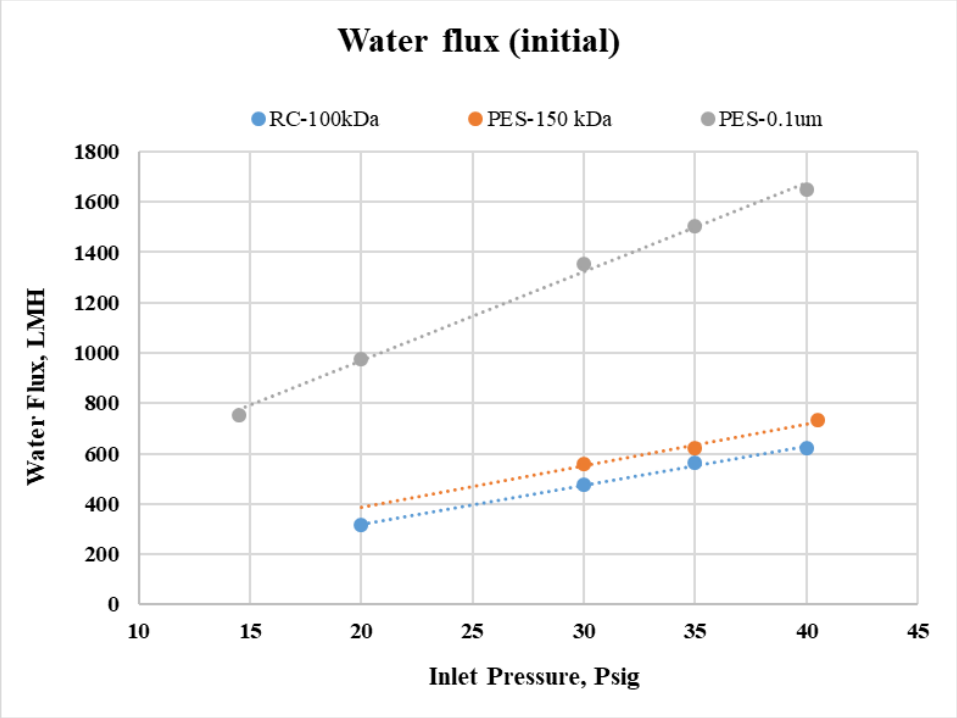

Figure 7-3. Water flux (initial) rate vs inlet pressure.

Indoor culture dewatering test: permeate flux with different membranes

To determine the optimal operating conditions, the impacts of inlet pressure (25-45 psig) and cross-flow velocity or recirculation rate (29-44 L/min) were tested on the permeate flux. With the RC-100 kDa membrane, the results with higher inlet pressure indicated a ~10% increase in flux, whereas a change in recirculation rate had insignificant effect on flux. For the PES-0.1 µm membrane, the flux increase was around 5% with an increase in pressure and an inverse relationship was observed with increasing recirculation rates. Recirculation rate or cross-flow velocity showed insignificant influence on flux rates and fouling behavior during membrane filtration. Typically, permeate flux increased with higher pressure. However, higher permeate flux may lead to higher foulant concentration close to the membrane surface due to concentration polarization, which would cause formation of a dense cake layer and increase filtration resistance.

To study the performance of different membranes with a more relevant liquid suspension, a pre-test to monitor flux through the different membranes over time was conducted at a constant inlet pressure of 35 psig and a recirculation rate of 37 L/min using culture having a cell concentration of ~1 g/L in complete recycle mode (open loop condition). Figure 7-4 shows change in flux over time for the different membranes. The results at a constant pressure and recirculation rate showed higher fluxes in the beginning of the filtration process, followed by a rapid decline within 10-50 min and finally leveling off at 40 LMH after 100-200 min of operation. In the higher MWCO PES-0.1 µm membrane, the initial liquid flux through the membrane was higher; however, a rapid decline was noticed over time and the flux leveled out at 40 LMH after 200 min. A rapid drop in flux implies faster membrane fouling, i.e., a quick build-up and compaction of a fouling layer on the membrane surface in a shorter amount of time. Lower MWCO membranes fluxes were not higher at the beginning, but remained stable at 40 LMH for a longer time. In the longer time scale

study with the RC-100 kDa membrane, the flux remained stable at 40 LMH from 200-500 min and then gradually declined to 30 LMH at 950 min, reached 20 LMH at 1080 min, and then leveled off.

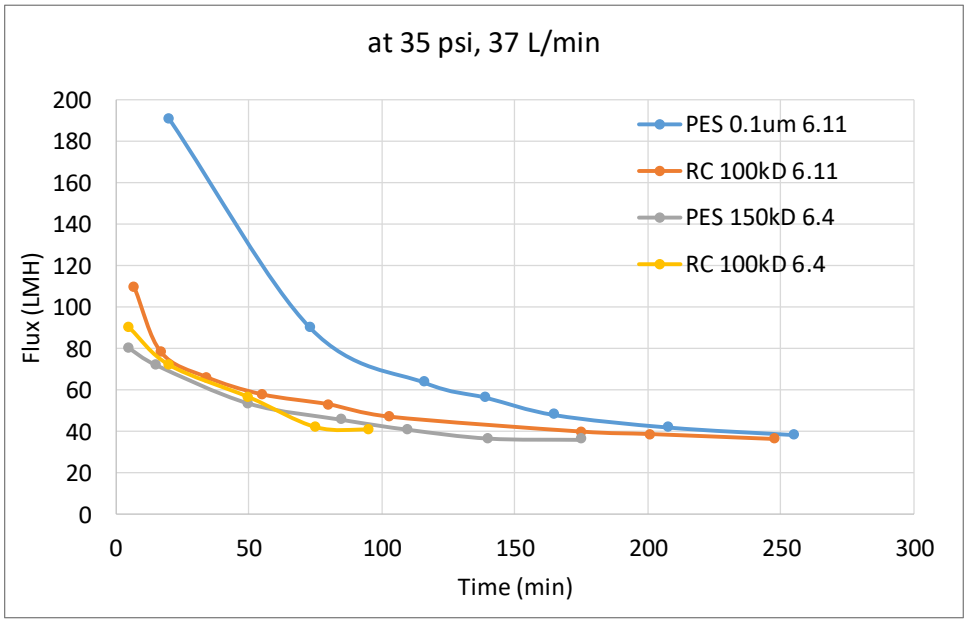

Figure 7-4. Permeate flux rate vs time at 35 psig, and recirculation flow rate at 37 L/min (~ 1 m/s) with 1 g/L culture in open loop operation.

The pressure drops for the different membranes are shown in Figure 7-5, which is another indicator of cake layer formation (fouling) and resulting flow resistance. In addition, exopolysaccharides (EPS) and algal organic matter (mainly protein, polysaccharides, *etc.*) released into the culture medium can also lead to the formation of a gel layer, which will cause flux drop. Both PES membranes (150 kDa and 0.1 µm MWCO) showed greater pressure drop ranging from 2.5-4 psig compared to the RC 100 kDa membrane. This may be explained by the biochemical composition of the feed combined with the properties of the membrane materials that cause different fouling behavior. The pressure drop in the RC membrane was noticed to be around 2-3 psig and the performance seems stable during long-term operation. This is associated with the pore size and properties of the RC membrane material, which is hydrophilic such that adsorption fouling by protein and dissolved macromolecules is minimized. Thus, the RC membrane was selected for further study of algal biomass dewatering and concentration.

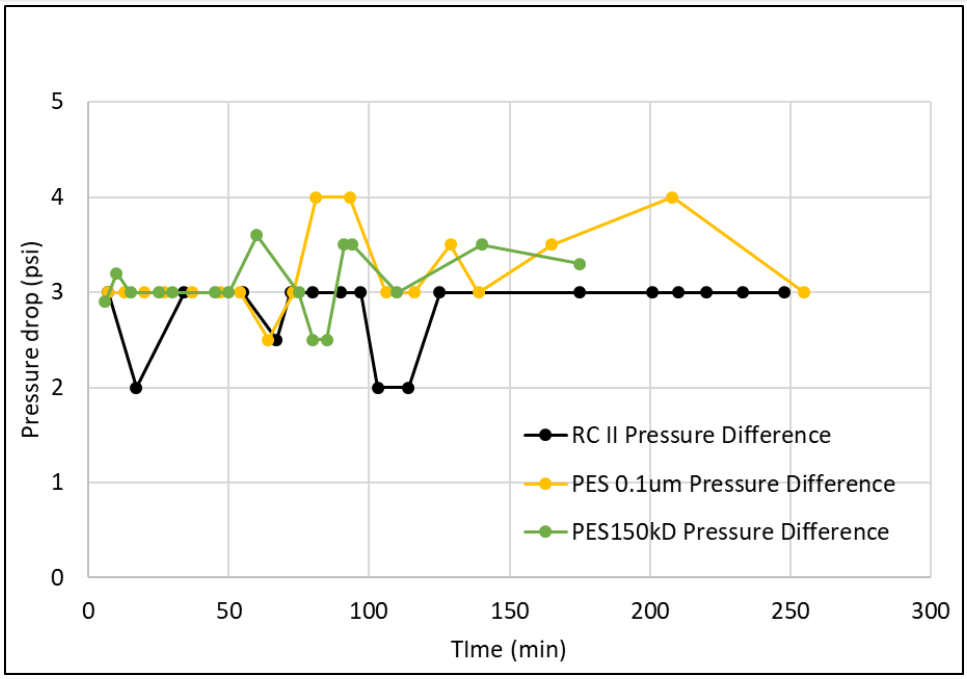

Figure 7-5. Pressure drop vs time at 35 psig, and recirculation flow rate at 37 L/min (~ 1 m/s) with 1 g/L culture in open loop operation.

Algal cell and permeate analysis during dewatering test

During the pre-tests, it was observed that the collected permeate was blue in color. The permeate was spectrophotometrically analyzed to confirm the increase of absorbance at 620 and 650 nm over test run, which corresponds to the blue color of PC. The release of blue color was noticed to be higher with the PES-0.1 µm membrane compared to the RC-100 kDa membrane. Microscopic analysis indicated that the cells harvested with the RC membrane were found to be largely intact whereas some lysis of cells was noticed for the PES membrane samples. These results indicate that the blue color was due to cell lysis and that PC and EPS-like biomolecules could pass through the PES-0.1 µm membrane more easily compared to the other membranes used in this study.

From these results, it was decided that further testing would be performed with the RC-100 kDa membrane. The next test used various feed stock concentrations and compared the ability to concentrate harvested AB1166 culture that was reconstituted after processing through the centrifuge. By taking the biomass solids from the centrifuge and re-suspending the material in a given amount of centrate, feed cultures with varying biomass concentrations could be produced.

Dewatering tests at varying feed concentrations

During July to August 2019, we conducted 15 test runs with harvested AB1166 culture from the 6,000-L outdoor PBR system. Feed biomass concentrations ranged from 0.1 to 3.6% (w/w). To carry out the dewatering and concentration experiment, we obtained biomass sludge from

centrifugation to prepare different concentration of feed culture. The operation was carried out with a starting inlet pressure of 35 psig and a recirculation rate of 37 L/min velocity, while maintaining a temperature around 35 °C. Initial experiments were carried out in a closed loop to concentrate the biomass, and after reaching the higher threshold concentrations, open loop was also operated to run the process in continuous mode.

The optimal feed concentration for running the ultrafiltration process was found to be 2.5-3%, which enabled biomass to be concentrated about 5-fold. The system became unstable after continuous running in closed loop operation mode, reaching the threshold capacity of the membrane system, and limits for pressure drop (20 psig) and temperature (50°C). To further concentrate of biomass and to run the system in continuous mode, the system was operated in open loop mode to maintain appropriate retentate flux rate with respect to the permeate flux rates.

Evaluate HTL Conversion and Fractionation with Advanced Strain

The ABY2 project did not have specific goals related to the development of hydrothermal liquefaction (HTL) or catalytic hydrothermal gasification (CHG) processes. However, experimental data are required for HTL applied to the biomass produced in the project in order to calculate BFI yields. Also, both HTL and CHG yields are required for TEA and LCA assessments. The original plan for the project was to utilize a pilot scale HTL unit that was designed and partially assembled during the DOE-funded Integrated Biorefinery project, the intended use in that project being processing of the spent biomass from ethanol production. PNNL is acknowledged for assisting with this HTL unit. This was a large unit (over 4 tons) capable of processing about 150 gal/h of slurry feed (typically 10-20% biomass). As such, it was oversized for the production scale of this project and work on the unit was discontinued in 2017 when a more attractive option became available at RIL. During that period, RIL was expanding its capabilities in the HTL area to include both batch and continuous process units, with and without the use of various catalyst compositions. RIL had historically tested spirulina (see US Patent application 2016/0130504 A1), which added value to the overall project. Their testing for the current project was limited to AB1, which they were producing at their outdoor testing site in India, both in Algenol's VIPER PBRs and in open ponds. The main test results from RIL we relied upon for this project was at a 300 mL scale in a batch mode at 350°C, with the commonly used dichloromethane (DCM) separation method. Reported values for BFI yield were 40-41% in two sets of experimental campaigns. Testing with an unidentified catalyst yielded only slightly higher results at 43.3% yield. Results for spirulina (performed outside the current project) were at bit higher: 43% without catalyst and 45-52% with two different catalysts. RIL also conducted HTL experiments in a continuous mode for AB1, though not in a manner allowing quantitative comparison to the small scale batch experiments.

We were not able to supply RIL with AB1166 biomass in the time window available to us. Thus, an alternative needed to be identified to meet the project requirements for HTL of our improved strain. NREL was working with a bench scale unit with a very small sample size (5 – 7 mL). The details of the testing procedure were given earlier in this report in the discussion of Tasks 2 and 5. It was not clear if these small scale experiments could be quantitative, i.e., representative of what can be expected in a large scale deployment. However, we reasoned that they should be adequate in a relative sense, allowing comparison between AB1 and AB1166. The BFI yield

results from three tests at 300°C were 34.7% ± 0.7% for AB1 and 35.1% ± 1.2% for AB1166. The AB1 yields determined by NREL were somewhat lower than the yields determined by RIL at about 50x larger scale and higher temperature (350°C for RIL *vs* 300°C for NREL). The same is true for testing of spirulina residue after PC extraction, 40.4% for NREL *vs* 48% for RIL. However, the latter comparison involves different spirulina strains and different extraction procedures (as well as different temperatures), so the differences are not unexpected.

Our final conclusion for a non-catalyzed HTL process is that a conversion efficiency of 38% ± 2% is a fair representation of the overall results for AB1 and AB1166. RIL's results suggest a slightly higher conversion for *Arthrospira*. Catalyzed HTL will almost certainly yield results above 40%, although the long term operability and economic impacts associated with catalyst use need to be better understood.

The quality of the BFI, as measured by the high heating value (HHV), was somewhat higher for the NREL *vs* RIL processes. The HHV for NREL-generated BFI was 35.9 MJ/kg while BFI from RIL was about 7% lower at 33.6 MJ/kg. The process temperature differences may be the main explanation for the differences in BFI quality and quantity for the two labs, although compositional differences in the AB1 biomass could also play a role. We have not fully addressed the issues with BFI quality and have not considered the impact of that quality on the TEA or LCA assessments.

Downstream Operations for Phycocyanin Extraction

As described previously, phycocyanin (PC) is a blue pigment marketed as a food colorant, and represents a potential co-product that can help support an early stage algal biofuel biorefinery. While the following section focuses on PC extraction from *Arthrospira platensis*, due to the ability to market PC from *Arthrospira* given is GRAS status, small scale extractions of *Cyanobacterium* sp. strains produced PC of similar quality and thus much of the following protocol could be used for PC recovery from those strains. The process to extract and purify PC from *Arthrospira* began with the field harvest, which underwent first stage dewatering as it passed through the Russell-Finex Liquid Solid Separator (LSS), introduced above in section 6.2. This resulted in a slurry with, on average, 6% solids content. The slurry was then passed to a second stage dewatering step, which at the DEMO scale was conducted indoors using vacuum-aided mesh filtration. At commercial scale, a vacuum belt filter would be used for second stage dewatering. The following extraction and purification processes were then performed: dehydrate then re-hydrate the biomass in an extraction buffer to lyse the cells and release PC, separate cell debris from the PC-enriched buffer solution, purify and concentrate phycocyanin using filtration, and dry into a storable powder. Dehydration functioned as the interface between semi-continuous upstream cultivation and downstream batch PC processing, where operations do not occur in unison with the daily cultivation field harvests. As such, the downstream system operated independently from the field, where two batches were run per week with dehydrated biomass as the main feedstock. The purpose of the DEMO extraction and purification system was to validate both individual unit operations and integrated downstream processing from biomass drying to final PC product, while at the same time producing samples for business development. Only a portion of the work described in this section was funded through the ABY2 program, but we have opted to include an

extensive description of work conducted in this area, whether funded internally or through the ABY2 program.

The downstream systems were constructed in the Algenol's Engineering High Bay (Figure 7-6). Continued process development at the various stages were conducted over the duration of DEMO operations. Limited optimization studies were performed beyond centrifugation with the recognition that the filtration systems in place at the DEMO unit were not representative of the commercial design. The processes described in detail below represent the baseline operational protocols determined for each stage that were conducted over the last six DEMO campaigns (Campaigns 4 through 9) for consistency and validation.

Figure 7-6. DEMO PC extraction and purification line in Algenol Engineering High Bay.

The overall PC downstream production process consists of the following unit operations:

1. First- and Second-Stage Biomass Dewatering
2. Biomass Dehydration
3. PC Extraction
4. Centrifugation of Extracted Biomass
5. PC Purification and Concentration (Microfiltration and Ultrafiltration)

The following sections provide details on these unit operations, including observations, operational data, and improvements made to the overall process. Based on observed large differences in the efficiency of the PC extraction step, particular emphasis was placed on improving this step for more complete and consistent extraction; the results and conclusions from these attempts are summarized at the end of this section.

1. First- and Second-Stage Biomass Dewatering

As described above and in section 6.2, biomass dewatering began with the passage of the field harvest through the LSS. The LSS was implemented at the start of Campaign 2, where during Campaigns 2 and 3, a design of experiment (DOE) was run to determine optimal operational parameters to achieve a concentrated sludge output of ~6% solids w/w (94% moisture content). An additional critical performance metric was also to achieve a harvest efficiency (i.e., biomass removal from the medium) of ≥ 95%, such that most of the biomass was collected, and ≤ 5% was lost or returned to the field.

Starting from Campaign 4, when harvest parameters were optimized, a total of 193 harvests were dewatered through the LSS. Throughout DEMO, the key harvest and dewatering metrics were at or near targets. Overall averages (Campaigns 4 through 9) were as follows; solids content = 5.4%, harvest efficiency = 93.0% and separation efficiency = 96.4%. On average, ~120 kg dewatered sludge was collected from the LSS on a daily basis.

From the LSS in the field, the biomass sludge was transported indoors to 2nd-stage dewatering in a mesh screening unit (Screening Tub). Further biomass dewatering is essential to reduce energy requirements during the subsequent dehydration step. The sludge was pumped into the Screening Tub, rinsed with RO water at a ratio of ~1:1 (RO water:sludge) to remove salts, and concentrated further using a 21 µm mesh under vacuum while manually mixing. The dewatered sludge was then sent to dehydration. Starting from DEMO Campaign 4 (see Section 6.2 for DEMO campaign description and results), when operational protocols became more consistent, a total of 164 harvests were dewatered through the Screening Tub. The target solids content out of the Screening Tub was 18-20%. The overall average solids content achieved was on target at 18.6%. A photograph of a representative sample of dewatered biomass is shown in Figure 7-7. On average, ~30 kg dewatered sludge was collected from the Screening Tub on a daily basis (a 4-fold decrease in weight from the LSS), and up to 125 kg could be obtained from a full harvest. During DEMO, successful dewatering trials were also conducted using a vacuum belt filter (VBF manufactured by BHS)), which will be the technology used in future pilot and commercial plants.

Figure 7-7. Dewatered biomass at ~20% solids content (80% moisture) after Screening Tub filtration.

2. Biomass Dehydration

For the dehydration step, dewatered biomass from the Screening Tub was manually spread in even strips and thickness onto metal trays using a specifically designed mold. Initially, trays were perforated with a silicone liner to prevent sticking, however later tests were performed on solid trays with a Teflon coating (no liner). A total of 14 trays were loaded per run, with a biomass target of 2.2 kg dewatered biomass at 18-20% solids content per tray. Therefore, a total of ~30 kg dewatered biomass could be processed daily through the dehydrator. Biomass was dried in a Harvest Saver food dehydrator (convective airflow; Commercial Dehydrator Systems (CDS)) for 24 h at 120°F (Figure 7-8). After 24 h, the dried biomass was removed from the trays, combined, crushed to achieve similar particle size, and stored at room temperature in airtight plastic bags until resuspension. From Campaigns 4 through 9, there were 121 batches run through the dehydrator, with an average solids content of 95% (5% moisture). On average, a total of 5.3 kg dried biomass was collected from the trays after each run, almost a 6-fold decrease in weight from the Screening Tub.

Figure 7-8. DEMO-style Harvest Saver dehydrator manufactured by Commercial Dehydrator Systems (CDS).

Dehydration trials conducted in process development included varying dehydration time (24-48 h) and temperature (120-130°C). Biomass dried at higher temperatures (>120°C) had greater PC losses, likely due to PC degradation. Under the standard protocol (120°C for 24 h), biomass moisture content varied both within and between trays, largely depending on location within the dehydrator. While this variability lessened when the dehydrator was relocated to a room with more consistent temperature and humidity, it was still observed throughout DEMO, namely when using the solid trays. PC loss calculated at the dehydration stage using the standard protocol was 8.2%, resulting in a PC yield of 91.8%.

3. PC Extraction

In the initial PC extraction protocol, dried (dehydrated) biomass was resuspended in a 0.2 M sodium phosphate buffer-salts solution (pH 6.0) to re-hydrate and lyse the cells, leading to release

PC into solution. A primary purpose of the phosphate buffer addition was to inhibit metabolic enzymes that could cause PC degradation, thus enhancing product stability. Rehydration was performed at room temperature (~25°C) in a 20-gal tank at a resuspension concentration of 12.5% w/w (dried biomass weight/total weight), under constant mixing using a paddle mixer for 16 h in the dark. The average amount of dried biomass used for resuspension was ~6.7 kg into 47 kg buffer (accounting for moisture content of the biomass). After 16 h, the slurry was transferred to a larger tank, diluted in 88 gal RO water (for a total of 100 gal) and homogenized for 15 minutes prior to centrifugation.

A total of 88 'dry-extraction' batches were processed through extraction and purification over the course of DEMO downstream operations; however only data from the 56 batches run from Campaigns 4 through 9 is reported here since this represents a more consistent period of operations. PC extraction efficiencies from tank resuspensions started being tracked January 2018 with dried biomass from Campaign 4, at which point it was determined that not all of the PC was being extracted from the cells. Upon further investigation, not only was PC extraction incomplete, but also highly variable and unpredictable from batch to batch; one day a batch would have 100% PC extraction, then the following day only 45% extraction (Figure 7-9).

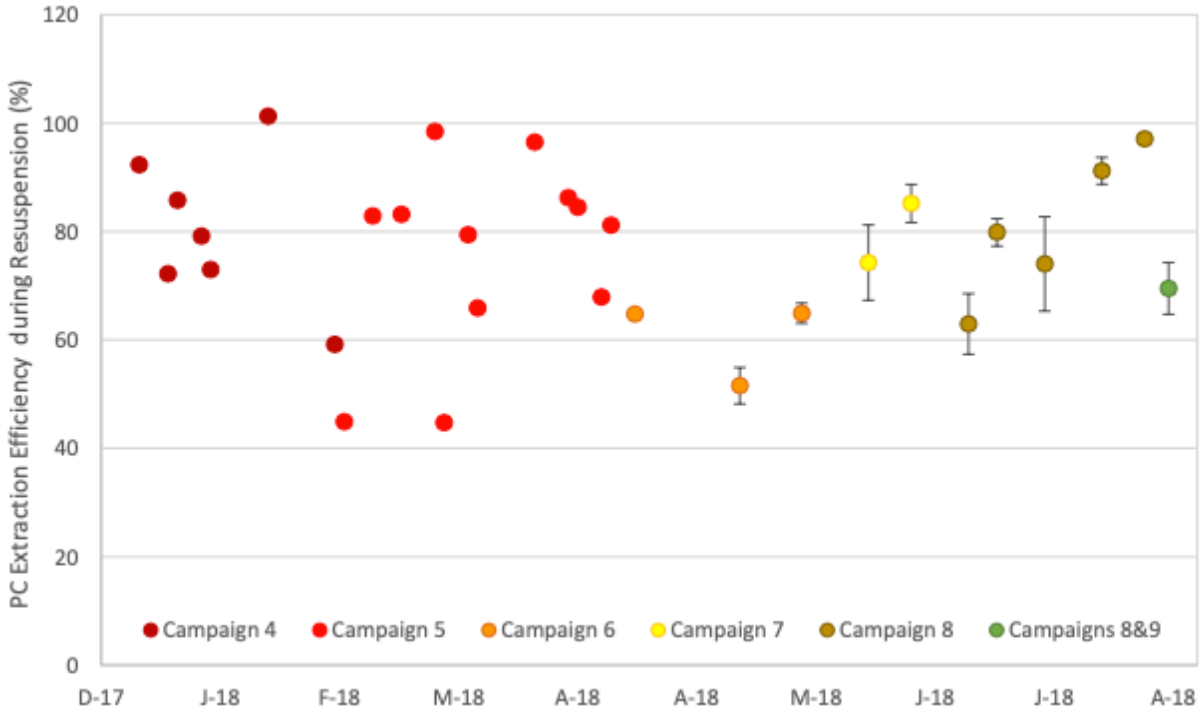

Figure 7-9. PC Extraction Efficiency (%) from DEMO downstream batches during tank resuspension starting Campaign 4 (processed starting January 2018). From mid-Campaign 6 to the end of DEMO, several dried biomass batches were combined prior to resuspension in attempts to mitigate variability; values represent the average extraction efficiency (% ±SD) of the combined batches run. A trend of increased extractability was seen as the campaigns progressed with the combined batches.

From mid-Campaign 6 to the end of DEMO, dried biomass from several harvests with the same dehydration parameters were combined and re-suspended together to mitigate variability in extraction efficiency. There appeared to be a trend showing increased extractability as the campaigns progressed with the combined batches. PC loss calculated at the resuspension stage was only 1.3%, resulting in a PC yield of 98.7%. While PC was not completely extracted from the cells, "total PC in" closely matched "total PC out" of the tank indicating minimal PC loss to degradation. The fraction of PC lost due to incomplete extraction showed up in the post-extraction centrifuge sludge. Investigations into the root cause of biomass 'resiliency' to lysis and PC extraction were then conducted, as summarized below.

Extraction Optimization

As discussed above, there was substantial variability in the efficiency of PC extraction from dried *Arthrospira* biomass. Multiple experiments were therefore performed to test several key variables hypothesized to enhance PC extraction. Experiments were conducted at lab scale using an assay developed to simulate the downstream extraction process from dehydration through resuspension/extraction. Due to scalability constraints, the centrifugation step was not included in the lab process, therefore a 5% PC loss was assumed. For this work stream, pre-dried AB2293 biomass (from DEMO), and/or fresh culture obtained from the PDU were used. The fresh biomass collected from PDU PBRs was dewatered indoors using the Screening Tub as per standard DEMO procedures (i.e., 21 µm mesh, RO water rinse, under vacuum). Note that no 1st-stage dewatering at harvest (i.e., LSS) was performed. Moisture content and PC of the dewatered biomass were taken as the 'T=0' values for yield calculations. Samples for microscopic analysis were also taken to look for cell lysis and/or PC leakage at this stage.

Extraction efficiency (%) was calculated at the end of dried biomass resuspension by dividing the supernatant PC by the total PC in the sample (i.e., supernatant PC + cell PC), such that if all of the PC was out of the cells, extraction efficiency would be 100%. PC loss during dehydration was calculated by dividing total PC of dried biomass at end of dehydration by total PC at 'T=0' (dewatered biomass), such that if these values matched, PC loss would be 0. PC loss during centrifugation was assumed at 5% (i.e., as hold-up volume of centrate coming out with the waste sludge).

Specific experimental details for the process optimization R&D efforts are provided below.

Resuspension tank heating and longer resuspension duration

For this experiment, pre-dried biomass from Campaign 4 (harvested December 2017) was used: i) batch D048, which had good PC extraction (>95% efficiency); and ii) batch D049, which had poor PC extraction (<60% efficiency). Both batches had been dehydrated for 48 h at 49°C (120°F). The biomass was resuspended in flasks incubated at 22°, 35° and 40°C, for 8, 12, 24 and 36 h to determine whether increasing resuspension temperature and/or time improved PC extraction from resilient biomass.

Dried biomass from batch D048 (previously demonstrated to be easily extracted) showed nearly 100% PC extraction regardless of resuspension temperature or time, with the exception of the 8 h resuspension at 22°C, which had an extraction efficiency of 86% (Figure 7-10). Extraction

results at standard operations (22°C for 16 h) from this experiment were consistent with previous lab results ("Lab 16 h" in Figure 7-10) and DEMO results. Dried biomass from batch D049 (previously demonstrated to be resilient to extraction) did show moderate improvements in PC extraction with increased temperature and resuspension duration, but there was not a large difference between 24 *vs* 36 h, or between 35° *vs* 40°C, and did not achieve the targeted ≥ 95% extraction efficiency (Figure 7-10).

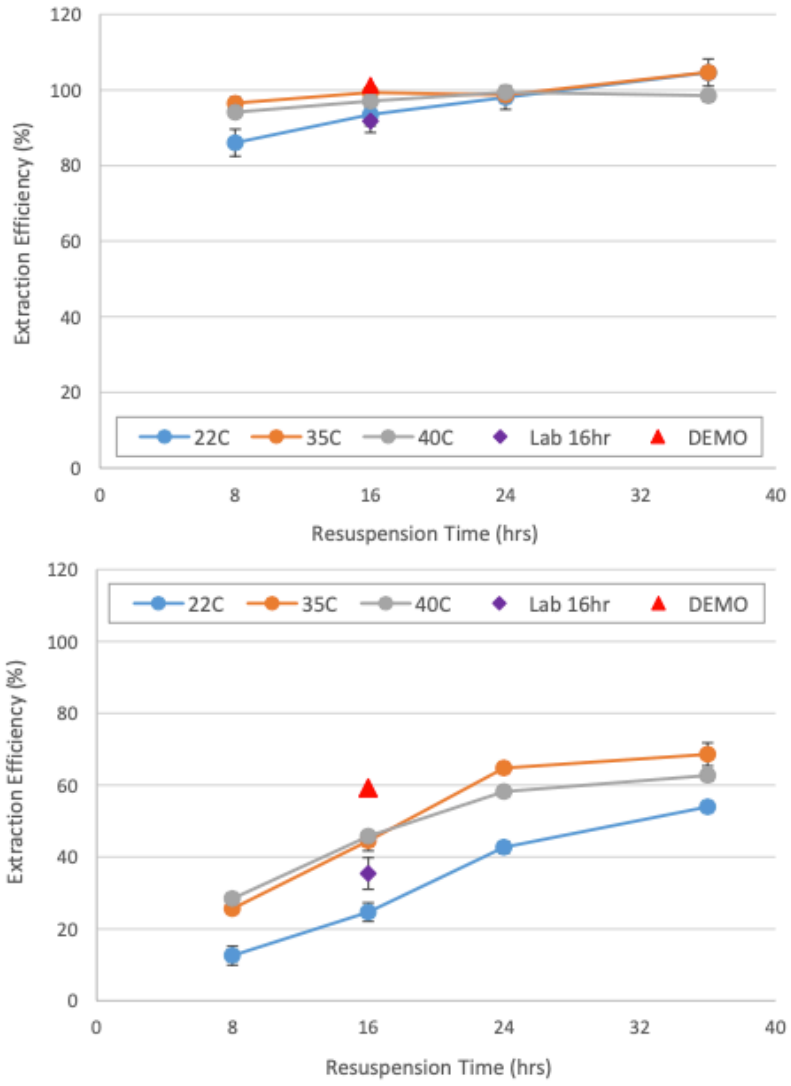

Figure 7-10. PC extraction efficiency (% ± SD) of DEMO dehydrated biomass from batch D048 (top) and batch D049 (bottom) during resuspension at various temperatures and durations. Extraction was compared to previous lab-scale ("Lab 16 h") and DEMO efficiencies conducted at standard operations (16 h resuspension at 22°C).

Enhanced lysis procedure and shorter dehydration duration

A side project was conducted at Algenol using internal funds to develop an enhanced cell lysis procedure to enable more complete and consistent extraction of PC from *Arthrospira*. A related

work stream was also conducted to determine whether shorter drying times improved PC extraction and/or mitigated PC loss during dehydration.

For these experiments, fresh *Arthrospira* biomass was harvested from PDU PBRs and dewatered as described above. After dewatering, the biomass was split in two: one sample was resuspended in phosphate buffer as described above ("control protocol"), and the other sample was subjected to an additional treatment step to facilitate cell disruption (referred to in this section as the "enhanced lysis protocol"). Biomass samples from these treatments were placed on trays and dried for various lengths of time (3 through 24 h) in the Excalibur dehydrator. A total of eight experiments using the enhanced lysis protocol *vs* the control protocol were conducted.

Standard resuspensions (i.e., 22°C for 16 h in the dark while continuously agitated) were performed with the treated and untreated (control) biomass from each drying interval to generate a PC extraction curve. The enhanced lysis protocol resulted in 100% PC extraction at all dehydration times tested from 4 to 24 h (Figure 7-11).

As mentioned previously, PC extraction from untreated biomass was variable from batch to batch, with most batches showing resiliency and incomplete extraction. In one experiment, the untreated biomass had very good extraction (near 100%), which is included in the data plotted below (Figure 7-11) to highlight the variability (large error bars) that was likewise observed at DEMO. Interestingly, untreated biomass after 6 h drying showed higher extraction, supporting the hypothesis that longer dehydration times may be adversely impacting cell lysis and extraction (at least for untreated biomass). On the other hand, the enhanced lysis protocol produced very consistent lab results, showing 100% PC extraction on nearly all biomass samples, including that dried for short (very wet) or long (very dry) periods of time.

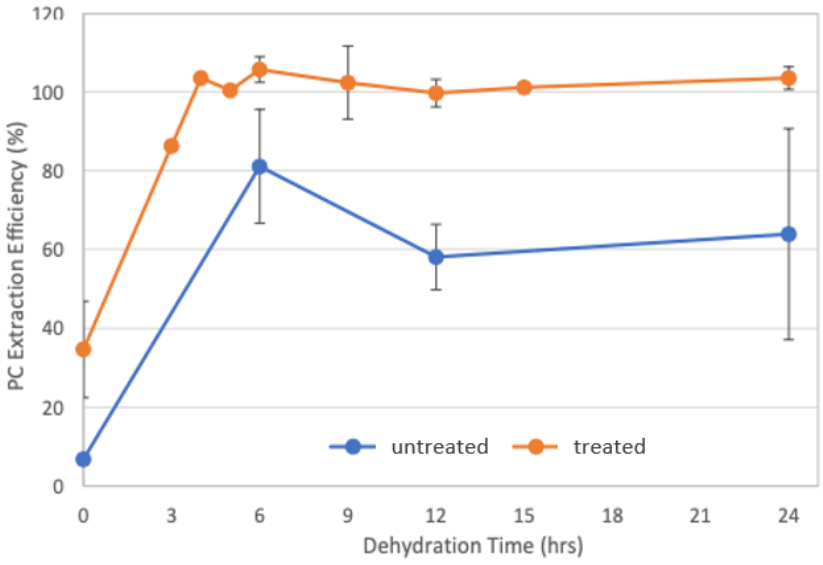

Figure 7-11. PC extraction efficiency (% ± SD) post-resuspension of treated and untreated biomass dehydrated for various lengths of time. Dewatered treated and untreated biomass, represented above as '0' dehydration time, were resuspended without drying, which resulted in low extraction efficiency.

DEMO validation

For the final experiment, a validation of the improved resuspension and extraction procedure was conducted at pilot scale using the DEMO downstream processing equipment. Biomass from PDU VIPER PBRs was dewatered and treated to achieve a final buffer concentration of 0.2 M in a biomass resuspension concentration of 12.5% (w/w). The dewatered biomass was dehydrated in the Harvest Saver unit for 24 h on lined solid trays at 49°C (120°F). The dried biomass was resuspended in a 7-gal tank in RO water, and mixed with the DEMO propeller mixer for 16 h in the dark. After 16 h, the biomass was sampled for pH and PC content (whole cells and supernatant, diluted 10x in 0.1 M buffer) to determine extraction efficiency.

Using the DEMO equipment, 98% PC extraction efficiency was achieved (Table 7-2). The lab comparison (12.5%) resulted in 100% PC extraction. As in previous experiments, the drier biomass (i.e., dried 24 h), typically resulted in lower dehydration loss (due to uniformity of biomass moisture) and lower resuspension loss (due to slurry homogenization). In this experiment, the lab 12.5% resuspension in the beaker showed slightly higher PC loss, reflective of the 'non-optimized' concentration used. The DEMO yield was on target at 80%, lending confidence to the scalability of the procedure.

Table 7-2. PC loss at each extraction stage, total PC loss, and overall PC yield for treated biomass dried for 24 h in the Harvest Saver (HS) dehydrator. Lab resuspensions were performed in beakers with rigorous agitation (stir bars). Centrifuge loss was assumed at 5%.

Treatment	Dehydration PC loss	Resuspension PC loss	PC not extracted	Centrifuge loss	Total PC loss	Overall PC Yield
12.5% lab	3.9%	12.6%	0%	5%	21.5%	78.5%
12.5% DEMO	3.9%	9.2%	2.0%	5%	20.1%	79.9%

4. Centrifugation of Extracted Biomass

Once PC was extracted from the cells, the diluted resuspension slurry was sent through a continuous centrifuge (GEA Westfalia SC-35 Disc-Stack, intermittent discharge) to remove cellular debris from the PC solution (see Table 7-3 for standard operational parameters). A total of 140 gal was processed through the centrifuge at 10 GPM for each batch (100 gal resuspension slurry + 40 gal resuspension tank flush). During DEMO operations, centrifugation parameters were optimized, including; solids ejection interval and bowl prefill duration, which produced highly clarified centrate (> 98% solids removal) and high solid compaction to minimize PC loss. On average, 133 gal of PC centrate (which was sent to the microfiltration unit) and 10.8 kg of concentrated sludge was produced per batch. A CIP of the centrifuge was conducted after each batch using a programmed protocol, where an RO water recirculation rinse, along with caustic and acid recirculation cycles were performed. Regular bowl inspections and additional manual cleaning were performed as needed.

Table 7-3. Standard operational parameters of the DEMO centrifuge (SC-35). There were three main stages of centrifugation that included: i) processing the PC slurry from the resuspension/extraction tank; ii) a 40 gal RO water rinse of the resuspension/extraction tank that was passed through the centrifuge (which also served to flush the centrifuge); and iii) waste recirculation, where the waste tote was diluted to ~500 L and recirculated through the centrifuge.

Centrifuge Parameter	PC slurry from tank	RO Water Rinse	Waste Recirculation
Processing Flowrate	10 GPM	10 GPM	20 GPM
Ejection Interval	3 min	4 min	2 min
Prefill Time	8 s	10 s	3 s
Centrate Backpressure	65 PSIG	65 PSIG	65 PSIG
Hood Flush	No	No	No
Cyclone Flush	No	No	No

5. PC Purification and Concentration

After separation of the residual biomass, PC was purified and concentrated through microfiltration and ultrafiltration steps.

Microfiltration (MF)

Any fine-solids debris remaining in the PC solution after the centrifugation step was removed through dead-end MF (Rosedale housings) in a decreasing pore-size filtration array of 0.5 µm, 0.45 µm then 0.2 µm, to increase overall purity and prevent fouling of ultrafiltration (UF) membranes. Permeate flow rates were tracked (as membrane flux in LMH) over the process to ensure proper filtration and operational efficiency. A typical batch (~133 gal) took ~3 h to process. An average of 153 gal clarified PC supernatant ('permeate') (including rinse volume) was produced from each batch. CIP of the membranes with acid and base solutions took place daily after processing was complete, however on average, the filters needed replacement over time due to severe fouling and clogging.

It is worth noting that the dead-end MF system used at DEMO resulted in large hold up losses and excessive filter use, and is not representative of commercial designs. Therefore, we began using a ceramic cross-flow MF unit from Novasep that is analogous to commercial design (Figure 7-12). Protein solutions are notoriously difficult to microfilter as they can create gel layers on or within membrane pores leading to reductions in flux and eventual clogging; therefore, maintaining a consistent flux is essential to efficient operations, especially at scale. Using a 0.45 µm ceramic membrane, permeate flux was maintained at relatively high levels with periodic, automated back pulsing. Additionally, using diafiltration to wash PC from the concentrated solids resulted in up to 95% PC recovery. Permeate from the ceramic system used as feed into the UF system showed very similar performance to that of feed from dead end filtration, and full recovery of clean water flux post-CIP of the ceramic membranes was demonstrated.

Figure 7-12. Ceramic cross-flow microfiltration (MF) unit leased from Novasep that is analogous to the commercial design.

Ultrafiltration (UF)

The clarified PC permeate was then further purified (primarily to remove salts) and concentrated using 2-stage ultrafiltration involving: i) primary concentration: using UF-1 spiral wound membranes (Alfa Laval, 10 kDa; Figure 7-13); and ii) secondary concentration using UF-2 hollow fiber membranes (General Electric, 10 kDa). Ultrafiltration took place across two days, where the retentate from UF-1 was stored at 4°C in the dark until processed. On average, 33.5 kg of post-diafiltration retentate was produced from UF-1 per batch at a PC concentration of 9.8 g-PC/L. Two concentrated 'liquid PC' streams were collected from UF-2: i) retentate, where an average of 3.5 kg was collected per batch at 12.4% solids at 73.0 g-PC/L; and ii) residual, where an average of 1.9 kg was collected per batch at 5.5% solids at 27.5 g-PC/L. In all, a total of 176 kg liquid PC retentate and 73 kg liquid PC residual were produced during DEMO from Campaigns 4 through 9. The calculated average E1% at 620 nm for the retentate and residual PC streams generated from UF-2 were 32.7% and 32.1%, respectively. CIP of the membranes took place daily after processing was complete (see Batch Plans for details). Liquid PC was stored at -20°C.

Figure 7-13. Alfa Laval ultrafiltration (UF) pilot system used at DEMO.

Task 7 Summary

- Dewatering studies were conducted with advanced strain *Cyanobacterium* sp. AB1166 cultivated outdoors with the objective of minimizing continuous centrifugation power draw while maintaining a high separation efficiency by means of altering feed solids content, feed flow rate, and bowl ejection intervals.
- Various tangential flow filtration (TFF) membrane types were tested under different operating parameters to identify conditions that enable energy-efficient harvesting and dewatering of AB1166 to achieve a solids content sufficient for use as an HTL feed.
- HMB data from centrifugation and TFF studies were provided as inputs to the TEA and LCA teams.
- Based on HTL experiments conducted at RIL and NREL using *Cyanobacterium* sp. AB1 and AB1166 biomass, a BFI yield of 38% ± 2% (w/w) was determined to be a representative value for biomass conversion *via* non-catalyzed HTL.
- In work partially supported by ABY2 funds, downstream processing of *Arthrospira platensis* biomass was performed at pilot scale to produce phycocyanin (PC) for use as a food colorant. This co-product could help support the economics of an initial algal biofuels biorefinery. A process was defined that could be scaled to commercial scale at competitive production costs. Residual biomass after PC extraction was converted *via* lab-scale HTL to BFI at a yield of ~40% (w/w).

Task 7 Milestones

Subtask Topic	Milestone Number	Milestone Description	Milestone Verification Process	End Quarter
Optimize dewatering	M7.1	Dewatering energy targets achieved and approach validated	Algenol delivers dewatering unit operations to 8.0. Initial unit operation HMB delivered to TEA team	11
Outcome: **Completed.** Centrifugation- and filtration-based dewatering steps optimized for energy efficiency. HMB results delivered to TEA team (Algenol and GIT).				
Optimize HTL	M7.2	HTL BFI yield, quality and economic targets achieved	Algenol delivers HTL unit operations and HMB to 8.0.	12
Outcome: **Completed**. Bench-scale HTL of *Cyanobacterium* sp. (AB1 and AB1166) and *Arthrospira* biomass completed by RIL and NREL scientists to determine BFI yields and quality. Data provided to TEA and LCA teams to assess economic and environmental aspects of algal biofuel production.				
Operate PC extraction unit	M7.3	*Cyanobacterium* sp. and *Arthrospira* phycocyanin extracted and characterized	Algenol verifies PC product and delivers extraction process and performance data.	10
Outcome: **Completed.** Process and equipment for phycocyanin (PC) extraction developed, optimized, and implemented at pilot scale. Although methods were developed for PC extraction from *Cyanobacterium* sp. strains, the primary focus was on *Arthrospira* because it is the only currently approved source of PC for use as a food colorant, which represents the primary market. PC samples met quality specifications and were provided to potential customers for business development purposes.				

Task 8 – Integrated operation and commercial assessment

Task 8 Objective

The main objective for Task 8 was to demonstrate integrated operation of improved, semi-continuous cultivation protocols and energy-efficient harvesting operations (determined in Task 7) at the 4,000 to 20,000-L scale, using the enhanced strain (AB1166) with improved biomass yield and dewatering traits. *Arthrospira* cultivation and downstream operation was demonstrated at this scale (24,000 L) in Task 6 above. The main goal was stable operations and use of the results to finalize the TEA and LCA models, assess co-product economics and potential, and identify remaining opportunities and challenges with operating a commercial facility for the production of algal biomass-based biofuels. An additional objective of this task involves documentation of all ABY2 project results in this final report

Expected outcome: Integrated system demonstrated at scale. Targeted values attained for TEA and LCA for algal BFI and co-products.

Task 8 Activities

Integrated Operation Demonstration

During this phase of the project, advanced strain *Cyanobacterium* sp. AB1166 was cultivated outdoors at a scale large enough to demonstrate operability under commercially-relevant

conditions, with downstream operations integrated to the daily harvest provided by the production field. Though the main focus of this work stream was operability, the specific objectives for Subtask 8.1 are:

1. Reconfigure DEMO Area 100 for advanced strain AB1166 cultivation and biomass production, and demonstrate successful system commissioning prior to inoculation.
2. Demonstrate stable cultivation and harvest under semi-continuous operations with the improved strain AB1166 at expected productivity yields.
3. Optimize biomass dewatering operations with AB1166 using both centrifuge and membrane separation options.
4. Demonstrate integrated cultivation and dewatering operations at scale for ≥ 7 consecutive days.
5. Using the integrated process, generate samples for NREL for HTL conversion.
6. Finalize TEA and LCA models based on generated data that includes identification of economic and environmental challenges and opportunities for algal biofuel and co-product commercialization; compare to open pond cultivations.

Field Cultivation Operations

Strain *Cyanobacterium* sp. AB1166 was cultivated in a new ~6,000-L PBR array from June through August 2019 (Figure 8-1). The Inoculum Array platform consisted of 55 inter-connected VIPER 3.4 PBRs in which culture liquid was circulated via turnover loop with a positive-displacement pump (Moyno). The array was inoculated twice, first on June 26, 2019 which cultivated continuously for 15 days with 11 harvests, where resulting cultures were used to optimize dewatering operations, then again on July 25, where integrated operations from cultivation to downstream dewatering at scale were demonstrated over nine consecutive days. There were some cultivation differences during this phase of the project based on the platform that was available for use: these included: i) orientation – PBRs faced north-south instead of the east-west orientation used for the productivity milestone experiment (Figure 4.1); ii spacing – PBRs were at a height to space ratio of 4:1, closer together than the previous 2.4:1 spacing; iii) circulation – turnover loop and pump instead of airlift; and iv) nitrogen source – nitrate instead of urea was used in the second inoculation. Table 8-1 and the text below summarizes the details and conditions for both AB1166 cultivations. The north-south orientation of the PBRs results in a 5-10% lower yield during the summer months compared to an east-west orientation. (Legere, 2017). The 4:1 spacing should yield a 10-15% boost in productivity on an annual basis, although we can say that with certainty only for the summer months. Our goal here was to determine productivity levels within that band of uncertainty to be sure our assessment of operability is valid.

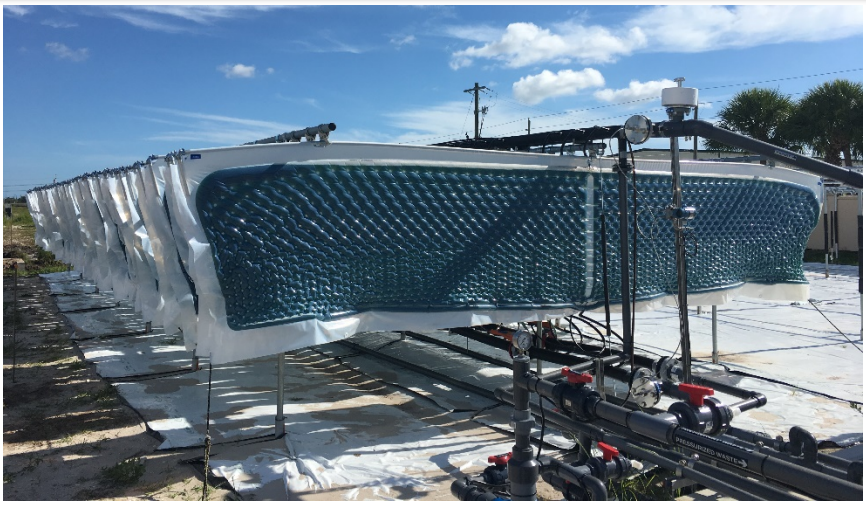

Figure 8-1: 6,000-L PBR Array fully inoculated with AB1166 culture. PBR faces are in a north-south orientation.

Scale-up

For both scale-up trains, AB1166 was grown in three 22-L flat panel "COBRA" PBRs supplied with CO_2-enriched air at 3.34 SLPM flow rate on the PDU pad under standard cultivation conditions analogous to the previous project phases. The only change included the COBRAs facing a N/S orientation (i.e., same as in the production field). Modified BG-11 medium using on-site saline well water was used. The COBRA cultures were inoculated in tandem through the inoculum port in the turnover loop.

Table 8-1: System and PBR parameters and cultivation conditions for AB1166 in the 6,000-L PBR Array.

Parameter	Description
Strain	*Cyanobacterium* sp. AB1166
Target inoculation density	0.3 sOD (3 PBRs)
Cultivation Platform (Area 100)	55 inter-connected PBRs, circulated by pump through turnover loop
PBR Type	VIPER 3.4, 3/8" liquid in and 5/8" liquid out tubing
PBR Plastic	CNX 130.23 (with TiO_2), patched over square tee
Diffuser	Laser perforated tubing
Total system volume (55 PBRs)	5843 L/1544 gal
Cascade interval volumes	3 PBRs = 340 L/90 gal (Appendix A)
	12 PBRs = 1295 L/342 gal (Appendix A)
Turnover pump	Moyno-style, positive displacement
Turnover pump rate - cultivation	3 PBRs = 3 LPM 12 PBRs = 12 LPM 55 PBRs = 55 LPM
Turnover pump rate - harvest	60 LPM
PBR flow rate - cultivation	1 LPM/PBR
System turnover rate	1 h 46 minutes
PBR Orientation	N-S
PBR Spacing	4.4:1
Diffuser Airflow	14 SLPM per 20-ft PBR

CO_2 Headspace	Set point PID; daytime initiated 1 h post sunrise, nighttime initiated 1 h pre-sunset, adjusted as necessary based on pH Day 1: cascade 1&2, grow-up: daytime = 0.5% (5,000 ppm), nighttime = 0.25% (2,500 ppm) Day 2: cascade 1&2, grow-up: daytime = 1% (10,000 ppm), nighttime = 0.5% (5,000 ppm) Day > 3: daytime = 2% (20,000 ppm), nighttime = 1% (10,000 ppm)
Target pH	7.3 (pH probe installed in turnover loop for continuous monitoring)
Gas Sterilization	0.2 µm micro-glass filter with a polyester felt backing (HEPA rated at 99.97% removal efficiency at 0.3 µm)
Medium	SW base, BG-11 nutrient medium
Medium Sterilization	0.2 µm PES filter
Nutrient dosing	Daily/bi-daily P dose
Cultivation Operations	Semi-continuous, daily morning dilutions based on OD delta, baseline density = 2 sOD (~0.6 g/L)
PBR cooling set point	Inoculation 1: no cooling set point, Inoculation 2: cooling set point at 38°C
Dye PBRs	On south side of cascade intervals (after PBRs 3 & 12) at ~4 sOD
Ground cover	White reflective film
Medium recycle	No
Gas recycle	No

System CIP

A robust acid-only CIP (peracetic acid (PAA) + sulfuric acid) was conducted prior to the first inoculation since the PBRs were new, and a full robust CIP (base + bleach followed by PAA + sulfuric acid) was conducted prior to the second inoculation. Oxidant and saline well water metrics were measured only in the first 3 PBRs, the other PBRs were backfilled with filtered freshwater until the cascade occurred. No residual chemicals were observed in the Go/No-Go metrics from the field prior to inoculation.

Field Operations

Three interconnected PBRs were initially inoculated from COBRA PBRs at a target inoculation density of ~0.3 sOD. The system was designed to support a cascade inoculation process with 3, 12, and 55 PBR intervals to decrease the amount of inoculum required. The culture grew up in batch mode to a given density before being passively cascaded to subsequent PBRs by opening isolation valves. Each cascade interval resulted in a ~4-fold culture dilution (i.e., 3 PBRs to 12, 12 PBRs to 55), with a target density post-cascade of ~0.3 sOD. The culture was grown in batch mode to a density > 2 sOD to begin daily dilutions. Semi-continuous operations with daily morning harvests were performed if the culture was > 2 sOD, where the culture was diluted back down to 2 sOD (~0.6 g/L biomass) baseline. The turnover loop was sampled daily for sOD to determine the volume of culture to harvest.

The medium used was a modified BG-11 in saline well water base (Table 8-2). Fresh 1x medium was made up in the tank every 2-3 days. Saline well water was added to the 1x medium tank on the MPP (main processing pad) ~ 24 h prior to use and recirculated for a minimum of 12 h prior to use to aerate and remove the sulfidic components. The dry nitrogen powder, either as tech-

grade urea (Inoculation 1) or tech-grade nitrate (Inoculation 2, Niterox) were added directly to the medium tank through a Silverson flash mixer. A concentration of 8-10 mM urea was targeted in the tank such that 2-5 mM urea would be added to the field daily based on the expected dilution volume, and the nitrate concentration in the 1x medium tank was 18 mM. The trace metal solution was made up in a 250x stock in RO water and dosed into the medium tank using a metering pump to the appropriate 1x concentration based on tank volume. During the second inoculation, the Fe concentration in the medium tank was doubled to 24.6 μM since it appeared Fe may have been consumed in the medium tank prior to use (Fe measured in the tank was typically below target) and/or filtered out after passing through the 0.2 um on the field processing pad (FPP).

Phosphoric acid (H_3PO_4) was added using a separate dosing system and tank on the FPP, which delivered directly into the turnover loop. Starting after the first cascade, 100 μM H_3PO_4 was dosed to the field daily from a 50 mM concentrated stock for the first inoculation, and every other day for the second inoculation. The concentrated stock was made up in softened water in the FPP tank once per week. The H_3PO_4 dose was delivered over 2 h (~1 system turnover) after the daily top-off was complete. The target was to have dissolved phosphate at or near zero, and particulate phosphate ≥ 50 μM/sOD.

Table 8-2: Modified BG-11 nutrient medium (at 1x) made in the medium tank during semi-continuous operations. Medium was made in on-site saline well water that had been recirculated to remove sulfidic compounds for ≥ 12 h. At several intervals during the second cultivation, more Fe was dosed directly into the field.

	Compound	Final concentration in the medium (mM)	
Macro-nutrients	Nitrogen source	8-10 mM urea (as CH_4N_2O)	18 mM nitrate (as $NaNO_3$)
	Phosphoric Acid (H_3PO_4) (liquid)	100 μM/dose from separate system on field processing pad (FPP)	
Trace metals	Citric Acid ($C_6H_8O_7$)	0.0312	
	Ferric Ammonium Citrate	0.0123 or 0.0246	
	$Na_2EDTA{\cdot}2H_2O$	0.00279	
	$MnCl_2{\cdot}4H_2O$	0.00915	
	$ZnSO_4{\cdot}7H_2O$	0.00077	
	$Na_2MoO_4{\cdot}2H_2O$	0.00161	
	$CuSO_4{\cdot}5H_2O$	0.00032	
	$Co(NO_3)_2{\cdot}6H_2O$	0.00017	

Upstream Results and Discussion

Inoculation 1; Provide biomass for downstream optimization

Two COBRA PBRs at an average of 2.65 sOD were used to inoculate the first three interconnected PBRs on June 26, 2019. The inoculation density in the field after the 2-h turnover time was 0.51 sOD. The grow-up and cascade process took 5 days, with the first dilution taking place on July 1. The culture was run in semi-continuous mode with daily dilutions for 11 consecutive days; the resulting culture was provided for downstream dewatering optimization operations.

The average overall productivity across 11 days was 14.9 g/m^2-d, which was lower than the ~30 g/m^2-d projected through modelling (Table 8-3). Since productivity was below the expected value for this time of year, several influencing factors were investigated. This cultivation used urea as the nitrogen source, where a total field concentration of 2-5 mM urea (equivalent to 4-10 mM ammonium) was targeted. Ammonium measured from the field showed concentrations upwards of 18 mM across several days during semi-continuous mode (data not shown). While this level has been tolerated well by AB1166 in previous lab and PDU trials, effective pH control at the distal surface edges of the PBRs at scale may not have been achieved and consequently a pH gradient may have been established. This high pH, paired with high ammonium concentrations, may have yielded conversion to ammonia that negatively impacted the culture. The average pH of the culture over 11 days was 7.32, measured by an in-line probe in the turnover loop, and right at target. However, mineral deposits on the PBR distal edges indicated bicarbonate precipitation, a symptom of high pH, and has also been seen in the past at larger scale with AB1. The high ammonium concentrations also appeared to be supporting a large bacterial population in the culture, which could also have influenced algal growth. No other contaminants, such as flagellates or ciliates, were observed.

The average daily integrated PAR during semi-continuous cultivation was 41.8 mol photons/m^2-d, with frequent afternoon rain storms. Given that a cooling system was not utilized, the culture temperature reached 44°C at one point, with several consecutive days above 40°C (data not shown). While this strain has shown tolerance to high temperatures, the strain may have been stressed during those particular days.

Another factor that could have affected low productivity was nutrient availability. While particulate phosphate overall what higher than target at 94 µM/sOD, Fe concentrations were typically at or near zero. While it is difficult to assess Fe limitation given that AB1166 may have luxury Fe uptake; chlorophyll and P_{max} measurements indicated some level of stress likely associated with nutrient limitation.

Given the above factors, several changes were made during the second cultivation in an attempt to mitigate any stress experienced by the culture which would lead to low productivity. These included: i) using nitrate as the nitrogen source instead of urea; ii) providing precautionary PBR cooling when 38°C was reached to avoid culture temperatures rising above 40°C; and iii) doubling the Fe concentration in the dilution medium.

Table 8-3: Environmental conditions, growth, harvest, and productivity averages for both field inoculations. Experimental values and annualized rates are shown for the indicated time period.

Inoculation	Duration (days)	PAR (mol photons/m^2-d)	Maximum Temperature (°C)	ΔOD/d	Biomass harvested (g/d)	Overall productivity (g/m^2-d)	Annualized productivity (g/m^2-d)
June 26, 2019	11	41.8	44	0.593	1,245	14.9	12
July 25, 2019	9	34.7	38	1.07	2,000	22.9	25

Inoculation 2; integrated cultivation and downstream processing operations

Three COBRA PBRs at an average of 3.36 sOD were used to inoculate the first three interconnected PBRs on July 25, 2019. The inoculation density in the field after the 2-h turnover time was 0.875 sOD. The grow-up and cascade process took 7 days, where the first dilution took place August 1. There was a lag observed in the grow-up phase of this inoculation due to an operational issue resulting in a missed H_3PO_4 dose and resultant P limitation. Once H_3PO_4 was added, the culture resumed expected growth. The culture was run in semi-continuous mode with daily dilutions for 9 days, where culture was provided for the downstream dewatering step for demonstration of integrated operations.

The average overall biomass productivity across 9 days was 22.9 g/m^2-d, which was comparable to that projected through modelling at 25 g/m^2-d (Table 8-3, Figure 8-2). The average daily integrated PAR over semi-continuous cultivation was below average by ~10%, at 32.6 mol photons/m^2-d (Figure 8-3), and since cooling was applied, the culture temperature did not exceed 38°C (data not shown). On one occasion (calendar day 215), the daily dilution could not be completed due to safety reasons, since a severe lightning storm was in the area.

The average baseline nitrate concentration in the culture medium was 9.7 mM, and the average particulate phosphate/sOD concentration was 49.6 μM/sOD, achieved by dosing the field every second day. Dissolved P in the medium was undetectable. As with the first inoculation, Fe concentrations measured in the field were at or near 0, therefore separate doses of just Fe were added directly to the turnover loop on 2 occasions; once during scale up and again during semi-continuous operations. Lower than expected Fe concentrations were also observed in the medium, therefore a CIP of the tank was performed to mitigate potential consumption by contaminants.

Photosynthetic parameters, modeling and annualization process

The algal cultures were monitored via oxygen PE (Photosynthesis-Irradiance) curve measurements and UV-Vis scans during the two experiments described in the preceding paragraphs. The PE curve data (Figure 8-4) were analyzed with the Webb Equation (Webb *et al*., 1974) to obtain photosynthetic parameters, P_{max}, E_k, and alpha (Figure 8-5 to 8-7). Note that the PE curves in Figure 8-4 all show essentially the same onset slope independent of temperature, thus indicating a limiting quantum yield (α) that is independent of temperature, a consistent observation for cyanobacteria in our laboratory. The rate at light saturation (P_{max}) is strongly temperature dependent indicating a strong temperature dependence for E_k as shown in Figure 8-7. Photoacclimation behavior of AB1166 is indicated by the correlation of E_k with average light (Figure 8-6); the slope of this curve is somewhat less than normally observed for AB1. Under the high light acclimated conditions, E_k was ~150 μmol photons/m^2-s, decreasing to ~60 μmol photons/m^2-s under very low light conditions. During semi-continuous cultivation (Day 5 to Day 14), the average P_{max} was 300 μmol O_2/L-hr, with some decline indicated over the 9 day run (Figure 8-5). However, the chl a/OD ratios displayed in Figure 8-5 are quite stable, indicating stable operation. The α values appear a bit low (table insert in Figure 8-7), but are not outside our experience with this strain. At the end of the semi-continuous run (Day 15) the experiment was continued in a batch mode, with one dilution at day 20, to generate biomass for other experiments (including HTL). During these later batch cultivations (Day 15 to Day 32), the average P_{max} was

230 µmol O_2/L-h (Figure 8-5). sOD (1 sOD = ~0.33 g/L) and Chl a/sOD are also shown in Figure 8-5, during the phase 2 experiment over 32 days. Under normal cultivation conditions, Chl a per sOD ratio is 6 to 7 mg/L for AB1166. Chl a/sOD below ~4 mg/L per sOD is likely an indication of culture stress by either temperature or nutrient limitation (see Day 1 to Day 4 in Figure 8-5).

The Algenol Productivity Model, discussed in more detail below, was used to annualize the experimental data with photosynthetic parameters used previously for the east-west orientation experiment in Task 6. The annualized rate was calculated from: Annualized rate = (Experimental rate)/(Model predicted rate) x (Model predicted FL annual rate). Temperature is generally accounted for *via* the E_k dependence shown in Figure 8-7, which is approximately Q10 = 2. The annualized rate is shown in Table 8-3 for semi-continuous operation as 25 g/m^2-d, which aligns well with experimental results. The annualized rate for two batch runs (from Day 15 to Day 20, Day 21 to Day 32) was 18 g/m^2-d, modestly higher than the batch reference productivity value of 15 g/m^2-d.

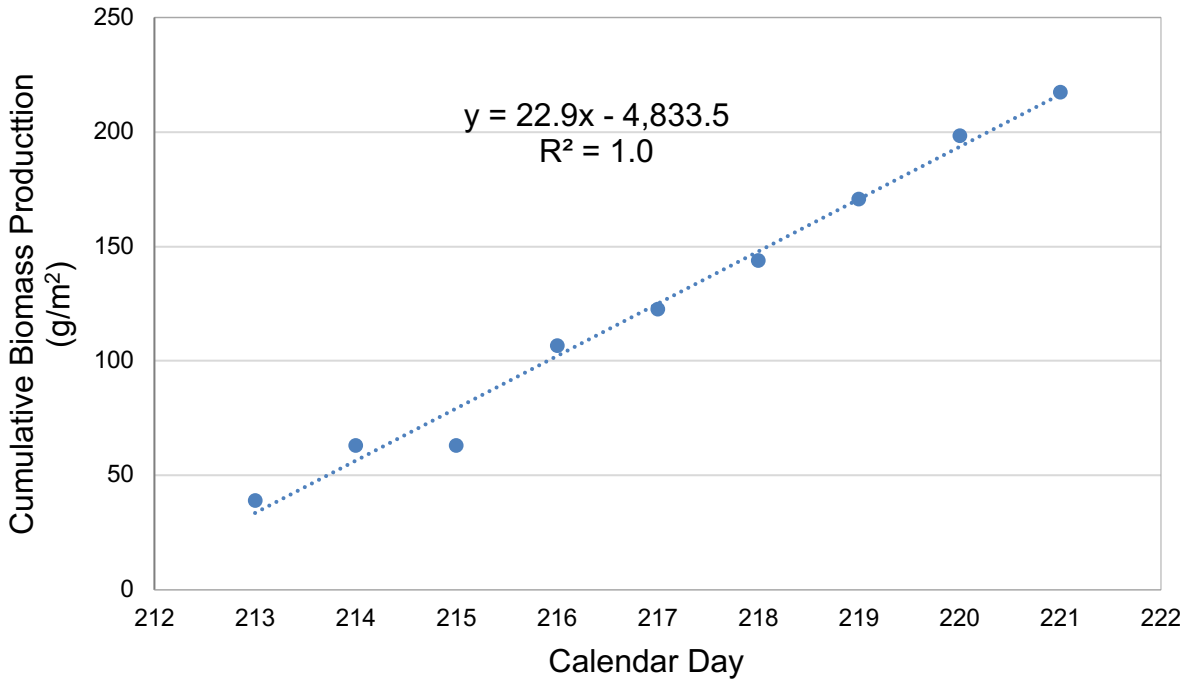

Figure 8-2: Cumulative biomass production (g/m^2) and overall daily productivity (measured as the slope of the line) over 9 days during the second cultivation. On calendar day 215, the daily dilution could not be completed due to safety reasons, since a severe lightning storm was in the area.

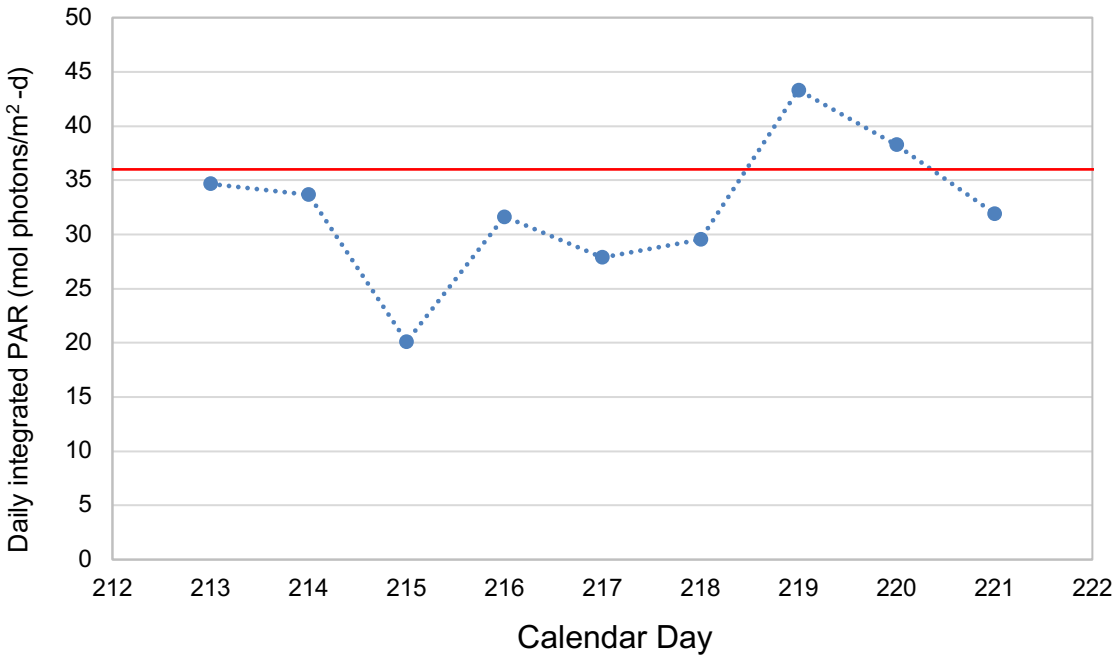

Figure 8-3: Average daily integrated irradiation (PAR) (mol photons/m^2-d), and the average yearly PAR for Fort Myers, FL for reference (red horizontal line).

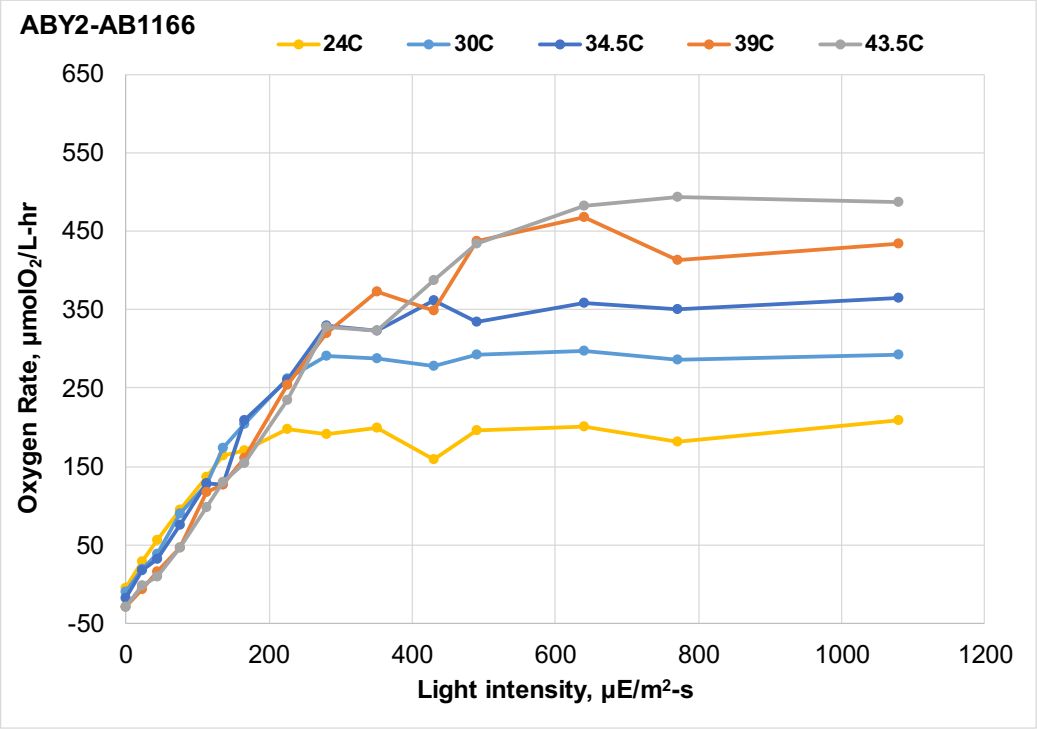

Figure 8-4: Oxygen PE curves of AB1166 at different indoor testing temperatures. Culture samples were taken from the outdoor PBR array on July-31 (Day-6) and diluted to k=0.1 cm^{-1} for testing in the MONK (automated PE curve measurement equipment).

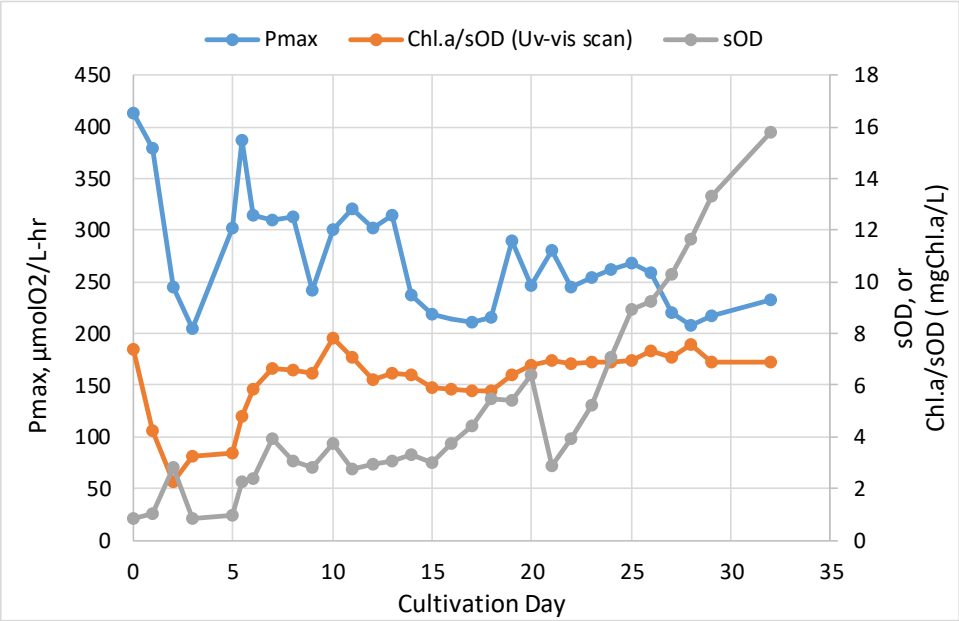

Figure 8-5: Photosynthetic parameter P_{max}, culture density (sOD) and Chl a content (Chl a/sOD) during the second AB1166 cultivation in Subtask 8.1. Day 5-14: semi-continuous operation, Day 15-20: batch-1 with a 2-fold dilution at day 20; Day 21-32 batch-2.

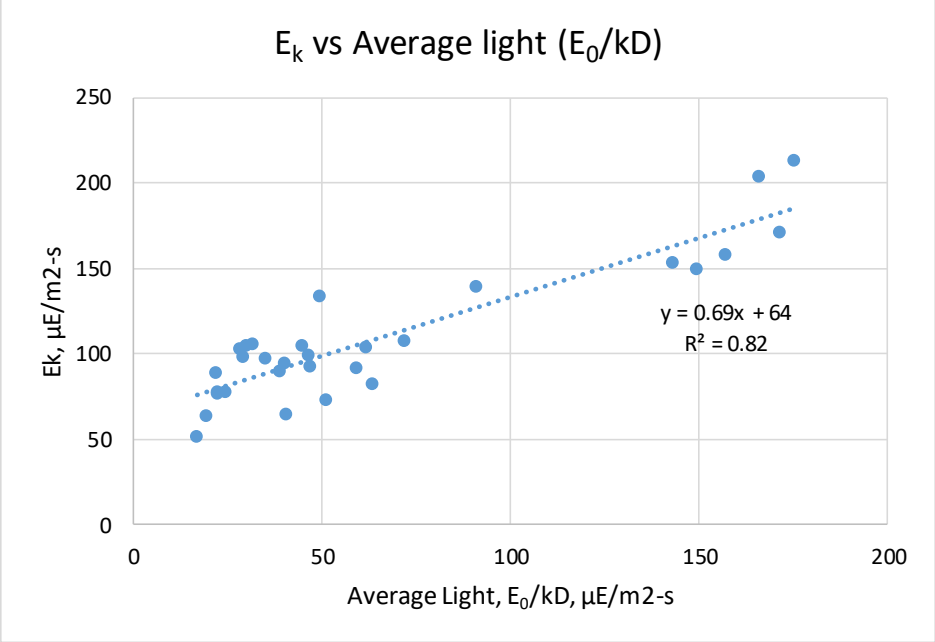

Figure 8-6: Light acclimation for AB1166: relationship between the photosaturation parameter (E_k) and the average light that the culture experiences.

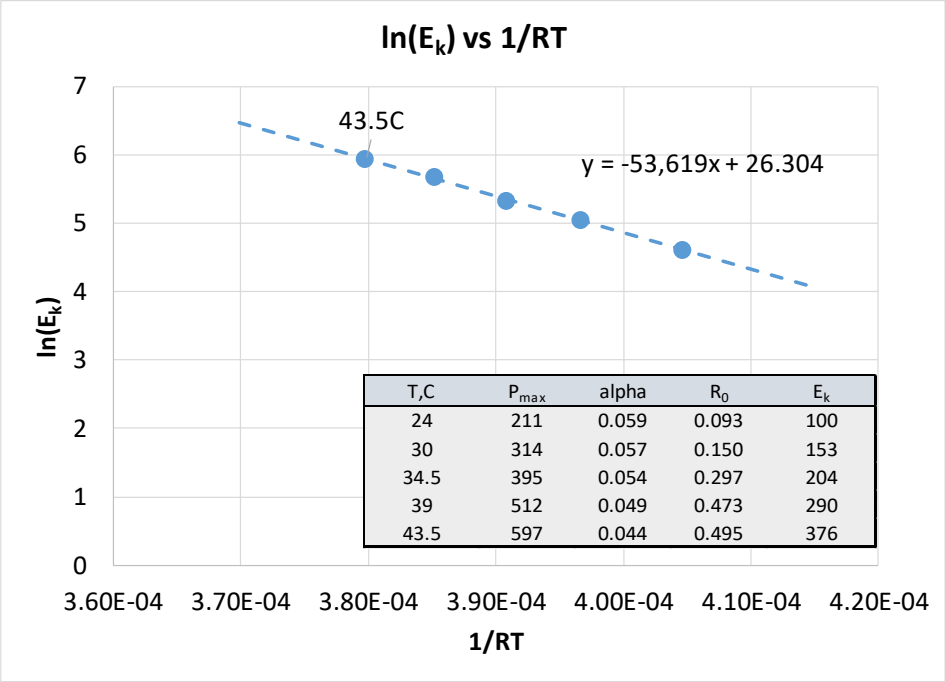

T,C	P_{max}	alpha	R_0	E_k
24	211	0.059	0.093	100
30	314	0.057	0.150	153
34.5	395	0.054	0.297	204
39	512	0.049	0.473	290
43.5	597	0.044	0.495	376

Figure 8-7 Arrhenius graph for the temperature dependence of the photosaturation parameter (E_k) for outdoor AB1166 culture samples (Webb Equation fitting analysis). Alpha (α), P_{max}, and R_0 values in the table are all shown on an O_2 (rather than carbon) basis.

Centrifuge operation

For the purpose of Task 8, the number of passes through the centrifuge was reduced to one. Centrifuge feed flow rate was maintained as fast as possible while still achieving the desired separation efficiency (as defined in Task 7). The bowl ejection interval was altered accordingly with the feed flow rate in order to maintain the separation efficiency. The purpose was to demonstrate stable operations of the centrifuge process integrated with daily input from the cultivation field.

Although a high feed flow rate was initially attempted, it was quickly determined that the incoming culture density (measured as sOD) was significantly higher than what was observed during the optimization runs in Task 7, therefore the feed flow rate needed to be reduced. Initially a 13 GPM flow rate was sufficient to achieve the desired separation efficiency; however, as the sOD trended upward, separation efficiency trended downward. In order to achieve a high separation efficiency (for further processing via the TFF), the harvest on 8 August was processed at a slower flow rate (7.5 GPM). A table detailing the parameters of the runs performed can be found below (Table 8-4).

Table 8-4: Separation efficiency and sludge solids content of different test runs.

Date / Run #	Flowrate (GPM)	Discharge rate (min)	Incoming sOD	Separation Efficiency (%)	Sludge Solids Content (%)
1 Aug / 1	20	1.5	4.93	75.4%	---
1 Aug / 2	15	1.5	4.67	74.9%	---
1 Aug / 3	15	1	4.20	97.7%	---

Date / Run #	Flowrate (GPM)	Discharge rate (min)	Incoming sOD	Separation Efficiency (%)	Sludge Solids Content (%)
2 Aug / 1	13	1	3.83	98.1%	7.15%
4 Aug / 1	13	1	3.99	89.5%	6.95%
5 Aug / 1	13	1	3.20	92.5%	7.11%
6 Aug / 1	13	1	3.37	94.7%	6.91%
7 Aug / 1	13	1	3.64	82.5%	5.00%
8 Aug / 1	7.5	1	4.00	99.1%	6.33%

A goal of this work stream was to try to achieve a target of ~20% w/w solids content. During optimization, however, we determined that we were not able to achieve anything greater than 9% w/w solids content; the average during optimization was ~7.5% w/w solids. During integrated processing, the average was ~6.6% w/w solids. With regard to power draw, the results described in Task 7 were confirmed by the operations performed in Task 8; as the centrifuge feed flow increases, the lower the specific energy required to operate the centrifuge.

Tangential flow filtration

The pre-test experiment with indoor cultures indicated better and more stable performance for the RC-100 kDa membrane compared to other membranes over a time scale of 240 min, the RC-100 kDa membrane was selected to carry out dewatering tests with the outdoor culture. At the end of all the experiments, we also checked the dewatering and concentration performance of PES-0.1 µm membrane, to confirm its faster fouling rate than RC-100 kDa membrane, especially in the case of higher concentrate biomass.

Tangential flow filtration operating conditions

The TFF membrane module could concentrate biomass sludge up to 20% (wt/wt), as claimed by manufacturer. However, during the period of July and August, we operated over 10 test ultrafiltration runs, and the highest concentration we obtained was around 12 to 15% (wt/wt). The system becomes unstable each time we attempted to concentrate the biomass further; we observed a rise in temperature, power usage and fluctuation in operating pressure and recirculation flow rate. The representative operating conditions for the August 1 run is shown in Figure 8-8. The rise in power usage was proportional to the increase in biomass concentration.

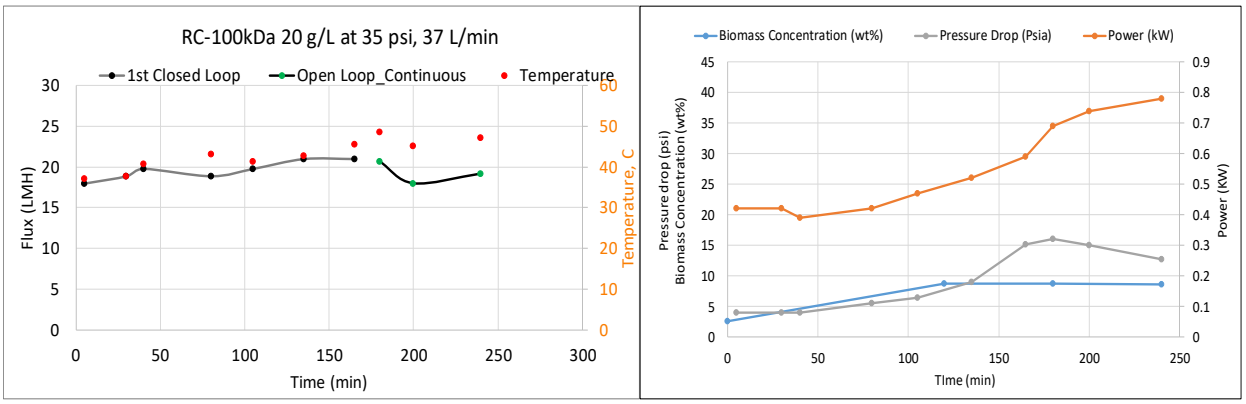

Figure 8-8: Permeate flux rate vs time at 35 psig, and recirculation flow rate at 37 L/min (~ 1 m/s).

Permeate flux rate vs concentration

From previous indoor culture dewatering tests, we noticed that the permeate flux rate decreases over time. It might indicate a cake layer had formed during the membrane dewatering process. This cake layer can be a function of biomass concentration, temperature, and recirculation rate. Figure 8-9 show the permeate flux rate at different biomass concentrations. At low concentrations, (0.1 to 0.2%), the permeate flux rate was stable around 40 LMH, whereas at higher concentrations (2-4 %), the permeate flux rate was about 20 LMH. When the biomass sludge concentration was above 10%, or when the membrane is fouled, the permeate flux rate could fall below 10 to 15 LMH.

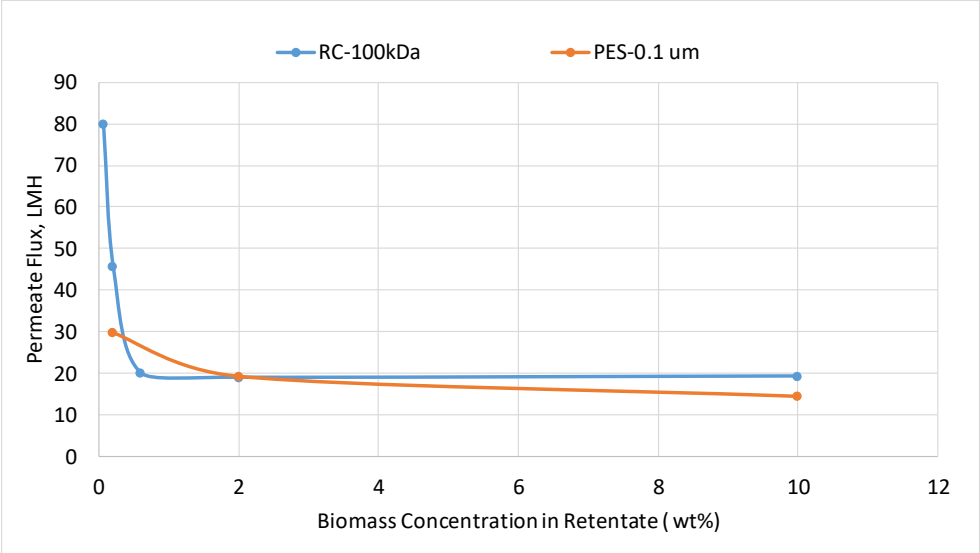

Figure 8-9: Permeate flux rate (pseudo-steady state) at different biomass concentration.

Diafiltration

Desalting algal biomass is beneficial for HTL since the salt concentration in the algal culture is around 3.5%. Diafiltration was used in an attempt to reduce the salt by 90%. The initial culture feed was processed in a closed loop to concentrate the biomass 3-fold to start the diafiltration process. However, due to the resulting high concentration of biomass (~8.3%), the recirculation rate was reduced. Subsequently, the biomass concentration was lowered to 5.8% for diafiltation. Diafiltration was carried out in continuous mode by adding one volume (1.3 L each) of RO water for each pass through the system; a total of five volumes of water was added and removed. After each cycle, the permeate sample was collected to monitor the reduction in conductivity and salinity. Figure 8-10(b) shows the change in salinity and conductivity of the permeate after each volume of RO water was added. The salinity and conductivity were reduced more than ten-fold after 3 h of operation.

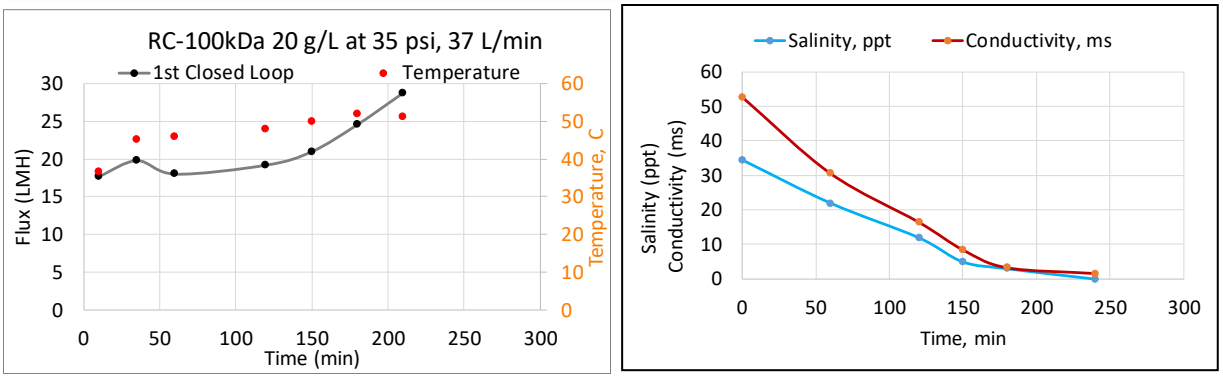

(a) (b)

Figure 8-10: (a) Diafiltration for 210 min pre-run (closed loop, without adding RO water); (b) Salinity and conductivity in diafiltration permeate over time (after adding 1.3 L RO water each half hour).

Energy Use and Cost of Biomass Dewatering

The energy use and overall cost of biomass dewatering for commercial scale (e.g., 2,000 acre) algal biocrude production, based on *Cyanobacterium* sp. strains, are very important components in techno-economic (TEA) and life cycle (LCA) assessments. Two stage dewatering technology was proposed to achieve the 15 to 20% (wt/wt) solids content target for the HTL feed.

The overall mass flow at a 60-acre module is shown below (Figure 8-11):

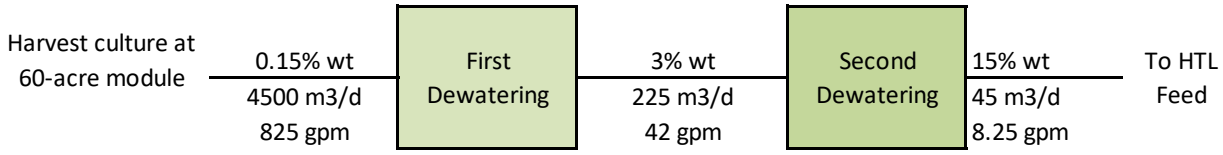

Figure 8-11: Process flow diagram of a 60-acre module for AB1 or AB1166 cultivation.

The first dewatering step could be accomplished with a hollow-fiber membrane or centrifuge, and the second dewatering step could utilize a TFF unit or continuous centrifuge. Based on the dewatering tests done by Algenol and with support from a commercial dewatering vendor (GEA) (Figure 8-12, Figure 8-13), we evaluated the dewatering cost for 60-acre module (Table 8-5) and a 2,000-acre facility (see Techno-Economic Analysis section below).

The energy usage in dewatering should be well controlled for biocrude production in terms of the LCA analysis. The heat content in dry algae biomass is about 6 kWh/kg biomass or 22 MJ/kg biomass. If we only choose centrifugation for dewatering, the dewatering energy expenditure would be about 13% the energy content of algal biomass. Therefore, dewatering primarily through centrifugation for biocrude production is not recommended, especially when harvest biomass concentration is below 0.15 wt% (1.5 g/L). On the other hand, membrane filtration as the first stage dewatering has great potential to reach the low energy dewatering target and has the added benefit of enabling culture medium recycle.

Table 8-5: Dewatering Process Design and Power Usage Analysis (60-acre module).

Dewatering Stage	Design	No. of units (GPM/unit)	CAPEX, Million $2019	Energy kWh/kg biomass	Vendor	Equipment Model
First Stage	Centrifuge	7 (120)	3.5	0.67	GEA	SST-400
First Stage	Hollow Fiber	6 (140)	2	0.33	Liquoflux	LF32AL22
Second Stage	Centrifuge	1 (120)	0.5	0.10	GEA	SST-400
Second Stage	TFF	1 (42)	1.3	0.09	Smartflow	7687-36
Total System	Centrifuge	-	4	0.77	-	-
Total System	Hollow Fiber + Centrifuge	-	2.5	0.43	-	-
Total System	Hollow Fiber + TFF	-	3.3	0.42	-	-

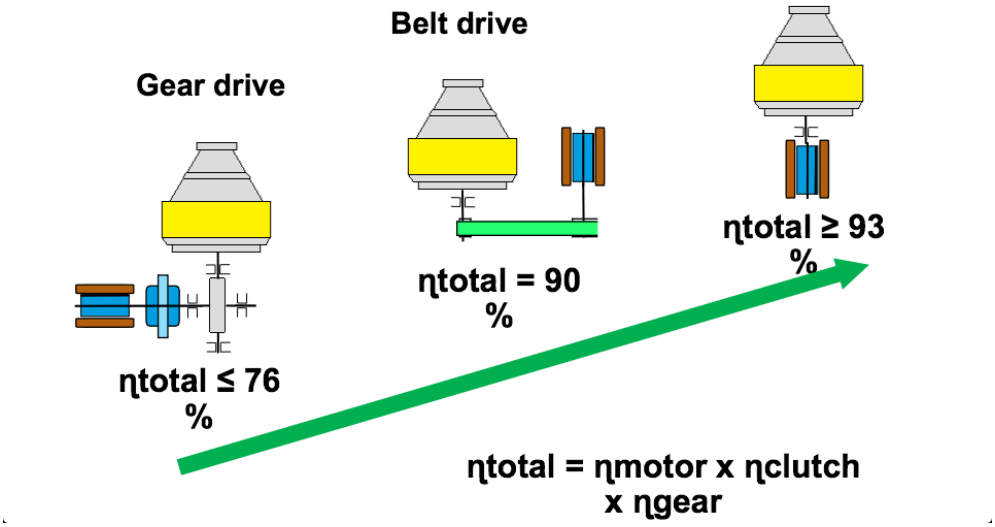

Drive system	Energy consuption / m3	Energy consuption / d at 120 m3/h
Gear drive	1.0 kWh	2,900 kWh
Flat belt	0.9 kWh	2,600 kWh
Direct drive	0.7 kWh	2,000 kWh

Figure 8-12: Power consumption for large scale centrifuges (4x SST-400 centrifuges for 120 m^3/h culture feed). Data provided by GEA.

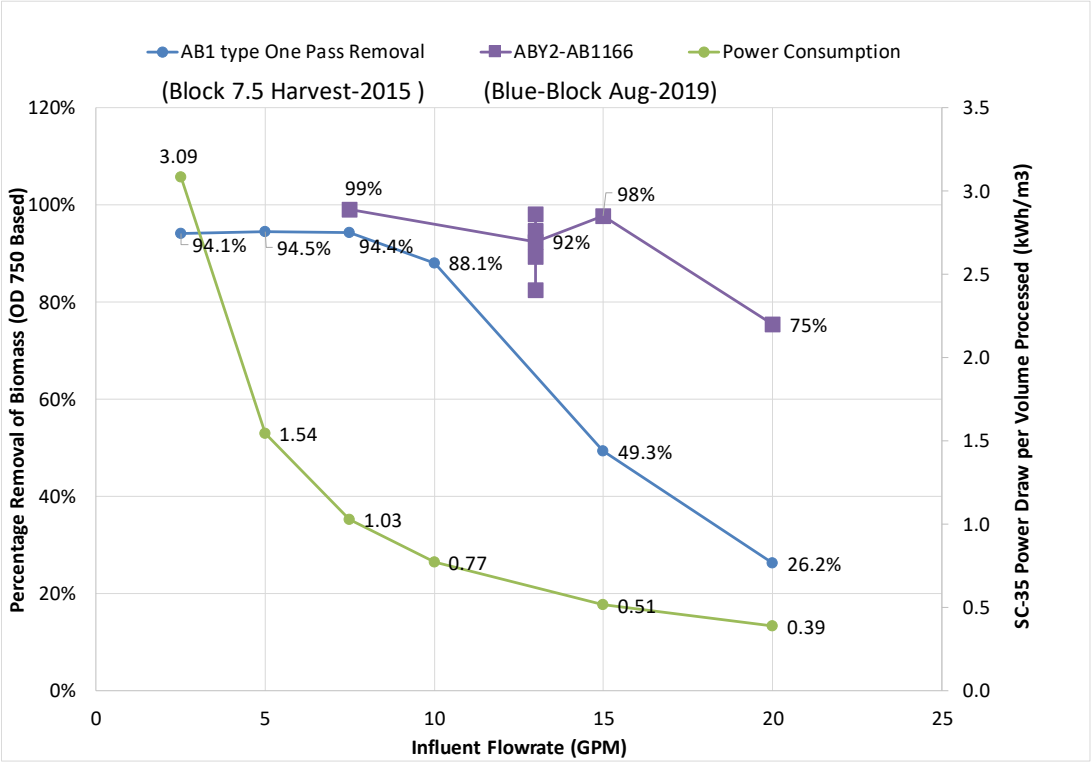

Figure 8-13: Power consumption from Algenol dewatering tests using a GEA SC-35 continuous centrifuge. Tested strains were Cyanobacterium sp. AB1 and AB1166.

The cost of the dewatering process can be calculated from the annualized CAPEX and OPEX. Power usage cost, membrane replacement cost, and maintenance cost are the major costs and are listed in Table 8-6 for 60-acre module. Power cost is calculated based on 0.05 $/kWh (same as for the Algenol 2,000-acre TEA), and membrane replacement cost is suggested from vendors (i.e., 5 year life time for hollow fiber filters and 3 year life time for TFF membranes). System maintenance is estimated to be 2% of long-term CAPEX (with a 20 year life time). The annualized CAPEX factor is 0.1. A hollow fiber + centrifuge option will provide the lowest dewatering cost, about 0.194 $/kg biomass.

Table 8-6: Dewatering Process OPEX and total dewatering cost analysis (60-acre module).

Case	***Design***	***Annualized CAPEX, $/kg***	***Energy $/kg biomass***	***Maintenance $/kg***	***Membrane replacement, $/kg***	***Total Dewatering Cost, $/kg***
1	Centrifuge	0.180	0.038	0.036	-	0.254
2	Hollow Fiber + Centrifuge	0.078	0.022	0.022	0.072	0.194
3	Hollow Fiber + TFF	0.089	0.021	0.030	0.095	0.235

Productivity Modeling, Annualized Productivities, and Comparison to Pond Cultivation

This section provides a summary of the Algenol Productivity Model aimed at understanding the productivities of cyanobacterial cultures at all scales. This model was developed and successfully applied to ethanologenic strains (Legere, 2017) and has now been deployed in this project for biomass production. The modeling efforts target understanding productivities in the laboratory, 2 mL through 1 L laboratory PBRs, as well as large outdoor PBR arrays. The model is applicable to horizontal PBRs, vertical PBRs, and highly mixed PBRs, as well as to pond cultivations. It enables an annualization process in which seasonally acquired data can be projected to an annual yield based on historical climate data. More generally, the modeling effort in the current project was aimed at:

- reconciling small-scale laboratory results with outdoor results
- quantifying incentives for various culture management strategies
- providing photosynthetic parameters as a monitor of culture health
- developing predictive capabilities for productivity given local climate inputs
- identifying phenomena that limit outdoor culture productivities
- providing guidance, and quantitative incentives, for research efforts aimed at higher productivities
- annualizing outdoor cultivation results obtained during different seasons

The general approach for use of the Algenol Productivity Model involves laboratory derivation of photosynthetic parameters and deployment in a phenomenological model constructed for the experimental situation being addressed, e.g., outdoor deployment of vertical PBRs. We begin by establishing the relationship between the Algenol-derived kinetic parameters from Photosynthesis-Irradiance (PE) curves and μ (the specific growth rate) which by definition is

$$\mu = (dC_c/dt)/C_c = P_v/C_c \qquad \text{(Eq. 8-1)}$$

where C_0 is the photosynthetically fixed carbon concentration (mol C/m^3), t is time (sec), and $P_v = dC_c/dt$ is the volumetric production rate. μ is a function of irradiance (E) except under saturating light conditions, when P_v is replaced by P_m (also referred to as P_{max}), the maximum photosynthesis rate obtained under high (saturating) irradiance conditions (ignoring photoinhibition effects). This would yield the maximum specific growth rate, μ_m. The determination of μ or μ_m is carried out under low light absorption (non-saturating) conditions where exponential growth is expected. Note that C_c contains both cellular and non-cellular (dissolved organic) components. As long as the proportionality of those components is unchanged over the time scale of the experiments, Equation 8-1 and the comparison below to kinetic parameters derived from PE curves are valid. In fact, because of the normalization in Equation 8-1, any physical property that provides a proper measure of growth (such as sOD in most cases) can be used to determine μ. PNNL was supplied with AB1 for their DISCOVR project (Huesemann, 2017) and generated growth rate (μ) data for

a wide range of temperatures. The comparison to our data set with μ derived from PE curves to PNNL's results is near perfect (See Algenol internal report in Appendix 3).

We now turn to derivation of the productivity model. Assume that irradiance (E) decays exponentially in the culture according to Beer's Law

$$E = E_0\, e^{-kz} \qquad \text{(Eq. 8-2)}$$

where k is the extinction coefficient (m^{-1} units), z (m) is the distance into the culture, and E_0 is the incident irradiance at the culture surface (μmol photons/m^2-s). k is determined as an average over the absorption spectrum in the Photosynthetically Active Radiation (PAR) range (400 to 700 nm) and is equal to KC_c, where K is the PAR averaged absorption cross section (m^2/mol C). We have shown Equation 8-2 to be valid for our organisms under wide ranging conditions, making only a small (wavelength uniform) scattering correction (Legere, 2017). We assume further that P_v in the culture at a point z below the surface can be described by a hyperbolic equation (the Monod equation, which is similar to a Michaelis-Menten formulation, see for example Bechet *et al,,* 2013)

$$P_v = P_m\, E/(E_k + E) \qquad \text{(Eq. 8-3)}$$

E_k is the half- saturation constant which describes photosaturation (μmol photons/m^2-s), and P_m (alternatively designated as P_{max}) is the maximum photosynthetic rate asymptotically approached at high irradiance. This formula can be adapted to include photoinhibition effects, but we find that under most lab and outdoor conditions now employed at Algenol (e.g., vertically oriented PBRs), those effects are small. The areal productivity (mol C/m^2-s) in a culture of depth D is derived by integrating Equation 8-3 over the depth (D) of the culture (Legere, 2017):

$$P_a = \int_0^D P_m\, E_0\, e^{-kz}/(E_k + E_0\, e^{-kz})\, dz = (P_m/k)\, \ln((E_k + E_0)/(E_k + E_0\, e^{-kD})) \qquad \text{(Eq. 8-4)}$$

where the z integration is performed over the limits 0 to D. In the limit when kD approaches zero (e.g., in the dilute limit), this expression reduces to:

$$P_a = Pm\, E_0 D/(E_k + E_0) \qquad \text{(Eq. 8-5)}$$

The amount of light absorbed in a very shallow culture is kDE_0. Hence the ratio of areal production to light absorbed in a very shallow culture (the quantum yield) is:

$$P_a/kDE_0 = P_m/(k\,(E_k + E_0)) \qquad \text{(Eq. 8-6)}$$

Now taking the limit as E_0 approaches zero, we find that the limiting quantum yield (α, reciprocal of the minimum quantum requirement) is

$$\alpha = P_m/k\, E_k \qquad \text{(Eq. 8-7)}$$

which, when multiplied by E, corresponds to the limiting areal production rate (mol carbon/m^2-sec) at low light levels.

Generally, the same relationships apply for the exponential version of Equation 8-3 (Bechet *et al,*, 2013). Both Monod and exponential forms of Equation 8-3 are used to fit the PE curves. The exponential form gives a better fit. However, for productivity analysis, the integration over culture depth described above to produce Equation 8-4 has to be done numerically for the exponential model. There is no significant difference in the application of the Algenol Productivity Model to productivity data analysis with the exponential form and Monod forms as long as they are used consistently, i.e., that the same approach is used for PE curves and productivity modeling. The simpler Monod process is used here.

From the PE curves we obtain the photosynthetic parameters described above and also an estimate of the respiration rate (R_0), expressed in units of µmol C/mg Chl a-min, C_0 is the Chl a concentration in mg Chl a/ m^3. The values from PE curves are only upper limit estimates as there are contributions attributable to the irradiance history of the sample. Both R_0 and α from the PE curves are based on O_2 evolution and must be corrected to the desired carbon basis by dividing by the photosynthetic quotient (PQ). This value is about 1.1 mol O_2/mol C for AB1 and 1.2-1.3 mol O_2/mol C for *Arthrospira platensis* AB2293.

The Algenol Productivity Model was developed in this manner and used in conjunction with PE-derived photosynthetic parameters to estimate expected average outdoor productivities for PBR deployments in Fort Myers (and elsewhere around the world). The daily biomass volumetric productivity can be described as:

$$P_{Biomass} = F(P_a \gamma \frac{t_1}{D} - R_0 C_c \gamma t_2) \qquad \text{(Eq. 8-8)}$$

where γ is the conversion between fixed C and dry weight biomass (g biomass/mol C), C_c is the chlorophyll concentration, t_1 is the time for illumination (sec), and t_2 is the time for respiration load (min). Illumination time (t_1) is about half of the respiration load time (t_2) for outdoor cultivation. γ is based on the carbon content of the biomass (about 50% for AB1 and about 46% for *Arthrospira*) combined with the amount of dissolved organic carbon (DOC) which is not harvested under normal circumstances. DOC is about 30% of dry weight carbon (DWC) for AB1 (23% of total carbon) and about 15% for *Arthrospira*, so that γ is about 18.5 and 22.7 g dry weight biomass/mol C for AB1 and *Arthrospira*, respectively. As shown earlier, AB1166 has significantly less DOC (~15% wt%) than AB1 and γ is about 20.9. (The increase in productivity for AB1166 versus AB1, as measured by AFDW, can be largely accounted for by the increased γ.) Conversion to areal productivity is done based on the actual outdoor deployment (PBR dimensions and spacing). The main element is the factor F in Equation 8-8, which is the ratio of incident solar irradiation to average irradiance on the surface of the PBRs. From optical models and geometric considerations, F is to a good approximation equal to H:S; therefore, F = 2.4 for AB1 and AB1166 cultivations, F=4 for *Arthrospira* cultivations, and F=1 for ponds or other horizontal systems including laboratory LvPBRs. E_0 in Equation 8-4 for P_a is divided by F, a reflection of one of the main advantages of vertical PBR systems related to light dilution. The E_0 value obtained from the weather station on site is averaged over the daytime hours (t_1), and reduced by 15% to correct approximately for reflection losses. More detailed discussion can be found in the temperature dependence manuscript attached in Appendix 1.

In the discussion to follow, the Algenol Productivity Model is applied to the *Arthrospira* results and AB1 results for outdoor deployment described earlier in this report. The parameters for the

modeling of the 24,000 L *Arthrospira* experiment are derived from indoor PE curve experiments as described in the temperature dependence manuscript in Appendix 1: α = 0.061 fixed C/photon, E_k = 240 µmol photons/m^2-s, and R_0 = 0.1 µmol C/mg Chl a-min. The geometry of the experiment is taken into account: Height to spacing ratio of 4:1; single 20 ft wide PBR volume of 100 L; PBR thickness of 2.5 cm on average; 240 interconnected PBRs for a total volume of 24,000 L. Included in the model fitting are single PBR experiments for 10 ft wide, 50 L volume, as well as 3 x 20-ft PBRs with a total volume of 300 L. The data, presented as weekly averages, are displayed in Figure 8-14, along with the fit based on the Algenol Productivity Model and the lab derived photosynthetic parameters. Some vertical adjustment in the fit is made; the adjustment is very minor, well within the uncertainty of the parameter determinations and the adjustments for DOC and PQ. The model includes the experimentally-derived temperature dependence of E_a = 60 kJ/mol which is applied to the E_k parameter and E_a = 20 KJ/mol applied to R_0. The temperature and incident irradiance are taken from a weather station positioned at the Fort Myers PDU. The fit is excellent, providing an annualized productivity of 22.6 g/m^2-d. The peak productivity is 30-35 g/m^2-day.

The same parameter set is applied to a simulated pond experiment (20 cm deep). Those results are shown in Figure 8-14 and suggest 7.1 g/m^2-d for the annualized productivity for a pond. The peak productivity is about 10 g/m^2-day. The average agrees well with typical results reported in the literature for commercial *Arthrospira* (Spirulina) pond systems (Lu *et al.*, 2011). The peak productivity result is in good agreement with results obtained at ASU during the summer of 2019 as part of this project. Overall the PBR:Pond productivity ratio is about 3.2:1.

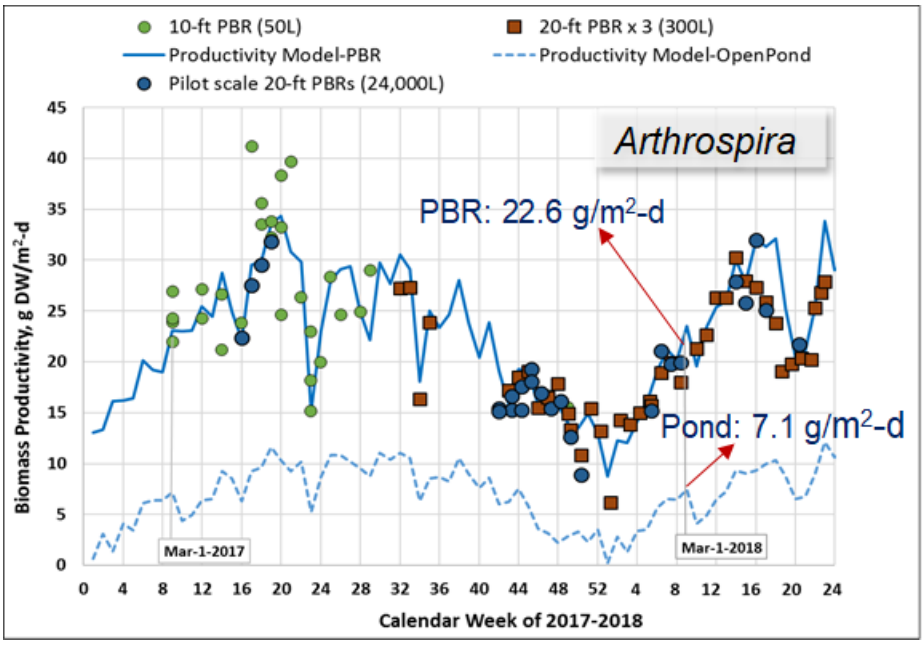

Figure 8-14: Experimental and modeled productivities for Arthrospira (AB2293) for semi-continuous PBR operation and prediction for corresponding open pond cultivation. All results, including models, are based on weekly averages. The same photosynthetic parameters are used for both PBR and pond modeling (Fort Myers climate conditions). Annual averages are shown for model results. The height-to-spacing ratio (H:S) is 4:1 for the PBR cultivation.

A second, less extensive series of experiments were conducted for *Cyanobacterium* sp. AB1, establishing the achievement of the milestone for the project related to productivity improvement. Those results are displayed in Figure 8-15 in a similar format to the previous slide. α, = 0.09 fixed C/photon, E_k is calculated from E_0/kD, for an average value at 100 µmol photons/m^2-s (at 30°C) for semi-continuous operations, and R_0 = 0.1 µmol C/mg Chl a-min. Temperature dependence is included in the model with an activation energy of 55 kJ/mol for E_k. The geometry of the PBR experiment is taken into account: Height to spacing ratio of 2.4:1, PBR thickness of 2.5 cm. For pond modeling, a 20 cm depth is assumed. Using this set of photosynthetic parameters, but different γ values, we obtained AB1 biomass annualized productivity of 24.2 g/m^2-d, and AB1166 biomass annualized productivity is 26.8 g/m^2-d. The major difference in γ between AB1 and AB1166 is explained by higher released EPS (DOC) in AB1 (about 30% of total DW) with γ = 18.5 g DW/mol C, while, with less released EPS in AB1166 (about 15% of DW) γ = 20.9 g DW/mol C. As noted earlier and described in Appendix 1, the γ value for *Arthrospira* is 22.7 g DW/mol C (carbon content of DW ~46% and DOC ~ 15% of DW).

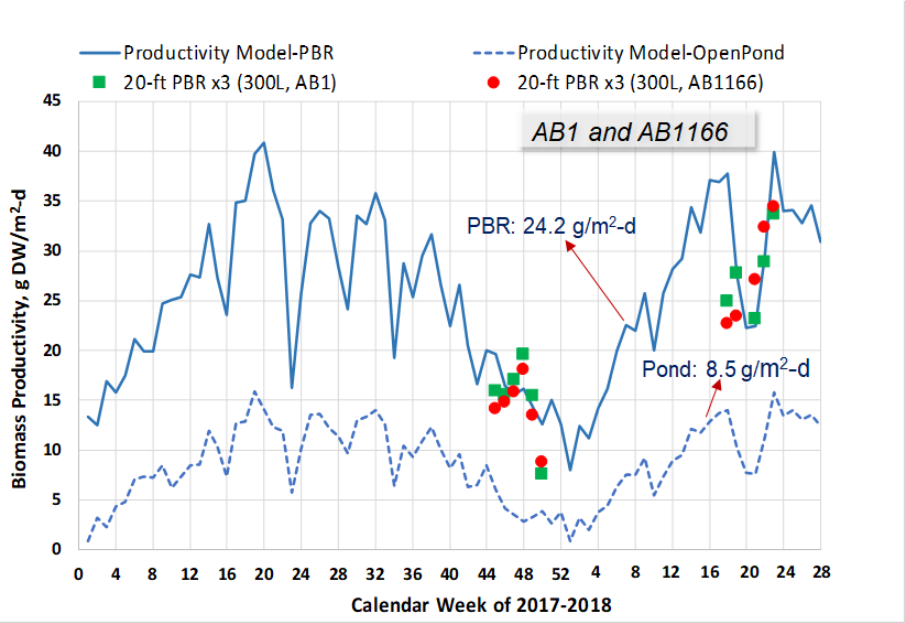

Figure 8-15: Experimental and modeled productivities for Cyanobacterium sp. AB1 and AB1166. AB1 (circles) and AB1166 (squares) experimental data, productivity modeling for semi-continuous PBR cultivation (solid line), and prediction for corresponding open pond cultivation (dashed line). All results, including models, are based on weekly averages. The same photosynthetic parameters are used for both PBR and pond modeling. Annual averages are shown for model fits. The height-to-spacing ratio (H:S) is 2.4 for the PBR cultivation.

We have systematically studied photosynthetic parameters for several strains, and a representative experimental dataset (measured at 30°C) for AB1 and AB1166 from the 2018 Milestone 4.1 experiment is shown in Table 8-7 (see also Figures 8.4 - 8.7.) The photosaturation parameter (E_k) and maximum photosynthetic capacity (P_m) acclimate with average light for AB1 and related strains (Legere, 2017). This is a major observation in batch cultivation with AB1-like strains; E_k can be reduced to 60 µmol photons/m^2-s or lower as culture density becomes dense. However, we can maintain E_k at range from 100-200 µmol photons/m^2-s through semi-continuous

operation. This is the main reason for the 60 to 80% higher productivity in semi-continuous operation (24-27 g/m^2-d) compared to the reference batch operation (15 g/m^2-d) with AB1-like strains (Table 4.3). We also found that E_k does not vary with average light as much for *Arthrospira* at a given temperature, and as a consequence, there is less difference between batch and semi-continuous operation for *Arthrospira.*

Table 8-7: Summarized photosynthetic parameters for AB1 and AB1166 during outdoor milestone experiments (2018)

1st Run (April-May 2018)	**AB1 (Batch)**	**AB1 (Semi-continuous)**	**AB1166 (Semi-continuous)**
sOD750	26.4	3.35	3.45
k-PAR	15.85	2.0	2.05
k-PAR/sOD	0.6	0.6	0.6
P_{max} (µmol O_2/L-hr)	227	449	497
alpha (mol O_2/mol photon)	0.1	0.09	0.09
R_0 (µmol O_2/L-min)	0.45	0.73	0.69
E_k (µmol photons/m^2-s)	60	140	157

2nd Run (May-June 2018)		**AB1 (Semi-continuous)**	**AB1166 (Semi-continuous)**
sOD750		3.71 ± 0.48	3.76 ± 0.30
k-PAR of culture (1/cm)		2.05 ± 0.25	2.38 ± 0.10
k-PAR/sOD		0.54 ± 0.02	0.59 ± 0.05
Chl-a (mg/L) Scan		18.1 ± 3.2	21.9 ± 4.8
Chl-a/sOD ratio Scan		4.8 ± 1.1	5.9 ± 1.5
PC % Scan		14.6 ± 0.9	16.9 ± 1.4
P_{max} (µmol O_2/L-hr)		422 ± 20	479 ± 24
alpha (mol O_2/mol photon)		0.12 ± 0.02	0.10 ± 0.01
R_0 (µmol O_2/L-min)		1.22 ± 0.2	0.79 ± 0.13
E_k (µmol photons/m^2-s)		100 ± 13	127 ± 6.4

A productivity modeling analysis was also carried out on the AB1 growth data from an early summer AzCATI pond experiment in Arizona. With light and culture temperature as model inputs, we could fit the pond data by productivity model parameters α and E_k. In Figure 8-16, we show the comparison of model and experimental data in optical density (sOD), the modeling fitting parameter were α = 0.07 mol C/mol photon, and E_k= 80 µmol photons/m^2-s at 30°C. The photosaturation parameter E_k is significantly lower than our PBR results (about a factor of 3, if we assume E_k ~ average light). This may indicate E_k could be also impacted by other factors besides light, such as nutrient level, and/or day-night temperature. It is also possible that the lower E_k is just a consequence of fitting results that are compromised by predation or other unknown factors. This was the only AB1 pond experiment that performed reasonably well at AzCATI or at RIL in India (i.e., predator contaminant levels were low). A semi-continuous AzCATI pond experiment on UTEX1926 (*Arthrospira*) performed in Mesa, AZ in Aug/Sept 2019 gave an average productivity of ~10-12 g/m^2-day (average PAR at 43 mol/m^2-day), which is consistent with our productivity model prediction of 11.2 g/m^2-day. See Appendix 2 for a more detailed discussion of both AzCATI and RIL pond experiments.

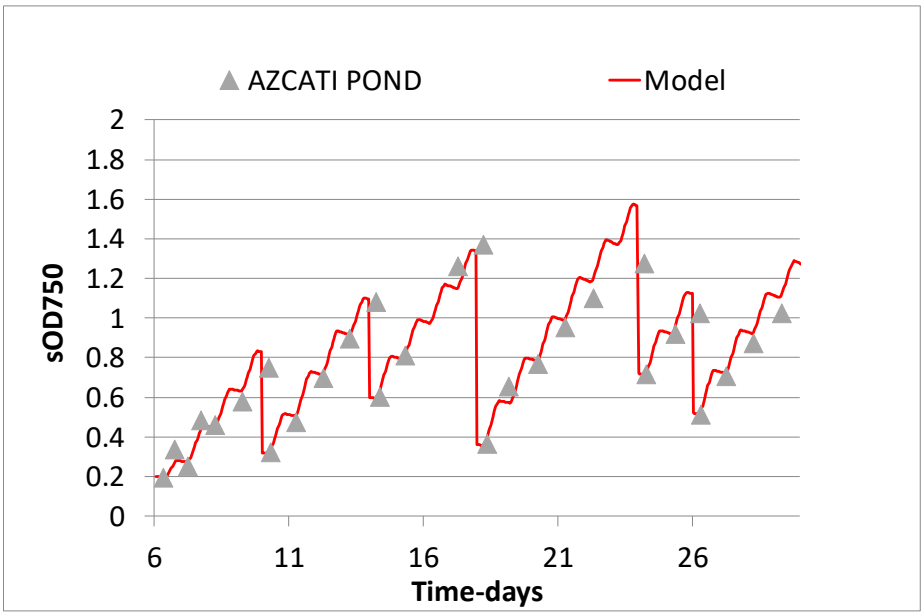

Figure 8-16. Productivity Modeling analysis on AB1 growth in AzCATI POND (June 6 to June 29, 2019).

Life Cycle Assessments

Life cycle greenhouse gas emissions of different CO_2 supply options for an algal biorefinery

The key component of the 2nd objective of this project is a 60% reduction in carbon footprint of the biofuel compared to fossil fuel being displaced. LCA analyses have been conducted throughout this work as a research guidance tool, and ultimately as a test of progress with respect to the project objectives. The energy efficiency of the biorefinery is obviously critical and much of the experimental work for both AB1 and *Arthrospira* cultivations has been devoted to reducing the energy consumption of both upstream and downstream processing. Another critical factor is the source of the CO_2 and the CO_2 burden (or credit) that it brings to the biorefinery boundary limit. We have considered a number of scenarios for that delivery as described in detail in the attached manuscripts (Appendix 1). The first manuscript deals with a variety of sources and the impact on biofuel production (ethanol and HTL processed biocrude). The second one, which we will focus on here, provides more details on the CO_2 sourcing and a case study for the simplest source, flue gas from a coal-fired power plant. The full list of cases considered is given in Table 8-8. The source burden is defined as the footprint of the CO_2 delivered to the boundary limits of the biorefinery. If production from ambient air were practical, say in a pond system where no energy is consumed in delivery, the source burden would be -1.0, i.e., full credit for taking CO_2 from the air. Since flue gas from a power plant (Case 1) would have otherwise been emitted to the environment, the situation is close to the ambient air case. With due consideration of some source management and delivery to the biorefinery (assumed 2 miles away), the source burden is 0.92. The other cases are described in the 2nd manuscript in the Appendix. We note that CO_2 sourced from biomass (Cases 9-11) can be produced with very favorable source burdens, sufficient to provide even relatively inefficient biorefinery processes with favorable carbon footprints.

Table 8-8: Source burden, g CO_2e per g CO_2 delivered to the biorefinery.

Source Description	Source Burden
Case 1: Legacy coal based power plant	-0.92
Case 2: Legacy coal based power plant with CO_2 capture	-0.76
Case 3: Legacy natural gas based power plant	-0.77
Case 4: Legacy natural gas based power plant with CO_2 capture	-0.73
Case 5: Purpose-built NGCC plant	-0.53
Case 6: Purpose-built NGCC plant with CO_2 capture	-0.40
Case 7: Purpose-built NGCC plant with CO_2 capture and refrigeration	-0.54
Case 8: Purpose-built NGCC plant with CO_2 capture and partial refrigeration	-0.60
Case 9: Biomass combustion	-1.30
Case 10: Biomass gasification	-1.62
Case 11: Biomass gasification with CO_2 capture	-1.56
Case 12: Direct air capture case	-0.61

For a detailed discussion of source-biorefinery integration, we choose the simplest example, Case 1. In this case, the flue gas is extracted from the stack of a coal-fired power plant. It is cooled and

compressed before being transported to the algal biorefinery as the primary source of CO_2. The plant is modeled as a pulverized coal plant burning Powder River basin coal. Flue gas from the power plant is assumed to be extracted from a single stack utilizing a stack fan. Since most coal-fired boilers have flue gas desulfurization, it is assumed that the flue gas is saturated with water and available at a temperature of 60°C. Thereafter, the flue gas is cooled in a direct contact cooler/scrubber to reduce the gas volumetric flow and remove as much of the water as possible before flowing through the transport compressor. A pressure drop of 0.055 bar per mile is assumed and the CO_2 is delivered to the biorefinery at a pressure of 2 bar. The flue gas leaves the transport compressor and travels through ductwork from the power plant to the biorefinery. The flue gas passes through a second direct contact cooler to cool the flue gas before it is utilized by the facility. The process is shown in Figure 8-17. The energy required for each component of flue gas processing, the energy required for flue gas transport, and the composition of the major streams for all the cases is in the supporting information.

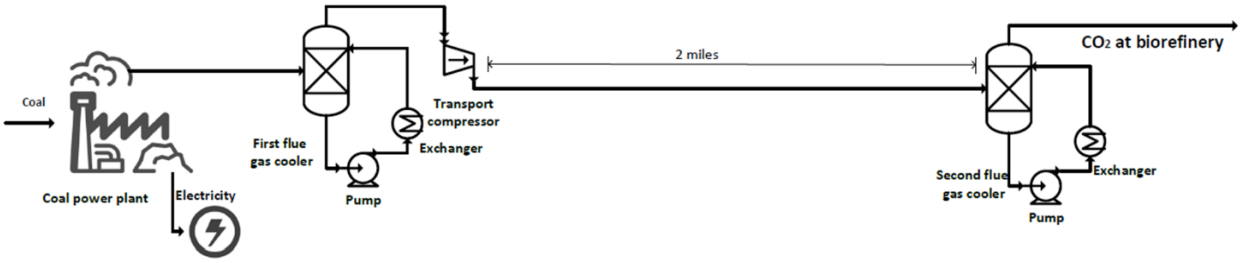

Figure 8-17: CO_2 supply from a coal based power plant.

To study the effect of CO_2 sourcing on the GHG footprint of the biorefinery, ASPEN Plus® models were prepared for biofuel production from hydrothermal liquefaction (HTL) of algal biomass. The simulation encompassed the Case 1 CO_2 supply, algae production, HTL of algal biomass and catalytic hydrothermal gasification (CHG) of the aqueous phase resulting from HTL reactor. The primary product is the biofuel produced from the HTL process. The productivity for the algae cultivation is taken from the AB1166 results reported earlier, annualized for Fort Myers, Florida climate. More details related to the modeling are given in Appendix 1. The CHG fuel-gas is utilized to provide heat for the HTL and CHG reactors. The electricity requirements of the biorefinery are met through an onsite natural gas powered CHP plant. The CHP is sized (15 MW) to meet the daytime electricity requirements of the algae biorefinery, which are higher than those at night. Excess electricity production is exported to the power plant. The daytime CO_2 emissions from the CHP plant are utilized by the biorefinery and the night-time emissions are vented to the atmosphere. The simulation incorporated separate day and night operations as well as recycles of CO_2, water and nutrients. The coal power plant is assumed to be located 2 miles from the biorefinery. The proposed size of the PBR-based refinery is 2,000 acres and an algae growth cycle of 60 days (between clean-in-place operations) is assumed. The system boundary of the LCA also includes hydro-treating of biocrude (BFI). The flowsheet depicting the biofuel production through HTL is presented in Figure 8-18.

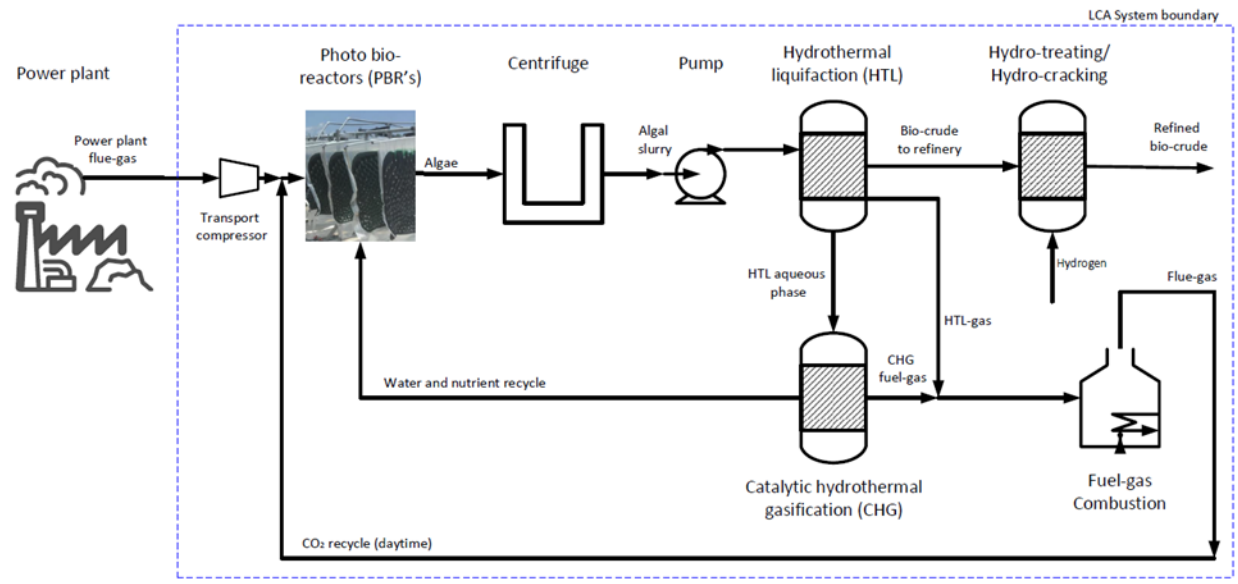

Figure 8-18: Flowsheet for biofuel production from algal biomass via HTL.

The LCA result is a GHG emission of 31.4 g CO_2 eq./MJ biofuel, as shown in Figure 8-19. This is a 66% GHG reduction compared with gasoline, which has a carbon footprint of 93.1 g CO_2 eq./MJ. The emissions associated with CO_2 delivery are highlighted in red in Figure 8-19. The figure highlights that the CO_2 delivery has a significant contribution to the final carbon footprint of biofuel production. The study assumes a grid average electricity emissions (750 g CO_2 eq./kWh) for plant electricity export to the coal-fired power plant. The largest source and sink of CO_2 emissions are the biofuel combustion and CO_2 delivery during algae growth, respectively. The emissions from the CHG and the CHP are night-time CO_2 emissions which are vented to the atmosphere. The other major contributors are likely to remain constant with the changing plant configurations except for the electricity export. If a grid average electricity emission of 500 g CO_2 eq./kWh (representative of average US grid) is assumed, the total carbon footprint for the biofuel would be 43.1 g CO_2 eq./MJ biofuel, which is a 54% emission reduction compared to gasoline.

For a given plant capacity, all the emission sources, except the CO_2 delivery and electricity export, are expected to remain constant. The contribution of CO_2 delivery would be different for different CO_2 supply cases. Furthermore, different CO_2 supply scenarios can offer a variety of heat integration avenues to the biorefinery. In the natural gas combined cycle (NGCC) and biomass CO_2 supply cases, the utilization of excess electricity and heat in the biorefinery can reduce the CO_2 footprint of the complete process. The direct air capture case, in particular, is expected to derive considerable benefit by the integration of the direct air capture process and the biorefinery. Exploring these heat integration scenarios is beyond the scope of this project.

Overall it is clear that a carbon footprint reduction of 60% compared to gasoline is achievable with the PBR-based biorefinery considered in this work. This satisfies the key element of the 2nd objective of this project.

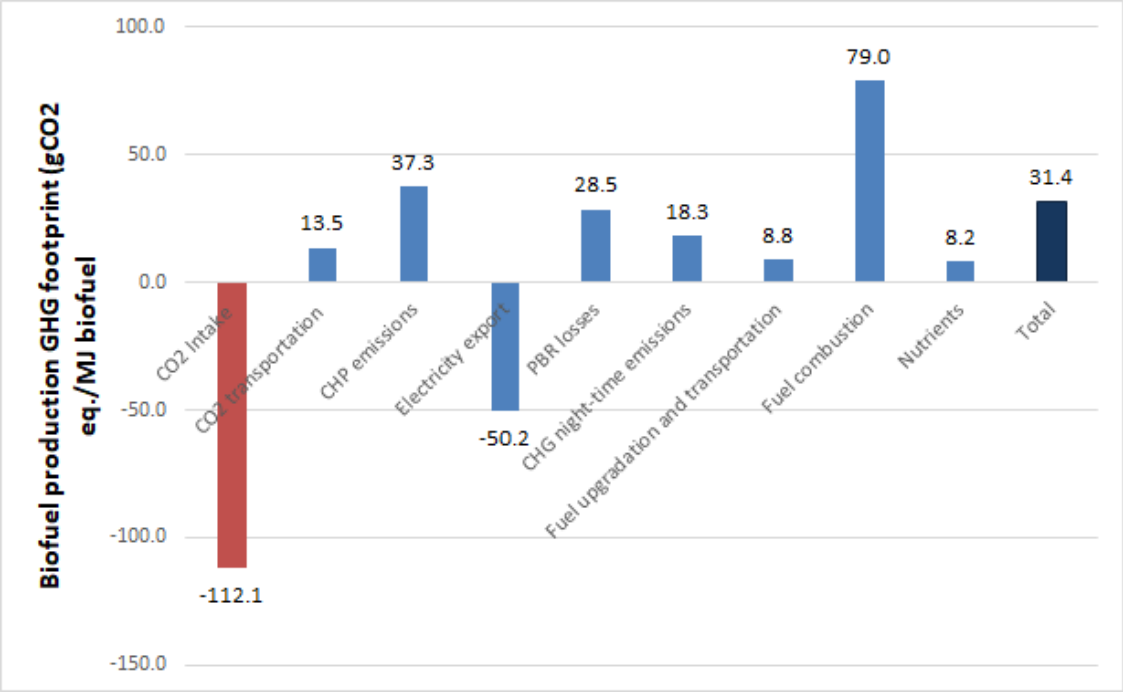

Figure 8-19: Biofuel production from algae HTL process utilizing CO2 from coal based power plant.

Techno-Economic Analysis for a BFI Biorefinery and Biomass Production

Techno-Economic Analysis (TEA) has been an integral part of Algenol's technical portfolio from company startup in 2006. TEA, combined with Algenol's financial model, provides an economic assessment of the viability of the algal biofuels technology under various scenarios for future economic conditions.

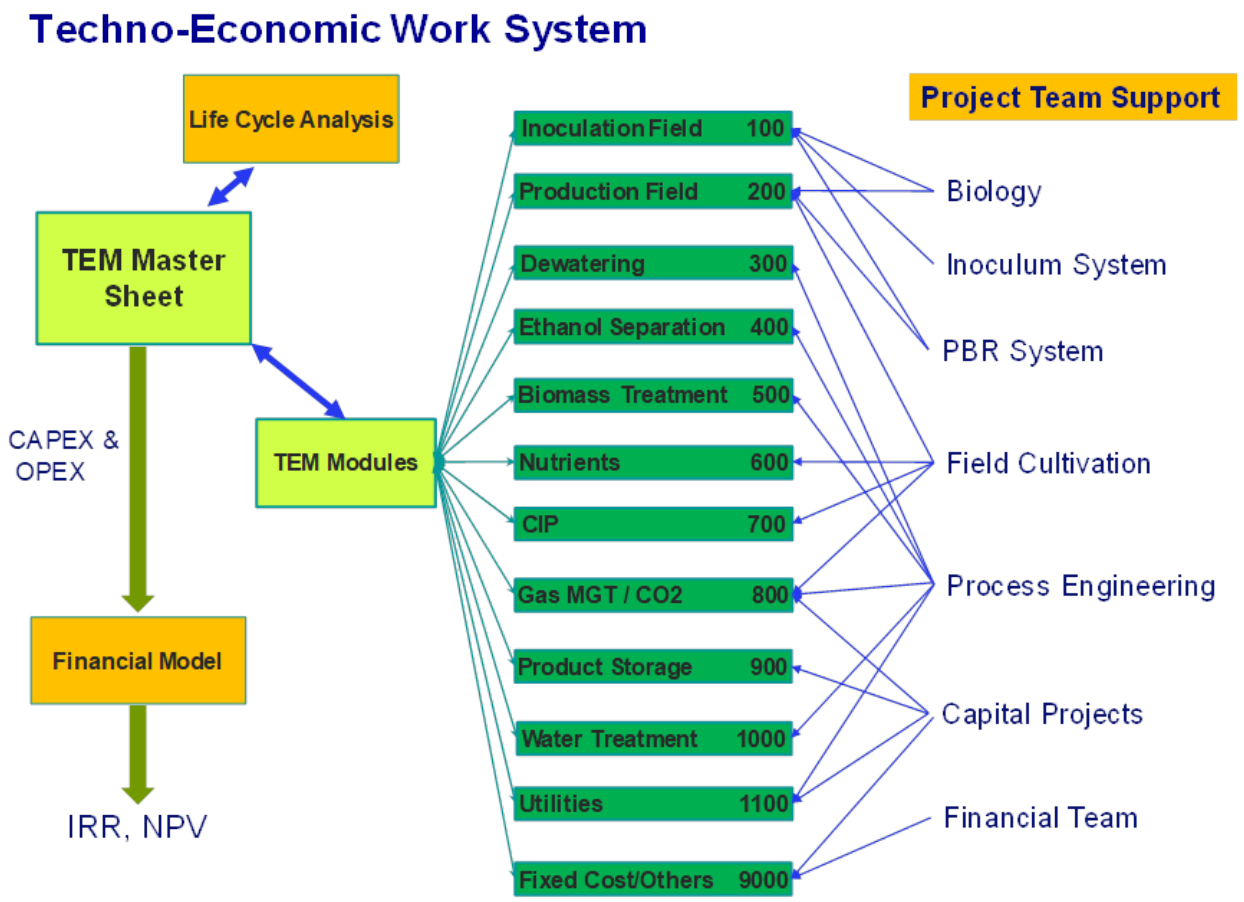

The TEA work system is illustrated in the above diagram. Georgia Tech played an important role as part of the process engineering team and as part of the LCA execution team, which relied on the same data base and plant design input as the TEA team. Other partners also contributed in their specialized areas. This structure was originally put in place for the ethanol DOE project (Legere, 2017), with ethanol separation assigned as area 400. That area is eliminated for the current program and other aspects modified somewhat for BFI and co-product production. For convenience, the number labeling is not adjusted for the absence of Area 400.

The following narrative addresses three TEA-related aspects of the current project: A. BFI Production Costs and Energy Expenditures; B. Biomass Production for Algal Co-Products; C. Ponds versus PBRs for Biomass Production Cost and D. Summary and Conclusions for TEA Studies.

A. *BFI Production Costs and Energy Expenditures*

As described in a previous Algenol-DOE report (Legere, 2017), Algenol has developed a 2,000-acre algal biofuels production plant TEA for ethanol production based on a capital projects design at FEL-2. The production platform was based on genetically modified AB1, with biocrude (BFI) production from the spent biomass as a secondary product. In the current project, we extend that work to BFI-only production, and BFI/co-product (phycocyanin) based on Algenol capital project designs at FEL-2 and FEL-3 level, respectively. TEA, with its Capital Expense (CAPEX) and

Operating Expense (OPEX) goals, provides research guidance for both performance improvements and cost reductions.

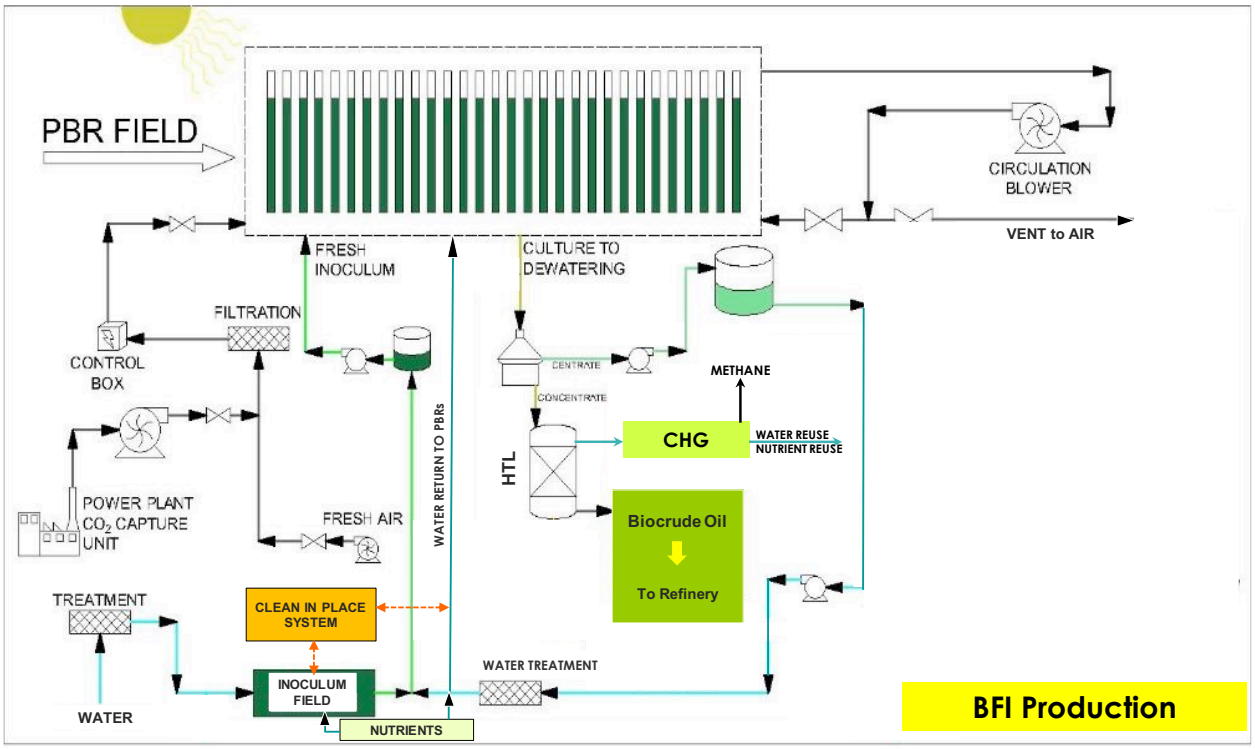

Figure 8-20. Block flow diagram that forms the basis for the Algal BFI Plant.

The CAPEX cost estimation is based on the Lang and Guthrieth factor method (Seider *et al*., 2010), which uses installation factors and individual purchased equipment cost to calculate overall plant cost. The OPEX is calculated from material and energy balance data, in conjunction with labor cost and PBR system maintenance cost. OPEX estimation is aided by Algenol's pilot plant operation experience (from 0.1 acre to 2 acre) over the past decade, including the pilot scale work in this project described in earlier sections. The cost estimation is based on the assumption that this is the "n^{th}" plant with 2,000-wet acre biofuel production field in USA (e.g., in Fort Myers for the climate assumptions). The biofuel strains considered are *Cyanobacterium* sp. AB1 and AB1166. Co-product work focused on *Arthrospira platensis* in smaller scale production platforms. In the 2,000 acre production field, there are 3.3 million Algenol 20-ft PBRs (100 L culture each). The basic process flow for biocrude is shown in Figure 8-20.

The costing summary for both CAPEX and OPEX is presented in a Target, P50, and P90 (current) format. The P90 values represent cost projections (or performance projections in some instances) that are viewed to have a ~90% probability of being achieved on the time scale of first-plant commercialization. P50 values are 50% probabilities, representing reasonable expectations for cost and performance for the nth plant. Target values are long term research and development targets, based on what has been established as being possible to achieve. The major assumptions are shown in Figure 8-21. PBR cost is the major CAPEX cost for the production field, set at $50 (Target), $100 (P50), $200 (P90) per 20-ft PBR. Life time of PBR (replacement, is a key OPEX factor) is set as 10 (Target), 8 (P50), or 6 (P90) years.

- Baseline CAPEX and OPEX alignment with Ethanol TEA
- Recycled gas and culture media
- Biomass Productivity: 27 (current), 32 (P50), 42 (target) gDW/m^2-d (HS=2.5) for Florida, rescaled to other regions based on irradiance and temperature
- Combined Heat and Power (CHP) provides both electricity and CO_2 as flue gas (CO_2 cost at 35 $/tonne as baseline, 0 at P50; 3$/MMBtu Natural Gas)
- HTL and CHG biomass processing process
- 40% HTL yield
- 330d per year operation at Fort Myers, FL

Figure 8-21. Major cost and productivity assumptions in TEA-BFI Plant.

The sub area CAPEX and OPEX values for USA deployment are given in Table 8-9 and Table 8-10. A Combined Heat and Power (CHP) unit (~ 9 MW electricity, in Area 1100) provides the heat and power for the upstream algae cultivation and downstream product processing operation: flue gas CO_2 from that unit can potentially be used for upstream algae cultivation. In the BFI biorefinery, the CHP will be sized to provide 6 MW thermal (~ 400°C for the HTL process) and 9 MW electricity (day-night average). The extra electricity is sold back to the grid at rate of $0.07 /kWh.

Table 8-9. TEA CAPEX for 2,000-acre BFI plant.

Long Term CapEX	24 yr		Target	P50	Current
	Area	Area code	CapEX ($/facility-acre)	CapEX ($/facility-acre)	CapEX ($/facility-acre)
	Innoculum	Area 0100	919	919	1,548
	Production Field	Area 0200	52,288	104,576	238,564
	Dewatering	Area 0300	34,000	34,000	64,000
	Biomass Treatment	Area 0500	47,942	40,725	36,778
	Nutrients	Area 0600	370	370	1,312
	CIP	Area 0700	4596	4596	9,562
	Gas Management/CO_2	Area 0800	17,206	17,206	22,775
	Product Storage Loadout	Area 0900	1869	1869	1,869
	Wastewater Treatment	Area 1000	7400	7400	7,400
	Utilities	Area 1100	11,301	11,301	11,301
	Others	Area 9000	12,000	12,000	12,000
	Sum.		189,892	234,962	407,110
			Target	P50	Current
Short Term CapEX	6 to 12 yr		10	8	6
	Area	Area code	CapEX ($/facility-acre)	CapEX ($/facility-acre)	CapEX ($/facility-acre)
PBR Bags	Innoculum	Area 0100	113	113	173
PBR Bags	Production Field	Area 0200	29,412	58,824	88,236
	Sum.		29,525	58,937	88,409
Total CapEx			219,416	293,899	495,518

Table 8-10. TEA OPEX for 2,000-acre BFI plant.

		Target	P50	Current
Area	Area code	OpEX ($/acre-yr)	OpEX ($/acre-yr)	OpEX ($/acre-yr)
Innoculum	Area 0100	537	537	752
Production Field	Area 0200	4,226	8,638	17,019
Dewatering	Area 0300	3,620	3,620	2,650
Biomass Treatment	Area 0500	828	631	533
Nutrients	Area 0600	1,770	1,696	4,969
CIP	Area 0700	618	618	1,485
Gas Management/CO_2	Area 0800	629	629	4,092
Product Storage Loadout	Area 0900	66	66	66
Wastewater Treatment	Area 1000	355	355	355
Utilities (not including power)	Area 1100	128	128	128
Fixed Cost	Area 9000	2,288	2,288	2,288
Sum.(excluding minor corrections related to specifics of power system)		15,000	19,200	34,137
Total- Productivity (gal BFI/acre-year)		6000	4600	3900
		Target	P50	Current
Opex per gallon BFI		$2.5	$4.20	$8.8

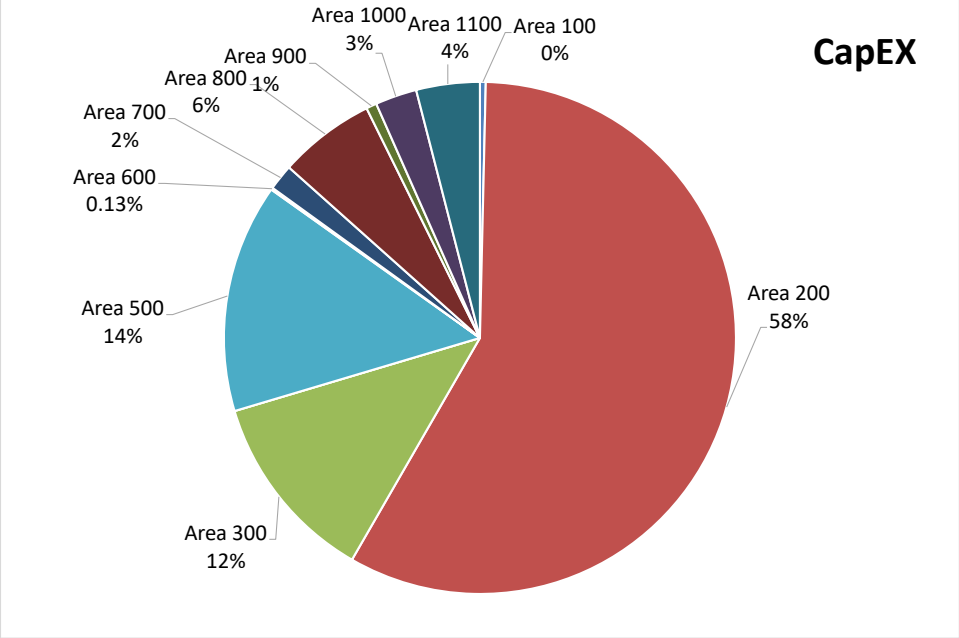

Figure 8-22. CAPEX breakdown for P50 Case

Figures 8-22 and 8-23 display the CAPEX and OPEX breakdowns for the P50 case. The majority of CAPEX costs are in the PBR field (Area 200), Dewatering (Area 300) and HTL (Area 500). The majority OPEX costs are for PBR bag replacement, nutrients, and fixed costs (labor, insurance, and tax). CO_2 cost is set as 0 $/tonne in P50 case, as we assumed a low cost CO_2 source (e.g., flue gas) with that cost offset by a CO_2 tax credit.

For biomass processing (Area 500), Algenol built, but did not commission an HTL unit (~120 gal/d 20% biomass sludge processing capacity). The HTL yield is critical to BFI productivity (as shown in Table 8-11). We have chosen 40% HTL yield in the P50 case, based on the data from NREL

and RIL, as described in the HTL section of this report. This is a fairly conservative value (the upper end of our current estimate of 38% ± 2%). However, we have not taken any debit for the low quality of the BFI, compared to conventional fossil crude.

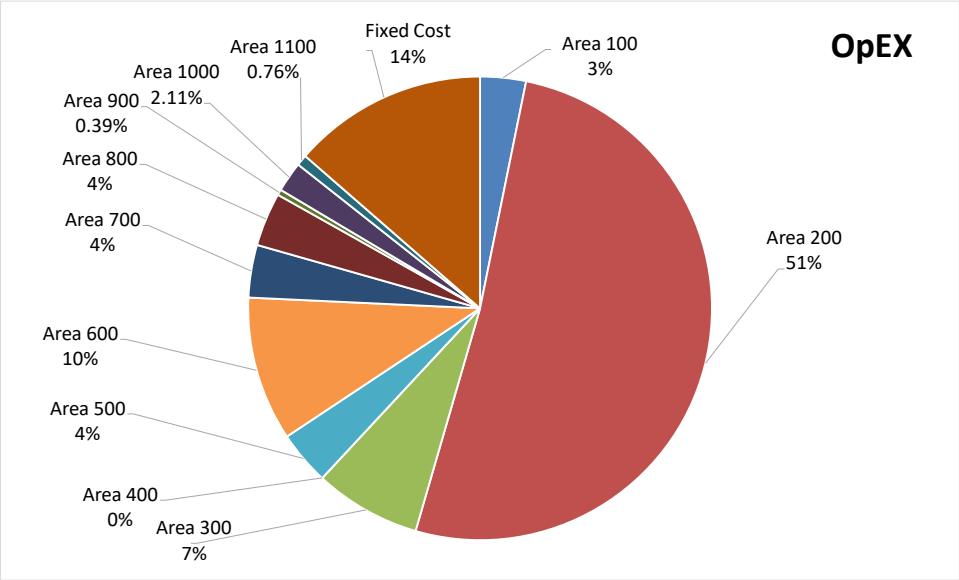

Figure 8-23. OPEX breakdown for P50 Case

Table 8-11. Annualized BFI productivities at different HTL yields and biomass productivities. The HTL BFI yields are lower limit values from PNNL and NREL (34%) to upper limit values from RIL with catalytic HTL (60% or more). The productivity ranges from 15 g/m^2-d (batch production of AB1) to 25-30 g/m^2-d (AB1 and AB1166 field results for semi-continuous operation) to 40 g/m^2-d (current view of the practical limit for known organisms).

Annualized Biomass Productivity	**HTL BFI Yield (η, AFDW basis)**			
	34%	40%	50%	60%
gAFDW/m^2-d	galBFI/acre-yr	galBFI/acre-yr	galBFI/acre-yr	galBFI/acre-yr
15	2,030	2,390	2,990	3,580
20	2,700	3,185	3,980	4,780
25	3,385	3,980	4,980	5,970
30	4,060	4,780	5,970	7,170
35	4,740	5,575	6,970	8,360
40	5,415	6,370	7,960	9,560

Total production cost per gallon of BFI for the base case is calculated from Annualized CAPEX + OPEX; the annualized CAPEX factor is 0.1. The reference P50 number for total production cost is 10.6 $/gal-BFI (or about 400 $/bbl) calculated from the CAPEX and OPEX Tables 8-11 and 8-12. Biomass productivity, PBR system cost, and CO_2 costs are the major drivers for Algal biofuels economics. When PBR system cost is increased by $50 per 20-ft PBR, the total production cost

of BFI will be increased by 1.9 $/gal BFI. When CO_2 price is increased by 50 $/tonne, the total production cost of BFI will be increased by 1.1 $/gal-BFI.

The BFI yield matrix is shown in Table 8-11. The HTL yield for AB1 and AB1166 found experimentally by RIL and NREL is quoted earlier as 38% ± 2%. Combined with their respective productivities of 24.2 and 26.8 g/m^2-d, the predicted BFI yields are 3,700 gal/acre-yr for AB1 and 4,100 gal/acre-yr for AB1166, meeting or exceeding the ABY2 target of 3,700. AB1166 also meets the stretch target of 4,000 gal/acre-yr set for this project. The ultimate yield of 9,560 gal BFI/acre-yr corresponds to about $100/bbl crude or about $4/gal refined fuel. The experimental result of about 4,000 gal BFI/acre-yr corresponds to about $250/bbl crude or about $10/gal refined fuel. We note again that the low quality of the BFI product from HTL is not taken into account in these fuel costs.

Regarding energy expenditures, the use of a CHP unit to provide heat and power for upstream algae cultivation and downstream biomass processing is a critical plant design element for managing energy usage. The electricity energy requirements for each area are listed in Table 8-12. The major electricity usage for upstream cultivation is the aeration of PBRs (7% of BFI energy content) to keep algae cells suspended, keep nutrients well mixed, and efficiently deliver CO_2. The main energy input for downstream is the dewatering (includes harvesting) process (Area 300, 9.3% of BFI energy content), which is to concentrate the culture harvest ~130x to 20 wt% biomass sludge with a two-stage algae dewatering process (UF + Centrifuge) developed in this project. The HTL and CHG processes (Area 500, 2.8% of BFI energy content) are thermal energy dominated processes requiring high-grade heat at 350-400°C. With our ASPEN model, the recovered CH_4 from CHG can provide all the required heat for HTL and CHG processes. The 2.8% value in the Table 8-12 represents the electrical requirement for HTL and CHG. As shown in Table 8-12, the total energy expenditure is about 20% of BFI energy content, where 4,600 gal/acre-yr (the P50 value) is assumed for the areal productivity. The total energy expenditure would be about 25% if the observed 3,700 gal/acre AB1 value were used.

The stretch target set for total energy cost was 10% of the BFI energy content and it was recognized in the original proposal that this was an ambitious goal. Good progress was made in various aspects of the plant design in terms of energy usage. That combined with the 60+% improvement in productivity got us close to the goal. The ABY2 (Priority Area 2) goal of <10% energy expenditure for intermediate processing (harvesting and dewatering) is met for the P50 case. With the AB1166 yield of 4,100 gal/acre-yr, the Area 300 energy usage is 10.4%. For the AB1 case, the value is 11.6%. Though these values are reasonable projections, many of the process improvements in the P50 plant model have not been demonstrated in the field.

Table 8-12. Cost and Energy input in each subarea for 2,000-acre BFI plant (P50)

Area Description	Area Coding	CAPEX	OPEX	Power	Energy input/Energy content in BFI
		$/acre	$/acre-yr	kwh/yr	
Inoculum	Area 0100	1030	537	811,360	0.2%
Production Field	Area 0200	163,400	8,638	-	
Dewatering	Area 0300	34,000	3,621	32,188,460	9.3%
Biomass Treatment	Area 0500	40,700	630	9,828,500	2.8%
Nutrients	Area 0600	370	1,696	42,650	0.0%
CIP	Area 0700	4600	618	1,610,900	0.5%
Gas Management/CO2	Area 0800	17,200	630	24,388,000	7.0%
Product Storage Loadout	Area 0900	1870	66	70,100	0.0%
Wastewater Treatment	Area 1000	7400	355	2,277,600	0.7%
Utilities	Area 1100	11,300	128		
Others (Civil)	Area 9000	12,000	2,288		
Sum.		**293,870**	**19,200**	**71,220,000**	**20%**

B. *Biomass Production for Algal Co-Products*

Algenol has developed techno-economic analyses (TEA) for dry algal biomass as a precursor to phycocyanin (PC) production as well as, potentially, other high value products.. Figure 8-24 displays a simplified block diagram for a dedicated biomass production facility for these products.

The economics of all of these applications, and BFI as well, is critically dependent on the production cost of biomass feedstock. The focus here, and in the next section, is on the production cost for *Arthrospira* biomass, which is a feedstock for dry biomass as a nutraceutical, PC as a food colorant, and algal protein, a potential alternative to animal-based protein. Though algal protein and biofertilizer applications could potentially achieve a scale relevant for biofuel production, neither has a well-established market. The high value co-product chosen for this project, PC, would never reach a scale that is close to that needed for fuels. However, it could potentially be a key part of a market entry strategy for future large scale algal BFI production, demonstrating operability and firming up the biofuel economics. PC also has an established, growing market, replacing fossil-based synthetic blue dyes in many food applications. That is the logic associated with the choice of PC, as expressed in the original proposal.

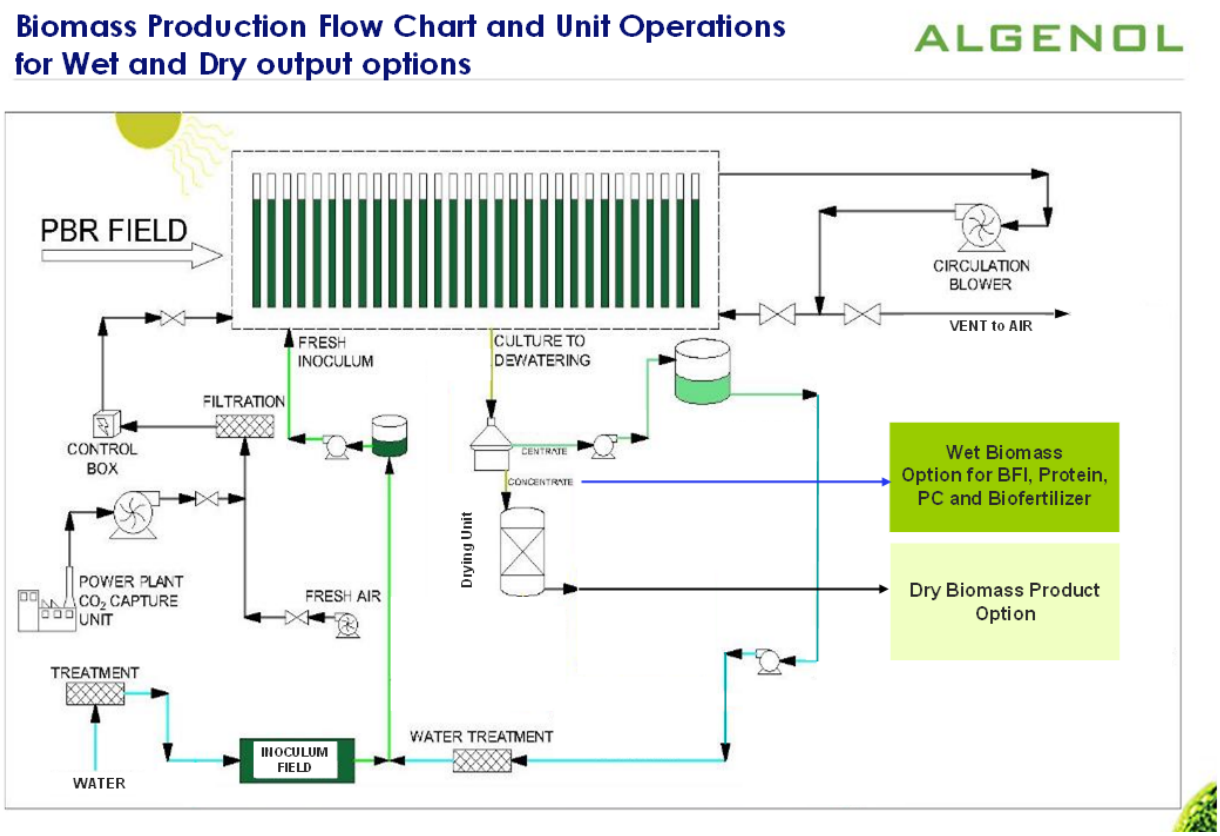

Figure 8-24. Block flow diagram that forms the basis biomass-derived co-products plant (wet option for BFI, protein, phycocyanin, biofertilizer; dry option for dry algae biomass).

PC is a key photosynthetic pigment in cyanobacteria. In *Arthrospira*, it comprises about 10 wt% of the AFDW, or about 25% of the protein content. The two main components of PC are cPC, absorbing at about 620 nm and aPC absorbing at about 650 nm (MacColl, 2004). This red spectral absorption is responsible for the intense blue color. The color quality or hue is primarily a function of the ratio of aPC/cPC. Algenol studied the spectral aspects of PC in detail and the variability of PC content with light and temperature, as described in Appendix 1. Algenol's PC product was tested with several potential end users, with consistently strong approval. Algenol gave serious consideration of a commercial PC venture at modest scale (compared to biofuels) but at significant scale (14 acre) for the existing PC market (roughly $100 million/yr at about $200/kg). That endeavor, though not pursued to date, produced a detailed plant design that has now informed the green-field economics to be discussed herein. That detailed commercial examination of this opportunity is not viewed as part of this project, though much of the pilot scale work represented an important part of this project as discussed in other sections of the report.

The calculations here will focus on the *Arthrospira* biomass production cost, $/kg, estimated as (0.1 CAPEX + total OPEX)/Production. Three scales are examined, 20, 200, and 2,000 acre PBR deployments with a height-to-spacing ratio of 4.0, which is appropriate for high value products. The 20 acre scale is appropriate for PC, the 200 acre scale for protein and perhaps future PC production. The 2,000 acre scale is included mainly for comparison purposes, but also represents

a potential future scenario for both protein and BFI. The following assumptions were used for these green-field calculations:

- The productivity levels are chosen as Conservative (18 g/m^2-d), Current (23 g/m^2-d) and Target (30 g/m^2-d).
- PBR assembly (PBR, supports, local piping) is taken as $200, $100, and $50 per 20 ft wide PBR.
- Gas and culture medium are recycled.
- A CHP system and CO_2 cost are employed as described in Figure 8-21 above.
- Labor rates are based on 50, 100, and 150 FTE (full time equivalents) for 20, 200, and 2,000 acre cases, respectively.
- Spray drying for biomass is assumed, though a wet option (80% moisture content) is also considered.
- Baseline CAPEX and OPEX aligned with detailed PC plant design (without PC extraction) for Conservative scenario, and learning curve assumptions for Current (or P50) and Target scenarios.
- 330 d per year operation under Fort Myers, Florida historical climate conditions.

Results for the 20-acre case are shown in Table 8-13. Though small (ounce) quantities of *Arthrospira* sell for about $1,000/kg, bulk (tonne) quantities are about $10/kg a selling price attributable to production from China (Lu *et al.*, 2011), where low labor rates and fully-depreciated capital have a dramatic impact on production costs. Trial calculations with 1/6 the labor rates assumed above yield production costs that are 20-30% lower than in Figure 8-20. Earthrise is the major US producer of *Arthrospira* at a facility in California that produces commercial biomass as well as PC food colorant, marketed as Linablue. We do not have bulk selling price information for Earthrise biomass or PC. It is important to note in making these comparisons that Chinese producers (for the most part) and Earthrise cannot operate year round. Typically, they only operate 6-8 months out of the year due to seasonal climate constraints.

Table 8-13. TEA analysis for 20-acre PBR facility producing dry Arthrospira biomass.

20-Acre Case	Conservative	Current	Target	Units
Biomass Productivity	**18**	**23**	**30**	**g/m^2-d**
PBR system cost	200	**100**	50	$/20-ft PBR
PBR life	6	**6**	6	yr
CAPEX per acre	2460	**1825**	1420	k$/acre
CAPEX	49	**37**	28	Million $
OPEX	14.5	**10**	7.2	$/kg
Production	480	**600**	800	tonne/yr
Total Production Cost	**25**	**16**	**11**	**$/kg**

Results for the 200 acre case are shown in Table 8-14. Production costs decrease as expected based on economy of scale considerations. The Current result of about $8/kg is similar to the wholesale, bulk selling price of dry *Arthrospira* biomass.

Table 8-14. TEA analysis for 200-acre PBR facility producing dry Arthrospira biomass.

200-Acre Case	Conservative	Current	Target	Units
Biomass Productivity	18	**23**	30	g/ m^2-d
PBR system cost	200	**100**	50	$/20-ft PBR
PBR life	6	**6**	6	yr
CAPEX per acre	1490	**1040**	765	k$/acre
CAPEX	300	**210**	150	Million $
OPEX	6.1	**4.2**	3	$/kg
Production	4,800	**6,000**	8,000	tonne/yr
Total Production Cost	**12.3**	**7.6**	**4.9**	**$/kg**

Results for the 2,000 acre case are shown in Table 8-15 and show the expected continued decline in production costs. This case is an academic exercise currently as the market demand for algae products (e.g., protein) at this scale has not been demonstrated.

Table 8-15. TEA analysis for 2,000-acre PBR facility producing dry Arthrospira biomass.

2,000-Acre Case	Conservative	Current	Target	Units
Biomass Productivity	**18**	**23**	**30**	g/m^2-d
PBR system cost	200	**100**	50	$/20-ft PBR
PBR life	6	**6**	6	yr
CAPEX per acre	1325	**900**	650	k$/acre
CAPEX	2650	**1800**	1300	Million $
OPEX	4.8	**3.2**	2.2	$/kg
Production	48,000	**60,000**	80,000	tonne/yr
Total Production Cost	**10**	**6**	**3.9**	**$/kg**

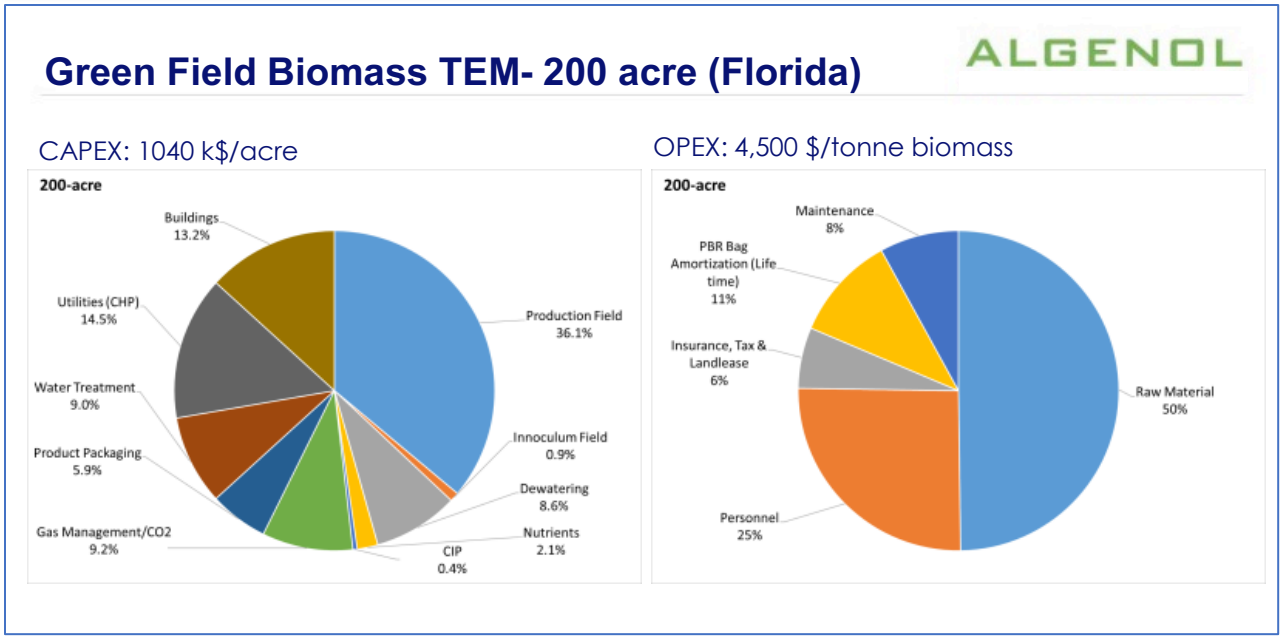

Figure 8-25. CAPEX and OPEX breakdown for 200-acre Greenfield PBR-based, Arthrospira biomass plant in Fort Myers, Florida

For completeness, Figure 8-25 displays a breakdown of CAPEX and OPEX costs for the 200 acre case. Similar to BFI TEA results, the PBR field and dewatering process are the major CAPEX components. Raw materials cost (nutrients, water, electricity) is about 50% of OPEX, and labor cost is about 25% of OPEX.

C. *Ponds versus PBRs for Biomass Production Cost*

PBR-based production of biomass has long been regarded as economically challenged with respect to production from ponds, and that is largely correct. However, Algenol has made great strides in developing a low-cost, high-productivity system. Continuous improvement took place during this project, with high throughput manufacturing demonstrated, and the PBR assembly cost was reduced to near $100. So the $200 Conservative value used in the previous section is truly conservative at this point. A future cost in the $50 range is certainly possible. Reports from NREL and PNNL using Algenol's cost information show that this PBR system is competitive with open ponds (Clippinger and Davis, 2019; Zhu *et al.*, 2018). Our own work described herein agrees with that conclusion.

The Algenol Productivity Model applies to pond cultivations as noted previously in the Productivity Modeling section. The predicted annualized pond productivity for *Arthrospira* in Fort Myers, Florida is 7.1 g/m^2-d. Data for China averages 7.5 g/m^2-d, as noted earlier (Lu *et al.*, 2011). That average is not an annual value; it is an average over the 6-8 month period of operation, scaled up to an annual value. The weather for northern China during the 6-8 month period is very similar to the annual average for Fort Myers. Thus the agreement between the China average and the model prediction is satisfying, as already noted. We use the 7.5 g/m^2-d value in the TEA modeling to follow, which is 3x lower than PBRs. As a mature technology, we do not allow for any learning curve improvements for pond cultivation and thus no distinction between Conservative, Current, and Target (as done above for PBRs). Other assumptions are:

- Open pond capital cost of $40,000/acre, upstream piping cost at $20,000/acre and upstream equipment cost at $20,000/acre (all from RIL, but consistent with NREL report TP-5100-647772).
- Labor rates are based on 50, 100, and 150 FTE (full time equivalents) for 20, 200, and 2,000 acre cases, respectively.
- $3/kg for raw material cost for 20-acre case and 20% less for 200 and 2,000 acre cases.
- Other assumptions are made consistent with approach for the PBR cases.

Results are shown in Table 8-16. The comparison to PBR systems is shown in Figure 8-26. According to this analysis, Algenol's PBR system is completely competitive with pond systems under Fort Myers climate conditions. This conclusion agrees with recent studies from NREL and PNNL (Clippinger and Davis, 2019; Zhu *et al.*, 2018). Earthrise is reported to have spent about $15M in current dollars for an additional 25 acre facility in 1996. That agrees well with the CAPEX estimate in Table 8-16. For the wet-biomass case (no spray drying) production costs are reduced 5-7% for both Pond and PBR cultivations.

Table 8-16. TEA analysis for Pond Cases based on biomass productivities obtained during up-time in commercial facilities, and economic assumptions comparable to PBR analyses described above.

Pond Cases	20-Acre	200-Acre	2,000-Acre	Units
Biomass Productivity	**7.5**	**7.5**	**7.5**	g/m^2-d
Open Pond Cost	40,000	**40,000**	40,000	$/acre
CAPEX per acre	665	**350**	240	K$/acre
CAPEX	13	**70**	475	Million $
OPEX	8.5	**5**	3.5	$/kg
Production	200	**2,000**	20,000	tonne/yr
Total Production Cost	**14**	**7.8**	**5.4**	**$/kg**

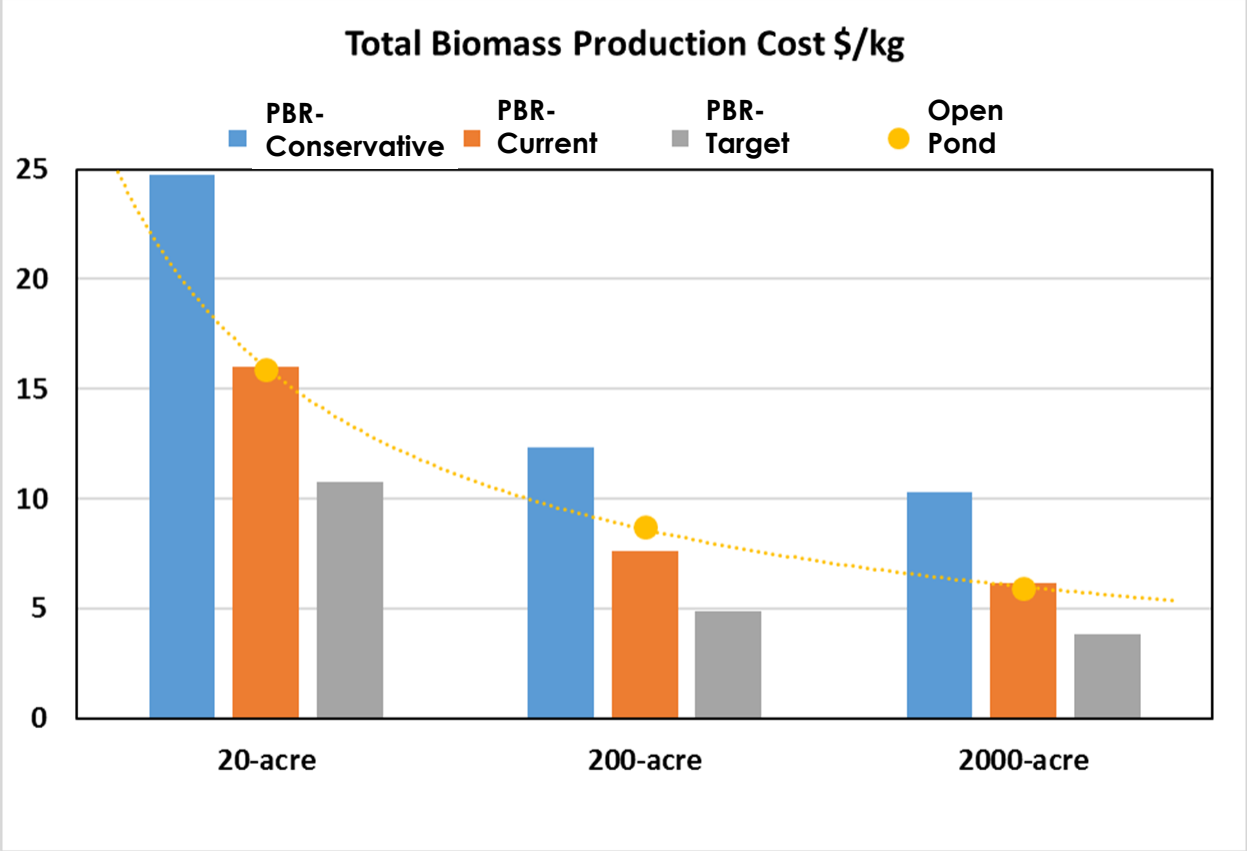

Figure 8-26. Comparison of Arthrospira production costs for PBR and Open Pond deployments under Fort Myers, Florida average climate conditions. Assumptions for Open Pond production most closely align with PBR-Current case.

Biomass pond production in the AB1 (or AB1166) case is not a practical consideration at this point based on the lack of success at both RIL and ASU due to predation and other issues. However, we can still do a thought experiment as has been done at NREL (Clippinger and Davis, 2019) and PNNL (Zhu e*t. al.*, 2018), both of which had input from Algenol regarding PBR costs and productivities. We assume the process is producing wet biomass suitable for HTL feed. Making rough corrections to productivities established herein, both studies yielded MBSP (minimum biomass selling price) of around 1,000 $/tonne at large scale (1,000 to 2,000 acre PBR system and 3,000 to 6,000 acre pond system). Our own studies (still in progess) yield similar results on the Production Cost basis we have been using throughout this section. We find PBRs are fully competitive with open pond systems on a green field calculation basis. In addition, PBR systems have much more room for improvement since they are still relatively early on the learning curve. The lower values for biomass cost for AB1 compared to *Arthrospira,* roughly 1 $/kg compared to 3.5 $/kg at the 2,000 acre scale, are due to several factors: wet *vs* dry biomass, PBR spacing (H:S ratios of 2.4 *vs* 4.0), carbonate cost for *Arthrospira*, high nutrient cost for *Arthrospira*, and higher productivity for AB1. Though many aspects of PBR technology need to be proven by sustained outdoor operation, it is clear that PBR systems have a high potential for competitive economics with respect to open pond systems.

D. Economics of Phycocyanin as a Co-Product

PC can be derived from any cyanobacterial strain, including the *Cyanobacterium sp*. strains considered here (AB1 and AB1166) and *Arthrospira.* Although not discussed in detail here, the PC extracts from *Cyanobacterium* sp. and *Arthrospira* are indistinguishable with respect to the color profile*. Arthrospira platensis* was chosen for emphasis mainly because the FGPC derived from this species already has broad regulatory approvals for use as a food colorant. As can be seen in the above TEA discussion, *Arthrospira* biomass is 3-4 times more costly to produce than AB1 or AB1166 when using current plant design specifications. Partially offsetting this cost disparity, downstream processing of *Cyanobacterium* to extract PC is expected to be more costly than that for *Arthrospira* due to the extra costs associated with dewatering and expected higher energy required to disrupt the strong cell wall of *Cyanobacterium*. In any case, the lack of existing approvals for PC derived from any source other than *Arthrospira* is a substantial barrier to developing alternative sources.

As discussed in the original proposal for this project, FGPC produced as a high value co-product for large-scale biocrude production is not a likely scenario. At a scale meaningful for the fuel market, with 10-12% of the biomass being used for the food colorant market, PC would quickly transition from a high-value specialty product to a low-value commodity. This would almost certainly be the fate of all high value, low volume co-product candidates. To quantify this assertion, the following formula for food grade PC productivity is useful (see also related Task 6 discussion):

$P_{FGPC} = P_{biomass}$ x harvest efficiency x PC content x g_{FGPC}/g_{PC} x extraction efficiency (Eq. 8-9)

$P_{biomass}$ is the biomass productivity (22.6 g/m^2-d annualized for Fort Myers), harvest efficiency is ~95%, PC content is about 12%, g_{FGPC}/g_{PC} is the ratio of the diluted FGPC product to pure PC (about 3.3), and the final term is the PC extraction efficiency (about 65% as described in Task 7 above). The result is P_{FGPC} = 5.5 g/m^2-d, or about 8 tonne FGPC/acre-yr for a PBR-based production facility. Thus a 20 acre PBR facility would be expected to produce about 160 tonne/yr, and a 200 acre facility would produce 1,600 tonne/yr. The projected FGPC market for 2025, as described in the original proposal, is about 1,000 tonne/yr. At 4,100 gal/acre-yr (and discounting by 12% for PC removal) those facilities would produce only 70,000 and 700,000 gal/yr of biocrude, respectively, an insignificant amount on the fuel market scale. The 20 acre case would modestly impact the PC market, while the 200 acre case would quickly saturate it.

To summarize, *Arthrospira* biomass can be produced competitively in a PBR-based facility compared to an open pond facility, both being modeled on a green-field TEA basis. Hence, PC can be produced competitively, assuming no differentiation in extraction technologies. This co-product cannot provide an economic crutch for biocrude production from algae. However, it can provide a market stepping stone toward algal biofuel production wherein PBR-based production technology can be demonstrated and optimized in a profitable enterprise.

E. *Summary and Conclusions for TEA Studies*

With regard to the economics of biomass and biocrude production from cyanobacteria, this project has advanced the state-of-the-art in a number of dimensions. The relationship between biomass

productivity for hanging bag PBR arrays *vs* open ponds has been firmly established for three organisms, making a strong argument for general application to all systems with light limited productivities. The observed 3x productivity advantage of PBRs will decrease for higher productivity systems with less pronounced photosaturation effects, but can be expected to be an important factor in any case. The productivity advantage is sufficient to overcome the CAPEX disadvantage in the PBR-pond comparison and has been convincingly shown by work in this project and work by others (Clippinger and Davis, 2019; Zhu et al., 2018). This project also demonstrated a clear advantage of PBRs in terms of predation risks, in that Algenol's lead strain, AB1, could be successfully grown for extended periods of time in PBR operations, whereas AB1 could not be grown consistently in ponds by two highly experienced organizations (ASU and RIL) due to frequent predation. Major advances in PBR operation were achieved in this project with the successful design and operation of a scalable semi-continuous production system. The resulting 60-80% improvement in productivity far exceeded BETO's established goals, and resulted in a major improvement in economics. Nevertheless, BFI costs are still in excess of 400 $/bbl (over 10 $/gal). A low carbon footprint, as discussed in the LCA section, can help, but the associated carbon credits are unlikely to overcome the economic deficiencies of the current technology in the near future. In addition, although the quality of biocrude was improved by NREL, biocrude quality is still an issue for displacement of most fossil fuel feedstocks. Improvements in BFI yield and quality, improvements in biomass productivity, and CAPEX/OPEX reductions are all required for advancing towards commercial viability.

Task 8 Summary

- PBR-based growth of *Cyanobacterium* sp. AB1166 at the 6,600 L scale integrated with downstream harvesting and dewatering operations were successfully conducted.
- A dewatering process for AB1166, consisting of first stage hollow fiber filtration followed by second stage continuous centrifugation, was determined to provide the lowest cost to achieve the required solids content for HTL.
- The Algenol Productivity Model was applied to *Cyanobacterium* sp. AB1 and AB1166 and *Arthrospira platensis*, enabling productivity comparisons between strains, including growth in open ponds *vs* PBRs. One outcome of these studies was that productivity obtained in Algenol's VIPER PBRs is approximately three-fold higher than open ponds (20 cm depth) for all strains tested.
- Life Cycle Assessments were determined for biocrude production from algal biomass, with a focus on the carbon footprint. Twelve different CO_2 supply cases spanning from fossil fuel-based power plant stack gases to direct air capture systems were compared. CO_2 supply for the combustion or gasification of biomass were determined to have the lowest carbon footprint for the supplied CO_2. A 60% reduction in carbon footprint was calculated for algal biofuels relative to fossil fuels.
- A detailed Techno-Economic Analysis (TEA) was completed for PBR-based production of biocrude. One aspect of this was a comparison of open pond- *vs* PBR-based production systems; the results indicated that Algenol's PBR system is completely competitive with pond systems under southwest Florida climate conditions. Despite the advancements achieved in this project, BFI costs were determined to still be in excess of 400 $/bbl (over 10 $/gal), indicating that Improvements in BFI yield and quality, improvements in biomass productivity, and CAPEX/OPEX reductions are all required for advancing towards commercial viability.

Task 8 Milestones

Subtask Topic	Milestone Number	Milestone Description	Milestone Verification Process	End Quarter
Integrated PBR operation	M8.1	Stable operation at 4,000-20,000 L scale and integrated HMB using commercial strain	TEA/LCA team receives integrated process HMB and performance data from commercial strain; TEA/LCA team identifies limitations and opportunities for commercial scale algae BFI facility	13
Outcome: **Completed**. TEA and LCA models fully developed and deployed with the latest process and performance data at 2,000 acre scale. Comparison to ponds completed. Limitations and opportunities for fuels and co-products identified and discussed.				
Deliver final report	M8.3	Project report complete	Project Team delivers final report to DOE	14
Outcome: **Completed.**				

Section References

Bechet, Q., Shilton, A., and Guieysse, B. 2013. Modeling the effect of light and temperature on algae growth: State of the art and critical assessment for productivity prediction during outdoor cultivation. *Biotechnology Advances* 31:1648-1663.

Clippinger, J. and R. Davis. 2019. Techno-Economic Analysis for the Production of Algal Biomass via Closed Photobioreactors: Future Cost Potential Evaluated Across a Range of Cultivation System Designs. National Renewable Energy Laboratory Report NREL/TP-5100-72716. https://www.nrel.gov/docs/fy19osti/72716.pdf

Huesemann, M. 2017. Algae DISCOVR Project: Development of Integrated Screening, Cultivar Optimization, and Validation Research. 2017 BETO Peer Review Meeting. https://www.energy.gov/sites/prod/files/2017/05/f34/Algae_Huesemann_132501-503%2C%20505.pdf

Legere, E. 2017. Algenol Integrated Pilot-Scale Biorefinery. DOE Final Project Report, https://www.osti.gov/servlets/purl/1360777.

Lu, Y., Xiang, Q. and Wen, Y. 2011. Spirulina *(Arthrospira)* industry in Inner Mongolia of China: current status and prospects. *Journal of Applied Phycology* 23:265-269.

MacColl, R. 2004. Allophycocyanin and Energy Transfer. *Biochimica et Biophysica Acta* 165:73-81.

Seider, W., Lewin, D., Seader, J., Widagdo, S., Gani, R. and Ng, K. 2016. Product and Process Design Principles: Synthesis, Analysis and Evaluation, 4th Edition ISBN: 978-1-119-28263-1.

Webb, W., Newton, M. and Starr, D. 1974. Carbon dioxide exchange of Alnusrubra: a mathematical model. *Oecologia* 17:281–291.

Zhu, Y., Anderson, D. and Jones, S. 2018. Algae Farm Cost Model: Considerations for Photobioreactors. Pacific Northwest National Laboratory Report PNNL-28201. https://www.osti.gov/servlets/purl/1485133

Publications, Presentations and Awards

Publications

Tao Dong, Wei Xiong, Jianping Yu and Philip T. Pienkos (2018) Co-production of fully renewable medium chain α-olefins and bio-oil via hydrothermal liquefaction of biomass containing polyhydroxyalkanoic acid. RSC Adv. 8, 34380-34387.

Tao Dong, Bo Wang, Wei Xiong, Nick Sweeney, Philip T. Pienkos, Jianping Yu (2020) System-level optimization to improve biofuel potential via genetic engineering and hydrothermal liquefaction. ACS Sustainable Chemistry and Engineering 8:2753-2762.

Pratham Arora, Ronald Chance, Howard Hendrix, Teresa Fishbeck, Matthew J. Realff, Valerie M. Thomas, and Yanhui Yuan (2020) Lifecycle Greenhouse Gas Emissions for an Ethanol Production Process Based on Genetically Modified Cyanobacteria: CO_2 Sourcing Options. (submitted)

Ankush Karemore, Yanhui Yuan, William Porubsky, and Ronald Chance (2020) Temperature Effects on Biomass and Pigment Production for *Arthrospira platensis* in Semi-Continuous Photobioreactor Cultivations. (submitted))

Pratham Arora, Ronald Chance, Howard Hendrix, Matthew J. Realff, Valerie M. Thomas, and Yanhui Yuan (2020) Life cycle greenhouse gas emissions of different CO2 supply options for an algal biorefinery. (submitted)

Presentations

Ron Chance (Algenol): “Biofuels and Bioproducts Produced in Photobioreactors.” School of Chemical and Biological Engineering, Georgia Tech, Atlanta, GA on April 11, 2017.

Laura Belicka (Algenol): “Algae-based Biofuel Production in the Algenol Direct-to-Ethanol Process.” Renewable Energy Systems and Sustainability Conference, sponsored by the Florida Energy Systems Consortium, in Lakeland, FL on July 31, 2017.

Ron Chance (Algenol): “Carbon Capture and Utilization in a Photobioreactor-based Biorefinery.” Invited lecture at ExxonMobil’s Corporate Strategic Research Laboratories in Annandale, NJ on September 7, 2017.

Ron Chance (Algenol): “Impacts of CO_2 Supply Systems for Algae-Based Biorefineries on Biofuel Life Cycle Assessments.” AIChE Meeting in Minneapolis, MN on October 29, 2017.

Philip T. Pienkos (NREL): “Outside the Box Thinking at NREL—New Feedstocks, New Targets, New Processes.” ABLC Next meeting held in San Francisco, CA, October 18, 2017.

Paul Roessler (Algenol): “Application of Synthetic Biology at Algenol Biotech.” Algae Biomass Summit in Salt Lake City, UT on October 30, 2017.

Ron Chance (Algenol): “High Value Products from a Photobioreactor-Based Biorefinery.” AIChE Meeting in Minneapolis, MN on October 31, 2017.

Jacques Beaudry-Losique (Algenol): “CO_2 Supply Systems for Algal Biorefineries.” Algae Biomass Summit in Salt Lake City, UT on October 31, 2017.

Ed Legere (Algenol): “Between the Pond and the Tube”. Algae Biomass Summit in Salt Lake City, UT on October 31, 2017.

Ron Chance (Algenol): "CO_2 Capture and Utilization in a Photobioreactor-Based Biorefinery." 10th CO_2 Utilization Summit in Tampa, FL on February 28, 2018.

Tao Dong (NREL): "An integrated biorefinery to co-produce linear α-olefins and bio-oil through hydrothermal liquefaction." AOCS Meeting in Minneapolis, MN on May 6-9, 2018.

Paul Roessler (Algenol): "Integrated Development of Novel Strains, Production Systems, and Downstream Processes for New Commercial Products at Algenol Biotech." 8th International Conference on Algal Biomass, Biofuels and Bioproducts held in Seattle, WA, June 10-14, 2018. He also served as a panel member at the "DOE Listening Day" held immediately after the ABBB Conference.

Ed Legere (Algenol): "The Algenol Photobioreactor: Evolution of Design and Performance." Algae Biomass Summit held in Houston, TX, October 14-17, 2018.

Ron Chance (Algenol): "The Algenol Photobioreactor System: Comparison to Pond Based Systems." Algae Biomass Summit held in Houston, TX, October 14-17, 2018.

Josee Bouchard (Algenol): "Biomass Production in an Advanced Photobioreactor-Based Biorefinery." Algae Biomass Summit held in Houston, TX, October 14-17, 2018.

Tao Dong (NREL): "Improving biofuel intermediate yield and quality by tuning algal composition." Algae Biomass Summit in Houston, TX on October 14-17, 2018

Ron Chance (Algenol): "CO2 Utilization in a Photobioreactor-Based Algal Biorefinery." 12th CO2 Utilization Summit in Houston Texas on February 28, 2019.

Paul Roessler and Ron Chance (Algenol) presented the current status of this project at the DOE BETO 2019 Project Peer Review Meeting in Denver, CO on March 6, 2019.

Lanny Miller (Algenol): "Execution of an Algal Biofuels Capital Project: Risks and Opportunities." US Microalgae Industry Summit in Fort Lauderdale, Florida on May 16, 2019.

Lisa Pickell (Algenol): "The Algenol Photobioreactor: Evolution of Design and Performance." US Microalgae Industry Summit in Fort Lauderdale, Florida on May 16, 2019.

Ron Chance (Algenol): "Carbon Capture and Utilization in a Photobioreactor-Based Algal Biorefinery." Plenary lecture at the Algal BBB Conference held in Boulder, Colorado on June 18, 2019.

Pratham Arora (GeorgiaTech): "Hydrothermal Liquefaction of Algae for Biocrude Production: Effects of CO_2 Sourcing on Economics and LCA", Foundations of Computer-Aided Process Design, Copper Mountain, CO, July 17, 2019.

Yanhui Yuan (Algenol): "Quantitative Translation of Small Scale Indoor Biomass Productivity Determinations to Large Scale Outdoor Determinations for Cyanobacteria." Algae Biomass Summit held in Orlando, Florida on September 16, 2019.

Yanhui Yuan (Algenol): "Life cycle greenhouse gas emissions of different CO2 supply options for an algal biorefinery." Algae Biomass Summit held in Orlando, Florida on September 16, 2019.

Paul Roessler (Algenol): "Product R&D at Algenol." Lecture for an online Algal Biotechnology course sponsored by ATEC (Algae Technology Educational Consortium). Recorded at the University of California – San Diego on November 21, 2019.

Paul Roessler (Algenol): “Algenol Biotech: Technology and Products.” Invited lecture at the University of California – San Diego for a course entitled “Advanced Topics: Biofuels and Bioproducts” on November 26, 2019.

Patent Applications

Budinoff, C., Hehman, L., Sweeney, K., McConnell, M., and Stegman, M. Methods for Extracting Phycocyanin. U.S. Patent Application No. 62,489,912, filed April 25, 2017.

Awards

Dr. Ron Chance was the recipient of the 2018 Lawrence B. Evans Award from the American Institute of Chemical Engineers. This is an institute level award recognizing lifetime achievement. The award carries with it a travel allowance and a $3,000 prize. The award was presented on October 28, 2018 at the annual AIChE meeting in Pittsburgh, PA.

Appendices

Appendix 1: Publications and Submitted Manuscripts Supported by this Award

Five manuscripts have been submitted for publication in peer reviewed journals, thus far two of these have been published (see Publications section for references). All five were supported in part by the current ABY2 project (DE-EE0007690), as noted in the acknowledgments. The remaining three submitted manuscripts are currently under review, and are attached. The first describes a detailed study of the production of *Arthrospira platensis*, the cyanobacterial strain that was the primary focus of the co-product scenario explored in this project. This paper establishes temperature constraints, including the impact on phycocyanin production; it also includes modeling fundamentals and predictions for outdoor performance that are well aligned with experimental observations. The second manuscript focuses more on CO_2 delivery options and discusses one biorefinery case study for biocrude production. This paper establishes numerous sourcing scenarios for achieving the 60% reduction in carbon footprint for an algal biorefinery that produces biomass for conversion to biocrude. The third manuscript describes lifecycle assessments for several CO_2 sourcing options for an algal biorefinery producing both ethanol and biocrude.

1.A. Biomass and Pigment Production for Arthrospira platensis via Semi-Continuous Cultivation in Photobioreactors: Temperature Effects

Biomass and Pigment Production for *Arthrospira platensis* via Semi-Continuous Cultivation in Photobioreactors: Temperature Effects

Ankush Karemore[1,2], Yanhui Yuan,[3] William Porubsky,[3] Ronald Chance[2,3]

[1]*School of Industrial and Systems Engineering, Georgia Institute of Technology Atlanta, GA 30332*

[2]*School of Chemical and Biomolecular Engineering, Georgia Institute of Technology Atlanta, GA 30332*

[3]*Algenol Biotech LLC, 16121 Lee Rd, Fort Myers, FL 33912*

Abstract
This study describes the response of *Arthrospira platensis* to a variety of temperature conditions as reflected in variations of photosynthetic parameters, pigmentation, and biomass productivity in indoor photobioreactor (PBR) cultivations. These experiments are designed to better understand the impact of temperature, seasonal variations, and acclimation effects on outdoor biomass production. The irradiance level and temperature range (20 – 39°C) are chosen to enable modeling of semi-continuous operation of large-scale outdoor PBR deployments. Overall, the cultivations were quite stable with some pigment-related instabilities after prolonged high temperature exposure. Changes in productivity with temperature, as reflected in measured photosynthetic parameters, are immediate and mainly attributable to the temperature dependence of the photosaturation parameter, a secondary factor being variation in pigment content on a longer time scale corresponding to turnover of the culture population. Though pigment changes have minimum impact on productivity, prolonged exposure at 35°C and above yields a clear degradation in performance. Productivities in a semi-continuous operation are quantitatively reproduced with a

productivity model incorporating photosynthetic parameters measured herein. This study confirms the importance of temperature for biomass and pigment production in *Arthrospira* cultivations and provides a basis for risk assessments related to temperature mitigation for large-scale outdoor cultivations.

Introduction

The filamentous cyanobacterium *Arthrospira platensis (Spirulina)* is an oxygenic photosynthetic organism able to grow in tropical and subtropical environments, and one of only a few microalgal systems that has been successfully commercialized and approved by United States Food and Drug Administration (FDA) as a food supplement (Trabelsi et al., 2009). *Arthrospira* cultivation and processing yields valuable biochemical components including protein, carbohydrates, fatty acids and pigments such as phycocyanin (PC), which can be used in nutritional, pharmacological, and cosmetic products. Due to these high value applications, as well as relatively easy harvesting and extraction processes, *Arthrospira* cultivation has been deployed commercially at moderate scale (10 – 100 acre open ponds) for many decades (Lu et al., 2011). It is important to note that *Arthrospira* is an extremophile, in that it can maintain high productivity under high alkalinity, high pH conditions; this limits predation and competition sufficiently to allow commercial production in open pond systems. Algal cultures are influenced by various abiotic variables such as temperature, irradiance levels, and nutrient availability, all of which play a significant role in regulating photosynthetic activity, biomass composition and overall productivity. Under outdoor cultivation conditions, temperature and light intensity are the two key external factors that determine photosynthetic activity and biomass growth rates. Obviously, both factors are highly variable on a daily and seasonal basis in the natural environment, and spatially within the culture as well (Chaiklahan et al., 2007; Vonshak and Novoplansky, 2008). Typically, *Arthrospira* is cultivated outdoors for mass production in raceway ponds, where cells encounter fluctuating environments in terms of irradiance, temperature, and nutrient supply. Though the PBR environment tends to be more homogeneous, similar fluctuations are present and temperatures are generally higher due to absorptive heating and the absence of evaporative cooling. Outdoor algal cultures are subjected to high light intensity as well as possible high temperature stress that can negatively impact photosynthetic activity (Torzillo et al., 1991b). These factors can change both the photosynthesis and respiration rates, thereby directly influencing the growth and the chemical composition of the biomass produced (Trabelsi et al., 2009).

Overall, the existing literature is consistent with an optimal temperature range for stable production of roughly 20-35 °C. Our screening studies are consistent with that range and also consistent with an activation energy of about 60 kJ mole^{-1} (Q10 ~2) under saturating light conditions over that temperature range. It is well-known that productivity is enhanced in semi-continuous operation where the impact of photosaturation effects is lessened. We know of no detailed studies dealing with the effect of temperature and acclimation response on growth and pigment content of *Arthrospira* in a semi-continuous production mode for extended time scales under tightly controlled (laboratory) conditions. The intention here is to determine what portion of previous learnings translate to semi-continuous operation and the dynamic (light/temperature) conditions experienced outdoors, and examine the responses to abrupt changes in temperature. Therefore, in the present work we will examine temperature effects at a longer time scale, and carry out the experiments in semi-continuous operation mode in PBRs at 20 °C, 30 °C and 35 °C. In subtropical conditions, the outdoor culture temperature in the summer months can be very high in PBRs, reaching up to 35-45 °C for several hours. We have only a limited understanding of temperature impacts on photosynthetic parameters, and pigment accumulation in that outdoor environment. Thus, the scope of this work includes *Arthrospira* growth under a variety of temperature conditions with a work plan that includes assessment of temperature response and recovery, and quantification of the dynamic change in biomass and pigment content of *Arthrospira* during the experiments. There is no doubt that high irradiance levels can be a confounding factor both at low and high temperatures. We limit the current study to “average” irradiance conditions in Fort Myers, Florida. The combination of vertical PBR arrays, which dilute the average irradiance levels from about 800 µE/m2-s to about 200 µE/m2-s, and the rapid mixing, which distributes the heat from light absorption more evenly within the PBR volume, lessen the potential for extreme effects due to high irradiance. That is born out by cultivation field observations of *Arthrospira* growth and laboratory studies of irradiance effects with the same approach used here. Regarding lower temperatures than the 20°C included here, our screening studies do not suggest any issues down to 10°C and field experience in the environment of interest shows that the concerns lie at high temperatures.

The work was performed in three phases (Figure 1a): Phase I employs constant temperature conditions (same for day and night cycles), Phase II shifts the Phase 1 cultures to opposing temperature conditions (low to high, and high to low), and Phase III continues the examination under dynamic summer temperature profiles (hourly variations) in a semi-continuous operation mode. The experimental setup, shown in Figure 1b, involves vertically oriented tubular photobioreactors, designed to be predictive of outdoor performance in large PBR arrays.

Material and Methods

1.

Algal Strain and culture condition

The algal strain used in this study was *Arthrospira Platensis* maintained in Zarrouk's medium with the following macro and micro ingredients (mM): $NaHCO_3$ (200), K_2HPO_4 (3.7), $NaNO_3$ (30), K_2SO_4 (5.7), NaCl (18), $CaCl_2$ $2H_2O$ (0.27), $FeSO_4$ $7H_2O$ (0.036), Na_2EDTA $2H_2O$ (0.215), NaOH (0.1), H_3BO_3 (0.045), $MnCl_2$ $4H_2O$ (0.009), $ZnSO_4$ $7H_2O$ (0.001), $NaMoO_4$ $2H_2O$ (0.000083), and $CuSO_4$ $5H_2O$ (0.00032) (Zarrouk, 1966). Unless stated otherwise, Zarrouk´s medium with 200 mM $NaHCO_3$ was used for all culture cultivations. The seed culture was sourced from a private collection and cultivated at 30 °C for one week to reach a biomass concentration of 0.75 gDW L^{-1} (optical density at 750nm, OD_{750}, equal to 1.5). Under most conditions the DW to OD_{750} ratio was about 0.5 gDW L^{-1} per OD_{750} which is regarded as normal for this organism. Although some variation within the relationship between OD and DW can occur with differing temperature conditions (Jahnke et al., 2011; Torzillo et al., 1991a), such variations were generally minor in the experiments reported here and only occurred at the latter stages of growth at 35 °C where the cultures displayed clear instabilities (declines) in pigmentation. Lower pigmentation, especially in the red spectral region, can lead to lower refractive indices at 750 nm, lower light scattering, and thus high DW/OD ratios, as observed. The DW measurements involve collecting algal cells on pre-rinsed glass fiber filters (1.5 µm pore size, 47 mm ProWeigh Filters, Cole-Parmer) by filtration, washing three times in deionized water, and then drying to a constant weight at 60 °C for 48 h. The specification for the drying method calls for a water content of no more than 3% after 24 h. The remaining salt content after this procedure was generally less than 2%, and to that extent our DW is equivalent to ash-free DW (AFDW).

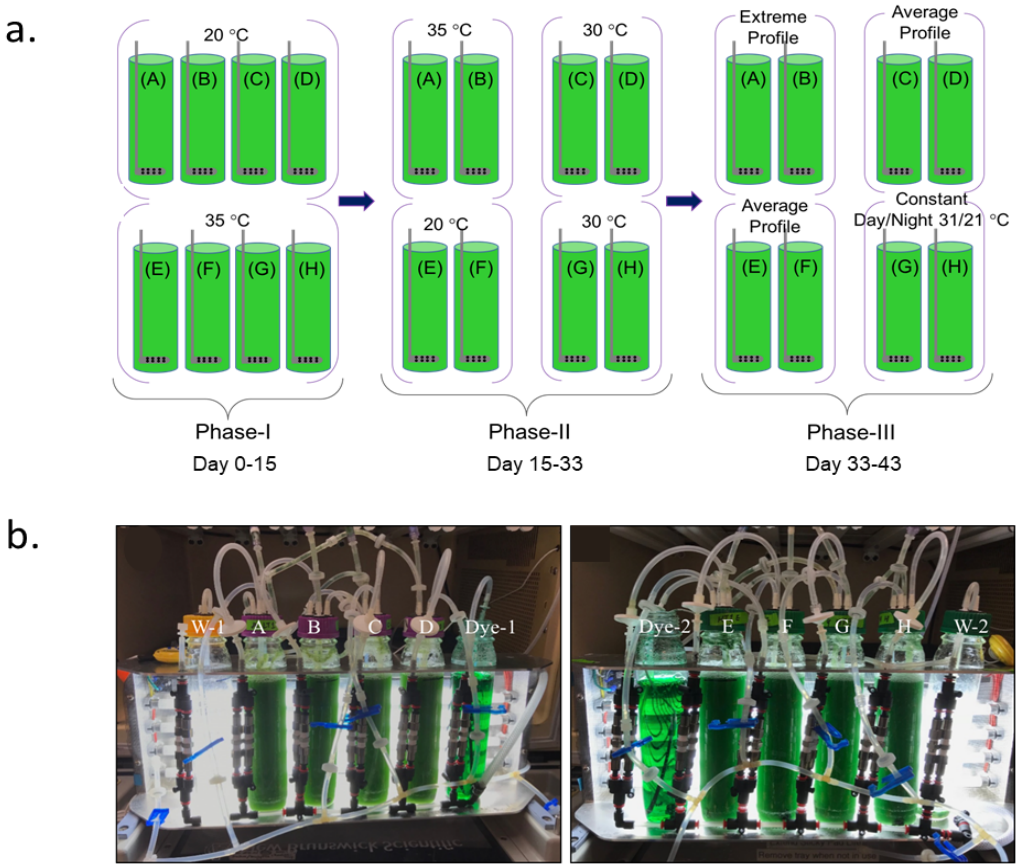

Figure 1. a) Experimental program illustrating timing for the three experimental phases and the sequencing of the eight reactors. The temperature profiles for Phase III are based on historical climate data in Fort Myers Florida. The Extreme Profile is based on summer temperatures only; the average profile is based on annual average. Both involve hourly temperature variations in the reactors. The Constant Profile has contant values on a 12-12 cycle based on annual day and night averages. b) Photobioreactor setup for cultures in Phase I where Reactors A, B and C, D were cultivated at 20 °C and (b) Reactors E, F and G, H were cultivated at 35 °C. Dye-1 and Dye-2 were the dummy reactors used for monitoring temperature, and reactors W-1 and W-2 were connected to the reactor exhaust and used as waste collectors due to minor foaming and evaporation loss. Reactors are brought outside of the incubator for sampling and photograph.

Arthrospira platensis, the most common commercial strain, is interchangeably referred to as "*Spirulina*" in the literature. We have used *Arthrospira* throughout this article to refer to the organism under study here and literature results cited for *Arthrospira platensis*.

0.35-liter PBR cultivation conditions

For 0.35 L PBR operation, the reactors were inoculated with the *Arthrospira* strain grown at 30 °C to a concentration of 0.5 gDW L^{-1}. The pH value was maintained between 9.2-9.8 with an aeration rate of 80 mL min^{-1} supplying 0.75 % CO_2 during the light phase and 0.20 % CO_2 in the dark phase for cultures grown at 30 °C and 35 °C. The cultures grown at 20 ° C were supplied with 0.38 % CO_2 during the light phase, and 0.2 % CO_2 in the night phase. The aeration rate chosen for these experiments is higher than normal due to the filamentous

nature of *Arthrospira* that leads to settling under less stringent conditions. Thus the CO_2 concentration, required to supply the cultures and replenish the bicarbonate consumed by the organism, appears low but is confirmed to be sufficient by the pH monitoring, as well as extensive experience with outdoor cultivations. The light regime for the cultures was a 12 h light:12 h dark cycle with light intensity of 230 µmol m^{-2} s^{-1} from one side of the PBRs using fluorescent lamps (Plusrite). This irradiance level was chosen to model annual average conditions for typical vertical PBR arrays deployed in Fort Myers, Florida. For CO_2 aeration and mixing of the cultures, a custom designed porous air diffuser (0.5 mm diameter) was used in order to generate mm-size gas bubbles for aeration at a constant flow rate of 80 mL min^{-1}.

Semi-continuous cultivation and experimental set-up in PBR

For semi-continuous cultivation, culture dilution with Zarrouk´s medium was carried out on alternate days maintaining OD_{750} = 2.0 (~1 gDW L^{-1}) as the starting point for the next production cycle. The experiment was continued over a time course of 43 days in this semi-continuous operation mode. The experimental program was divided into three phases with eight PBRs designated in alphabetical order from A to H. These eight PBRs were divided in four sets of duplicate PBRs indicated as 'AB' for A and B, 'CD' for C and D, etc. (Figure 1). OD750nm was monitored as a surrogate for biomass concentration, with the OD-concentration relationship periodically monitored. That relationship (typically DW in g L^{-1} = 0.5*OD750nm) varied only slightly during the course of these experiments as discussed above.

In Phase I, four reactors each were cultivated at constant 20 °C (AB, CD) and 35 °C (EF, GH) for 15 days. In Phase II, the four reactors at 20°C were shifted to 30 °C (CD) and 35 °C (AB) whereas the other set of four reactors at 35°C were shifted to 20 °C (EF) and 30°C (GH). The Phase II shift was started on the 15th day and kept in place until the 33rd day. To acclimate the cultures to the newer temperature conditions, cultures were grown in batch mode for four days (15 – 19) without performing any dilution. In the final Phase III, the culture conditions were shifted from constant temperature to dynamic summer temperature profiles (derived from historical climate data for Fort Myers, Florida) with hourly changes in temperature over the course of 24 hours. This phase lasted from day 33 to day 43. In this phase, the cultures grown at constant 20 °C (EF) and 30 °C (CD) in Phase II were shifted to average summer profile with 35/21 °C as maximum/minimum temperatures, the culture at constant 35 °C (AB) was moved to extreme summer profile with 39/26 °C as maximum/minimum temperatures, and final set of two reactors cultured at constant 30°C (GH) were shifted to constant day (31 °C) and night (22 °C) temperature based on summer average of day and night temperatures. Summer is defined as June 1 through August 31 for creating these profiles from historical data.

Determination of chlorophyll and phycocyanin

Chlorophyll-a (Chl-a) was measured using a standard methanol-based methodology (Marsac and Houmard, 1988).

PC extraction and quantification was carried out using repeated freeze-thaw cycles based on Yoshikawa and Belay (2008). Briefly, this method extracts PC from fresh biomass using a repeated freeze-thaw and soaking regime and then quantifies PC spectro-photometrically based on absorbance at three wavelengths: 620 nm, 650 nm and 680 nm. PC content is calculated following the Yoshikawa equation, where cPC is C-phycocyanin and aPC is allophycocyanin:

$$\text{cPC, mg/mL} = 0.162 \times OD_{620} - 0.098 \times OD_{650} \quad (1)$$

$$\text{aPC, mg/mL} = 0.180 \times OD_{650} - 0.042 \times OD_{620} \quad (2)$$

Photosynthetic parameters

The oxygen PE (O_2 production vs irradiance) curves were determined in Algenol's custom-designed system. The system is comprised of a white light LED source, photosynthetically active radiation (PAR) light sensor, and an O_2 sensor, all in a temperature-controlled cassette (Legere, 2017). The optical path length, d, is 1 cm. The cell contains 4 ml of fluid stirred at 400rpm with no head space. For measurement of O_2, needle-type oxygen sensors (OXR50, Pyroscience) composed of fiber-optical cable connected to FireSting O_2 sensors were used. Response times to changing conditions were rapid with no indication of mass transfer limitations. The temperature is controlled to ±1 °C over the range from 10 °C to 50 °C. The culture samples were taken from the PBR and incubated at 30 °C for 1.5 hr for dark acclimation, and then diluted to an absorptivity of exp(-kd)=0.1 (concentration~ 1 mg Chl.a L^{-1}) using fresh Zarrouk's media, where k is the absorption coefficient for the whole cell *Arthrospira* averaged over the PAR range (400-750 nm). In determining k, spectra are first corrected

for scattering (approximately) by subtracting at all wavelengths the absorbance at 750 nm (OD_{750}). The first 10 min of oxygen uptake data in the dark is used to calculate the dark respiration rate. The light is then ramped up to 1000 µE m^{-2} s^{-1} stepwise with 3 min at each step (typically 15 steps). The oxygen evolution rate is fitted with a Monod model (Bechet 2013) form to report photosynthetic parameters: α, E_k, and P_{max} (limited quantum yield in low light limit, photosaturation parameter, and max photosynthetic rate in high light limit). The Monod mathematical model is used in order to be consistent with the approach taken for the Algenol Productivity Model (see Supplementary Material). All measurements are carried out in duplicate.

Productivity Modeling

Ethanol productivity from genetically modified cyanobacteria has been successfully modeled by Algenol using a Monod modeling approach (Legere 2017). The Algenol Productivity Model has been adapted for biomass-only production and used in conjunction with PE-derived photosynthetic parameters to estimate expected outdoor productivities for PBR deployments in Fort Myers (and elsewhere around the world). The daily biomass volumetric productivity can be described as:

$$P_{Biomass} = \alpha E_k \gamma ln\left[\frac{E_k+E_0}{E_k+E_0 e^{-kD}}\right]\frac{t_1}{D} - R_0 C_c \gamma t_2 \qquad (3)$$

where α is the quantum yield in the low light limit (mol C /mol photons), E_k is the photosaturation parameter (µE m^{-2} s^{-1}), γ is the conversion between fixed C to dry weight biomass (gDW mol C^{-1}), E_0 is the incident light intensity (µE m^{-2} s^{-1}) at the culture surface (corrected approximately for reflection losses), k is the absorptivity coefficient of biomass (m^{-1}), D is the effective light path (m), R_0 is the specific respiration rate (µmol C $mgChl.a^{-1}$ min^{-1}), C_c is the Chl.a concentration (mgChl.a m^{-3}), t_1 is the time for light-on (sec), and t_2 is the time for respiration load (min). Light-on time (t_1) is about half of the respiration load time (t_2) for outdoor cultivation. For the indoor PBR experiment, 12 hr light/12 hr dark cycle, E_0 is constant at 230 µE m^{-2} s^{-1}, and the average light path (D) is approximately the radius of the reactor tubes with illumination from one side. The productivity data are quoted as the mean values ± SD (n = 2) for the two independent replicate cultures. The derivation of Equation (3) is included in Supplementary Material along with application of model to a large scale outdoor PBR cultivation of *Arthrospira* (Chance and Roessler 2019). The model applies to a static system, in that none of the mixing rates involved in these cultivations involve significant movement of culture components on the time scale of the photosynthetic reactions. (See Supplemental Material.)

Results and Discussion

Cell growth characteristics

Cell growth was evaluated based on the determination of optical cell density (OD_{750}), converted to dry weight (DW). Pigment content was determined by extraction and quantification as described above. All results reflect duplicate measurements, plus at least two biological replicates.

Startup: Phase I

The biomass growth profiles of *Arthrospira* under photoautotrophic conditions in three phases are shown in Figure 2. In Phase I, the growth response to constant low temperature (LT) (20 °C±1) (AB & CD) and high temperature (HT) (35°C±1) (EF & GH) was assessed. PBRs were cultivated in batch mode for initial 5 days to reach OD_{750} 2.0 and beyond, and then operated in semi-continuous mode maintaining the OD_{750} = 2.0 starting point from day 5 to 15 with harvest/dilution every two days. For the chosen temperatures of 20°C and 35°C, the average pre-dilution concentrations of the cultures were 1.30 gDW L^{-1} (OD_{750} = 2.6) and 1.62 gDW L^{-1} (OD_{750} = 3.2) respectively (Figure 2) yielding biomass growth rates 0.17 gDW L^{-1} d^{-1} and 0.20 gDW L^{-1} d^{-1} at 20 °C and 35 °C, respectively. These results are summarized in Table 1. As can be seen in the table, good reproducibility is found for all results (including pigment contents to be discussed later).

Transition: Phase II

As noted earlier, in Phase II (day 15 to 33) the four cultures (ABCD) grown previously at 20 °C were shifted to 35 °C (AB) and 30 °C (CD), and the four cultures at 35 °C (EFGH) were shifted to 20 °C (EF) and 30 °C (GH). As a recovery phase and to acclimate the cultures after transition from Phase I to Phase II, the cultures in the newer temperature conditions were grown in batch mode without dilution for four days from day 15-19. The

responses to temperature change were assessed at the end of the fourth day. As expected, the culture shifted from lower temperature (LT) (20 °C) to higher temperatures (30 °C and 35 °C) showed higher growth to 1.90 gDW L^{-1} (from 0.93 to 1.90 gDW L^{-1} over 4 days). The cultures shifted from higher temperature (35 °C) to low temperature (20 °C and 30 °C) grew more slowly, with biomass concentration reaching around 1.71 gDW L^{-1} (from 1.17 to 1.71 gDW L^{-1}) on day 19 after four days of batch cultivation (Figure 2 a and b). The time scale of temperature response for *Arthrospira*, as judged from these OD750nm measurements, is essentially instantaneous within the noise of these measurements.

Table 1. Summarized results indicating various growth and pigment parameters in response to temperature conditions in Phase I, II and III. Phase I starts with 20 °C for both AB and CD, shifted to 35 °C (AB) and 30 °C (CD) in Phase II, then to ExSP (AB) and AvSP (CD) in Phase III, whereas culture EF and GH start with 35 °C in Phase I, shifted to 20 °C (EF) and 30 °C (GH) in Phase II, then to AvSP (EF) and CtSP (GH) in Phase III, respectively. Biomass Concentration is the concentration prior to dilution, averaged over the relevant Phase period (semi-continuous operation regions only). Error bars are +/- one standard deviation.

Parameters/Temperature treatments	**AB**	**CD**	**EF**	**GH**
Phase I: 0-15 Days (n=4)	**20°C**	**20°C**	**35°C**	**35°C**
Biomass Concentration (g L^{-1})	1.29±0.07	1.30±0.05	1.62±0.05	1.61±0.08
Biomass Productivity (g L^{-1} day^{-1})	0.17±0.03	0.17±0.02	0.20±0.04	0.21±0.03
PC % (%DW)	8.08±0.3%	8.09±0.4%	9.95±1.1%	9.73±0.8%
aPC % (%DW)	2.85±0.09%	2.83±0.10%	2.68±0.21%	2.61±0.15%
cPC % (%DW)	5.22±0.22%	5.26±0.35%	7.27±0.57%	7.11±0.42%
Chl-a %	1.61±0.10%	1.61±0.13%	0.98±0.17%	1.0±0.12%
Phase II: 15-33 Days (n=4)	**35°C**	**30°C**	**20°C**	**30°C**
Biomass Concentration (g L^{-1})	1.57±0.17	1.48±0.18	1.40±0.09	1.58±0.14
Biomass Productivity (g L^{-1} day^{-1})	0.18±0.04	0.21±0.02	0.15±0.03	0.23±0.06
PC % (%DW)	11.50±0.8%	11.31±0.6%	7.45±0.3%	10.35±1.0%
aPC% (%DW)	3.20±0.13%	3.49±0.15%	2.22±0.08%	2.91±0.23%
cPC% (%DW)	8.30±0.36%	7.82±0.39%	5.23±0.23%	7.44±0.45%
Chl-a %	1.32±0.05%	1.70±0.11%	1.14±0.23%	1.42±0.18%
Phase III: 33- 43 Days (n=4)	**Ext. Summer (39/26°C)**	**Ave. Summer (35/21°C)**	**Ave. Summer (35/21°C)**	**Ct. Summer (31/21°C)**
Biomass Concentration (g L^{-1})	1.59±0.03	1.52±0.02	1.45±0.05	1.58±0.04
Biomass Productivity (g L^{-1} day^{-1})	0.22±0.02	0.25±0.02	0.24±0.02	0.25±0.02
PC % (%DW)	10.85±0.4%	12.42±0.5%	11.85±0.6%	11.49±0.4%
aPC% (%DW)	2.81±0.07%	3.61±0.18%	3.57±0.14%	3.34±0.12%
cPC% (%DW)	8.04±0.40%	8.81±0.39%	8.28±0.54%	8.15±0.33%
Chl-a %	1.08±0.12%	1.83±0.16%	1.93±0.09%	1.86±0.04%

During semi-continuous operation in Phase II, different algal growth patterns are found under the chosen temperature conditions. The average pre-dilution DW biomass concentrations for the different temperature treatments are shown in Table 1. The 20 °C average is the only one that is clearly distinguishable. The most favorable temperature appears to be 30 °C, which is close to the optimum temperature for *Arthrospira* for achieving maximum productivity under our growth conditions. The results are consistent with that of Colla et al. (2007), where higher temperatures had a clear negative effect on *Arthrospira* biomass production. An optimization study carried out by Sánchez-Luna et al. (2007) in batch cultivations reported 29 °C as best growth temperature. For the two cultures in our Phase II study maintained at 30 °C (one originating from the 20 °C Phase I experiment and the other from the 35 °C Phase I experiment), the results are essentially the same. Thus, the extreme of temperatures and prolonged exposure to high temperatures at 35 °C in Phase I is thought to have caused stress to the cells, and that has been observed by others to result in decline in biomass production and protein content, with simultaneous accumulation of carbohydrate and EPS (Panyakampol et al., 2015; Trabelsi et al., 2009). There was some decline in growth rate at 35 °C, though a stress response is clearer in the pigment content, as discussed below. Noticeable decline in growth and a lower cell density were observed in the cultures that were shifted from 35 °C→20 °C. This is normal temperature dependence (Kumar et al., 2011). The relative dilution rates were 0.12 day^{-1} at 20 °C, 0.16 day^{-1} at 30 °C, and 0.13 day^{-1} at 35 °C. The highest dilution rate, and therefore productivity, was seen at 30 °C. This agrees with the results cited above and also with Trabelsi et al. (2009) where maximum growth rate for *Arthrospira platensis* was found at 30 °C.

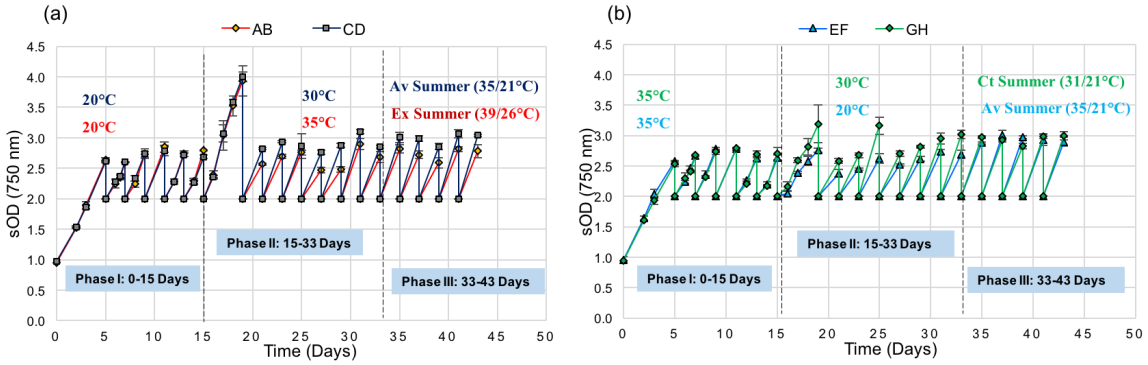

Figure 2. OD (750 nm) results for cultures in three different phases (a) AB and CD and (b) EF and GH at various temperature treatments. Results shown are the average of two determinations with error bars showing the range of values. Temperature conditions for the various phases are shown.

Table 2. Summary of photosynthetic parameters at different temperature treatments in the three phases obtained from Monod fits to the PI response curve

	Phase I		Phase II			Phase III		
Temperature treatments	20 °C	35 °C	20 °C	30 °C	35 °C	31/21 °C	35/21 °C	39/26 °C
PI Temperature	20 °C	35 °C	30 °C	30 °C	30 °C	30 °C	30 °C	30 °C
sOD750	2.6	2.7	2.5	2.75	2.5	3.0	2.95	2.8
Chl.a-Extract/sOD (mg/L)	7.5	8.15	6.7	8.0	7.7	10.3	10.1	7.3
P_{max} (µmolO_2/L-hr)	240	620	583	650	510	730	710	580

α' (molO$_2$/mol photon)	0.075	0.075	0.060	0.075	0.070	0.090	0.080	0.060
E$_k$ (μE/m^2-s)	85	230	270	240	200	220	240	270
R$_0$' (μmolO$_2$/L-hr)	0.12	0.48	0.47	0.37	0.55	0.49	0.25	0.35

Outdoor Simulation: Phase III

Phase III involved exposing the cultures to dynamic temperature profiles with hourly changes in temperature that are representative of outdoor summer culture temperature profiles (Supplementary Material). This final phase of cultivation was carried out from day 33-43 with scheduled alternate day dilutions and with no adaptation period. The cultures grown at constant 20 °C (EF) and one set of the constant 30 °C (CD) cultures were shifted to average summer profile (AvSP) with 35 °C/21 °C as maximum/minimum temperatures during the course of day/night temperature ramping. The cultures at constant 35 °C (AB) were shifted to an extreme summer profile (ExSP) with 39 °C/26 °C as maximum/minimum temperatures, and the final set of two photobioreactors at constant 30 °C (GH) were shifted to constant summer profile (CtSP) where day/night temperature were maintained at constant 31 °C/21 °C, selected based on Fort Myers summer profile and averaging the day and night temperatures separately.

The average pre-dilution cell concentration in gDW L^{-1} for the temperature profile treatments are shown in Table 1. The relative dilution rates were about 0.16 day^{-1} in AvSP (CD), AvSP (EF) and CtSP (GH), and about 20% lower (0.135 day^{-1}) for ExSP (AB).

From visual observations, it is worth noting that during the processing of biomass samples for the various analyses, agglomeration or clumping of the algal cultures occurred for cultures grown at higher temperature (constant 35 °C and ExSP). This is attributed to a stress response. In addition, the dried samples from these temperature exposures showed a flaky texture on the dry weight plate membrane surface. In cyanobacteria, high temperature stress can result in a rise in fluidity of membranes which can cause disintegration of the lipid bilayer and many other alterations in the physical properties of the cells that result in the loss of functionality of photosynthetic machinery (Panyakampol et al., 2015; Panyakampol et al., 2016).

Biomass Productivity

Table 1 summarizes productivity results obtained in different phases of temperature treatment. These productivities are averaged over the entire phase and indicate an apparent peak at 30 °C. Figure 3 summarizes the productivity results found towards the end of the various phases with average values plotted against average daytime temperatures. This plot is intended to explore the final results of the extended periods at the various temperature conditions. The variation from 20 °C to 30 °C is attributed to the temperature dependence of P_{max} (and thus E_k) and is less than the commonly observed Q10 = 2 behavior due to the irradiance level (230 μE m^{-2} s^{-1}) being substantially below E_k as shown below. This is the expected behavior when the system is stable and unstressed. No acclimation, other than the normal E_k dependence on temperature, is indicated. The slight downturn at 35 °C and higher in Figure 3 is attributed to a stress response that is more apparent in the pigment results discussed below. The consequences of the stress response are continuing throughout the time period of the phases, consistent with a degradation as opposed to an acclimation process. The downturn in productivity and pigmentation was enhanced for batch experiments at 35 °C to 45 °C that are not discussed here.

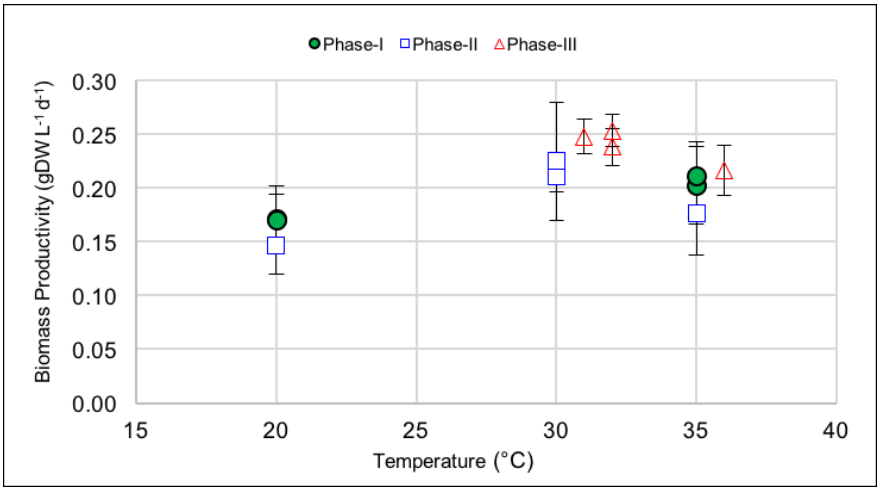

Figure 3. Average biomass productivities of *Arthrospira platensis* at various temperature treatments in three phases: Phase I temperature were 20 and 35 °C; in Phase II temperature were 20, 30 and 35 °C and in Phase III 31 °C (CtSP), 32 °C (AvSP) and 36 °C (ExSP), where temperature designations are the average daytime values. Error bars are +/- one standard deviation for the averages over multiple days of semi-continuous operation.

The choice of 230 µE m^{-2} s^{-1} was based on the average annual irradiance at the exposed culture surfaces of PBR arrays in Fort Myers, Florida with a height-to-spacing ratio chosen to maximize productivity (Legere, 2017). To convert the quoted biomass productivities from g L^{-1} d^{-1} to g m^{-2} d^{-1}, multiply by a geometric factor of 95 L m^{-2}. Thus, taking 30 °C as a reasonable estimate of the annual average daytime temperature in Fort Myers, a biomass productivity of 21 g m^{-2} day^{-1} is obtained. This is very close to the observed annual average of 23 g m^{-2} day^{-1} found experimentally for large PBR arrays (24,000 L culture) tested for over 1 year at the Algenol site in Fort Myers (Chance and Roessler, 2019; see also Supplementary Material).

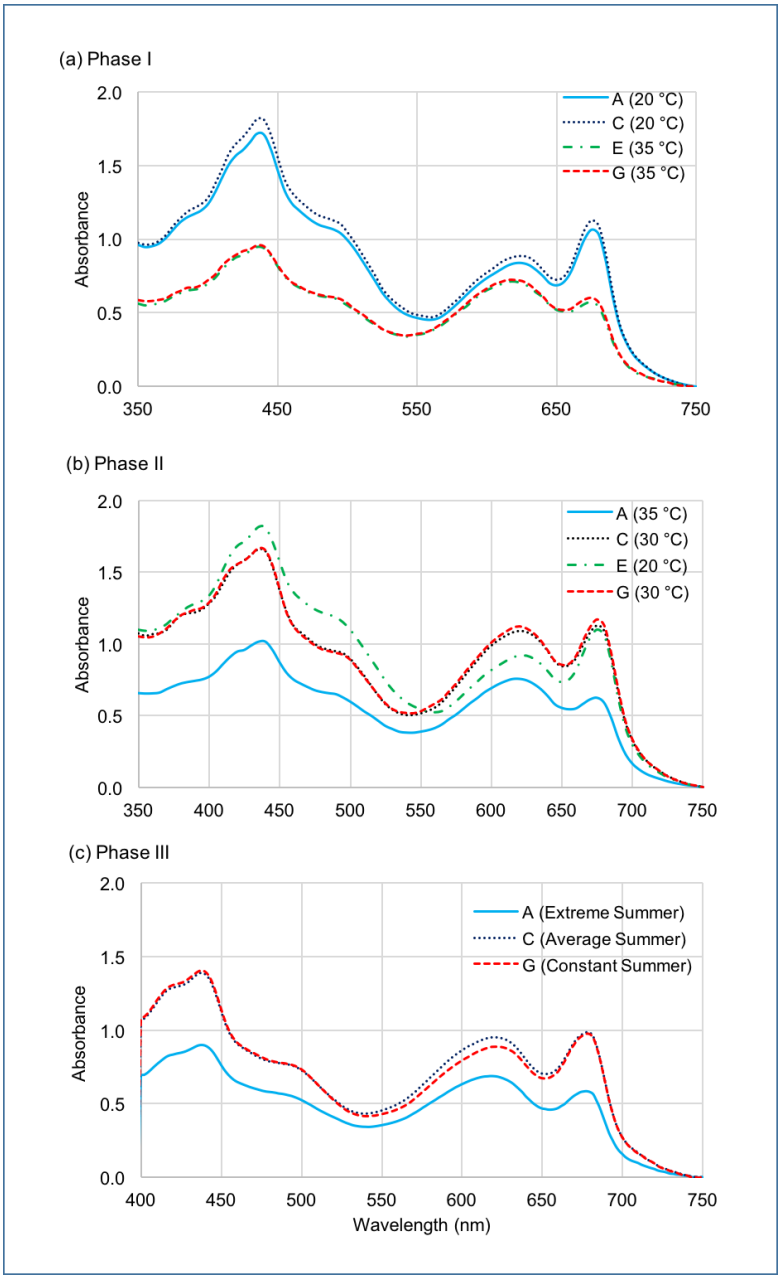

Figure 4. Representative whole cell (WC) spectra of cultures at different temperature treatments in the three phases of the experiment (a) Phase I at 20 °C (A and C) and 35 °C (E and G), (b) Phase II at 35 °C (A), 30 °C (C) 20 °C (E) and 30 °C (G), and (c) Phase III with Extreme Summer, ExSP (A), Average Summer, AvSP (C) and Constant Summer, CtSP (G). The absorbance values are normalized to 1 gDW L^{-1}.

Chlorophyll and Phycocyanin Production

During the cultivations, chlorophyll (Chl-a) content and phycocyanin (PC) content for *Arthrospira* were monitored. The two main components of the PC content were determined separately: allophycocyanin (aPC) and C-phycocyanin (cPC) via spectroscopic determination (Yoshikawa and Belay, 2008). In addition, whole cell (WC) absorption spectra were measured (Figure 4) for qualitative pigment analysis. Results for pigment content are summarized in Table 1 and displayed in detail in Figure 5. All quoted contents are expressed as a percentage of whole cell dry weight.

First, from the Phase I results in Table 1, good reproducibility between the biological duplicates (AB-CD and EF-GH) is found for all the measurements. It can also be seen from Figure 5 that the AB and CD experiments at 20 °C are very stable in their pigment content, both PC and Chl-a. That is not the case for the 35 °C results where both PC and Chl-a are decreasing steadily throughout the Phase I residence time in Figure 5c. The decline in PC is about 20% and the decline in Chl-a is about 40% over the course of the Phase I experiments at 35 °C. It is unlikely that the degradation in pigment content in either case is due to thermal damage to the pigments, as these pigments are known to be stable to much high temperatures. It is more likely due to a slow alteration of the photosynthetic apparatus, which we regard as biologically irreversible (as distinguished from recovery from culture turnover in the semi-continuous mode). The decrease in PC content could in fact be a consequence of the decrease in Chl-a content as the light harvesting machinery re-balances the optimal ratio for these pigments.

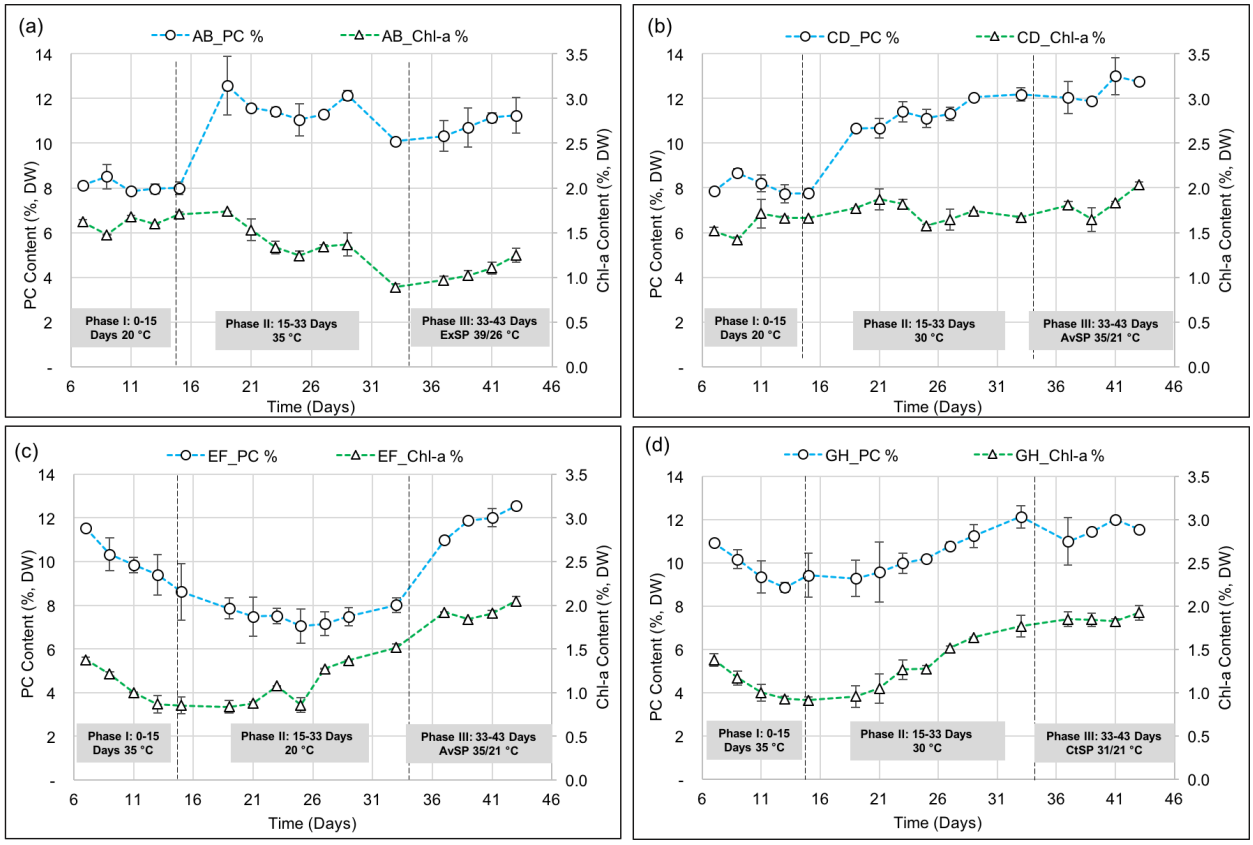

Figure 5. PC and Chl-a content (%, DW) in the three phases of the experimental plan at different temperature conditions. Experiments were performed in duplicate.

In Phase II, the AB culture goes from 20 °C to 35 °C with an initial sharp increase in PC content followed by a slow decline (Figure 5a). The Chl-a content stays constant initially and then declines slowly over the Phase II residence time, the overall decrease being similar to that for EF in Phase I (Figure 5c). The CD culture, which transitioned from 20 °C to 30 °C (Figure 5b), shows much more stable behavior, with a slower increase in PC content before reaching an apparent steady concentration of about 12%. The Chl-a concentration is stable at about 1.7%, similar to Phase I at 20 °C. There is no indication of instability at 30 °C. The CD culture, transitioned from 35 °C to 20 °C (Figure 5c), shows a steady decline in PC to the expected level for 20 °C production (~8 %). The Chl-a content increases slowly, eventually reaching the level expected for 20 °C production (~1.5%). The time scale for these changes are consistent with the expected time scale for culture turnover (roughly 20-30% per 2 day cycle). At the end of Phase II, the EF culture is almost exactly at the expected pigment contents found in the AB and CD Phase I experiments. The GH culture, transitioned from 35 °C to 30 °C (Figure 5d), achieves

an overall increase in PC content and Chl-a content, with a slightly enhanced time scale for reaching stable levels for both pigments.

Phase III observations from Figure 5 are consistent with the above observations. AB (35 °C to ExSP) shows an initial decline in pigment contents and then some recovery over time. CD shows essentially no change in going from 30 °C to AvSP. EF shows expected changes in going from 20 °C to AvSP. GH (30 °C to CtSP) shows little or no change in pigment content.

According to the literature for shorter duration experiments, there is a narrow temperature range between 35 °C and 37 °C for optimal growth with 40 °C being definitely detrimental for *Arthrospira* (Kumar et al., 2011; Torzillo et al., 1991b). Our results suggest extended periods at 35 °C are also not favorable for sustained growth, though the effects are largely reversible on a culture basis and most of the variation is in pigment production. A similar trend was seen in whole cell spectrum in Figure 4, where relatively higher peak at ~680nm (Chl-a) and lower peak at 620 nm (cPC) was found at lower temperatures, and thus indicates a higher Chl-a to PC ratio for low temperature cultures compared to those after prolonged high temperature exposure. The culture at 35 °C turned bluish green with Chl-a reduction (by >50 %) after prolonged exposure to this modestly elevated temperature. The spectra in Figure 4 are consistent with this visual observation. These results are generally consistent with Watras et al., (2017) where a progressive decrease in chlorophyll and phycocyanin fluorescence with increasing temperature was reported in most of the cultures of green and blue-green algae (e.g., *Scenedesmus dimorphus, Selenastrum minutum, and Synechococcus leopoliensis*).

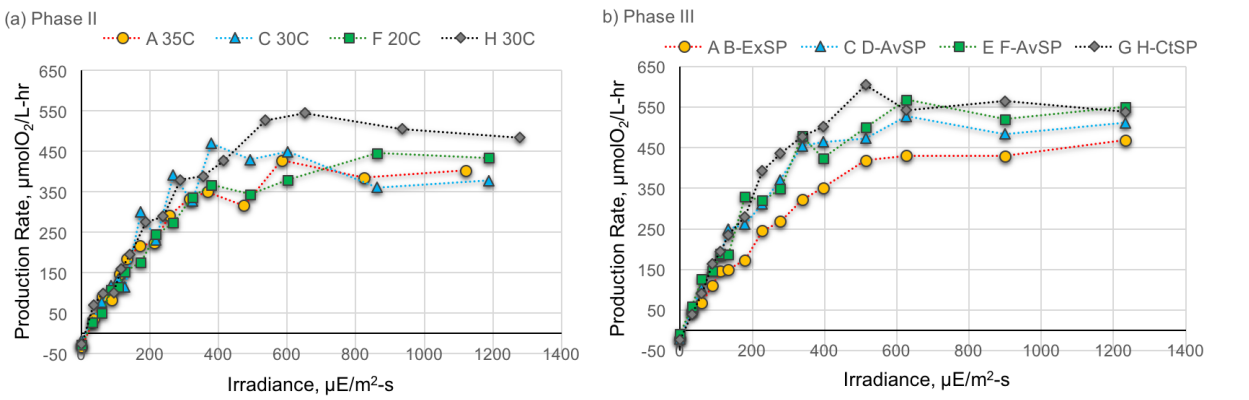

Figure 6. Photosynthesis irradiance (PI) response curves (measured at 30 °C) for the algal cultures at different temperature treatments in (a) Phase II on day 27, A-35 °C, C-30 °C, F-20 °C, and H-35 °C, and (b) Phase III on day 43, AB-ExSP, CD and EF-AvSP and GH-CtSP.

Photosynthetic parameters

Photosynthesis-irradiance (PI) curves have been extensively used to evaluate the photosynthetic response to various abiotic stresses experienced by algae (Falkowski and Raven, 2007). Photosynthetic parameters, including P_{max} (µmol O_2 L^{-1} hr^{-1}), α' (mol O_2 mol $photon^{-1}$), R_0' (µmol O_2 L^{-1} min^{-1}) and E_k (µE m^{-2} s^{-1}), were evaluated at different temperature treatments during Phases I and II using PE curves (Figure 6 and Table 2) to test consistency with the above observations for changing conditions and provide parameters for productivity modeling. The culture samples from different temperature treatments were first incubated at 30 °C under dark conditions for 1 h. Testing for the different treatments was conducted at a single temperature (30 °C) to avoid the normal temperature dependence wherein P_{max} and E_k display a Q_{10} = 2 dependence (about 60 kJ mol^{-1}). The PE curves were measured (in duplicate) for all treatments, with average values reported. The photosynthetic response patterns from cultures grown at 20 °C, 30 °C and 35 °C Phase I are shown in Figure 6, with results summarized in Table 2. It is clear that with this experimental protocol none of the samples in Figure 6 shows a significant difference from the others, the only possible exceptions being the AB-ExSP sample exposed to the most severe summer profile conditions and the A sample from Phase II (constant 35 °C). PE curves measured at 20 °C for culture samples from Phase I (20 °C treatment) yield a P_{max} of 240 µmol O_2 L^{-1} hr^{-1} and E_k as 85 µE m^{-2} s^{-1}, which is roughly Q_{10} of 2 when compared to results from PE curves measured at 30 °C. In fact a more

extensive testing (not presented here) of PE curves measured over the temperature range 15-35 °C yields an activation energy for P_{max} of 60 kJ mol^{-1}. This activated process can be attributed entirely to E_k, as the limiting quantum yield (α) has been shown to be independent of temperature over the range studied. As noted earlier, these observations are typical of temperature response in photosynthetic organisms (Falkowski and Raven, 2007). The constant exposure to 35 °C, also measured at 35 °C, (Table 2) yields photosynthetic parameters similar to the other tests at 30 °C. In Phase I there is some indication of a stress response at sustained high temperatures in these results, though this is not as clear as the pigment variation. There is no indication in Phase III of dynamic high temperature exposure having an adverse effect. These observations are consistent those made in conjunction with biomass and pigment production.

Table 3: Productivity Model Parameters

Model Parameters	Unit	Culture Density 1 gDW/L
α	*mol C/mol photon*	***0.061***
E_k	*μE/m^2-s*	*240 @ 30C*
R_0	*μmolC/mgChl.a-min*	*0.1 @30C*
F	*-*	*1*
E_s	*μE/m^2-s*	*230*
D	*m*	*0.0254*
k	*1/m at 1 gDW/L*	*175*
kD	*-*	*4.45*
C_0	*mgChl.a/m^3 at 1 gDW/L*	*18,000*
γ	*gDW/molC*	*22.68*
t_1	*sec*	*43,200*
t_2	*sec*	*86,400*

There was no significant difference in values of α' (limited quantum yield for O_2 production) which were close to ~ 0.070 mol O_2/mol photon for all the treatments. The lowest R_0' (respiration rate) of 0.12 μmol O_2/L-min was observed at 20°C while the maximum of 0.55 μmol O_2/L-min was found at 35°C. R_0' determinations have effects due to the light exposure history (Falkowski and Raven, 2007). Little temperature dependence is expected for α', consistent with the results from this study. The ratio α'/α is the photosynthetic quotient (O_2 per fixed carbon) which is expected to be in the range 1.1-1.3 (Falkowski and Raven, 2007). We use 1.2 for the modeling analysis to follow. The same value applies to R_0, the respiration rate on a carbon basis required for application in the Algenol Productivity Model, Equation 3.

It is noteworthy that large changes in pigment content and light absorption level are seen with very little change in biomass productivity, whether measured directly or inferred from the PE curves. This is consistent with the relatively minor impacts of low pigment mutants on productivity in other organisms (Kirst et al., 2014; Lea-Smith et al., 2014).

Productivity Modeling Analysis

The Algenol Productivity Model (Legere, 2017; Chance and Roessler, 2019) is used to analyze these indoor PBR experiment results, and determine if a set of photosynthetic parameters can be developed to adequately represent all experimental results. A representative model parameter set for the productivity model is derived from the PE data sets with [α, E_k, R_0] = [0.061 fixed C/photon, 240 μE m^{-2} s^{-1}, 0.1 μmol C mgChl.a^{-1} min^{-1}] at 30 °C providing a reasonable representation of the entire data base. The R_0 value at the reference 30 °C temperature was taken as 0.1 μmol C mgChl.a^{-1} min^{-1} consistent with conclusions from outdoor experiments on a carbon basis (Legere 2017; Chance and Roessler, 2019) and recognizing that R_0' determinations from PE curves will show an irradiance-related enhancement (Falkowski and Raven, 2007). To model temperature effects, E_k is set as a function of temperature (activation energy 60 kJ mol^{-1}), and the respiration rate (R_0) was modeled as a function of temperature (activation energy as 27 kJ mol^{-1}), with the activation energy estimates being consistent with previous studies (Legere, 2017). Table 4 gives a summary of the model parameter values. Comparison between the modeled and experimental productivities are shown in Figure 7. The model results are in good in agreement with experiment results for all cases considered here. Even at 35 °C, where clear

changes in pigmentation are seen, the agreement is satisfactory. For example, with temperature increased from 20 °C to 30 °C, the biomass productivity increases by 28% (experimental) and 26% (productivity model). At higher light intensities >>E_k, an increase of 100%, or Q_{10} = 2, would be expected. Good agreement between biomass productivities for the small, L scale, experiments reported here and the large, 24000 L scale, outdoor experiments (Chance and Roessler 2019) was noted earlier. This consistency can be extended to the PE experiments (mL scale) where the derived photosynthetic parameters are in good agreement with those employed for model representations of large scale outdoor experiments (Chance and Roessler, 2019; Supplementary Material).

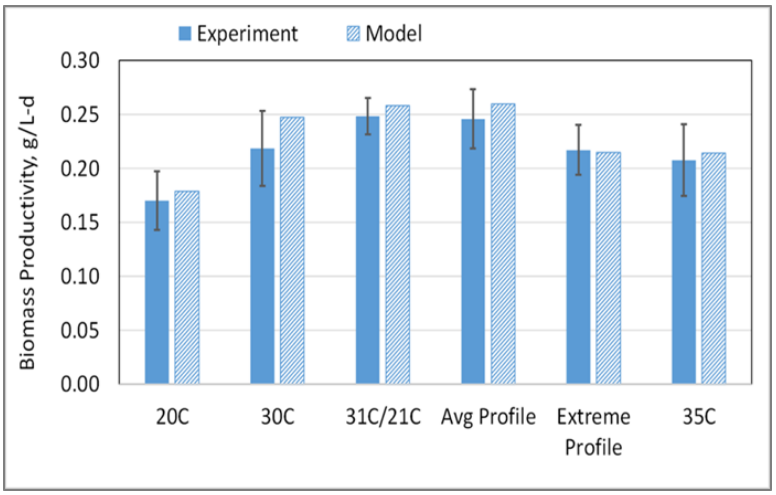

Figure 7. Experiment results of biomass productivity in comparison to the productivity model simulation. The productivity model parameter set, representative of the PI database at 30 °C, is [α, E_k, R_0] = [0.061 fixed C/photon, 240 μE/m^2-s, 0.1 μmolC/mgChl.a-min].

Conclusions

We have provided here a detailed study of temperature impacts on *Arthrospira platensis* biomass production in semi-continuous operation. This temperature study of *Arthrospira platensis* in photobioreactor cultivations demonstrates that temperatures in the 20 - 35 °C range are favorable for achieving consistent productivities, though long term exposure to 35 °C caused some modest changes in productivity and more obvious changes in pigmentation. Exposure to simulated conditions for summer temperature profiles for Southwest Florida shows some issues for the most extreme conditions but a general tolerance for the short term, mid-day exposures to higher temperatures. The response of the cultures to abrupt changes in temperature is immediate for biomass production and quantitatively consistent with the temperature dependence observed for P_{max} in smaller scale photosynthetic response experiments. Pigment variations with abrupt changes in temperature occurrs on a time scale that was essentially the same as that expected for turnover of the cell population under semi-continuous operation. No other acclimation effects were identified. These results all involve annual average irradiance conditions. Extension of this study to higher irradiance conditions in the summer may cause additional issues in combination with extreme temperature exposures, high or low. Productivity modeling based on photosynthetic parameters derived from periodic sampling of the cultures provides excellent agreement with experiment and consistency with the performance of large scale outdoor PBR cultivations.

Acknowledgements

We thank Professor John Coleman and Dr. Paul Roessler for many helpful discussions and suggestions. We thank Professors Valerie Thomas and Matthew Realff for their support and helpful comments. We acknowledge Matthew Anderson, Vedanta Malhoe, and Lucas Eastham for technical support. This material

is based upon work supported by the U.S. Department of Energy's Office of Energy Efficiency and Renewable Energy (EERE) under the Bioenergy Technologies Office Award Number DE-EE0007690.

Authorship

All authors made substantive contributions to the experimental design, data analysis, and interpretation of results.
All authors actively participated in the drafting and revision of the manuscript.
All authors have approved the final version of the manuscript and agree to be accountable for all aspects of the work
All authors have agreed on the order in which their names are listed on the manuscript

References

Bechet, Q,, Shilton, A., and Guieysse, B., (2013). Modeling the effect of light and temperature on algae growth: State of the art and critical assessment for productivity prediction during outdoor cultivation, *Biotechnology Advances* **31**, 1648-1663.

Chaiklahan, R., Khonsarn, N., Chirasuwan, N., Ruengjitchatchawalya, M., Bunnag, B., Tanticharoen, M. (2007). Response of Spirulina platensis C1 to high temperature and high light intensity. *Kasetsart J. - Nat. Sci.* **41**:123–129.

Chance, R.& Roessler, P. (2019). Production of Biocrude in an Advanced Photobioreactor-Based Biorefinery. *DOE Bioenergy Technol. Off.* https://www.energy.gov/sites/prod/files/2019/03/f61/Production of Biocrude in an Advanced Photobioreactor-Based Biorefinery_EE0007690.pdf.

Colla, L.M., Oliveira Reinehr,C., Reichert, C., Costa, J. (2007). Production of biomass and nutraceutical compounds by Spirulina platensis under different temperature and nitrogen regimes. *Bioresour. Technol.* **98**:1489–1493. https://www.sciencedirect.com/science/article/pii/S0960852405004761.

Falkowski, P.G., Raven, J.A. (2007). *Aquatic photosynthesis*. Princeton University Press.

Jahnke, J., Mahlmann, D.M., Jacobs, P., Priefer, U. (2011). The influence of growth conditions on the cell dry weight per unit biovolume of Klebsormidium flaccidum (Charophyta), a typical ubiquitous soil alga. *J. Appl. Phycol.* **23**:655–664.

Kirst, H., Formighieri, C., Melis, A. (2014). Maximizing photosynthetic efficiency and culture productivity in cyanobacteria upon minimizing the phycobilisome light-harvesting antenna size. *Biochim. Biophys. Acta - Bioenerg.* **1837**:1653–1664. http://www.sciencedirect.com/science/article/pii/S0005272814005362.

Kumar, M., Kulshreshtha, J., Singh, G. (2011). Growth and biopigment accumulation of cyanobacterium spirulina platensis at different light intensities and temperature. *Brazilian J. Microbiol.* **42**:1128–1135.

Lea-Smith, D., Bombelli, P., Dennis, J., Scott, S., Smith, A., Howe, C. (2014). Phycobilisome-Deficient Strains of Synechocystis sp. PCC 6803 Have Reduced Size and Require Carbon-Limiting Conditions to Exhibit Enhanced Productivity. *Plant Physiol.* **165**:705–714.

Legere, E. (2017). Algenol Integrated Pilot-Scale Biorefinery. *DOE Final Proj. Rep.* https://www.osti.gov/servlets/purl/1360777.

Marsac, D., Houmard, J. (1988). Complementary chromatic adaptation: Physiological conditions and action spectra. *Methods Enzymol.* **167**:318–328.

Panyakampol, J., Cheevadhanarak, S., Senachak, J., Dulsawat, S., Siangdung, W., Tanticharoen, M.,

Paithoonrangsarid, K. (2016). Different effects of the combined stress of nitrogen depletion and high temperature than an individual stress on the synthesis of biochemical compounds in Arthrospira platensis C1 (PCC 9438). *J. Appl. Phycol.* **28**:2177–2186. https://doi.org/10.1007/s10811-015-0765-4.

Panyakampol, J., Cheevadhanarak, S., Sutheeworapong, S., Chaijaruwanich, J., Senachak, J., Siangdung, W., Jeamton,W., Tanticharoen, M., Paithoonrangsarid, K. (2015). Physiological and transcriptional responses to high temperature in arthrospira (Spirulina) platensis C1. *Plant Cell Physiol.* **56**:481–496. http://dx.doi.org/10.1093/pcp/pcu192.

Sánchez-Luna, L., Bezerra, R., Matsudo, M., Sato, S., Converti, A., de Carvalho, J. (2007). Influence of pH, Temperature, and Urea MolarFlowrate onArthrospira platensisFed-BatchCultivation: A Kinetic and Thermodynamic Approach. *Biotechnol. Bioeng.* **96**:702–711.

Torzillo, G., Sacchi, A., Materassi, R. (1991a). Temperature as an important factor affecting productivity and night biomass loss in Spirulina platensis grown outdoors in tubular photobioreactors. *Bioresour. Technol.* **38**:95–100.

Torzillo, G., Sacchi, A., Materassi, R., Richmond, A. (1991b). Effect of temperature on yield and night biomass loss in Spirulina platensis grown outdoors in tubular photobioreactors. *J. Appl. Phycol.* **3**:103–109.

Trabelsi, L., Ben Ouada, H., Bacha, H., Ghoul, M. (2009). Combined effect of temperature and light intensity on growth and extracellular polymeric substance production by the cyanobacterium Arthrospira platensis. *J. Appl. Phycol.* **21**:405–412.

Vonshak, A., Novoplansky, N. (2008). Acclimation to low temperature of two Arthrospira platensis (cyanobacteria) strains involves down-regulation of PSII and improved resistance to photoinhibition. *J. Phycol.* **44**:1071–1079.

Watras, C., Morrison, K., Rubsam, J., Hanson, P., Watras, A., LaLiberte, G., Milewsk,i P. (2017). A temperature compensation method for chlorophyll and phycocyanin fluorescence sensors in freshwater. *Limnol. Oceanogr. Methods* **15**:642–652.

Yoshikawa, N. & Belay, A. (2008). Single-Laboratory Validation of a Method for the Determination of c-Phycocyanin and Allophycocyanin in Spirulina (Arthrospira) Supplements and Raw Materials by Spectrophotometry. *J. AOAC Int.* **91**:650–655.

Zarrouk, C. (1966). Contribution a L'etude D'une Cianophycee: Influence de Divers Facteurs Physiques Et Chimiques Sur la Croissance Et la Photosynthese de Spirulina Maxima (Setch. Et Garndner) Geitler. Faculte des Sciences, Universite de Paris. https://books.google.com/books?id=Hq5EcgAACAAJ.

1.B. Life Cycle Greenhouse Gas Emissions of Different CO_2 Supply Options for an Algal Biorefinery

Life cycle greenhouse gas emissions of different CO_2 supply options for an algal biorefinery

Pratham Arora[1,2], Ron Chance[3,4], Howard Hendrix[5], Matthew J. Realff[4], Valerie M. Thomas[1], Yanhui Yuan[3]

[1]School of Industrial and Systems Engineering Georgia Institute of Technology Atlanta GA 30332, United States
[2]Department of Hydro and Renewable Energy, Indian Institute of Technology-Roorkee, Uttarakhand 247667, India

[3]Algenol Biotech 16121 Lee Road, Suite 110 Fort Myers, FL 33912, United States
[4]School of Chemical and Biomolecular Engineering Georgia Institute of Technology Atlanta GA 30332, United States.
[5]Hendrix Engineering Solutions, Inc. 136 B Marketplace Circle PMB 164 Calera, AL 35040, United States

Abstract: This paper characterizes the greenhouse gas (GHG) emissions from the provision of CO_2 for twelve hours of the day from a range of sources. Twelve CO_2 supply cases spanning from fossil fuel power plant stack gases to direct air capture (DAC) systems are modeled. The results are compared in an LCA framework. The CO_2 supply from the combustion or gasification of biomass has GHG emissions of –1.62 gCO_2 eq./g CO_2 delivered and is the case with the lowest carbon footprint for supplied CO_2. A purpose built Natural Gas Combined Cycle (NGCC) power plant CO_2 source has the highest GHG emissions of -0.40 gCO_2 eq./gCO_2 delivered of the cases considered because of nighttime emissions and natural gas supply chain losses. The impact of a diurnal cycle can be mitigated by using capture and refrigeration systems as part of the CO_2 management system. The results are sensitive to the GHG emissions of the grid electricity which is imported or exported in different cases. A case study highlighting the effect of GHG emissions of CO_2 transport on the LCA of biofuel production from algae is presented. The results provide a benchmark for comparison of different CO_2 supply options for establishment of a sustainable algal biorefinery.

Introduction

Sustainable chemicals and fuels can potentially be produced from algal biomass. One production route is thermochemical conversion either of the entire algal mass or after extraction of other valuable products. The major advantage of biomass fuels is their potentially low net contribution of CO_2 to the atmosphere, due to photosynthetic fixing of CO_2 that is then returned to the atmosphere during fuel combustion. Thus, biofuels produced from algae have been predicted to have low greenhouse gas (GHG) emissions when compared to conventional fossil fuels [1].

Addition of CO_2 from an external source is often required for the efficient cultivation of algae [2]. Given the typical 50% carbon content in algae, 1.83 kg of CO_2 is required for each kg of dry algae produced. The actual requirement can be higher, depending on the CO_2 utilization efficiency of the algal biorefinery. The CO_2 utilization efficiency can be lower than 10% for open raceway ponds or higher than 75% for photobioreactor (PBR) based systems [3]. The CO_2 requirement means the algal biorefinery has to be close to an existing CO_2 source, such as a power plant, or have a source of CO_2 on site. It has been reported that the CO_2 requirement is responsible for 36 % of the raw material cost for a biorefinery [4]. An important consideration, often overlooked while quantifying the carbon footprint of algal biorefinery, is the CO_2 emission associated with production and transport of CO_2. Pate *et al* [5] conclude that a sustainable supply of CO_2 is the most significant challenge for the scale-up of an algal biorefinery.

Different algae species have optimum productivities at different CO_2 concentrations ranging from 2 % to 70 % [6][7]. The supply of CO_2 can also vary, from low concentration CO_2 available as power plant stack gas, to very high purity commercially purified CO_2. Zheng *et al* [8] compare the advantages and disadvantages of different CO_2 supply sources including air, flue gas, and purified CO_2. They report that while power plant stack gas has many economic advantages, more concentrated CO_2 streams can reduce gas volumes and pumping energy, and increase mass transfer efficiency. Though the economic aspects of different CO_2 supply scenarios have been studied [9], a comparison of CO_2 supply options from a life cycle assessment (LCA) perspective has not yet been provided. A

recent study [10] provides the economic potential and GHG emissions of hydrothermal liquefaction of algae, utilizing different CO_2 sources. They report the GWP results utilizing a functional unit 1 MJ of biocrude production. Furthermore, that study does not address the impact of different supply configurations on the night-time emissions from the CO_2 supply.

The present study compares the GHG emissions of different CO_2 supply scenarios, utilizing a functional unit of 1 g of CO_2 delivered to an algal biorefinery during the 12 daylight during which sunlight is available for algae growth. The study primarily highlights the GHG emissions from the production and transportation of CO_2, independent of the CO_2 use within the boundary of a production system or the subsequent release of CO_2 from products. Thus, the results can be used for any study focusing on utilization of CO_2 for algal growth or other diurnal systems. Twelve different CO_2 supply cases are modeled, with concentrations ranging from 5 % to 97 % CO_2. The analysis includes both day- and night-time emissions, which clarifies the quantification of CO_2 sources for algal biorefineries. The results can also be utilized by other CO_2 utilization facilities such as greenhouses, where the diurnal cycle of biomass growth is an important factor, and can be adjusted to different fractions of time of CO_2 delivery. This is presented with the help of the case study towards the end of the study.

Methodology

Different CO_2 supply scenarios have been modelled in a steady state process simulation software utilizing the Redlich Kwong Soave (RKS) thermodynamic model. ASPEN Plus® has been used in previous studies that have quantifyed the mass and energy balance of algal biorefineries [11] [12]. The CO_2 supply scenarios that are considered in the present study can be broadly classified into:

- Flue gas from a legacy coal based power plant, with and without carbon capture
- Flue gas from a legacy natural gas based power plant, with and without carbon capture
- Flue gas from a purpose-built natural gas combined cycle (NGCC) plant, with and without carbon capture and refrigeration
- Flue gas from purpose-built biomass combustion and biomass gasification plant.
- CO_2 supply from a purpose-built direct air capture (DAC) system [13]

The algal biorefinery is assumed to be located 2 miles from the legacy coal or natural gas power plants. This distance impacts the energy requirement, and hence CO_2 emissions, for moving any gases from the power plant to the algal biorefinery. Two miles was considered to be a representative distance. The purpose-built natural gas and biomass power plants and the direct air capture plant are assumed to be constructed at the algal biorefinery.

We distinguish the sourcing of CO_2 from existing “legacy” fossil fuel power plants, in contrast to the sourcing of CO_2 from new “purpose-built” power plants. For existing, legacy power plants the addition of carbon capture reduces the emissions of carbon dioxide to the atmosphere; it has the same effect as capturing carbon dioxide from the air, albeit with different technology processes. However, if a new power plant is built in order to provide CO_2 and energy to the biofuel facility, this is combusting fuels that otherwise would not be combusted, and these fuels must be completely included within the boundary of the analysis.

We consider separate day and night operations for the CO_2 supply, based on algae growth only taking place during daytime (12 hours). For legacy power plant flue gases this means that the night-time emissions from the plant are vented to the atmosphere, and not counted as part of the algal biorefinery operation, as only the day time emissions are sent to the algal biorefinery. The greenhouse gas emissions of the complete power plant is allocated to its electricity production and

the greenhouse gas emissions of its electricity production remains unchanged even though its daytime carbon dioxide emissions are being used by the algal biorefinery. For other cases, where a source is built specifically to provide CO_2 and power to the algal biorefinery, the emissions associated with day and night-time operation must be taken into account. Thus, for example, for biomass power plants emissions from the feedstock supply and night-time emissions are included.

Figure 1a illustrates the acquisition of CO_2 from the atmosphere or legacy power plants, with the CO_2 utilized and emitted to the atmosphere. Figure 1b illustrates the acquisition for CO_2 with purpose-built facilities that extract sequestered CO_2. Both 1a and 1b are typical of biofuel production processes, with CO_2 emitted to the atmosphere with the fuel is combusted. For completion, Figure 1c shows a utilization process in which the CO_2 is sequestered, which could occur with use of biofuel for stationary power production accompanied by CO_2 capture and sequestration.

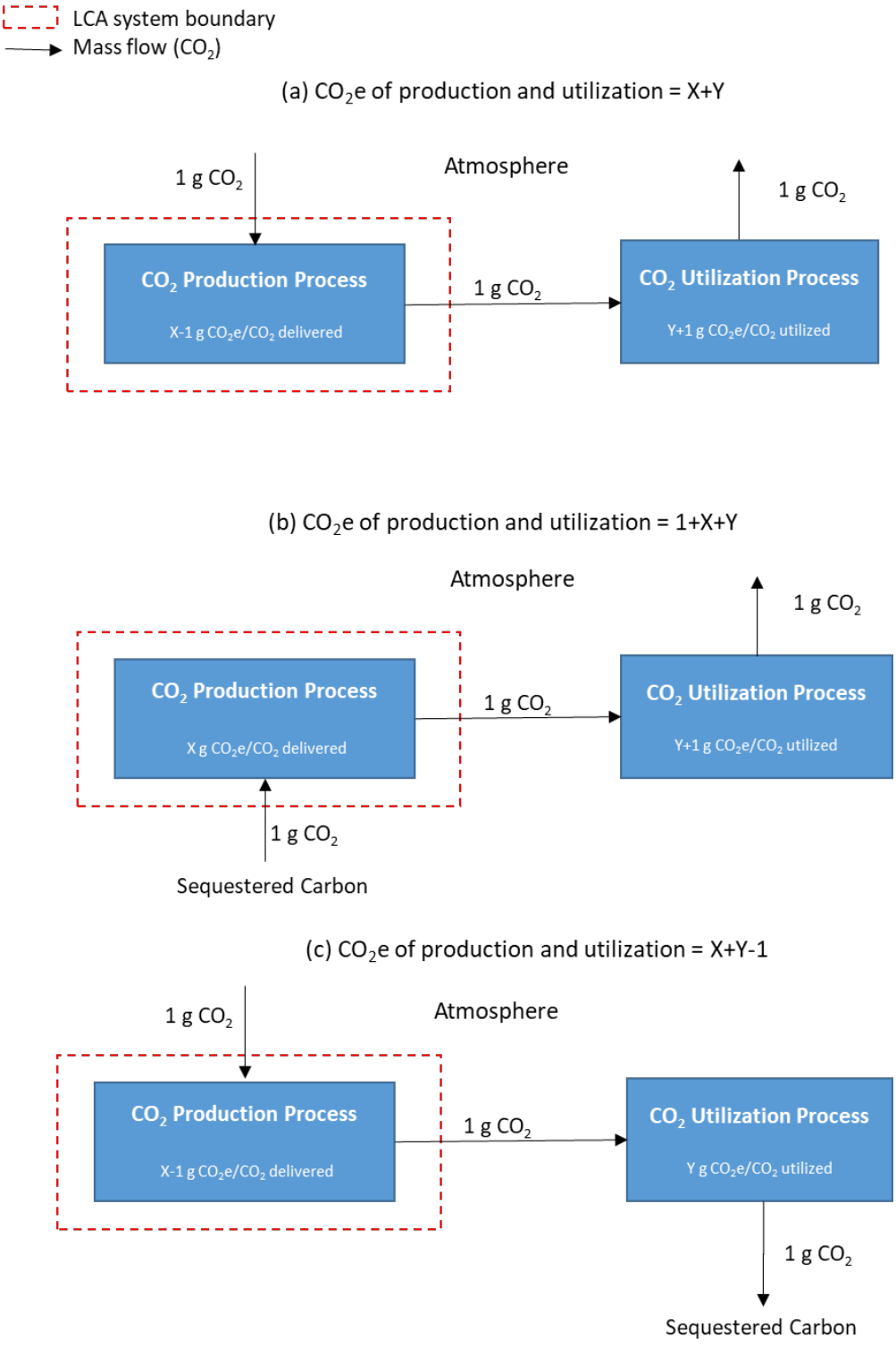

Figure 1: Illustration of CO_2 acquisition and disposition pathways and their effect on lifecycle greenhouse gas emissions. (a) CO_2 is captured from the atmosphere, utilized, and released to the atmosphere; (b) CO_2 is acquired from sequestered carbon, utilized, and released to the atmosphere; (c) CO_2 is captured from the atmosphere, utilized, and sequestered. In each case, excepting the direct CO_2 flows, there is a lifecycle greenhouse gas emission of x g CO_2e for the CO_2 production process, and y g CO_2e for the CO_2 utilization process; these differ for different CO_2 production and CO_2 utilization processes.

Case 1: Legacy coal power plant (LC)

In this case, the flue gas is extracted from the stack of a coal-fired power plant. It is cooled and compressed before being transported to the algal biorefinery as the primary source of CO_2. The plant is modeled as a pulverized coal plant burning Powder River basin coal. Flue gas from the power plant is assumed to be extracted from a single stack utilizing a stack fan. Since most coal-fired boilers have flue gas desulfurization (FGD), it is assumed that the flue gas is saturated with water and available at a temperature of 60 ^{o}C. The composition of flue gas in given in Table 1. Thereafter, the flue gas is cooled in a direct contact cooler/scrubber to reduce the gas volumetric flow and remove as much of the water as possible before flowing through the transport compressor. A pressure drop of 0.055 bar per mile is assumed and the CO_2 is delivered to the biorefinery at a pressure of 2 bar. The flue gas leaves the transport compressor and travels through ductwork from the power plant to the biorefinery. The flue gas passes through a second direct contact cooler to cool the flue gas before it is utilized by the facility. The process is shown in Figure 2. The energy required for each component of flue gas processing, the energy required for flue gas transport, and the composition of the major streams for all the cases is in the supporting information.

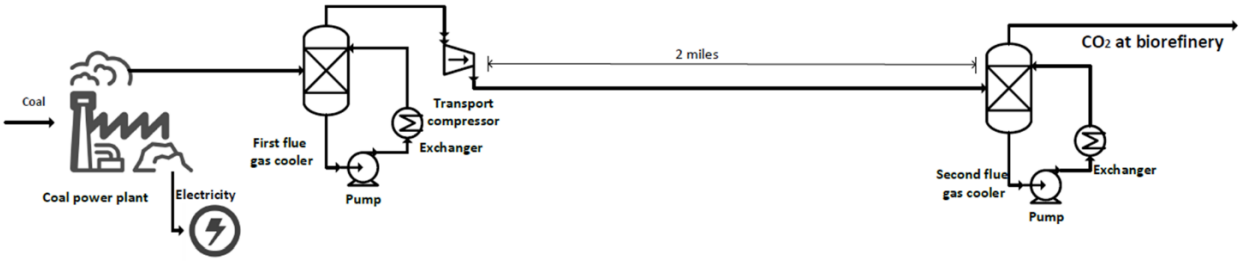

Figure 2: CO_2 supply from a coal based power plant.

Case 2: Legacy coal power plant with carbon capture (LCCC)

In this case, the CO_2 from flue gas is captured utilizing standard amine solvents. The flue gas is pretreated in a similar way to the case without capture. This prevents water entering the capture system and diluting the solvent in addition to reducing the gas volumetric flow. The heat gained by the circulating water is rejected to the cooling tower. The excess water condensed from the flue gas is purged from the process. The flue gas exiting the flue gas scrubber enters a flue gas blower which increases the pressure of the gas by approximately 0.1 bar to give the flue gas the driving force required to get through the absorber and the stack. The flue gas enters the bottom of the absorber where it flows upward through packing as the "lean" solvent is flowing downward. This is an exothermic reaction and it is assumed that the flue gas exiting the absorption portion of the column is at 60 ^{o}C, and the solvent leaving the bottom of the absorber is at 63 ^{o}C. The low concentration CO_2 flue gas exits the absorber and then flows through a stack to the atmosphere.

The "rich" solvent leaving the absorber flows through a rich/lean solvent exchanger where it is heated by the hot "lean" solvent exiting the regenerator. For this study it is assumed that the lean solvent entering this exchanger is at a temperature of about 125^{o}C. In the regenerator column, the CO_2 is steam "stripped" from the solvent utilizing heat supplied by the reboiler. The "lean" solvent exits the bottom of the regenerator, is cooled in the previously described rich/lean solvent exchanger and then further cooled with cooling water to 46^{o}C before re-entering the absorber. The process is shown in Figure 3. The steam for regenerating the carbon capture reboiler is supplied by a natural gas fired package boiler which is located adjacent to the carbon capture system. The rationale behind using a separate gas fired boiler rather than utilizing the steam directly from the coal-based power plant is that the latter may be disruptive to the highly constrained operation of a

legacy power plant. Furthermore, gas-based boiler systems would have a much lower carbon footprint compared to the steam that could be imported from a coal power plant. This package boiler generates a 3.1 bar steam needed for the carbon capture system. The CO_2 capture efficiency by the carbon capture system is assumed to be 90%. The remaining CO_2 escapes to the atmosphere and is counted in the carbon footprint of the delivered CO_2. The capture energy requirement is 2500 kJ/kg CO_2 captured, corresponding to aqueous ammonia based solvents [14]. The flue gas exiting the package boiler flows via an Induced Draft fan and combines with the flue gas from the coal-fired power plant before entering the Flue Gas Cooler. Therefore, the CO_2 from this boiler is also captured.

The CO_2 exiting the column is saturated with water. It flows through an overhead condenser where it is cooled to 46°C, allowing more than 95% of the water to condense from the CO_2. This is separated by the reflux drum and returned to the column. The delivered CO_2 has a concentration of approximately 95%. In this case, both the CO_2 supplied by the coal-fired power plant and the CO_2 coming from the natural gas boiler facility contribute to the total CO_2 delivered. The concentrated CO_2 leaving the regenerator is at a pressure of approximately 2 bar.

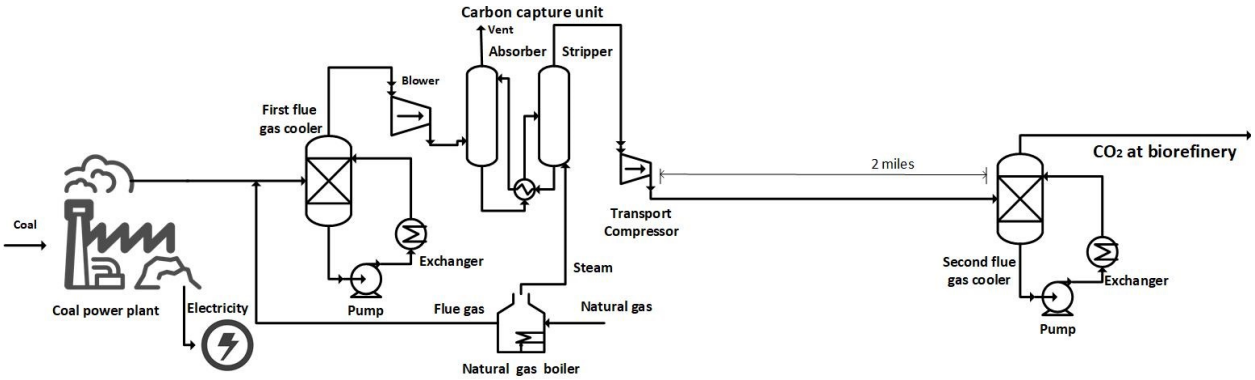

Figure 3: CO_2 supply from a coal based power plant with carbon capture.

Case 3: Legacy Natural gas power plant (LN)

There is a significant difference in the CO_2 concentration and water content of flue gas from a natural gas-based power plant compared to flue gas from a coal-based power plant. Essentially all existing coal-fired power plants have FGD units to remove sulfur. The effect is that the coal power plant flue gas is saturated with water when it exits the FGD at approximately 60°C. The different compositions are shown in Table 1. The process flowsheet is similar to Figure 2, with a natural gas power plant replacing a coal power plant.

Table 1: Flue gas composition (%) and temperature for natural gas based and coal based power plants:

	Natural gas based power plant	Coal based power plant
N_2	75.6	65.4
O_2	11.6	4.1
H_2O	8.5	18.6
CO_2	4.3	11.9
Temperature (°C)	82	60

Case 4: Legacy natural gas power plant with carbon capture (LNCC)

This case is analogous to case 2, with the flue gas being supplied from a natural gas power plant. Flue gas is extracted from the power plant stack using stack fans. The flue gas then flows into the carbon capture system as described in the previous section. The process flowsheet is similar to Figure 3 with a natural gas power plant replacing a coal power plant.

Case 5: Purpose-built NGCC plant (PN)

This case considers building a natural gas combined cycle (NGCC) plant near the biorefinery in order to supply CO_2, steam and power. The plant operates 24 hours a day. This study assumes a 84 MW NGCC plant that uses a 66 MW gas turbine to generate electricity. The hot exhaust from the gas turbine flows into an attached heat recovery steam generator (HRSG) where steam (80 t/h) at 10 bar and 500 C is generated. This steam is expanded to a pressure of 0.17 bar through a series of high, medium pressure and condensing turbines. This would produce another 18 MW of electricity. The excess electricity (74 MW) not required for CO_2 capture and distribution is supplied to the grid. The flue gas produced during the daytime is supplied to the biorefinery after cooling and scrubbing. At night all the emissions are vented to the atmosphere. The process flowsheet is similar to Figure 2 with the NGCC plant located at the biorefinery. The greenhouse gas emissions calculations are presented in the supporting information.

Case 6: Purpose-built NGCC plant with carbon capture (PNCC)

This case is an extension of case 5, with the addition of a carbon capture unit to supply a concentrated stream of CO_2 (20 t/h), using the same concentration and recovery assumptions as in earlier cases. After accounting for the energy required for CO_2 delivery and carbon capture, approximately 69 MW (daytime) and 74 MW (nighttime) of electricity can be supplied to the grid. At night this unit is assumed to operate at full load. Contrary to conventional plants, the carbon capture facility in this case does not operate at night, and all of the night-time CO_2 is vented to atmosphere. Since no steam extraction is required for the carbon capture facility at night, the steam turbine generates additional power (5 MW). The process flowsheet is similar to Figure 3 with the NGCC plant located at the biorefinery and without a natural gas boiler.

Case 7: Purpose-built NGCC plant with carbon capture and refrigeration (PNCR)

An enhancement to the previous case could be the inclusion of a refrigeration unit to capture the night-time emissions from the NGCC plant (Figure 4). This would reduce the required NGCC plant size to almost half (34 MW). During the day, a portion of the required CO_2 would be supplied by the NGCC system and the balance would be withdrawn from storage, and vaporized in an atmospheric vaporizer. At night, the NGCC would continue to run at full load, but the CO_2 would be liquefied and stored to replace what was withdrawn during the day. The benefits of this case are a smaller NGCC system and reduced CO_2 emissions.

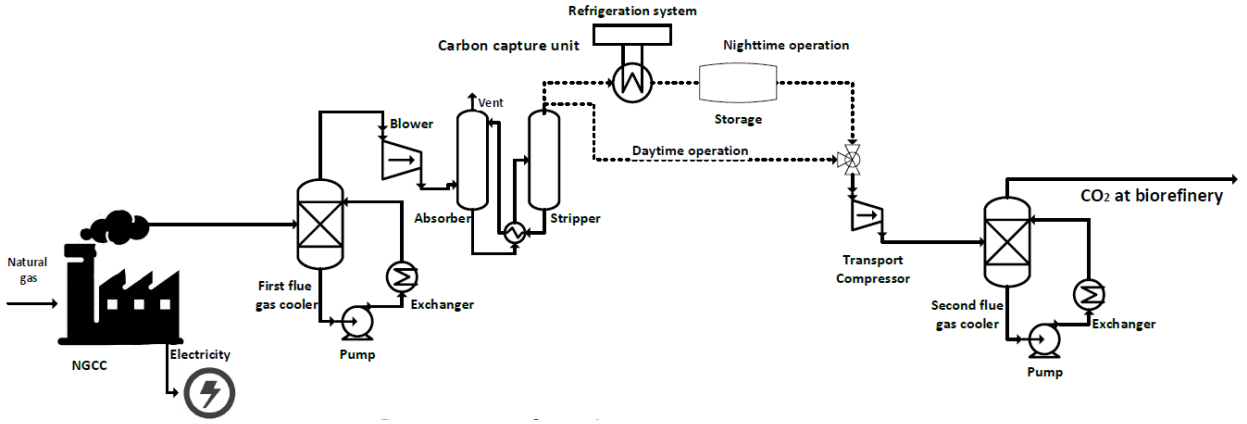

Figure 4: CO_2 supply from a standalone NGCC unit with carbon capture and refrigeration.

Case 8: Purpose-built NGCC plant with carbon capture and partial refrigeration (PNCPR)

Another possible modification to the standalone NGCC case is partial capture and refrigeration of flue gas. In this case the CO_2 would be captured and refrigerated only during the night-time operation. This concentrated CO_2 would be mixed with the flue-gas from the NGCC plant and supplied during the day to the algal biorefinery. This would help in increasing the CO_2 concentration in the supplied flue gas without the requirement of continuous operation of the carbon capture unit. The flowsheet is similar to flowsheet in Figure 4, with the CO_2 for daytime operation being supplied before carbon capture unit.

Case 9: Biomass combustion (BC)

This case considers building a biomass-fired boiler at the algal biorefinery. The steam produced from the boiler is used to generate electricity and the flue gas is supplied to the biorefinery. In this case biomass chips, which are pre-dried off-site to a moisture content of 20%, are fed into a circulating fluid bed combustor and combusted with air. Steam is generated in the unit and superheated to 10 bar and 500 °C before being supplied to a steam turbine. This steam is expanded to a pressure of 0.17 bar, producing 16 MW electricity. During the day, all of the flue gas from the biomass combustor is compressed and cooled and supplied directly to the biorefinery. At night, the unit would operate at 100% capacity and vent the flue gas to atmosphere. The process flowsheet is similar to Figure 2 with the biomass combustion plant located at the biorefinery.

Case 10: Biomass gasification (BG)

Biomass gasification is a thermo-chemical process that converts biomass into syngas, char, and tars. Biomass chips would be fed into an entrained flow gasifier which would result in a syngas stream rich in hydrogen and carbon monoxide. This syngas is utilized to run a 45 MW gas turbine. The hot exhaust from the gas turbine flows into an attached HRSG, where steam at 10 bar and 500 °C is generated. This steam is expanded to a pressure of 0.17 bar. The process flowsheet is similar to Figure 2 with the biomass gasification plant located at the biorefinery.

Case 11: Biomass gasification with carbon capture (BGCC)

This case is the extension of case 10, with a carbon capture unit used to supply a concentrated stream of CO_2. The carbon capture facility removes 90% of the CO_2 from the flue gas and concentrates it to 95% before supplying it to the biorefinery. After accounting for the power required by the biorefinery and the carbon capture facility, over 22 MW is available for sale to the grid. At night this unit is assumed to operate at full load. The process flowsheet is similar to Figure 3 with a biomass gasification plant replacing a coal-based power plant.

Case 12: Direct air capture (DAC)

Contrary to the cases described above, which capture CO_2 from flue stacks having relatively high concentration of CO_2, direct air capture (DAC) refers to technologies that can capture industrial-scale quantities of CO_2 from atmospheric air [15]. Different DAC strategies have been discussed by Sanz-Perez *et al.* [14]. We model a process developed by Carbon Engineering (CE) [13], which has a mass and energy balance available in the open literature.[12] Air is filtered through a chemical absorbent that captures about 80% of the air's carbon dioxide. The absorbent drops to the bottom, while the CO_2-depleted air is released. The collected CO_2 is concentrated in a process with two connected chemical loops (Figure 5). The first loop captures CO_2 from the atmosphere using an aqueous solution of potassium hydroxide and potassium carbonate. In the second loop the carbonate ions are precipitated to form calcium carbonate. The calcium carbonate is then calcined to liberate CO_2. A natural gas combined heat and power (CHP) unit provides the process steam requirements, and the electricity for CO_2 compression and air contactors. Natural gas also provides heat for the calciner. Thus the DAC process extracts a significant portion of CO_2 from flue gases generated in the CHP and the calciner, as well as from the atmosphere. The ASPEN Plus® model for the process was prepared based on the mass and energy balance reported for the CE pilot plant facility by Keith et al. [12].

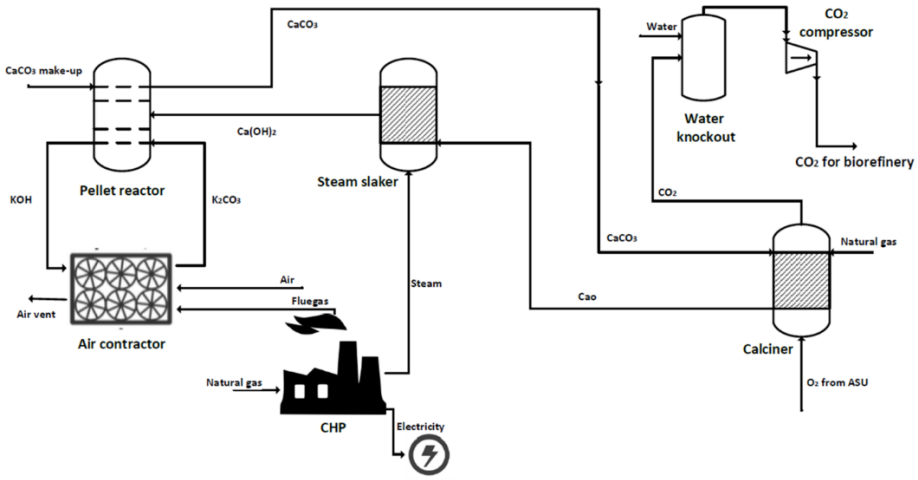

Figure 5: CO_2 supply from direct air capture system from Carbon Engineering.

LCA methodology

The major component of the GHG emissions is carbon dioxide. There are also some minor emissions of other GHGs. A global warming potential is used to characterize the relative contributions of different GHGs. These global warming potentials can be calculated for any time horizon; we use the global warming potentials for the 100-year time horizon from the IPCC Fifth Assessment Report including climate-carbon feedback [16].

The purpose of this study is to compare the carbon footprint of different CO_2 feedstock supply scenarios for a generic algal biorefinery. The study highlights the CO_2 delivery process configurations, to assist in understanding and reducing the GHG burden of transportation of CO_2. A cradle-to-gate LCA study was carried out with the help of Excel worksheets. The life cycle inventory (LCI) data was extracted from ASPEN Plus® flowsheets as well as the other databases such Ecoinvent [17]. The ASPEN Plus® flowsheets provided the material and energy balances for major process unit operations. Ecoinvent data were used for background processes such as transportation and electricity production. A functional unit of 1 g of CO_2 delivered to the biorefinery is used. The study

highlights the carbon footprint resulting from the production and transportation of CO_2, and does not address the carbon footprint associated with algae growth and processing, or with the subsequent release of CO_2 from use of the algae biorefinery products [18].. . The CO_2 produced in the different cases should be considered a product rather than an emission. The process matrix approach for inventory analysis that was developed by Heijungs and Suh [19] has been used. The approach usees matrix algebra to reconcile the unit process inventories.

In the NGCC cases (Cases 5-8), the upstream leakage of methane also needs to be accounted for. Methane leakage and additional supply chain emissions rates vary and are not well characterized. We assume GHG emissions of 14 g CO_2eq./MJ of natural gas utilized to account for natural gas production, processing, transmission, storage, and distribution [20]. Approximately half of these emissions are attributed to transmission, storage, and distribution. The emissions for import or export of electricity are assumed to occur at grid average electricity emissions of 500 g CO_2eq./kWh electricity.

Biomass GHG Calculation

For the biomass related cases (Cases 9-11), growing and harvesting trees will have GHG emissions associated with site preparation, use of fertilizers, and harvesting. Dwivedi *et al* [21] have characterized these for non-intensive forest management, intensive forest management with harvesting at 10 or 11 years, and intensive forest management with harvesting at greater than 12 years. These are summarized in Table 2, in kg CO_2e per hectare.

Table 2: GHG emissions from growing and harvesting trees.

Growing and harvesting trees	Total	Site prep	Fertilizers	Harvesting
Intensive forest management, >12yrs	4803	1127.4	2541.7	1134.2
Intensive forest management, 10 or 11 yrs	2432	1127.4	170.3	1134.2
Non-intensive forest management	2200	1065.5	0	1134.2

The present study focusses on 11 year harvesting. The products from harvesting are presented in Table 3 green tonnes per hectare from [21]. “Green” refers to fresh, undried biomass.

Table 3: Products from biomass harvesting.

Biomass component	Tonnes per hectare
Logging residues	28
Pulpwood	122
Logging residues + Pulpwood	150
Chip-N-Saw	50
Total biomass produced	200

The upstream carbon dioxide emissions can be allocated on the basis of mass, of energy content of the product, or value of the product. We allocate based on mass and on value. A key question is not only what type and age of trees are used, but what portion of these trees is used for wood chips. In this study logging residues and pulpwood are used to make wood chips. If the pulpwood were used for making pulp, the cost of wood for wood chips would be less and the portion of the upstream GHG

emissions allocated to the wood chips would be smaller. On the other hand, use of pulpwood for chips makes it easier to get wood locally to provide a large amount of wood chips.

Assuming an average of 50 km from the point of harvest to the chip mill, the GHG emissions association with transport are as shown in the Table 4,

Table 4: Emissions from biomass transport.

Transport to chip mill		
Log truck capacity	22.7	tonne
Log truck fuel use loaded	1.91	km/l
Log truck fuel use empty	2.34	km/l
Transport distance - wood to chip mill	50	km
GHG emissions of diesel	2.68	kg CO2e/l
GHG emissions wood to chip mill & backhaul	4.19	kg CO2e/tonne

We assume a chipping machine which uses 1.67 liters of diesel fuel per tonne [22]. Transport to the point of use may be another 50 km; if the truck is the same as the logging truck this contributes an additional 4.2 kg CO_2e per tonne of dry wood chips. Drying the biomass can consume 4.2 MJ/kg of water evaporated [21]. This is assumed to be accomplished with wood-based heat. With a typical energy density for dry wood chips of 18 MJ per kg, an additional 0.23 kg of wood chips will be needed for each finished kg of wood chips.

When the biomass is combusted during CO_2 production it will release carbon dioxide into the atmosphere. A global warming potential approach is utilized, which weights the impact of the biogenic carbon based on its lifetime in the atmosphere compared to the emission of fossil carbon [23]. The global warming potential for 11 year biomass with no storage and with a 100 year time horizon is 0.04. The CO_2 emissions from combustion of the biomass is 1.83 kg CO_2 per kg dry biomass. Therefore, the CO_2eq. emissions are 0.04 times that, or 0.08 kg CO_2 per kg biomass. In total, the result is 138 kg of CO_2eq. per tonne of biomass.

Results

The GHG emissions of different CO_2 supply scenarios are presented in Table 5. The three major contributors to the GHG emissions are described as the carbon source, electricity production and feedstock production respectively. The carbon source refers to the power plants, NGCC units, biomass combustion/gasification units and the DAC unit. Electricity production refers to the import or export of electricity. Feedstock production refers to the production and transportation of natural gas or biomass. The contribution of these three sources to the overall carbon footprint of different cases is presented in Table 5. Not surprisingly, the biomass CO_2 supply cases (cases 9-11) were found to have the lowest carbon footprint, as much of the CO_2 supplied was removed from the atmosphere during the growth of biomass. The CO_2 intake for feedstock production for biomass cases shown in Table 5, corresponds to the CO_2 that is released with the night time and carbon capture emissions. An additional GHG benefit is derived from the export of electricity which would displace predominantly fossil based electricity. The scenarios having a NGCC plant near the biorefinery (Cases 5-8) are predicted to have the highest carbon footprint. It should be noted that in all the cases, the electricity which is imported or exported is assumed to have grid average emissions. The NGCC with carbon capture scenario (Case 6-8) has a poorer carbon footprint in spite of utilizing the night-time NGCC emissions. This may be attributed to smaller electricity production and export. The size of the

NGCC facility with carbon capture and refrigeration (case 7) is almost half of the size of the facility without refrigeration (Case 6). The high carbon footprint for the carbon source in the NGCC (case 5-6) and biomass (case 9-11) scenarios correspond to the night time CO_2 emissions which are vented off to the atmosphere. In the cases that employ a refrigeration unit (cases 7-8), the emissions are smaller and result from the release from the carbon capture and refrigeration units. The emissions mainly correspond to the inefficiency of the capture and refrigeration systems. The emissions from carbon source in certain cases involving carbon capture (cases 6 & 11) are reported to be greater than one. The reason is for this is the CO2 losses in the carbon capture unit as well as the normalization of results with respect to the functional unit of 1 g of CO_2 delivered. The most promising carbon negative CO_2 supply cases are dependent on the growth of biomass to off-set the high amount of CO_2 released during night-time operation or the carbon-capture and refrigeration units.

The coal and natural gas power plant cases (cases 1-4) have significantly better GHG emissions for the transport of CO_2. The major contributors to the coal (cases 1-2) and natural gas (cases 3-4) plant scenarios are the electricity requirement for the transport compressor as well as the natural gas requirement as a source of heat for the scenarios (cases 2 & 4) involving carbon capture. The direct air capture (case 12) scenario also has a high carbon footprint due to the energy requirement for operating the compressors, air contactors, steam slaker and calciner. Additionally, in the DAC system 69 % of the CO_2 is absorbed from the atmosphere, with the remaining 31 % being emissions from the natural gas combustion in the CHP and the calciner. The emissions from natural gas combustion are captured and utilized by the DAC technology. Furthermore, since the CHP system in the DAC case is designed to meet the heat and electricity requirement of the air capture plant, the DAC case does not benefit from the export of electricity as in the other scenarios.

Table 5: GHG emissions (g CO_2e) for for 1g CO_2 delivered to the biorefinery.

	Carbon source	Electricity Production	Feedstock production	Total emissions
Case 1: Legacy coal based power plant	-1.00	0.08	0.00	-0.92
Case 2: Legacy coal based power plant with carbon capture	-0.84	0.04	0.04	-0.76
Case 3: Legacy natural gas based power plant	-1.00	0.23	0.00	-0.77
Case 4: Legacy natural gas based power plant with carbon capture	-0.84	0.08	0.04	-0.73
Case 5: Purpose-built NGCC plant	1.00	-2.06	0.53	-0.53
Case 6: Purpose-built NGCC plant with carbon capture	1.25	-2.25	0.60	-0.40
Case 7: Purpose-built NGCC plant with carbon capture and refrigeration	0.16	-1.01	0.31	-0.54
Case 8: Purpose-built NGCC plant with carbon capture and partial refrigeration	0.09	-0.99	0.29	-0.60
Case 9: Biomass combustion	1.00	-0.46	-1.84	-1.30
Case 10: Biomass gasification	1.00	-0.78	-1.84	-1.62
Case 11: Biomass gasification with carbon capture	1.25	-0.73	-2.07	-1.56
Case 12: Direct air capture case	-0.69	0.00	0.09	-0.61

Discussion

This section presents a critical discussion of the process modeling and LCA approach that has been adopted in this study. The power plants are included in the system boundary in the on-site NGCC and biomass power cases; they are omitted in the off-site coal and natural gas power plant cases. The rationale is that NGCC and biomass power plants at the CO_2 utilization site would be exclusively built for the purpose for providing CO_2. In contrast, the off-site coal and natural gas plants are existing, legacy power plants, operating as per their normal operations, and all the CO_2 delivered to the algal biorefinery would otherwise have been emitted to the atmosphere. However, for the on-site NGCC and biomass cases, which would be specifically built to provide CO_2 for the biorefinery, the emission from the feedstock supply as well as night-time emissions are part of the footprint of the CO_2 delivery. The excess electricity that is produced in these cases is exported to the grid and is assumed to have average grid emissions, whereas no credit for the off-site coal and natural gas power plant electricity is taken.

There is a difference in the DAC case and the power plant cases. In the DAC case, there is no additional energy (electricity) production and, thus, the carbon footprint of the complete facility is allocated to the CO_2 produced. In the power plant case, however, the carbon footprint of the complete power plant is already allocated to the electricity production from the power plant. The carbon footprint for the CO_2 supply from the power plant cases comes primarily from the compression of CO_2 and the capture process. These results show that for effective utilization of DAC systems for providing CO_2 to biorefineries, the energy consumption of the DAC system would need to be reduced.

Different algal bio-refineries would require different CO_2 concentrations for the optimal performance of the facility. Not all the scenarios presented in this study provide the same concentration of CO_2 at the biorefinery. The scenarios having the carbon capture and refrigeration provide a concentrated CO_2 stream having a 95% or greater of CO_2 concentration. These scenarios include the CO_2 transport from natural gas power plant, NGCC and biomass gasification cases. Other scenarios provide a more dilute CO_2 concentration. A comparison of CO_2 concentration delivered by different scenarios are presented in Table 6. The case 10, which is predicted to have the lowest carbon footprint for CO_2 delivery would be transporting the CO_2 at a concentration 8 %. If a more concentrated CO_2 stream is required, the biomass gasification flue gas must be captured as presented in case 11. The results indicate that transportation of dilute CO2 has a low carbon footprint. However, the required CO_2 purity depends on the size of the refinery, the specific demand of the organisms, and the spatial arrangement of the CO_2 generation and utilization units. These considerations are beyond the scope of the present work.

Table 6: CO_2 supply composition for different CO_2 supply scenarios.

Cases	CO_2	N_2	O_2	H_20
Case 1: Legacy coal based power plant	0.14	0.79	0.05	0.02
Case 2: Legacy coal based power plant with carbon capture	0.97	0.01	0.00	0.02
Case 3: Legacy natural gas based power plant	0.05	0.81	0.12	0.02
Case 4: Legacy natural gas based power plant with carbon capture	0.96	0.02	0.00	0.02
Case 5: Purpose-built NGCC plant	0.05	0.81	0.12	0.02
Case 6: Purpose-built NGCC plant with carbon capture	0.96	0.02	0.00	0.02

Case 7: Purpose-built NGCC plant with carbon capture and refrigeration	0.98	0.01	0.00	0.01
Case 8: Purpose-built NGCC plant with carbon capture and partial refrigeration	0.09	0.77	0.11	0.03
Case 9: Biomass combustion	0.18	0.78	0.03	0.02
Case 10: Biomass gasification	0.08	0.78	0.12	0.02
Case 11: Biomass gasification with carbon capture	0.97	0.01	0.00	0.02
Case 12: Direct air capture case	0.95	0.02	0.02	0.01

The import or export of electricity to the grid influences the footprint of CO_2 supply scenarios. While the off-site power plant CO_2 supply cases are importing electricity from the grid, the on-site NGCC and biomass scenarios are exporting excess electricity to the grid. The DAC case is self-sufficient in energy because of the presence of a CHP unit. This study assumes average grid electricity emissions for both the import and export of electricity. This assumption was made to facilitate a consistent comparison. This assumption might be questioned in the cases where the electricity is imported from the grid. Particularly in coal power plant scenarios, there is a reasonable probability that electricity required for CO_2 compression would be coming from the coal power plant itself. Coal electricity production has higher GHG emissions than the U.S. grid average. If coal electricity is assumed to be utilized in case 1 and case 2, the carbon footprint for the two cases would be -0.82 and -0.71 gCO_2 eq./g CO_2 eq. delivered, respectively. Alternately, case 3 and case 4 would have a slightly lower carbon footprint, since the carbon footprint of natural gas electricity production is slightly lower than grid average electricity production. A difference would be noticed in NGCC based cases, where excess electricity is supplied to the grid. In the NGCC based cases, the actual emissions for electricity emissions would be lower than carbon footprint of grid electricity. However, since they would be displacing grid electricity, those cases would derive the benefit of averting the grid emissions. The sensitivity of the NGCC based cases to the footprint of exported electricity is elaborated in the next section.

Sensitivity

The distance between the biorefinery and the legacy power plants affects the CO_2 delivery power requirements. A pressure drop of 0.055 bar is assumed for every mile. The energy requirements and corresponding greenhouse gas emissions results are shown in Figure 6. The emissions are greater for the natural gas power plant because of the dilute concentration of CO_2. Sensitivity of the carbon footprint with respect to distance to CO_2 transport doesn't make much difference in the carbon capture scenario, as the regenerator is assumed to operate at an elevated pressure and the flowrate is significantly smaller once the nitrogen and other gases are removed. It may be inferred that power plant CO_2 supply from natural gas based plant is only reasonable when the biorefinery is located near of the power plant. The CO_2 supply for coal based plant is comparatively less sensitive to the transport distance. The increase is distance, however, is expected to be coupled with increasing capital and operating cost. In the absence of a power plant as a source of carbon near the biorefinery, building a NGCC plant, biomass plant or DAC plant near the refinery are expected to be more viable options.

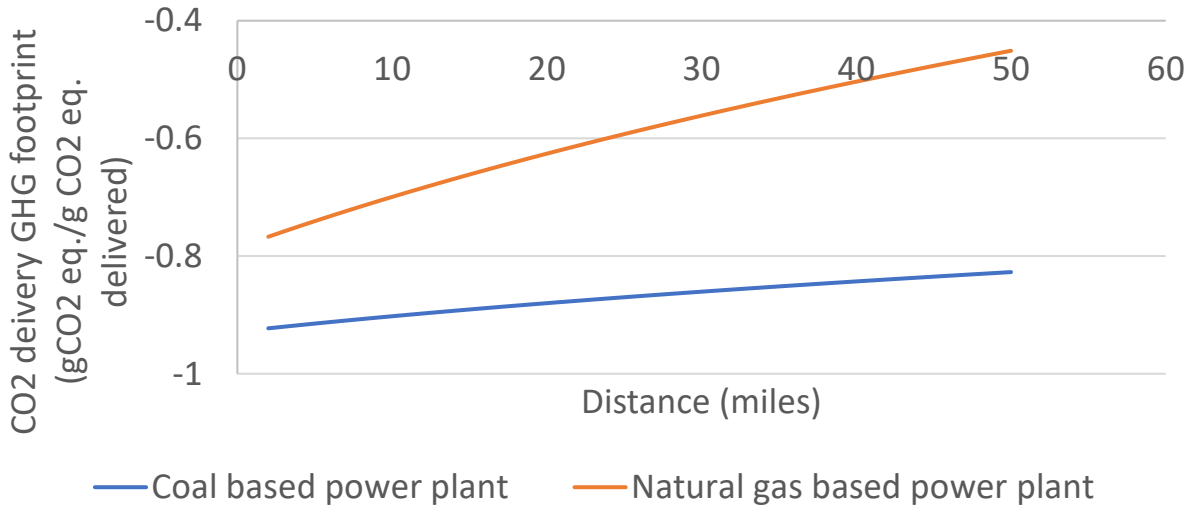

Figure 6: Sensitivity of power plant based CO_2 supply with increasing distance from the biorefinery.

The GHG emissions for the NGCC cases are very sensitive to the GHG emissions of the grid electricity as well as emissions from natural gas supply chain. These factors vary by location and are changing with time as renewables and natural gas displace coal as the major fuel for electricity consumption. A sensitivity analysis was performed for case 8, of CO_2 supply from a standalone NGCC unit incorporating carbon capture and refrigeration. The grid electricity carbon emissions were varied from 450 to 800 g CO_2 eq./kWh and the natural gas supply chain emissions were varied from 2 to 30 g CO_2 eq./MJ HHV natural gas. The GHG emissions of supplied CO_2 can go as high as 0.69 gCO_2 eq./g CO_2 delivered when the grid electricity has emits 450 g CO_2 eq./kWh and the natural gas supply chain emits 30 g CO_2 eq./MJ HHV Natural gas. On the other extreme the GHG emissions of the supplied CO_2 can go as low as -1.95 gCO_2 eq./g CO_2 delivered when the grid electricity has high GHG emissions and the natural gas supply chain has the lowest possible emissions. The carbon footprint for the intermediate cases can be calculated utilizing Equation 1,

$$GHG = 0.0428*NG - 0.0041*EL + 1.248 \quad (1)$$

where GHG refers to the GHG emissions of the delivered CO_2 (gCO_2 eq./g CO_2 delivered), NG refers to the natural gas supply chain emissions in g CO_2 eq./MJ HHV natural gas and EL refers to grid electricity GHG emissions in g CO_2 eq./kWh.

Case Study

To study the effect of CO_2 sourcing on the GHG footprint of the biorefinery, ASPEN Plus® models were prepared for biofuel production from hydrothermal liquefaction of algae [24]. The CO_2 supply scenario corresponding to Case 1 (Legacy Coal) has been modeled. The simulation encompassed the CO_2 supply, algae production, hydrothermal liquefaction (HTL) of algae and catalytic hydrothermal gasification (CHG) of aqueous phase resulting from HTL reactor. The primary product is the biofuel produced from the HTL process. The algae production was modelled utilizing a methodology reported by NREL [11]. The HTL and the CHG process were simulated by updating the models proposed by PNNL [12]. The CHG fuel-gas is utilized to provide heat for the HTL and CHG reactors. The electricity requirements of the biorefinery are met through an onsite natural gas powered CHP plant. The CHP is sized (15 MW) to meet the daytime electricity requirements of the algae biorefinery, which are higher than those at night. The daytime CO_2 emissions from the CHP plant are utilized by

the biorefinery and the night-time emissions are vented to the atmosphere. The simulation incorporated separate day and night operations as well as recycles of CO_2, water and nutrients. The coal power plant is assumed to be located 2 miles from the biorefinery. The proposed size of the PBR based refinery is 2000 acres and an algae growth cycle of 60 days is considered. The system boundary of the LCA also includes the hydro-treating of bio-crude. The flowsheet depicting the biofuel production through HTL is presented in Figure 7. The composition of major streams is presented in the supporting information.

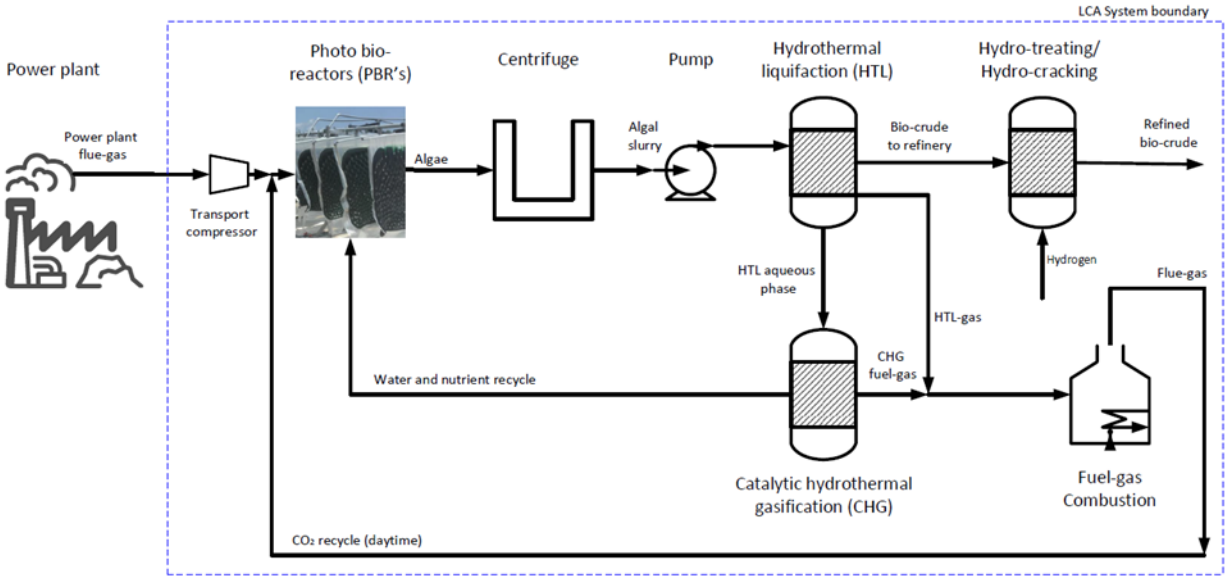

Figure 7: Flowsheet for biofuel production from algae HTL.

The LCA results indicates a GHG emission of 43.1 g CO_2 eq./MJ biofuel, as shown in Figure 8. This is a 54% GHG reduction compared with gasoline, which has a carbon footprint of 93.1 g CO_2 eq./MJ . The emissions associated with CO_2 delivery are highlighted in red in Figure 8. The figure highlights that the CO_2 delivery has a significant contribution to the final carbon footprint of biofuel production. The study assumes grid average electricity emissions (500 g CO_2 eq./kWh) for plant electricity export. The largest source and sink of CO_2 emissions are the bio-oil combustion and CO_2 delivery during algae growth, respectively. The emissions from the CHG and the CHP are night-time CO_2 emissions which are vented to the atmosphere. The other major contributors are likely to remain constant with the changing plant configurations except the electricity export. If a grid average electricity emission of 750 g CO_2 eq./kWh (appropriate for a typical coal-fired plant) is assumed, the total carbon footprint for the biofuel would be 31.4 g CO_2 eq./MJ biofuel.

For a given plant capacity all the emission sources, except the CO_2 delivery and electricity export, are expected to remain constant. The contribution of CO_2 delivery would be different for different CO_2 supply cases. Furthermore, different CO_2 supply scenarios can offer a variety of heat integration avenues to the biorefinery. In the NGCC and biomass CO_2 supply cases, the utilization of excess electricity and heat in the biorefinery can reduce the CO_2 footprint of the complete process. The direct air capture case, in particular, is expected to derive considerable benefit by the amalgamation of the utilities for the direct air capture process and the biorefinery. Presenting these heat integration scenarios is beyond the scope of the present study, and is a promising direction for future research.

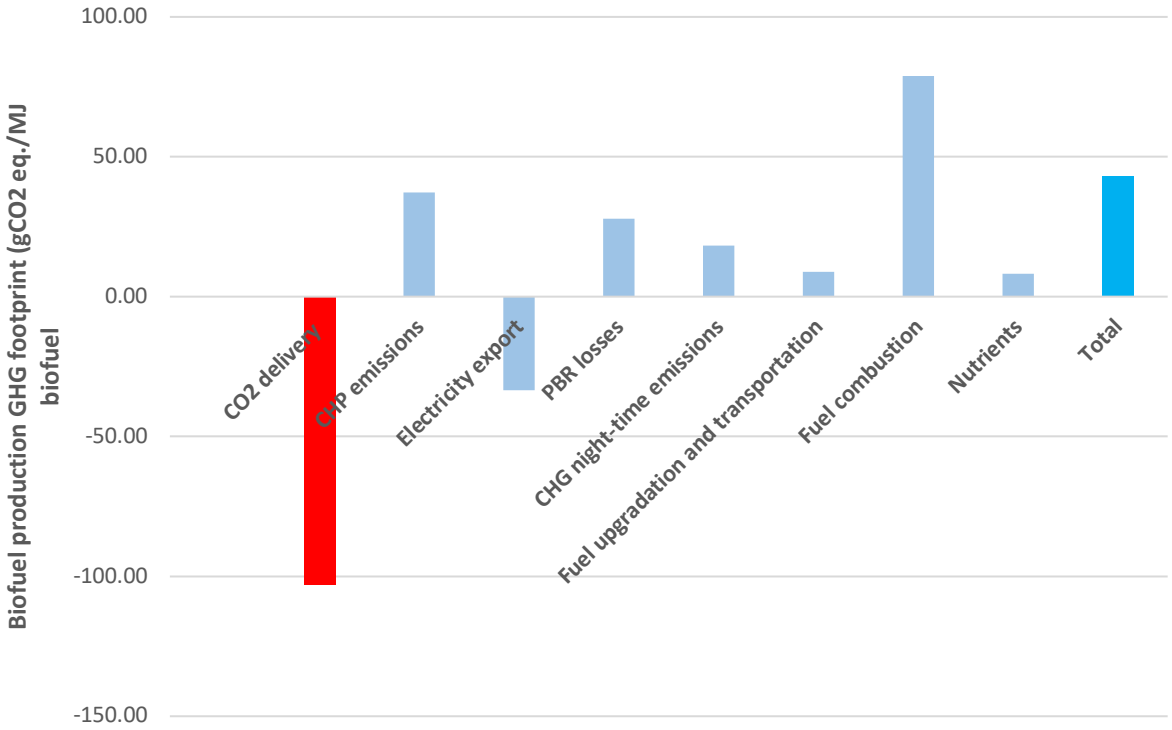

Figure8: Biofuel production from algae HTL process utilizing CO_2 from coal based power plant.

Conclusions

One of the prominent challenges in the production of algal biofuels is the sustainable supply of carbon dioxide. While some studies of the sustainability of algal biorefineries assume the availability of the required CO_2 without any additional carbon footprint, the present study quantifies the carbon footprint of CO_2 supply from different potential sources. Twelve different CO_2 supply cases spanning from fossil fuel based power plant stack gases to direct air capture systems have been compared. The results include both day and night-time emissions to provide a comprehensive comparison. CO_2 supply for the combustion or gasification of biomass are calculated to have the lowest carbon footprint for the supplied CO_2. Three scenarios involving construction of NGCC units near the biorefinery are found to have the least favorable carbon footprints. However, the greenhouse gas emissions are very sensitive to the grid electricity carbon footprint as well as emissions from supply chain of natural gas feedstock. CO_2 supply from existing fossil fuel based power plants have favorable carbon footprints for supplying their stack gases over short distances (<2 miles) but become less favorable as the distance between the power plant and biorefinery increases. The direct air capture system, which can eliminate the logistical constraint associated with CO_2 sourcing, has a relatively high energy demand, which would need to be reduced for optimal symbiosis with algal biorefineries.

Reference

[1] R.M. Handler, D.R. Shonnard, T.N. Kalnes, F.S. Lupton, Life cycle assessment of algal biofuels: Influence of feedstock cultivation systems and conversion platforms, Algal Res. 4 (2014) 105–115. https://doi.org/10.1016/j.algal.2013.12.001.

[2] T.C. de Assis, M.L. Calijuri, P.P. Assemany, A.S.A. de P. Pereira, M.A. Martins, Using atmospheric emissions as CO 2 source in the cultivation of microalgae: Productivity and economic viability, J.

Clean. Prod. 215 (2019) 1160–1169. https://doi.org/10.1016/j.jclepro.2019.01.093.
[3] R. Slade, A. Bauen, Micro-algae cultivation for biofuels : Cost , energy balance , environmental impacts and future prospects, Biomass and Bioenergy. 53 (2013) 29–38. https://doi.org/10.1016/j.biombioe.2012.12.019.
[4] F.G. Acién, J.M. Fernández, J.J. Magán, E. Molina, Production cost of a real microalgae production plant and strategies to reduce it, Biotechnol. Adv. 30 (2012) 1344–1353. https://doi.org/10.1016/j.biotechadv.2012.02.005.
[5] R. Pate, G. Klise, B. Wu, Resource demand implications for US algae biofuels production scale-up, Appl. Energy. 88 (2011) 3377–3388. https://doi.org/10.1016/j.apenergy.2011.04.023.
[6] S.P. Singh, P. Singh, Effect of CO 2 concentration on algal growth: A review, Renew. Sustain. Energy Rev. 38 (2014) 172–179. https://doi.org/10.1016/j.rser.2014.05.043.
[7] J.C.M. Pires, COP21: The algae opportunity?, Renew. Sustain. Energy Rev. 79 (2017) 867–877. https://doi.org/10.1016/j.rser.2017.05.197.
[8] Q. Zheng, X. Xu, G.J.O. Martin, S.E. Kentish, Chinese Journal of Chemical Engineering Critical review of strategies for CO 2 delivery to large-scale microalgae cultures, Chinese J. Chem. Eng. 26 (2018) 2219–2228. https://doi.org/10.1016/j.cjche.2018.07.013.
[9] G. Reiter, J. Lindorfer, Evaluating CO<inf>2</inf> sources for power-to-gas applications-A case study for Austria, J. CO2 Util. 10 (2015) 40–49. https://doi.org/10.1016/j.jcou.2015.03.003.
[10] M.D. Somers, J.C. Quinn, Sustainability of carbon delivery to an algal biorefinery: A techno-economic and life-cycle assessment, J. CO2 Util. 30 (2019) 193–204. https://doi.org/10.1016/j.jcou.2019.01.007.
[11] R. Davis, J. Markham, C. Kinchin, N. Grundl, E. Tan, D. Humbird, Process Design and Economics for the Production of Algal Biomass: Algal Biomass Production in Open Pond Systems and Processing Through Dewatering for Downstream Conversion, Natl. Renew. Energy Lab. (2016) 128. https://doi.org/10.2172/1239893.
[12] S.B. Jones, Y. Zhu, D. Anderson, R.T. Hallen, D.C. Elliott, Process Design and Economics for the Conversion of Algal Biomass to Hydrocarbons : Whole Algae Hydrothermal Liquefaction and Upgrading, 2014. https://doi.org/10.2172/1126336.
[13] D.W. Keith, G. Holmes, D. St. Angelo, K. Heidel, A Process for Capturing CO2 from the Atmosphere, Joule. 2 (2018) 1573–1594. https://doi.org/10.1016/j.joule.2018.05.006.
[14] H. Jilvero, F. Normann, K. Andersson, F. Johnsson, Heat requirement for regeneration of aqueous ammonia in post-combustion carbon dioxide capture, Int. J. Greenh. Gas Control. 11 (2012) 181–187. https://doi.org/10.1016/j.ijggc.2012.08.005.
[15] E.S. Sanz-Pérez, C.R. Murdock, S.A. Didas, C.W. Jones, Direct Capture of CO2 from Ambient Air, Chem. Rev. 116 (2016) 11840–11876. https://doi.org/10.1021/acs.chemrev.6b00173.
[16] IPCC, Working Group 1, Summary for Policymakers, in: Clim. Chang. 2013 Phys. Sci. Basis. Contrib. Work. Gr. I to Fifth Assess. Rep. Intergov. Panel Clim. Chang., 2013: p. 78. https://doi.org/10.1017/CBO9781107415324.Summary.
[17] ecoInvent, Data quality guideline for the ecoinvent database V 3.0, 3 (2009).
[18] D. Luo, Z. Hu, D.G. Choi, V.M. Thomas, M.J. Realff, R.R. Chance, Life cycle energy and greenhouse gas emissions for an ethanol production process based on blue-green algae, Environ. Sci. Technol. 44 (2010) 8670–8677. https://doi.org/10.1021/es1007577.
[19] R. Heijungs, S. Suh, The Computational Structure of Life Cycle Assessment, Springer Netherlands, 2002.
[20] P. Balcombe, K. Anderson, J. Speirs, N. Brandon, A. Hawkes, The Natural Gas Supply Chain: The Importance of Methane and Carbon Dioxide Emissions, ACS Sustain. Chem. Eng. 5 (2017) 3–20. https://doi.org/10.1021/acssuschemeng.6b00144.
[21] P. Dwivedi, R. Bailis, T.G. Bush, M. Marinescu, Quantifying GWI of Wood Pellet Production in the

Southern United States and Its Subsequent Utilization for Electricity Production in The Netherlands/Florida, Bioenergy Res. 4 (2011) 180–192. https://doi.org/10.1007/s12155-010-9111-5.

[22] M.D. Westbrook, W.D. Greene, R.L. Izlar, Utilizing forest biomass by adding a small chipper to a tree-length southern pine harvesting operation, South. J. Appl. For. 31 (2007) 165–169.

[23] G. Guest, F. Cherubini, A.H. Strømman, Global Warming Potential of Carbon Dioxide Emissions from Biomass Stored in the Anthroposphere and Used for Bioenergy at End of Life, J. Ind. Ecol. 17 (2013) 20–30. https://doi.org/10.1111/j.1530-9290.2012.00507.x.

[24] D.C. Elliott, T.R. Hart, A.J. Schmidt, G.G. Neuenschwander, L.J. Rotness, M. V. Olarte, A.H. Zacher, K.O. Albrecht, R.T. Hallen, J.E. Holladay, Process development for hydrothermal liquefaction of algae feedstocks in a continuous-flow reactor, Algal Res. 2 (2013) 445–454. https://doi.org/10.1016/j.algal.2013.08.005.

Acknowledgements
This material is based upon work supported by the U.S. Department of Energy's Office of Energy Efficiency and Renewable Energy (EERE) under the Bioenergy Technologies Office Award Number DE-EE0007690.

1.C. Lifecycle Greenhouse Gas Emissions for an Ethanol Production Process Based on Genetically Modified Cyanobacteria: CO_2 Sourcing Options

Lifecycle Greenhouse Gas Emissions for an Ethanol Production Process Based on Genetically Modified Cyanobacteria: CO_2 Sourcing Options

Pratham Arora[1,a], Ronald R. Chance[2,3], Howard Hendrix[4], Teresa Fishbeck[2], Matthew J. Realff[3], Valerie M. Thomas[1]*, Yanhui Yuan[2]

[1]School of Industrial and Systems Engineering
Georgia Institute of Technology
Atlanta GA 30332

[2]**Algenol Biotech**
16121 Lee Road, Suite 110
Fort Myers, FL 33912

[3]School of Chemical and Biomolecular Engineering
Georgia Institute of Technology
Atlanta GA 30332

[4]Hendrix Engineering Solutions, Inc.
136 B Marketplace Circle PMB 164
Calera, AL 35040
hendrixengineeringsolutions@gmail.com
205-382-3088

***corresponding author**

Keywords: diurnal, carbon capture, carbon storage, carbon refrigeration, biofuel

Author Information

*Corresponding Author
Email: valerie.thomas@isye.gatech.edu

Present Addresses
[a] Department of Hydro and Renewable Energy, Indian Institute of Technology Roorkee

Author Contributions
The manuscript was written through contributions of all authors. All authors have given approval to the final version of the manuscript.

Abstract

We evaluate the lifecycle energy and greenhouse gas inventory for ethanol produced by genetically modified cyanobacteria in photobioreactors. The diurnal cycle of algal growth significantly affects the design and impacts of CO_2 sourcing. Several CO_2 sourcing designs are evaluated: direct transport and use of coal flue gas or natural gas flue gas, carbon capture at coal or natural gas power plants with transport, and on-site production of heat, electricity, and CO_2 via a combined heat and power (CHP) unit fueled by either natural gas or biomass. The on-site CHP and CO_2 production cases can produce excess electricity which can be sold back to the grid; the scale of the on-site CHP and CO_2 production can be reduced by night-time capture and refrigerated storage of CO_2 on-site. The lifecycle greenhouse gas emissions for 1 MJ ethanol are about -19 g CO_2e for onsite biomass CHP-CO_2, +19 g CO_2e for direct use coal flue gas, and +31-35 CO_2e g for natural gas on-site energy and CHP-CO_2 options, compared to 91.3 g CO_2e for 1 MJ of conventional gasoline. Both natural gas and biomass fueled CHP facilities could be co-located with an ethanol biorefinery, capturing and utilizing carbon dioxide to make biofuel.

Introduction

Algal biofuels can be produced with a range of technologies, typically centered on lipid production.[1,2] Previous research has evaluated options for biodiesel production from algae, mainly considering open pond technology and typically assuming that the biofuel facility is located near a coal-fired power plant.[3]

We consider here a process in which ethanol is produced by cyanobacteria genetically engineered for that purpose. The cyanobacteria are grown in photobioreactors designed and

utilizing a process developed by Algenol Biotech.[4] Previous studies have evaluated the energy and greenhouse gas emissions for earlier versions of this system.[5,6] Over the past several years a great deal of progress has been made in the development of the associated upstream and downstream processes, with fundamental design changes that affect energy demand and product composition.[4] Detailed engineering analysis of both the biofuel facility processes and the delivery of electricity, process heat, and CO_2 have been undertaken along with process integration. In the first study of this process the energy and emissions from capturing and transporting the CO_2 were not included.[5] In the second study CO_2 was modeled as captured from power plants with amine scrubbing technology.[6]

Sourcing of CO_2 for algal biofuel production has been evaluated in previous studies.[7,8] Here we take a closer look at several approaches to CO_2 sourcing: use of flue gas directly from coal or natural gas power plants; use of captured CO_2 from coal or natural gas power plants; use of natural gas combined heat, power and CO_2 on site; and use of biomass combined heat, power and CO_2 on site. Unlike previous work the study includes the diurnal cycle of algae growth which impacts the CO_2 delivery system, particularly in the case of on-site CO_2 generation. More broadly, this study examines the role that on-site generation of heat and power, combined with carbon dioxide capture and utilization provides in the production of biofuels.

Ethanol Production Process Description

The cyanobacteria are grown in photobioreactors in a medium consisting of brackish water supplemented with nitrogen and phosphorus fertilizers. CO_2 is supplied via the aeration-based mixing system. The cyanobacteria produce ethanol which diffuses through their cell walls into the culture medium. Of the carbon that is consumed by the cyanobacteria, typically 66% is carbon in ethanol, with the balance being carbon in the biomass, based on the Algenol experience for ethanol production rates and the biomass concentrations in the photobioreactors.[4] An additional 15% CO_2 is supplied above the stoichiometric requirements, corresponding to the CO_2 that is not taken up into the biomass or ethanol due to loses largely attributable to mass transfer limitations. In the current system model, the target ethanol production rate is 73,000 liters/ha-year (7800 gal/acre-year), about 30% higher compared to the 56,000 liters/ha-year (6000 gal/acre-year) modeled previously.[5]

The entire contents of the photobioreactor, including culture medium, cyanobacteria, and ethanol, flow from the photobioreactors into a series of separation processes. The process design is different from that described previously in which ethanol was separated from the culture medium at the photobioreactors by evaporation and subsequent condensation.[5] As a result, the relative fraction of ethanol to cyanobacterial mass is lower, and fertilizer usage is higher, both due to the higher frequency of biomass harvesting and differences in the overall process inventories.

The process plant electric load is about 10,000 kW during the day and 4700 kW during the night for a PBR system that has a 1000-hectare (2500-acre) production footprint. The separation processes operate on a 24-hour basis, producing the separated ethanol product. However, the total load is lower at night as there is no active creation of ethanol by the cyanobacteria at night which means the supply of CO_2 to the cyanobacteria can be turned down. There is some electric load for the photobioreactors to keep the system fluids circulating; this is neglected for the purposes of this study. It is assumed that the day/night cycles are 12 hours in length and no variation during the year is assumed; this approximation has minimal impact on the lifecycle calculations. The process heat requirement is 636 kg/hr of natural gas (9 MW).

Figure 1 shows the process at the envisioned 1000-hectare facility, starting with the photobioreactor (PBR) field, from which the culture is removed for dewatering. The dewatering results in two streams: biomass and a mixture of brackish water and ethanol. In the process evaluated here, the biomass is disposed through deep well injection. Alternative dispositions of the biomass are discussed elsewhere.[4] The water-ethanol mixture is separated using vapor compression steam stripping,[9] with membrane dehydration used for final purification to fuel grade ethanol.[10]

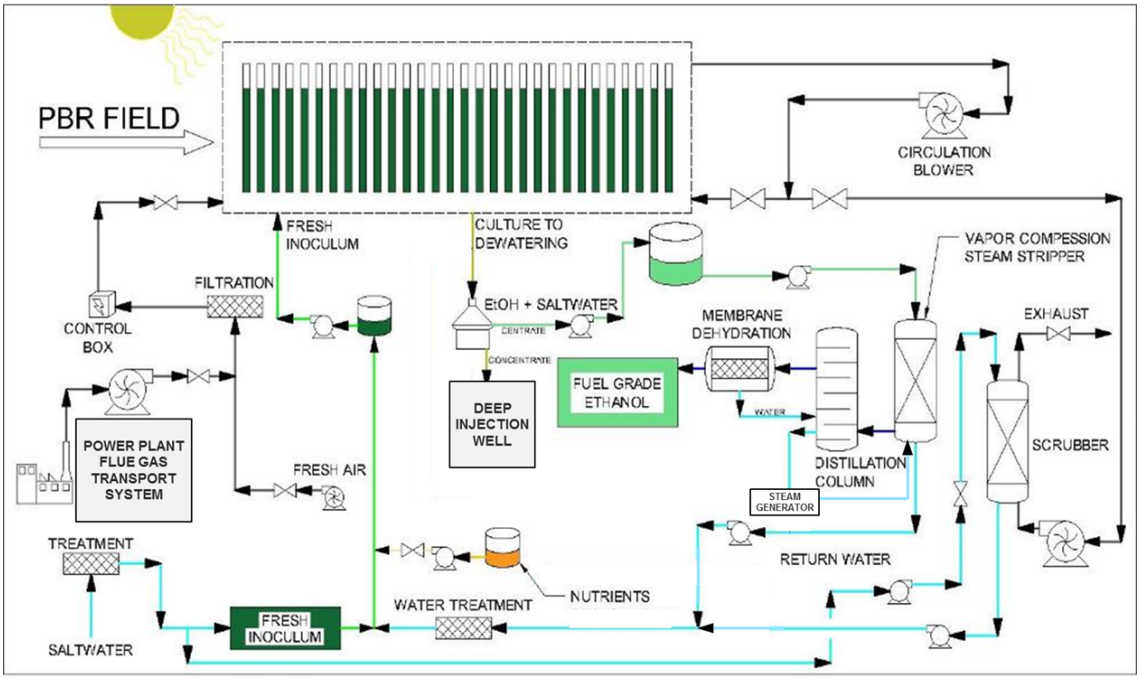

Figure 1. Biorefinery flow chart and unit operations. In addition, the LCA system boundary includes upstream lifecycle emissions for fuels, electricity, CO_2, nutrients, biorefinery infrastructure and ethanol product supply chain and use, see SI Figure S1.

Each photobioreactor contains about 100 liters of culture; the photobioreactor contents are assumed to be replaced every 69 days during a clean-in-place process; see Supporting Information (SI) Table S1.[4] The harvested material from the photobioreactors is sent through a centrifuge. The heavy fraction is disposed by deep-well injection. The light fraction is an ethanol-water mixture. It is sent to the vapor compression steam stripper which increases the concentration 10-fold. This is followed by a series of membrane dehydration steps to produce fuel-grade ethanol. The remaining water is sent through an on-site water treatment system. The treated water is mixed with fresh inoculum and returned to the photobioreactors. An alternative, not considered here, is a standard Stripper-Rectifier-Dehydration (SRD) system.[4]

Table 1 shows the carbon dioxide source systems considered.

CO_2 Source	**Notes**
Coal Flue Gas	Flue gas is transported 2 miles from a coal-fired power plant
Natural Gas Combined Cycle Flue Gas	Flue gas is transported 2 miles from a natural gas-fired power plant. The low CO_2 concentration makes this option too dilute for application; this case is included for comparison purposes only.

CO_2 Captured from Coal Plant	A CO_2 capture facility is constructed near the power plant to remove CO_2 from the coal-fired power plant's flue gas. A natural gas fired boiler would be constructed as part of the CO_2 capture facility to generate steam for the CO_2 regenerator. Concentrated CO_2 is transported 2 miles to the biofuel facility.
CO_2 Captured from Natural Gas Combined Cycle Plant	A CO_2 capture facility is constructed near the power plant to capture the CO_2. Concentrated CO_2 is transported 2 miles to the biofuel facility.
On-Site Natural Gas CHP Plant	Natural gas is combusted on site for production of CO_2, electricity and heat. Excess electricity is sold to the grid, and the power plant continues operations at night to maximize revenue from electricity sale.
On-Site Natural Gas CHP Plant with CO_2 capture and refrigeration	A carbon capture and refrigeration unit is constructed on site to capture night-time CO_2 for use during the day. This minimizes the natural gas requirement and reduces the electricity for sale to the grid.
On-Site Biomass CHP Plant	Biomass is combusted on site for production of CO_2, electricity and heat. Excess electricity is sold to the grid, and the power plant continues operations at night to maximize revenue from electricity sale.
On-Site Biomass CHP Plant with CO_2 capture and refrigeration	A carbon capture and refrigeration unit is constructed on site to capture night-time CO_2 for use during the day. This minimizes the biomass requirement and reduces the electricity for sale to the grid.

Table 1. Systems considered for providing CO_2 for the cyanobacterial production of ethanol

Carbon Dioxide Delivery Cases

Facility designs with external delivery of CO_2 will also consume natural gas on site for process heat. Since this natural gas at the production facility provides 1.75 t/hr of CO_2, 35.7 t/hr needs to be supplied from an external source. The 1.75 t CO_2/hr is mixed with the external CO_2 source during the day and fed to the production field; at night it is assumed that the facility's CO_2 is vented to the atmosphere and therefore its emission contributes to the carbon footprint.

Coal and Natural Gas Flue Gas Cases

In the scenarios described in this section, flue gas from either a natural gas combined cycle power plant or a coal-fired power plant is piped to the production facility.

Since coal plants and NGCC plants use different fuels and different power generating technologies, the CO_2 concentration is significantly different, 4.3 vol % for NGCC and 11.9% for coal (see SI Table S3). To obtain 37.4 t/hr of CO_2 from the NGCC flue gas a mass flow of 560 t/hr of flue gas is required. To obtain the same CO_2 flow from the pulverized coal plant, 202 t/hr of flue gas is required. The higher concentration of CO_2 in the coal flue gas decreases the size of the transport pipe, the power required to transport the flue gas between the power plant and the biofuel facility, and the power required to transport CO_2 within the biofuel facility.

An additional consideration is the required CO_2 concentration at the receiving facility. The CO_2 concentration in the NGCC flue gas may be too low for many algal production systems at rational aeration rates;[4] this will depend on the species of algae and the design of the system. The concentration is too low for the cyanobacteria considered here for ethanol production; even so the calculation is included to provide information that could be useful for algal strains with lower CO_2 or aeration constraints.

The overall power and natural gas demands for the production facility and the CO_2 delivery are shown in the SI Flue Gas Extraction and Transport section. Coal and natural gas flue gas are assumed to be piped two miles to the biofuel facility. For the coal flue gas case the power to transport the flue gas through the piping system is approximately 6190 kW; this power is not used at night. Compared to the baseline power requirements of about 10,000 kW for the biofuel facility itself, this power requirement for CO_2 transport is significant.

Carbon Capture from Coal and Natural Gas Power Plants Cases

Rather than transporting flue gas to the biofuel facility, the carbon dioxide in the flue gas can be captured at the power plant and sent to the biofuel facility in concentrated form. Carbon capture is modeled assuming an advanced solvent with a regeneration energy of 2500 kJ/kg CO_2 captured. The CO_2 capture efficiency is 90% and the delivered CO_2 will have a concentration of at least 95%. Due to the lower concentration of CO_2 in the flue gas from the NGCC unit, the moles of CO_2 removed from the flue gas per mole of solvent is assumed to be less than would be captured from coal derived flue gas, and therefore the circulation rate of solvent through the NGCC carbon capture system would be higher.

The SI section on CO_2 Capture and Transport shows modeling details and the overall power and natural gas demands for the production facility and the CO_2 delivery. While the electricity required for delivery of the concentrated CO_2 stream is lower than for delivery of raw flue gas, the natural gas requirements for capture of the flue gas are significant.

Natural Gas On-site 88 MW Heat, Power and CO_2 Case

In this case, natural gas is combusted on-site at the biofuel facility to provide electricity, heat and CO_2. A natural gas combined cycle system, described in the SI, is sized to provide just enough CO_2 for the 1000 hectare biofuel facility. Some power is used by the biofuel production facility, but substantial power is available for export to the grid. Heat and power are needed at night for the biofuel separation processes, but the cyanobacteria do not require CO_2 at night. A carbon capture system is included here because the concentration of CO_2 in the flue gas is too low for the cyanobacteria used in the Algenol ethanol-production facility. During the daytime operation, the extracted steam is used as process heat for the biofuel production process and the CO_2 capture and regeneration process. At night, we assume the unit would continue to be operated at full load to maximize revenue. Because carbon capture and steam are not required at night, 88 MW is available for sale to the grid. Process diagrams for day and night operation of this system, and summary heat and electricity requirements are shown in the SI.

Figure 2 shows the day and night carbon flows through the facility. Due to the capture of carbon dioxide with 90% capture efficiency, the input CO_2 requirement is 10% more than for the external CO_2 delivery cases with direct utilization of the delivered CO_2 or flue gas.

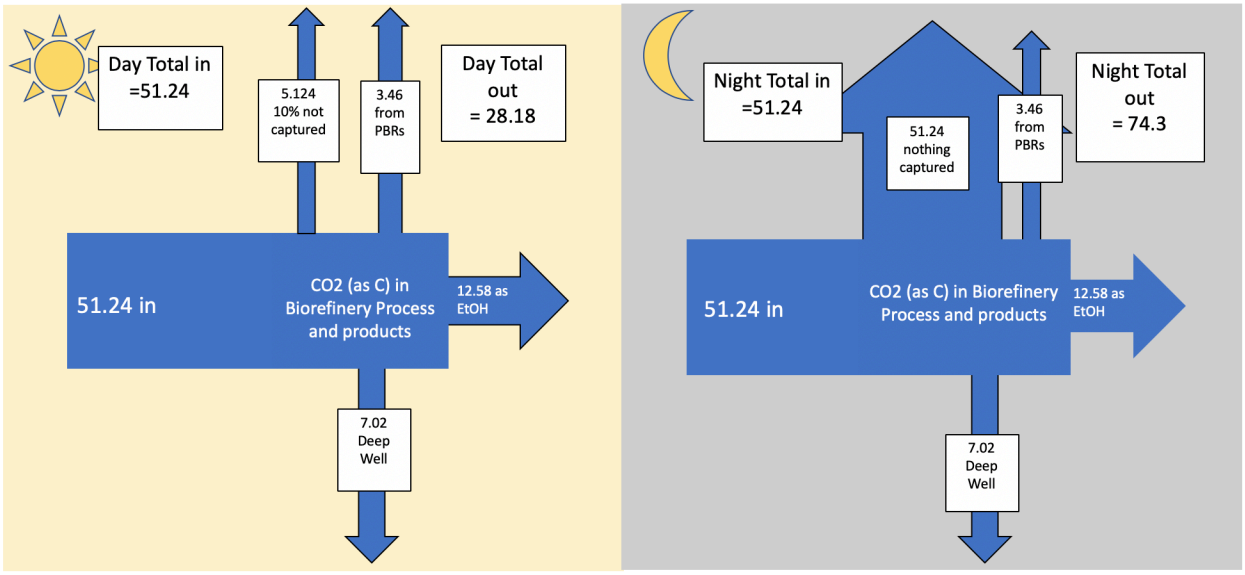

Figure 2. Day and night carbon flows through the facility with combined power, heat and CO_2 (t CO_2/hr).

Natural Gas On-site 31 MW Combined Heat, Power and CO_2 with Refrigeration

To minimize the natural gas requirement, CO_2 can be captured and refrigerated as liquid CO_2 at night for use during the day, as shown in Figure 3. The carbon capture system removes 90% of the carbon dioxide from the flue gas. During the day, this CO_2-rich stream can be compressed, cooled, and supplied to the photobioreactors for aeration. This case uses a 31 MW gas turbine to provide electricity. After consuming 9 MW for biofuel production and carbon capture, approximately 22 MW is available for sale to the grid. Summary heat and electricity requirements are shown in the SI.

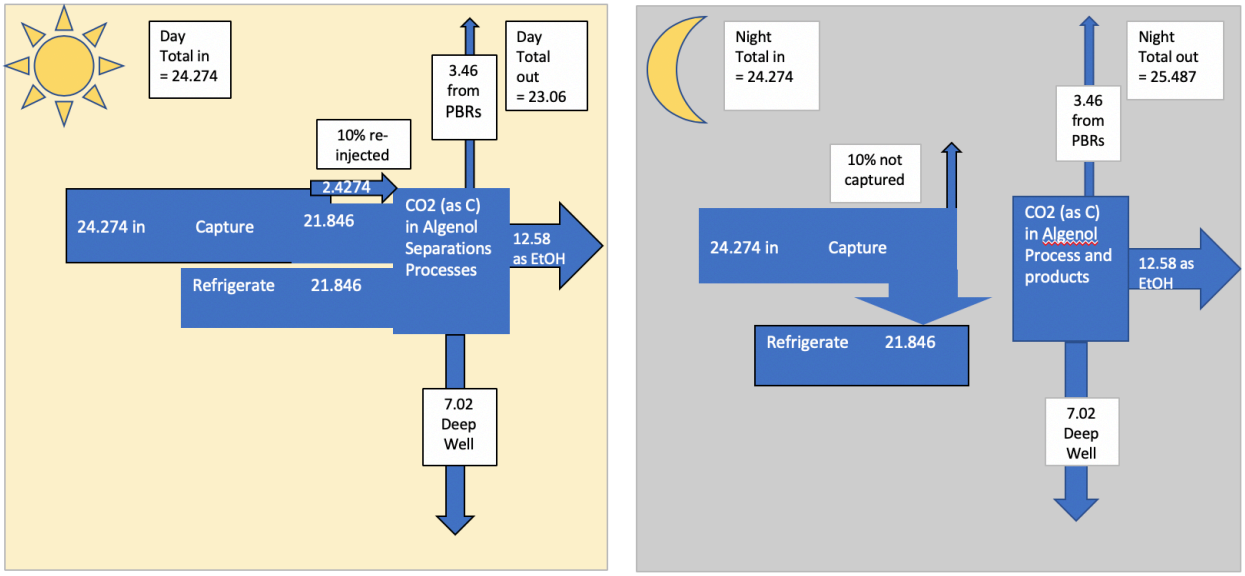

Figure 3. Day and night carbon flows through the biofuel facility with onsite generation of CO_2, heat, and power and with capture and refrigeration of CO_2 at night, using natural gas or biomass.

Biomass On-site 67 MW Heat Power and CO_2 Case

Biomass can be used as the source of CO_2, electricity and process heat. In this case, 24,060 kg/hr of biomass (wood) chips are pre-dried off site to a moisture content of 20%. On site they are fed to a circulating fluid bed combustor and combusted with air. During the day, all the flue gas from the biomass combustor is compressed and cooled and supplied directly to the photobioreactors. At night the unit would operate at 50% of the design load and vent the flue gas to the atmosphere. This co-production of electricity and fuel is more energy and CO_2-efficient than bioelectricity alone.[11] The heat and electricity requirements are summarized in the SI.

Biomass On-site 39 MW Heat Power and CO_2 Case with Refrigeration

In an alternative design, the CO_2 from the biomass combustion would be captured and refrigerated at night to reduce the biomass requirements. This approach reduces the biomass requirement and reduces the excess electricity to be sold back to the grid, but requires the addition of a carbon capture and refrigeration unit. The heat and electricity requirements are summarized in the SI.

Greenhouse Gas Emissions from Electricity and Natural Gas

There are two main uses of electricity in this system: to provide the CO_2 from external sources to the facility, and to run the facility. The CO_2 is required during the 12 hours of daytime; the electricity to run the facility is being used on a 24-hour basis although with more electricity used during the day than during the night.

For externally sourced CO_2, the flue gas or CO_2 capture and transport-powering activities occur within or near the power plant boundary. Accordingly, we calculate that the electricity used for this part of the CO_2 delivery comes from the coal-fired or natural gas power plant respectively. The lifecycle greenhouse gas emission factor from a coal-fired power plant is approximately 1 kg CO_2e/kWh. Utility-wide or state-wide electricity emissions factors vary widely and will change over time. As of 2016 the direct CO_2 emissions from electricity production in Florida, the location of the Algenol facility, was 0.462 kg/kWh.[12] As of 2018, the total lifecycle greenhouse gas emissions from US power was 0.48 g CO_2e/kWh (detailed calculations are provided in the SI). For the purpose of calculation we use 0.5 kg CO_2e/kWh for the grid-provided electricity.

There is no consensus on methods for quantifying emissions for specific electric loads.[13] The electricity used at the biofuel facility could be attributed to the state-wide or utility-wide average or marginal grid lifecycle electricity, or it could be calculated from the marginal emissions on an hour-by-hour basis for a specific power system. We assume that the electricity used to provide flue gas or CO_2 is all provided by the source power plant; we assume that the rest of the electricity is provided by grid electricity. For the cases in which grid electricity is used, higher CO_2 emissions from the grid result in higher lifecycle CO_2 for the biofuel. However for the combined heat, power and CO_2 cases in which CO_2 is produced on site and sold back to the grid, higher grid emissions result in a higher CO_2 credit for these electricity sales and thus result in a net lower biofuel lifecycle CO_2 emissions.

In a review of LCA studies of natural gas, a supply chain central estimate emission of 10.6 g CO_2e/MJ HHV is reported.[14] We use this value.

Allocation between Electricity and Biofuel

In the process models involving on-site power generation, there is some electricity available to sell back to the grid. In the models of CO_2 provided by power plant flue gas, this can also be seen as a combined system of power generation and biofuel production.

In the cases of using flue gas or CO_2 from coal or natural gas power plants, these are modeled as existing, legacy power plants whose CO_2 emissions previously, before construction of the biofuel plant, were released to the atmosphere. We calculate the CO_2 from the flue gas of existing power plants as being taken from the atmosphere.

For the cases of on-site fuel combustion, for both the natural gas and biomass combined heat, power and CO_2 systems, all of the lifecycle CO_2e from these fuels is from the combined system that is producing biofuel and some electricity for export. We take a systems expansion perspective. For the purpose of comparing the benefit of these combined biofuel and power systems with the other biofuel production scenarios, we can attribute the CO_2 emissions reduction to the biofuel. That is, we consider the entire system to be one MJ of transportation fuel and the corresponding amount of electricity exported and we compare the greenhouse gas emissions of the biofuel plus electricity system with a gasoline plus grid electricity system.

Greenhouse Gas Emissions from Biomass

Growing and harvesting trees will have greenhouse gas emissions associated with site preparation, use of fertilizers, and harvesting. We model use of biomass from slash pine plantations in Florida operated on a 21-year rotation.[15]

Overall the upstream CO_2 emissions of the wood chips is 338 kg CO_2e/ton chips, of which 283 is CO_2 from biomass combustion and 55 kg/ton is from diesel and other non-biomass sources. Alternative sourcing of biomass could reduce these numbers: bringing in the biomass by water transport may reduce the costs and greenhouse gas emissions.

When the biomass is combusted it will release carbon dioxide into the atmosphere. If the biomass comes from a managed plantation, the biomass will be regrown, drawing carbon dioxide out of the atmosphere. Over the ensuing 21 years, the emitted CO_2 will all be sequestered back in to biomass. However, because the CO_2 will have been in the atmosphere for some portion of the 21 years, it cannot be considered to be net zero. We use a global warming potential approach, which weights the impact of the biogenic carbon based on its lifetime in the atmosphere compared to the emission of fossil carbon.[16] The global warming potential for 21 year biomass with no storage and with a 100 year time horizon is 0.084. The fraction of dry wood biomass that is carbon is approximately half.[17] The CO_2 emissions from combustion of the biomass is 1.83 kg CO_2 per kg dry biomass. The CO_2e emissions are 0.084 times that, or 0.15 kg CO_2e per kg biomass. Details are shown in the SI.

Ancillary Processes

Ancillary processes include all the lifecycle processes not included in the operation of the product field, the separation processes, and delivery of the CO_2. These include site preparation, emissions related to fertilizer production and use, the lifecycle of the photobioreactors, transportation of the ethanol to the point of use, and ethanol combustion in the vehicle, and are detailed in the SI. The fertilizer use and photobioreactor production values represent current process design.[4]

Results

Lifecycle Greenhouse Gas Emissions for Ethanol Under Different CO_2 Supply Scenarios

GHG emissions for the facility production system are shown in Table 2 and Figure 4, with all values reflecting the current IPCC 2013 global warming potentials in the 100-year time horizon.[18]

The lifecycle CO_2 emissions for the biofuel production process has four main components:

1. the avoided CO_2 that is pulled into the facility rather than being emitted to the atmosphere and converted either into ethanol or biomass. This is calculated based on a branching ratio of carbon to ethanol of 65.6% and does not include the CO_2 that is transported to the facility but then released from the production field as CO_2;
2. the emitted CO_2 due to the combustion of the ethanol that releases the avoided CO_2 back into the atmosphere;
3. the CO_2 emitted due to the use of electricity and natural gas to power the biofuel facility and provide the CO_2 to the facility; and
4. the emissions from the other activities associated with the production of ethanol, essentially the fertilizer requirements and photobioreactor manufacture.

	Biomass	Biomass w Refrigeration	Coal Flue Gas	NG Flue Gas	Coal Plant Gas Capture	NG CHP	NG Plant Carbon Capture	NG CHP w Refrigeration
CO_2e from Atmosphere	-162.2	-114.1	-98.6	-98.6	-98.6	0.0	-98.5	0.0
EtOH Combustion	55.9	55.9	55.9	55.9	55.9	55.9	55.9	55.9
On-site Combustion Emissions	51.2	5.4	3.9	3.9	3.9	125.3	3.9	5.4
Electricity	-17.0	-1.4	17.6	17.6	17.6	-223.7	17.6	-73.8
Electricity for CO_2 Capture and Transport	0.0	0.0	14.0	19.1	11.0	0.0	9.6	0.0
NG for CO_2 capture	0.0	0.0	0.0	0.0	10.0	0.0	14.6	0.0
CO_2 loss from PBRs	15.4	15.4	15.4	15.4	15.4	15.4	15.4	15.4
Upstream Energy Life Cycle	27.9	19.9	1.6	1.6	3.8	48.3	4.8	22.9
Ancillary	9.4	9.4	9.4	9.4	9.4	9.4	9.4	9.4
Total	-19.3	-9.5	19.2	24.3	28.3	30.6	32.5	35.1

Table 2. Lifecycle greenhouse gas emissions for production of ethanol from cyanobacteria in photobioreactors, with a range of CO_2 sources, g CO_2e/MJ.

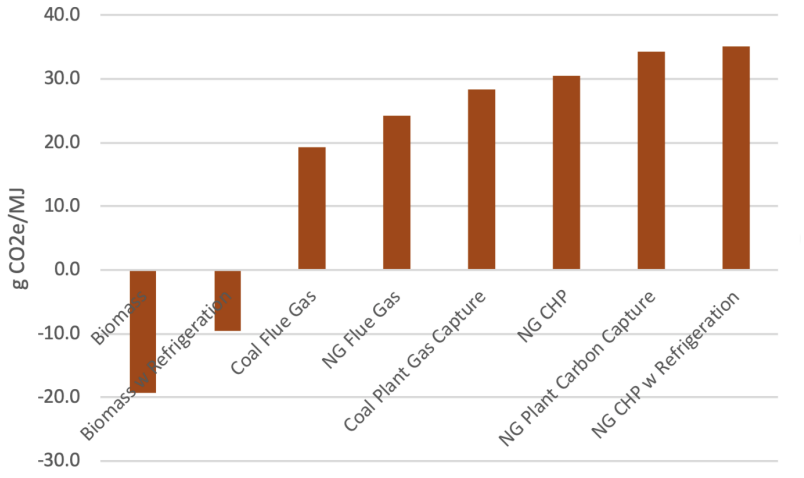

Figure 4. Greenhouse gas emissions from ethanol production for various CO_2 source options.

Sensitivity Analysis

Grid electricity emission factor

In the calculations above the greenhouse gas emissions from grid electricity are assumed to be 0.5 kg CO_2e/kWh. This electric grid emission factor is expected to decrease over time, the degree dependent on the extent to which policies to reduce greenhouse gas emissions are implemented. The scenario most sensitive to the grid electricity emissions factor is the natural gas CHP case, in which there is substantial export of electricity from the power plant. In a scenario with a 0.4 kg CO_2e/kWh emission factor for grid electricity, the natural gas CHP case and the natural gas CHP with refrigeration case would have ethanal emissions of 75 and 50 g CO_2e/MJ of ethanol, respectively, as shown in the SI. That is, the natural gas CHP scenarios become unattractive for ethanol production with the lower grid electricity emission factor. The other CO_2 sourcing options are less affected by grid electricity values: the biomass scenarios become less negative, yet remain negative. The scenarios that capture CO_2 from coal or natural gas power plants benefit from lower grid electricity emissions because these scenarios use grid electricity.

In calculating the lifecycle greenhouse gas emissions for delivery of coal flue gas or CO_2 captured from a coal power plant, we used a greenhouse gas emission factor for the coal plant for the electricity needed to capture and transport the CO_2, but we used a grid average emission factor, 0.5 kg CO_2e/kWh for the grid power used at the biofuel facility. If instead the coal power plant emission factor of 0.99 kg CO_2e/kWh were used for all the electricity, the lifecycle emissions for the scenarios with CO_2 from coal plants would rise from the baseline values of 19 and 28 g CO_2e/MJ for the flue gas and concentration CO_2 cases to 36 and 46 g CO_2e/MJ, respectively.

Productivity

In the baseline model, the facility is assumed to produce 73,000 liters/ha-year (7800 gal/acre-year). If the facility were only producing 56,000 liters/ha-year, as in the previous study, more of the incoming CO_2 would end up disposed in the biomass.[5] The fall in productivity would actually reduce the lifecycle greenhouse gas emissions of the ethanol produced by the system, see in SI Figure S5, because more carbon – nearly half of the incoming carbon - would be stored in waste biomass per MJ of ethanol produced. This would, however, also increase the cost of ethanol production.

Discussion

In the United States, the lifecycle greenhouse gas emissions of biofuels must be substantially less than that of the corresponding petroleum fuel to meet the requirements of the renewable fuel standard. The U.S. EPA uses year 2005 gasoline as its baseline for comparison, with life cycle greenhouse gas emissions of 91.3 g CO_2e/MJ gasoline.

The onsite generation of carbon dioxide, electricity and heat is advantageous for biofuel production. If the biofuel facility is not generating its own CO_2, then it must be located near a fossil fuel power plant, substantially reducing location flexibility. Moreover, if the CO_2 is sourced from a local power plant, then the biofuel facility is subject to the economic dispatch decisions of the power plant. As power requirements change throughout the day, generating units are turned on and off. As fuel prices change with time, the hours per year a particular unit operates will change. Also, all power plants require upgrades and maintenance. The operation of a biofuel facility that sources its CO_2 from a fossil fuel power plant would be totally dependent on the

power plant's operation, with the only backup being expensive industrial CO_2 delivered to the site.

The lowest lifecycle greenhouse gas emissions from this process can be achieved by using biomass as the source of CO_2, heat and electricity. Both on-site biomass scenarios have negative lifecycle greenhouse gas emissions. The coal flue gas case is the next-lowest emission scenario, with a total of 19 g CO_2e/MJ. There are substantial advantages in using the flue gas from a coal-fired power plant: rather than being emitted to the atmosphere, the carbon dioxide is utilized for biofuel production. If the biofuel facility can be located within about 2 miles, as assumed for these calculations, the energy and emissions from transporting the CO_2 is low enough, even using electricity from a coal plant, that the resulting ethanol has a greenhouse gas footprint substantially lower than gasoline. However, there are few coal plants in the US with sufficient nearby space to site a biofuel facility, and the low price of natural gas is leading to coal plant retirements. The natural gas flue gas case is also a relatively low-emitting option; however, the concentration of CO_2 in the natural gas flue gas is too low to support the cyanobacteria requirements; this is not a feasible case for the biofuel technology considered here although it may be an option for other algal biorefinery technologies. The natural gas carbon capture case does provide sufficiently concentrated CO_2, but at the expense of greater energy use and consequently a higher CO_2 footprint, approximately 33 g CO_2e/MJ.

The scenarios with on-site production of heat, power and CO_2, either from biomass or from natural gas, have benefits beyond the production of low carbon biofuel. The electricity produced by these facilities can provide low-carbon baseload power to the grid, and the carbon dioxide is utilized to make biofuel. Natural gas combined cycle power plants continue to be constructed; the joint production of biofuel with electricity may be an attractive model for biofuel production.

The production of electricity from biomass is an option for low carbon baseload power.[11] While biomass, considered in isolation as a carbon source for algal biofuel production, can appear to be an expensive option, in the broader context of on-going development of biomass electricity power plants, colocation of bioelectricity and algal biofuel production can be both economically attractive compared to biopower alone, and provide biofuel and carbon benefits.

Associated Content

Supporting Information: Tables S1-S13, Figure S1-S6, and text.

Acknowledgement

This material is based on work supported by the US Department of Energy Bioenergy Technologies Office Advanced Algal Systems Program (DE-FOA-0001471) award DE-EE0007690. This report was prepared as an account of work sponsored by an agency of the United States Government. Neither the United States Government nor any agency thereof, nor any of their employees, makes any warranty, express or implied, or assumes any legal liability or responsibility for the accuracy, completeness, or usefulness of any information, apparatus, product, or process disclosed, or represents that its use would not infringe privately owned rights. Reference herein to any specific commercial product, process, or service by trade name, trademark, manufacturer, or otherwise does not necessarily constitute or imply its endorsement, recommendation, or favoring by the United States Government or any agency thereof. The views and opinions of authors expressed herein do not necessarily state or reflect those of the United States Government or any agency thereof.

References

(1) Quinn J. C. and Davis, R.. The potentials and challenges of algae based biofuels: A review of the techno-economic, life cycle, and resource assessment modeling. *Bioresource Technology* **2015**, *18*, 444-452.

(2) Sills D. L.; Paramita V.; Franke M. J.; Johnson M. C.; Akabas, T. M.; Greene, C. H.; Tester J. W. Quantitative Uncertainty Analysis of Life Cycle Assessment for Algal Biofuel Production. *Envir. Sci. Technol*. **2013**, *47*, 687-694.

(3) Vasudevan, V.; Stratton R. W.; Pearlson, M. N.; Jersey G. R.; Beyene, A. G.; Weissman, J. C.; Rubino, M.; Hileman, J. I. Environmental Performance of Algal Biofuel Technology Options *Envir. Sci. Technol*. **2012**, 46, 2451−2459

(4) Legere, Ed, 2017. "Integrated Pilot-Scale Biorefinery for Producing Ethanol from Hybrid Algae", Award Number DE-EE0002867, (May 26). Public Version Final Report: https://www.osti.gov/servlets/purl/1360777

(5) Luo, D.; Hu, Z.; Choi, D. G.; Thomas, V. M.; Realff, M. J.; Chance, R. R. Lifecycle Energy and Greenhouse Gas Emissions for an Ethanol Production Process Based on Blue-green Algae, *Environmental Science and Technology* **2010**, *44*(22), 8670-8677. http://dx.doi.org/10.1021/es1007577

(6) Lively, R. P.; Sharma, P.; Luo, D.; McCool, B. A.; Beaudry-Losique, J.; Thomas, V. M.; Realff, M.; Chance, R. R. Anthropogenic CO_2 as a Feedstock for the Production of Algal-based Biofuels. *Biofuels Bioproducts & Biorefining* **2015,** *9*(1), 72-81. http://dx.doi.org/10.1002/bbb.1505

(7) Gutiérrez-Arriaga C. G.; Serna-Gonzalez M.; Once-Ortega J. M., El-Halwagi M. M. Sustainable Integration of Algal Biodiesel Production with Steam Electric Power Plants for Greenhouse Gas Mitigation. *ACS Sustainable Chem.& Eng*. **2014**, *2* (6), 1388-1403.

(8) Somers M. D.; Quinn J. C. Sustainability of carbon delivery to an algal biorefinery: A techno-economic and life-cycle assessment. *J. CO_2 Utilization* **2019**, *30*, 193-204.

(9) Moll, B. et al. 2016. Vapor Compression Steam Stripping. U.S. Patent 9.272,229 B2

(10) Vane, L. M.; Alvarez, F. R.; Huang, Y.; Baker, R. W. Experimental validation of hybrid distillation-vapor permeation process for energy efficient ethanol-water separation. *J. Chem. Technol. Biotechnol*. **2010**, *85* (4), 502–511.

(11) Brown, M. A.; Favero A.; Thomas V. M.; Banboukian A. The Economic and Environmental Performance of Biomass as an Intermediate Resource for Power Production. *Utilities Policy* **2019**, *58*, 52-62. https://doi.org/10.1016/j.jup.2019.04.002

(12) EIA (Energy Information Administration), 2018. Florida Electricity Profile 2016. US Department of Energy. https://www.eia.gov/electricity/state/florida/

(13) Ryan, N. A.; Johnson J. X.; Keoleian G. A. Comparative Assessment of Models and Methods to Calculate Grid Electricity Emissions. *Envir. Sci. Technol.* **2016**, *50* (17), 8937-8953.

(14) Balcombe, Paul, Kris Anderson, Jamie Speirs, Nigel Brandon, and Adam Hawkes.. "The Natural Gas Supply Chain: The Importance of Methane and Carbon Dioxide Emissions."

Sustainable Chemistry and Engineering **2017**, *5*, 3-20.
https://doi.org/10.1021/acssuschemeng.6b00144

(15) Dwivedi P.; Bailis R.; Bush T. G.; Marinescu M. Quantifying GWI of Wood Pellet Production in the Southern United States and Its Subsequent Utilization for Electricity Production in The Netherlands/Florida. *Bioenerg. Res.* **2011**, *4*, 180-192. doi:10.1088/1748-9326/9/2/024009.

(16) Guest G., Cherubini F., Stromman A. H.. Global Warming Potential of Carbon Dioxide Emissions from Biomass Stored in the Anthroposphere and Used for Bioenergy at the End of Life. *J. Indust. Ecol*. **2013**, *17* (1), 20-30. DOI: 10.1111/j.1530-9290.2012.00507.x

(17) FAO 2005. Knowledge Reference for National Forest Assessments. 5. Carbon Content Estimation. http://www.fao.org/forestry/17111/en/

(18) IPCC (2013). Climate Change 2013: The Physical Science Basis. Working Group I Contribution to the Fifth Assessment Report of the Intergovernmental Panel on Climate Change. Chapter 8: Anthropogenic and Natural Radiative Forcing

Appendix 2: Reports from Partner Organizations

2.A. Outdoor pond experiments performed at the Arizona Center for Algae Technology and Innovation (AzCATI) at Arizona State University

Introduction and Experimental Setup:

From June 6, 2019 through September 29th, 2019, ASU-AzCATI conducted two cultivation experiments for Algenol. The first experiment conducted from June 6th through August 20, 2019 utilized the Algenol supplied ABI strain and was run in modified f/2 media as shown in Table 1 (recipe supplied by Algenol). Other key operational parameters were as follows:

- Pond type: 5.6 m^2 surface area, on the ground
- Pond depth/volume: 20 cm/900 L
- Paddlewheel speed 20 hz (~7.5 RPM)
- Sparger type: 4" ceramic (Sweetwater)
- CO_2 flow rate (when dosing): 2 ml/min
- pH control/setpoint: 7.2 (7.3/7.1 upper/lower control limits)
- Operational strategy: Semi-continuous with up to 3x/week harvests and reset. Target harvest volume % of 50-75% depending on growth and frequency of harvest. No medium recycle.

Table 1. Media formulation for ABI cultivation trials at AzCATI.

STOCK Solution	Mass of Primary Stock g/L	Vol. Primary Stock for 1 L Secondary Stock	Volume for 1x Final Media
Sodium Nitrate			0.42 g/L
PHOSPHATE STOCK			
Potassium Phosphate Dibasic	87.1	250 mL/L	2 mL/L
Na2EDTA	2		
TRACE METALS			
Citric Acid	12		
Ferric Ammonium Citrate	12		
Manganese Chloride Tetrahydrate	3.62	250 mL/L	2 mL/L
Zinc Sulphate Heptahydrate	0.444		
Sodium Molybdate Dihydrate	0.78		
Copper Sulphate Pentahydrate	0.158		
Cobalt Nitrate Hexahydrate	0.0988		
Crystal SeaSalt			33 g/L

From August 6 through September 29th, 2019, the second experiment utilized the publicly available *Arhrospira platensis* (UTEX1926). The media for UTEX1926 is shown in Table 2 ("Z-media"). Other key operational parameters for the UTEX1926 cultivation trials were as follows:

- Pond type: 5.6 m^2 surface area, on the ground, hypalon liner

- Pond depth/volume: 20 cm/900 L
- Paddlewheel speed 20 hz (~7.5 RPM)
- Sparger type: 4" ceramic (Sweetwater)
- CO_2 flow rate (when dosing): 2 ml/min
- pH control/setpoint: 9.9 (9.95/9.85 upper/lower control limits)
- Operational strategy: Semi-continuous with 1-2x/week harvests and reset. Target harvest volume % of 50-75% depending on growth and frequency of harvest. No medium recycle.

Table 2. Media formulation for UTEX cultivation trials at AzCATI.

Z-Media

	Chemical Name	Chemical Formula	Amount (g)
1	Sodium Bicarbonate	$NaHCO_3$	16.8
2	Potassium Phosphate Monobasic	KH_2PO_4	0.5
3	Sodium Nitrate	$NaNO_3$	2.5
4	Potassium Sulfate	K_2SO_4	1
5	Sodium Chloride	NaCl	1
6	Magnesium Sulfate	$MgSO_4$	0.2
7	Sodium EDTA	NaEDTA	0.08
8	Calcium Chloride	$CaCl_2$	0.04
9	Iron Chloride	FeCl	0.01
10	BG-11 Trace Metals #6		1 mL
	Dissolve in 900 mL DI water. Filter Sterilize		

Parameters/metrics to be collected for all pond runs included:

- Daily pond measurements for pH, temperature and depth (morning and afternoon)
- Daily (M-F) 3x50 ml grab samples for OD750/680, AFDW, nutrients (N and P)
- At harvest/reset: Bulk sample (1-2 L) spun down biomass for proximate analysis. Note – no biomass compositional analysis performed as part of this project, but samples are preserved and stored (frozen as paste or freeze dried)
- Minimum 1x/week microscopy observation

Strain scale up (both strains):

AB1 was received from Algenol as liquid culture (100 ml) and subsequently split into 3x 100 ml shake flasks at 50 ml in fresh media. Throughout the project AzCATI maintained the ABI strain on plates on in liquid flask culture. UTEX1926 was maintained on Z-media agar plates and brought into liquid culture in a 100 ml shake flask at 50 ml volume in Z-media. Strain scale up for both strains followed the same pathway as shown in Figure 1. 50 ml of shake flask culture into 800 ml bubble column (16:1 dilution). From 800 ml bubble columns, culture is scaled into 15 L airlift flat panels (1.5" light path). Bubble columns and 15 L flat panels are cultivated indoors on cool white fluorescent bulbs at ~ 150 µmol photons/m^2-s light intensity. UTEX1926 was cultivated at constant 24 h light and ~29-30 ^oC culture temperature in z-Media and pH of 9-10 (no CO_2 supplementation) and air flow rate of ~ 5 ml/min. ABI was cultivated in modified f/2 media under

12/12 light dark cycle at ~29-30 °C culture temperature with a 2% v/v CO2/Air at ~5 ml/min. 1-2x15 L FP-PBR from indoor cultivation were then used to inoculate 1-2 110 L FP PBRS in the greenhouse (GH). Temperatures were maintained so as not to exceed a peak afternoon culture temperature of 35 °C using a stainless-steel heat exchangers placed in the FP-PBRs and an external evaporative cooling system loop. pH was monitored in the GH but is open loop (constant CO2 flow at 2% CO_2/air). CO2 was only used for UTEX1926 if pH values exceeded 10.5. pH for ABI was typically 6.9/7.5 under the open-loop conditions in the GH. Typical strain morphology/seed quality out of the GH is shown in Figure 2.

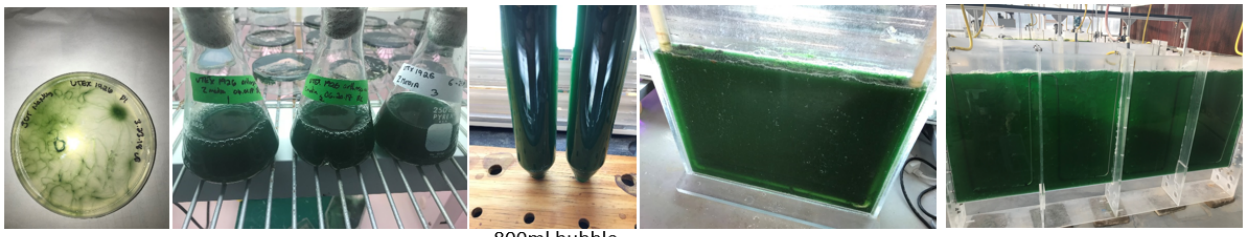

Figure 1: Seed train scale up for ABI and UTEX1926 at AzCATI. Greenhouse (GH) cultivation in the 100 L FP-PBR was on natural diurnal lighting in a temperature-controlled greenhouse.

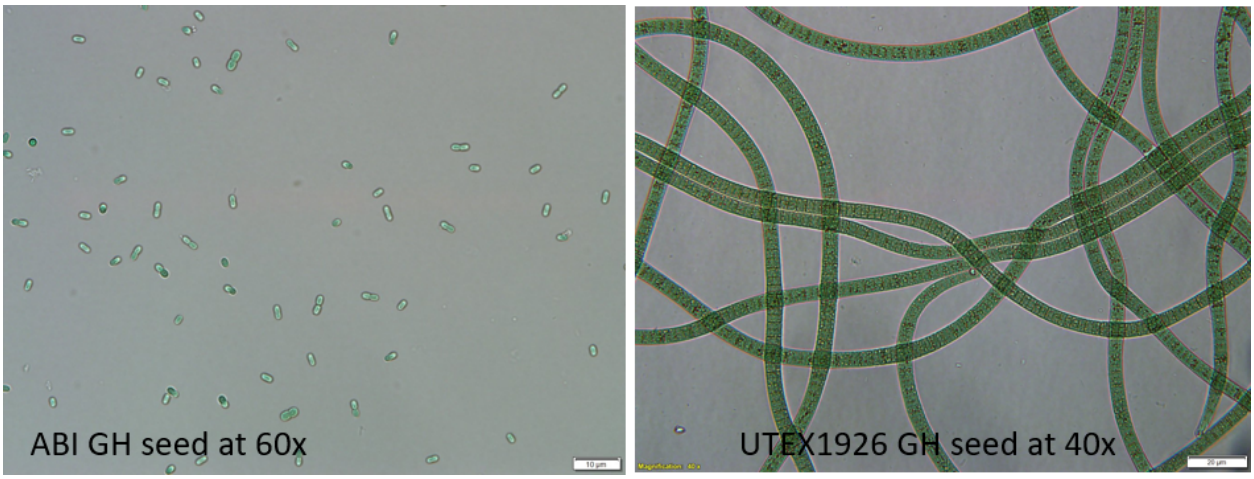

Figure 2: Typical optical micrographs for seed cultures in GH panels for ABI (left image) and UTEX1926 (right image) prior to going outdoors.

One 110 L GH panel was used to seed 1x5.6 m2 pond at 20 cm/900 L (9:1 dilution). Target starting density for AB1 and UTEX1926 was ~0.05-0.1 g/L. A single pond would then be used to inoculate an additional two ponds for a total of three ponds as biological replicates. The ponds utilized in this experiment are shown in Figure 3. pH monitoring and control and temperature monitoring was done with a Neptune APEX controller and Neptune pH/ORP and temperature probes. Weather data was provided by a weather station (HOBO RX3000 Weather Station) with collection of Air Temperature, Solar insulation and PAR, relative humidity, wind speed and direction, and precipitation.

Figure 4 shows as an example, the starting conditions of the miniponds and the qualitative progression in culture density for the ABI cultivation trial. Figure 5 shows the weather data (air temp and RH and PAR) for the ABI cultivation trail along with pond pH and pond water

temperature. There was one significant rain event at the end of July but otherwise a fairly typical summer for Mesa, AZ. Figure 5 shows the weather data for the duration of the UTEX1926 run

Figure 3: 5.6 m^2 ponds at AzCATI

early August through late September. Morning and afternoon water temperatures throughout the ABI cultivation trial were 20-25 °C and 32-36 °C, respectively. Similarly, for the UTEX1926, 20-25 °C for morning temperatures and 30-35 °C for peak afternoon temperatures in August and then dropping to below 30 °C in September for peak afternoon temperatures.

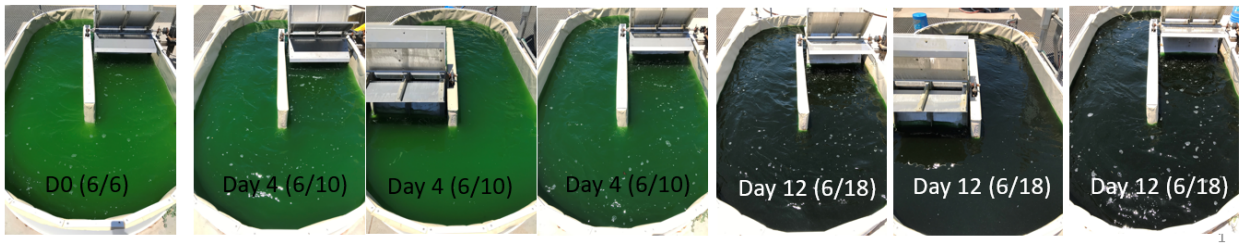

Figure 4: Pond progression for initial start up of ABI cultivation trial in 5.6 m2, 900 L outdoor miniponds.

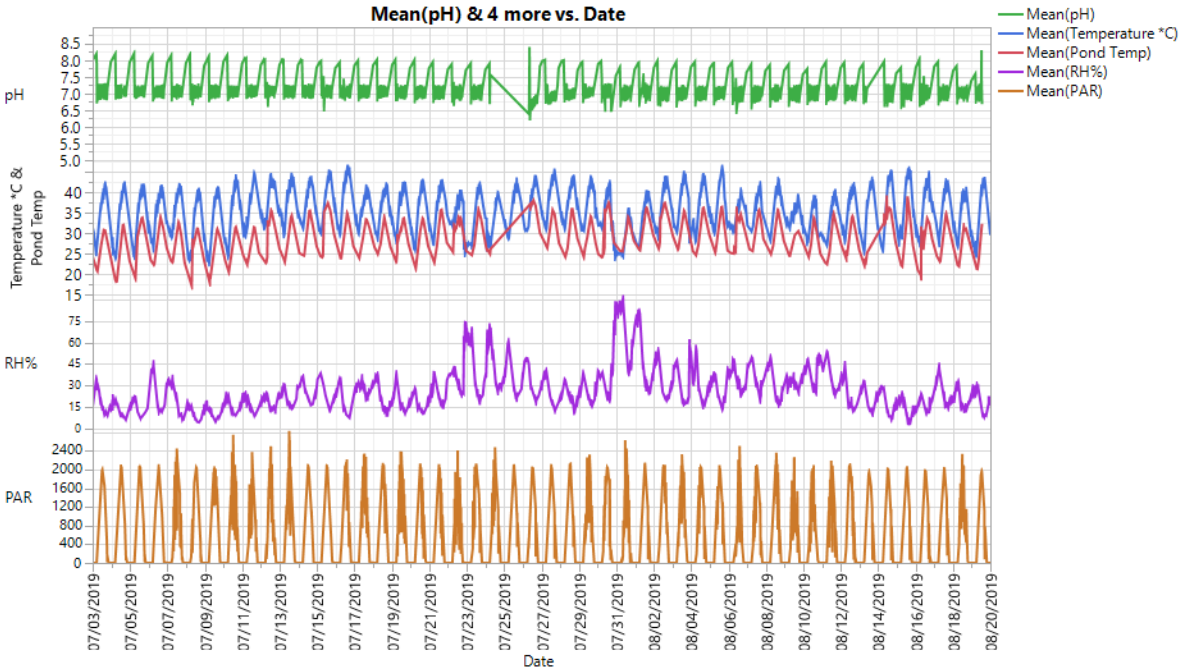

Figure 5: Weather and pond parameters for the second half of the AB1 cultivation trial.

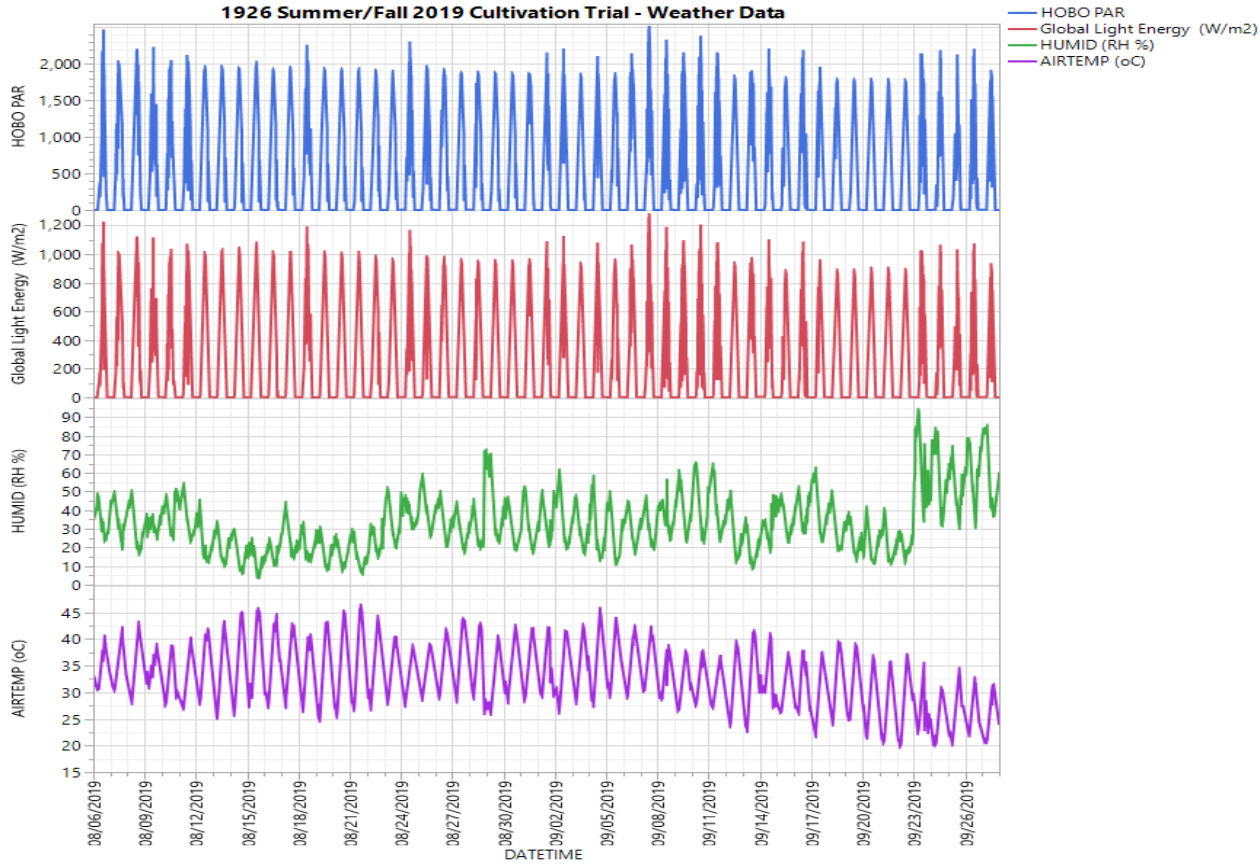

Figure 6: Weather data for the UTEX1926 cultivation trial.

Cultures were run under N-replete conditions. Nitrate and Phosphate data was measured on a Lachet Quickchem 8500 nutrient analyzer. Values reported are for N (measured as NO3) and P (measured as PO4) in mg/L (ppm) of N and P, respectively. N and P data is shown in Figures 7 and 8 for AB1 and UTEX1926, respectively.

AFDW data was measured and productivity was calculated in two ways, 1) [concentration at harvest (g/L) X volume harvested (L)] divided by [area of pond (m2) X days of cultivation between harvests (days) represented as "AHYP-H2H" in g/m^2-d (Average Harvest Yield Productivity, Harvest to Harvest), and 2) the Average Slope Productivity (ASP) from each AFDW point to AFDW (except on after reset) is also calculated. The later, ASP represents the "instantaneous" productivity on a day to day basis. Finally for the UTEX1926 we also calculated the overall slope productivity by linear line fit of the AFDW data between harvest points.
AFDW and productivity data for the UTEX1926 cultivation trial is shown in Figure 9. The run consisted of 8 grow periods starting with a single pond inoculated on 8/6/2019 at a starting depth of 15 cm and then volume up to 20 cm after a couple days. This pond was reset and used to inoculate two additional ponds but due to a mechanical drain issue the new ponds were lost as they slowly leaked overnight. The original pond was reset again to start one additional pond on 8/16 and then a third pond on 8/20/2019 all running at 20 cm. AS shown in Figure 9, concentrations at harvest ranged from a low of 0.3 g/L to a max of 0.7 g/L. Peak ASP productivities observed were in excess of 25 g/m^2-d but on average closer to 10-12 g/m^2-d for most of the run showing signs of decline in later September. The overall average productivity across the run was 8.9 g/m^2-d based on the harvest yields. However, the average slope productivities for the entire run were 10.1 g/m^2-d. The difference between harvest yields and the slope productivity indicates a lack of optimization in harvest frequency/dilution rate and we were essentially "leaving some productivity "on the table". However, no optimization of growth rate through manipulation of dilution rate/harvest frequency was attempted during this cultivation trial as it simply represented the establishment of a baseline benchmark. A summary of the slope productivities and those calculated based on actual volume harvested are shown in Table 3 for comparison.

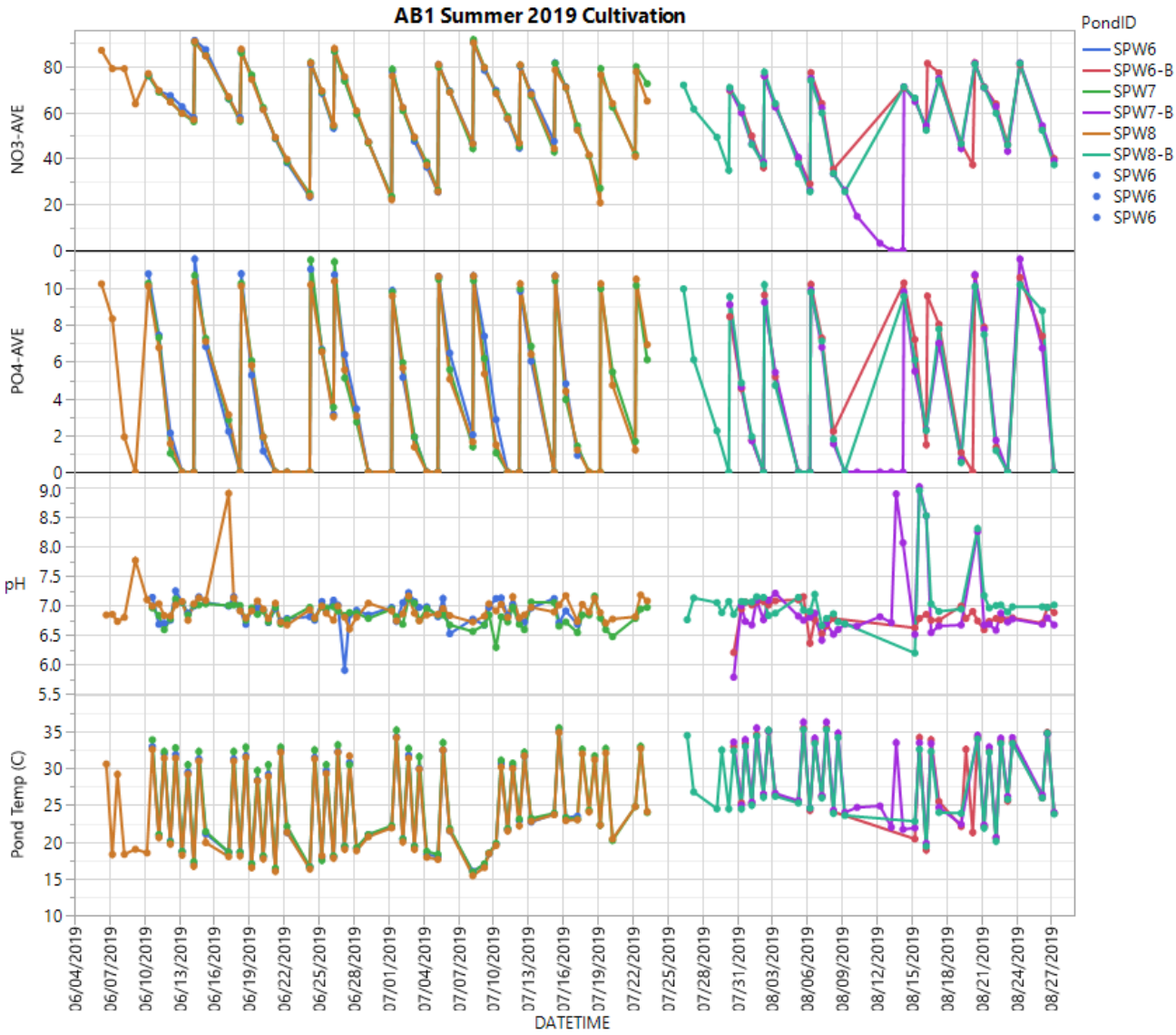

Figure 7: ABI pond cultivation trends for nutrients (NO3-N mg/L, PO4-P mg/L), pond pH and water temperature from AM/PM manual checks with handheld pH and temperature probes.

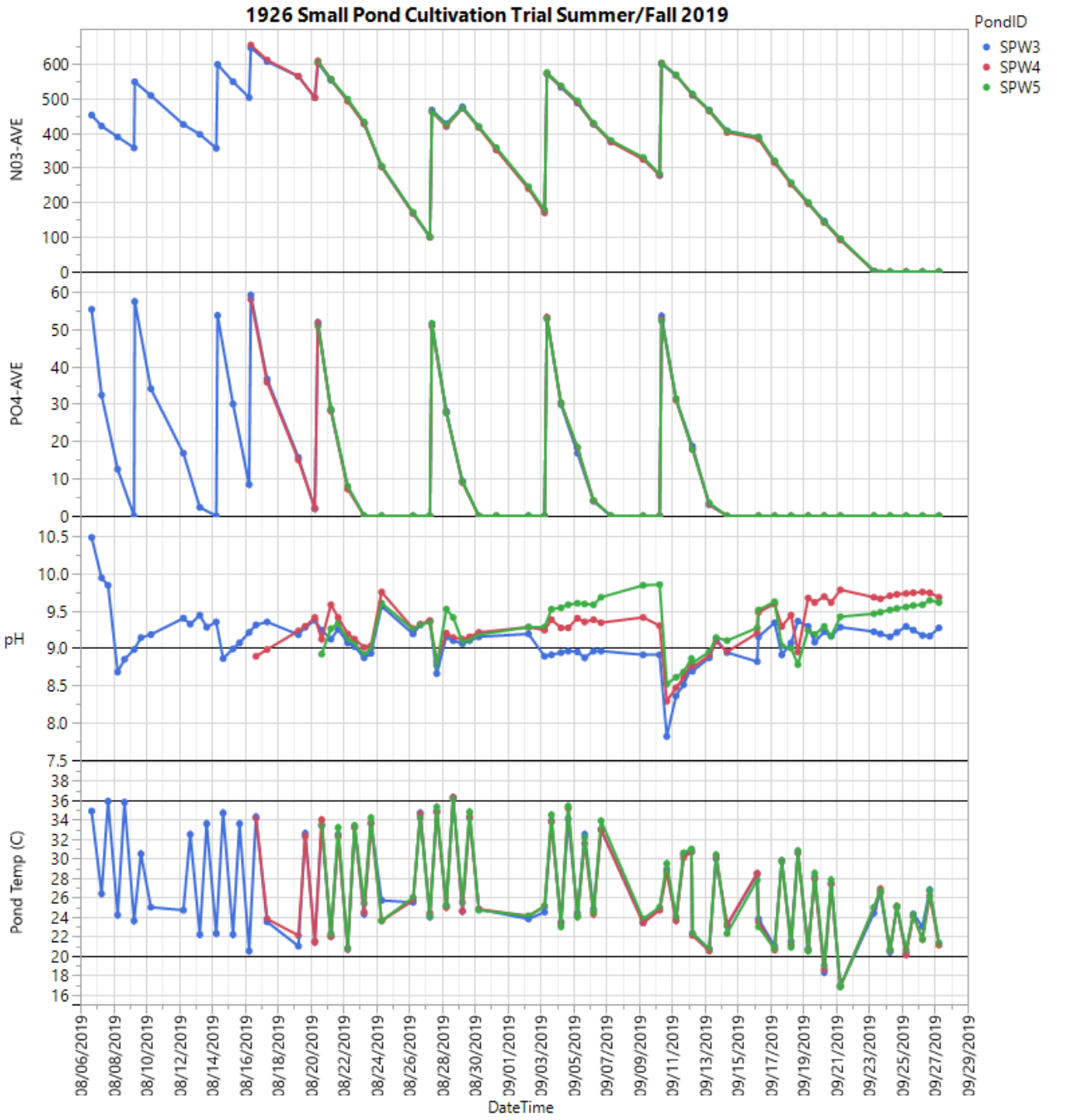

Figure 8: UTEX1926I pond cultivation trends for nutrients (NO3-N mg/L, PO_4-P mg/L), pond pH and water temperature from AM/PM manual checks with handheld pH and temperature probes.

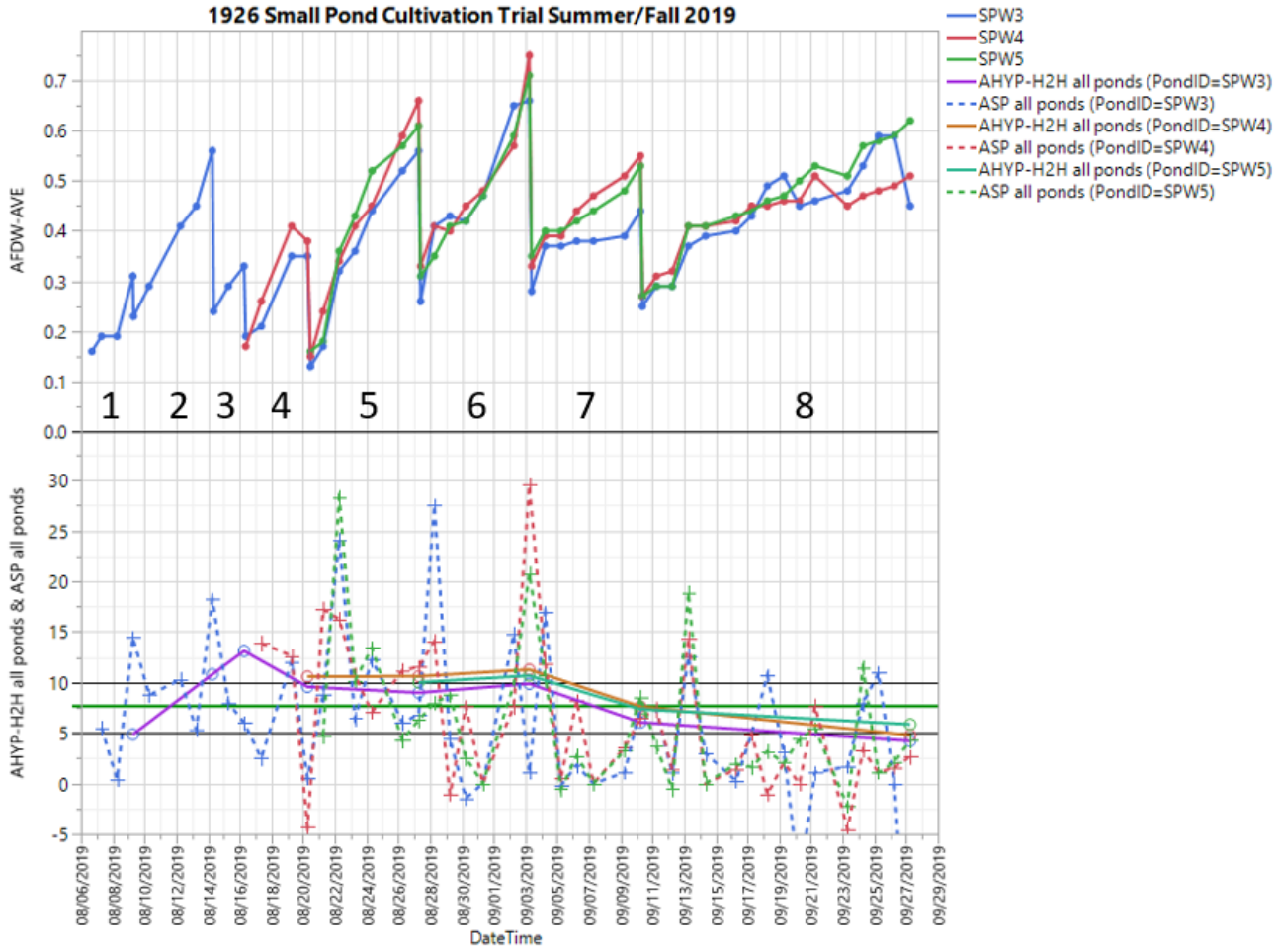

Figure 9: UTEX1926 AFDW (g/L) and calculated productivity (AHYP-H2H and ASP). Peak ASP productivities observed were in excess of 25 g/m^2-d but on average closer to 10-12 g/m^2-d for the most of the run.

Table 3. Slope and AHYP-H2H productivity summary for UTEX393 Cultivation trial. G1-G8 indicate the grow out periods as indicated in Figure 9.

Growout Period	Slope Prod. g/L-day	Slope Prod. g/m2-day	Days between reset	% Harvest	Avg. AHYP-H2H g/m2-day	Stdev AHYP-H2H
G1	0.053	11.36	2.6	33.3	4.9	
G2	0.055	11.79	5.0	60.0	10.8	
G3	0.048	10.29	2.0	50.0	13.1	
G4	0.053	11.36	4.0	67.5	10.1	0.71
G5	0.068	14.57	7.1	70.0	9.9	0.81
G6	0.053	11.36	7.0	65.0	10.6	0.70
G7	0.03	6.43	7.0	60.0	7.0	0.83
G8	0.016	3.49	17.0	100.0	5.0	0.83
Average	**0.047**	**10.1**			**8.9**	

The productivities observed for UTEX1926 under these environmental and nutrient/media conditions are in line with what we would expect for this strain. Spirulina in general is not a fast grower and we were not expecting to see more than low double-digit growth rates. Culture stability, as expected, was very good for UTEX393 operating at high alkalinity and high pH. No grazers or other harmful contaminants were observed although we did see a progression to shorter and shorter filament lengths as the culture progressed over time (Figure 10). This is a typical observation for this strain when cultivated outdoors.

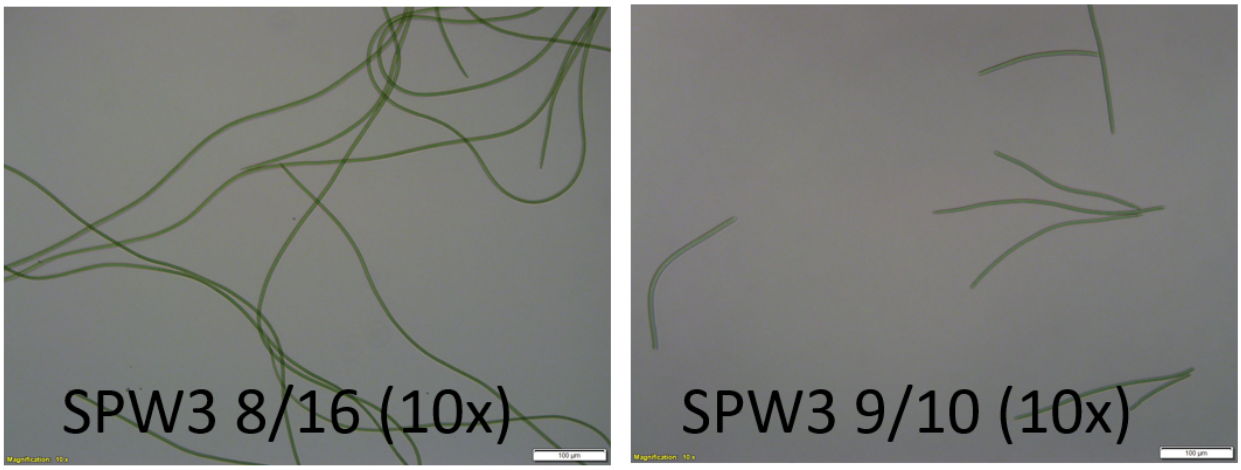

Figure 10: Optical micrographs of UTEX1926 from pond SPW3 early (left image) and late (right image) showing shortening of filament length over time.

AFDW and productivity data for the ABI cultivation trial is shown in Figure 11. The run consisted of two separate cultivation trials as ponds all crashed in mid-July and were restarted with fresh inoculum from the GH. A single pond was started on 6/6/2019 at a starting depth of 20 cm and was split on 6/10 and used to inoculate two additional ponds also at 20 cm creating three biological replicates. Ponds were reset every 4-5 days and as shown in Figure 9, concentrations at harvest ranged from a low of 0.3 g/L to a max of 0.7 g/L. Peak ASP never exceeded ~15 g/m^2-d and most averaged in the mid to upper single digits. The overall average productivity across the run was 7.0 g/m^2-d based on the harvest yields and did not change over the course of the run (Figure 12). However, the average slope productivities for the entire run were 10.1 g/m^2-d. The difference between harvest yields and the slope productivity indicates a lack of optimization in harvest frequency/dilution rate and we were essentially "leaving some productivity "on the table". However, no optimization of growth rate through manipulation of dilution rate/harvest frequency was attempted during this cultivation trial as it simply represented the establishment of a baseline benchmark. A summary of the slope productivities and those calculated based on actual volume harvested are shown in Table 3 for comparison. AB1 ponds under cultivation 6/6/2019-8/27/2019

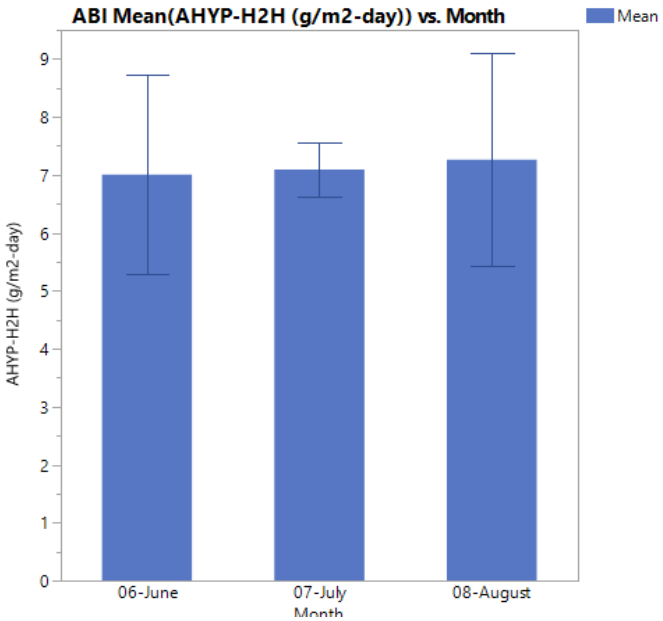

Figure 11: Average harvest yield productivity by month for ABI.

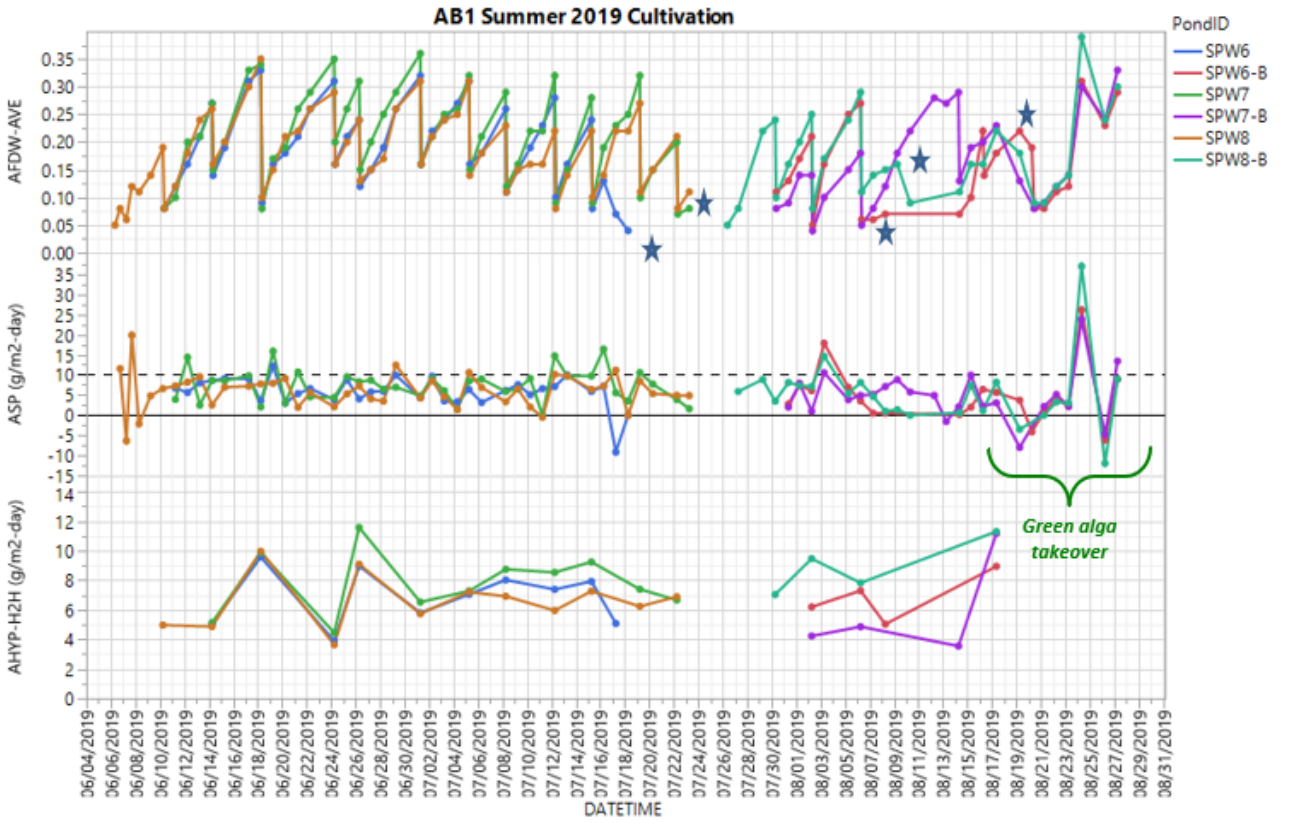

Figure 12: AFDW and productivity for the ABI cultivation trials at AzCATI. AFDW (top) in g/L and ASP and AHYP-H2H in g/m^2-d. Stars indicated where ponds crashed due to contamination. Note that after 8/18/2019, a green alga contaminant (Pichochlorum sp.) took over the ponds so productivity is not calculated post 8/18/2019 for AB1.

Culture remained healthy and relatively free of contamination through mid-July with pond SPW6 showing signs of major flocculation and settling post reset but still maintained a blue-green color. However, within a day bacterial contamination increased along with a browning of the culture. Grazers (amoeba) were also present. Ponds SPW7 and SPW8 followed a similar pattern of decline and were terminated one week later on July 22, 2019. A similar pattern of contamination (increased flocculation, then discoloration to brown) occurred again during the second cultivation trial beginning around 8/7/2019. The progression of second round of culture crash is illustrated in Figure 13 again starting in SPW6 and progressing. At the end of the cultivation run we observed a wholesale takeover by a small green alga whereby productivity returned but little or no ABI was observed under microscopic observation.

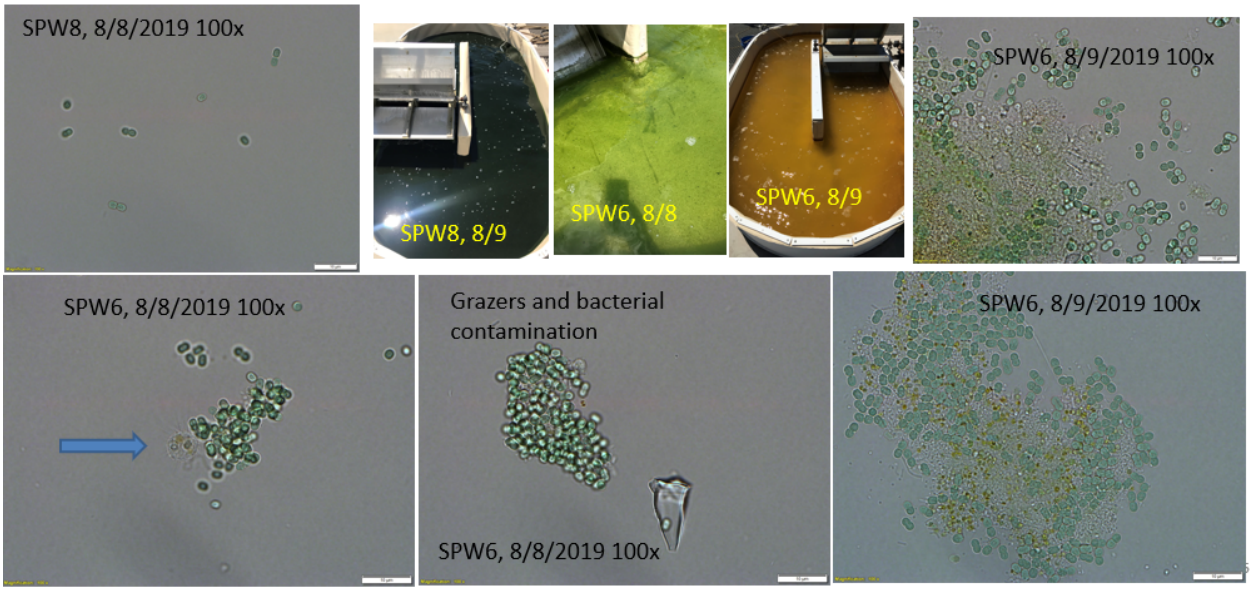

Figure 13: Progression of culture collapse with AB1 in early August 2019.

In conclusion, the UTEX1926 performed as expected for Mesa, AZ in Aug/Sept with an average productivity of ~ 9 g/m^2-d for Aug/Sept and the ABI perhaps underperformed showing only 7 g/m^2-d for June-Jul-Aug. By way of comparison to other cultivation trials being conducted on site during this time period, we observed sustained productivities for a number of cultivars in excess of 25 g/m^2-d in June/July/Aug with our benchmark summer strain UTEX393 (*Acutodesmus obliquus)* showing a sustained 30 g/m^2-d for the month of July and a summer average of 25.4 g/m^2-d for all of June/July/Aug.

2.B. Reliance Industries Report on Open Pond Cultivation and HTL R&D Activities

1

DOE ABY2 Update Meeting with Project Partners

by

Makarand Phadke
Rajaram Ghadge

Reliance Industries Ltd

November 14, 2017

2

RIL Scope in Overall DOE Program

Task	Subtask	Responsible	Timing (month)
6.0 Operation and Biomass Harvest at Scale	**6.3 Determine productivity potential and economics of AB1 in open** pond raceways 6.3.1 Operate ATP3 open pond raceway 6.3.2 Operate RIL open pond raceway 6.3.3 Analyze cultivation and productivity data 6.3.4 Develop TEA/LCA, CAPEX/OPEX for pond/PBR comparisons	ATP3/ RIL	22–36
7.0 Downstream Processing Optimization	**7.2 Evaluate HTL conversion and fractionation with advanced strain** 7.2.1 Complete base performance runs with AB1 *(begin in Phase 2)* 7.2.2 Characterize advanced HTL strain product and performance 7.2.3 Characterize RIL HTL product and performance 7.2.4 Complete HMB on unit operation and update TEA/LCA	Algenol/ RIL	12–36

3

Performance Summary of AB1

Batch No.	OD @ Inoculation	OD @ Crash	No of pond	Days of Cultivation	Mode of Crash	Crop Protection	Remarks
1	2.0	0.270	2	10	Dominated by Ciliates	-	
2	4.5	0.332	2	13	Heavy rain and Ciliates	2ppm BAC	
3	13.0	0.200	2	6	Heavy rain and Ciliates	-	
4	7.7	0.290	7	19	Dominated by ciliates and rain dilution	2ppm BAC	
5	7.3	0.584	3	9	Clumping, Bleaching of Cells and Ciliates	-	
6	10.0	0.360	5	26	Heavy rain and Domination of Ciliates	2ppm BAC	

4

Accomplishments

- We are able to scale up AB1 outdoor in 1m^2 ponds.
- To date, the strain was able to scale to maximum seven 1m^2 ponds and maximum period of cultivation was 26 days.
- Preliminary crop protection sensitivity test was carried out.
- Potential harvesting methodology tested in collaboration with up stream team and preliminary data was generated.

Flow-Cam Analysis of AB1 Cells (6th Batch)

5

- The ciliate contaminated culture of AB1 was analyzed through Flow-Cam for population dynamic study.
- In 2-5µm size filter category target algal cells of AB01 in singlet were observed.
- In 5-10µm filter category doublets target algal cells of AB01 were observed.
- In 10-20µm size filter range mostly doublets and triplets cells of AB01 were observed.
- Amongst contaminants Amoeba and Ciliates were observed in filter range of 10-35µm.

Flow-Cam Analysis of AB1 Cells (6th Batch)

6

Targeted AB01 Cells

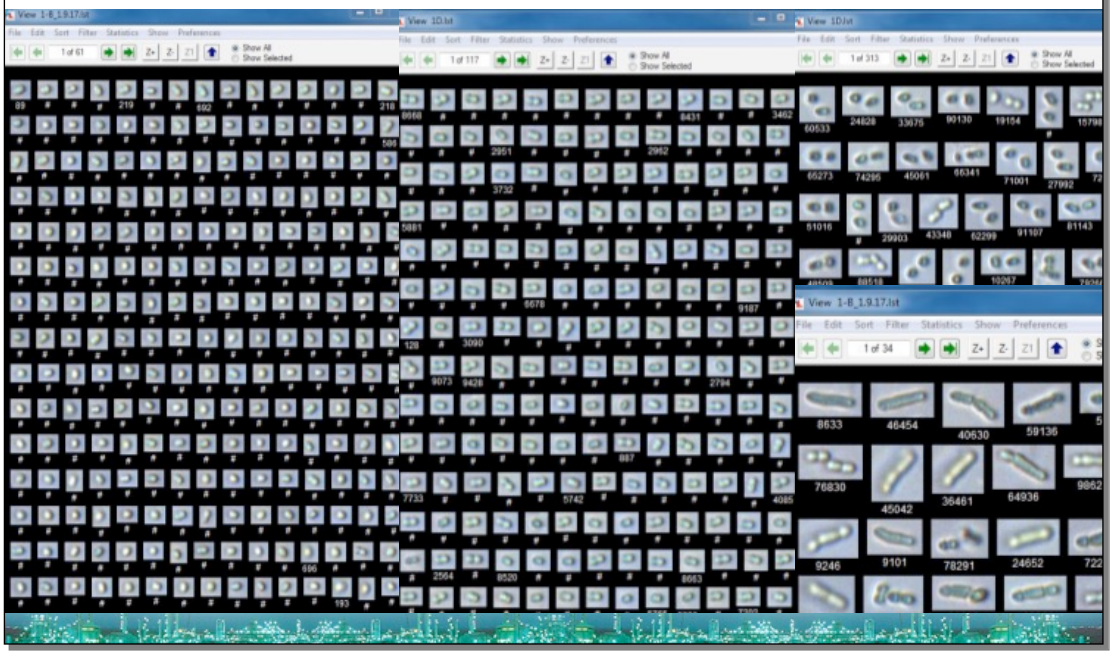

7

Flow-Cam Analysis of AB1 (6th Batch)

Contaminant – Ciliates and Amoeba

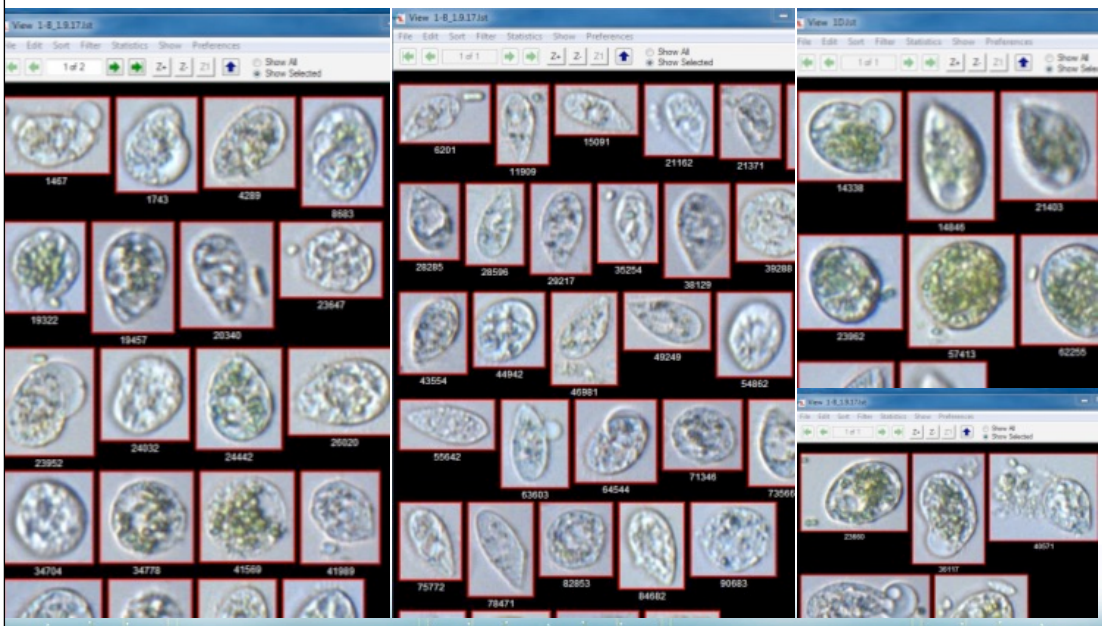

8

Harvesting Efforts for AB1

Coagulant and flocculent dosage optimization for strain AB1

		Comb-1	Comb-2	Comb-3	Comb-4	Comb-5
Strain	Unit	**AB-01**	AB-01	AB-01	AB-01	AB-01
pH adjusted to		**7**	7	7	7	7
Coagulant Dosage	ppm	**15**	20	25	25	30
Vol of Coagulant Stock Used	µL	**375**	500	625	625	1250
Flocculant Dosage	ppm	**2**	2	2	2	2
Vol of Flocculant Stock Used	µL	**500**	500	500	500	500
OD of Virgin Culture	nm	**1.188**	1.188	1.188	1.188	1.188
OD of Supernatant	nm	**0.033**	0.024	0.02	0.015	0.011
% Cell Recovery	%	**97.22**	97.98	98.32	98.74	99.07
OD to AFDCW Correlation	mg/L	**438**	438	438	438	438
AFDCW of Virgin Culture	mg/L	**520.344**	520.344	520.344	520.344	520.344
Coagulant Dosage Per unit Harvested Biomass	m/m	**0.03**	0.04	0.05	0.05	0.06
Settling Distance	cm	**3.5**	3.5	3.5	3.5	3.5
Settling Time	sec	**1800**	1800	120	1800	120
Settling Velocity	cm/s	**0.0019**	0.0019	0.0292	0.0019	0.0292
Clarity		**Fine Particles Remained**	Fine Particles Remained	Fine Particles Remained	Fine Particles Remained	Fine Particles Remained
Flock Characteristics		**Medium Density & Rice Like Flocks**	Medium Density & Rice Like Flocks	Medium Density & Rice Like Flocks	Medium Density & Rice Like Flocks	Medium Density & Rice Like Flocks

9

HTL as Platform technology: Evaluation of Algenol strain AB1

Characterization of AB1 Slurry

AB1 Slurry → Evaporation at 105 °C under vacuum → **AB1 Dry Solids**

Solids: 9.91 %
Moisture: 90.09 %

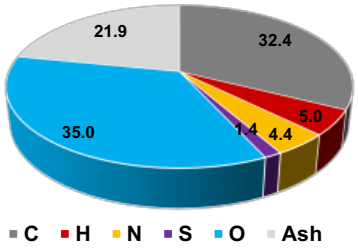

AFDW elemental distribution of AB001 (%)

C	41.47
H	6.38
N	5.58
S	1.79
O	44.78

Energy HHV
15.30 MJ/Kg

Elements in Ash (dry algae basis)

Total Ash	21.9	%
Na	98291	ppm
Mg	15542	ppm
K	9771	ppm
Ca	3683	ppm
P	1764	ppm
Fe	447	ppm
Si	262	ppm

AFDW yields of HTL products (%)

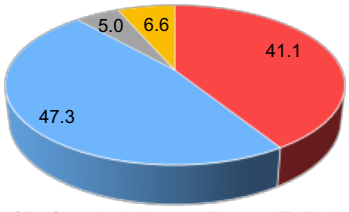

HTL conditions: Slurry, 350 Deg C, 200 bar, 30 min.

- Ash content of the slurry solids was observed to be high (21.9%) though the algae was cultivated in PBR
- HTL produced 40 wt % of the crude bio-oil under near super critical conditions

10

HTL as Platform technology: Evaluation of Algenol strain AB1

AFDW Elemental recovery in HTL products

- Around 70% of the biomass carbon is recovered in BFI
- Most of the biomass oxygen content (78%) ends up in Aqueous phase
- The HTL derived BFI possessed HHV of 33.6 MJ/Kg
- The biomass ash content ends in both HTL Aqueous and Residue products
- The gas phase mostly contained CO_2 (85% approx.)

Distribution of various elements in HTL products

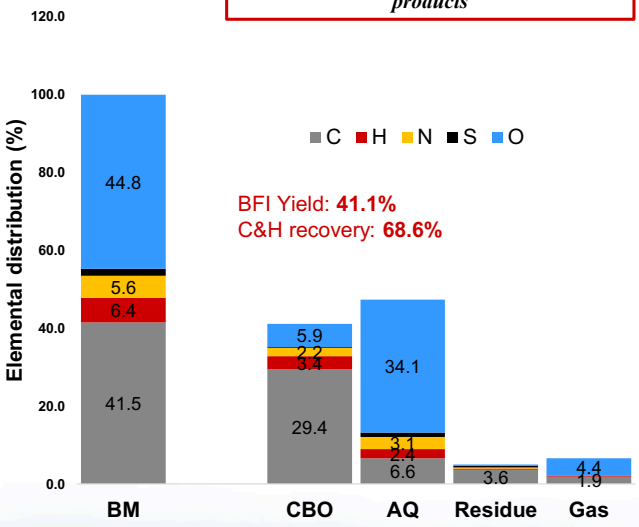

BFI Yield: **41.1%**
C&H recovery: **68.6%**

- The energy content of the HTL-derived BFI is 2.3 times higher than biomass feed. This is due to the removal of oxygen atoms from the feed during HTL.

11

HTL as Platform technology: Evaluation of Algenol strain AB1

GC-MS of Crude Bio-Oil (BFI) obtained from HTL of AB1 slurry

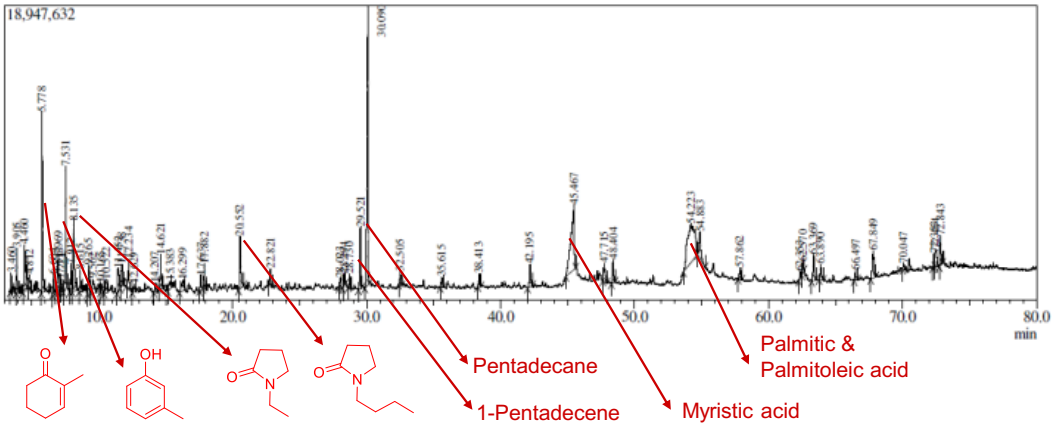

- GC-MS of CBO showed the presence of fatty acids and their decarboxylated derivatives
- 2-pyrrolidinone derivatives originated from amino acids of protein component
- Cyclic ketones and phenols are derived from carbohydrates portion of the microalgae

❖ **Nitrogenaceous heterocycles, ketones, phenols were found along with fatty acid derivatives in the HTL-derived crude bio-oil.**

12

HTL as Platform technology: Evaluation of Algenol strain AB1

GC-MS of Aqueous phase obtained from HTL of AB1 slurry

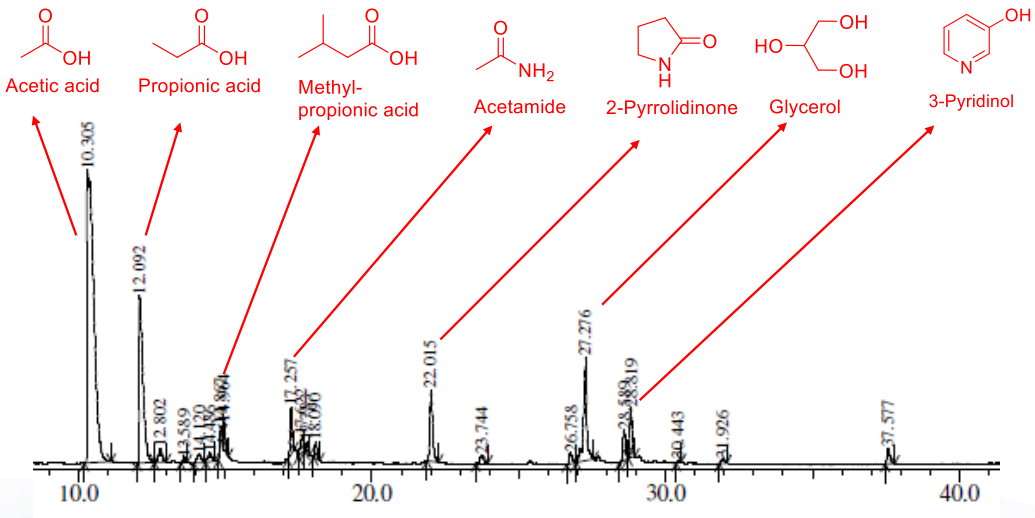

❖ **HTL aqueous phase mainly contained small organic acids, amides, glycerol and pyridinol.**
❖ **The magnitude of peak area will correspond to the relative quantity of the components.**

13

Bench-scale Unit: Commissioning of HTL

Features of Bench Scale Unit

- ✓ Capacity~30 kg/day
- ✓ Staged pumping and heating
- ✓ Reactor flexibility : CSTR/ PFR/Ebullated bed reactor
- ✓ High & Low pressure separation option

"System & process for biofuel production" Patent Application No 3641/MUM/2015

14

Continuous HTL Operation

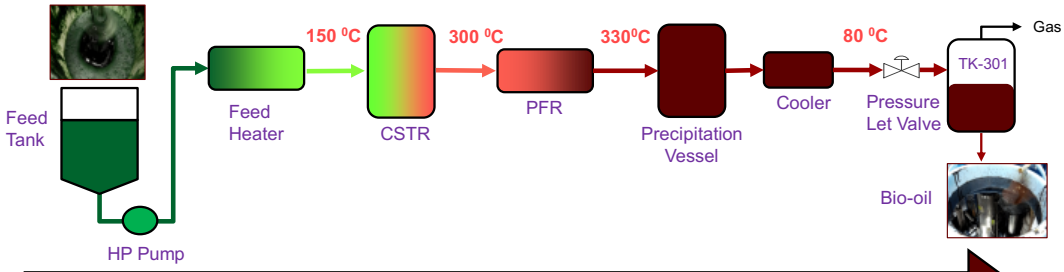

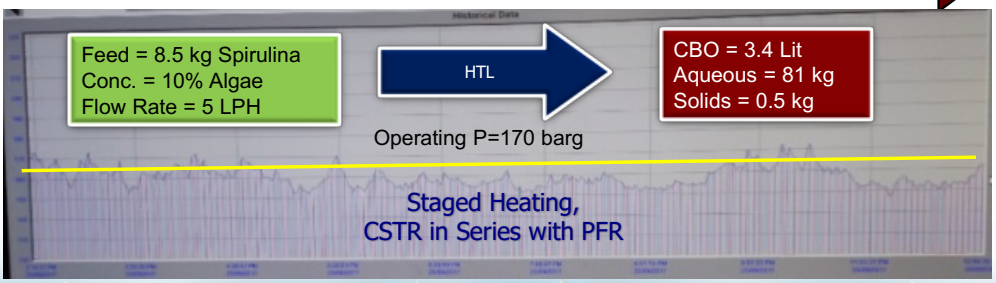

No pressure drop observed over the run of 17 hours of continuous operation

Path Forward

15

- Optimization of OD and media concentration for AB01 in open pond cultivation
  - Getting ~3 OD culture from aPBR team
  - Inoculation @ 0.5 OD in outdoor 1m^2 ponds
  - Testing different media composition
- Optimizing and validating harvesting system with upstream team
- Scale up of AB1 to 20m^2, 100m^2 and finally to 500m^2 pond
- Conducting HTL trials in bench scale HTL unit for 24 hrs continuous operation

16

ALGENOL DOE Update - RIL Contribution

by

Reliance Industries Ltd

July 09, 2018

17

HTL of AB1 in batch and bench scale with & w/o RCAT

S.no.	Deliverables	Status	Plan
1	Evaluate HTL conversion and fractionation with advanced strain	HTL conversion is done	Fractionation is in progress
1.1	Complete base performance runs with AB1	Done	
1.2	Characterize advanced HTL strain product and performance	Done	
1.3	Characterize RIL HTL product and performance	In progress	
1.4	Complete HMB on unit operation and update TEA/LCA	HMB on unit operation is done.	TEA/LCA is to be started

Bench-scale HTL Facility

18

- Bench Scale HTL unit. Capacity: 30 kg/day
- Reaction performed in CSTR (1 Lits)
- Operating parameters – 350 ºC, 200 barg
- Low pressure separation option.
- Reaction performed with & woithout catalyst.
- Experiments were also performed in batch scale reactor of 2 lit , 300 ml reactor

HTL of AB1 Block B slurry- Bench scale continuous run- Non-catalytic

19

Characterization of AB1 Slurry- Block B

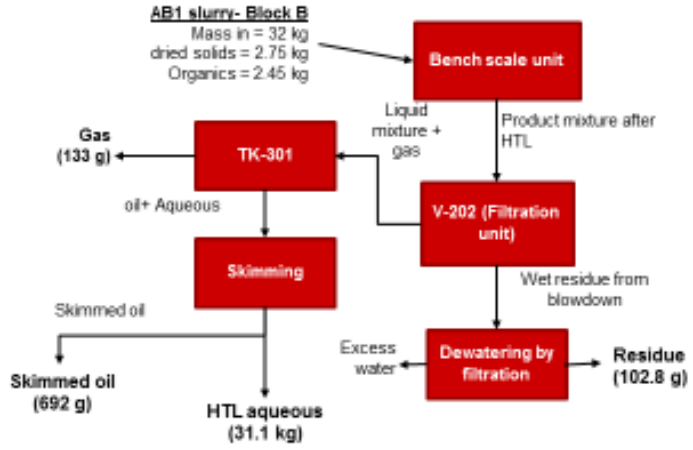

AB1 Slurry — Solids: 8.6 %, Moisture: 91.4 %, Ash (dried solids): 11 %

Evaporation at 105 ºC under vacuum

AB1 Dry Solids

AFDW elemental (%)

C	45.4
H	8.5
N	9.3
S	1.7
O	35.1

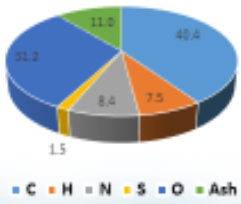

- Total of 692 g of oil was obtained with a yield of 28.2 %
- Product separation (oil/aqueous) difficulties observed in non-cat HTL

HTL of AB1 Block B slurry- Bench scale continuous run- Non-catalytic

20

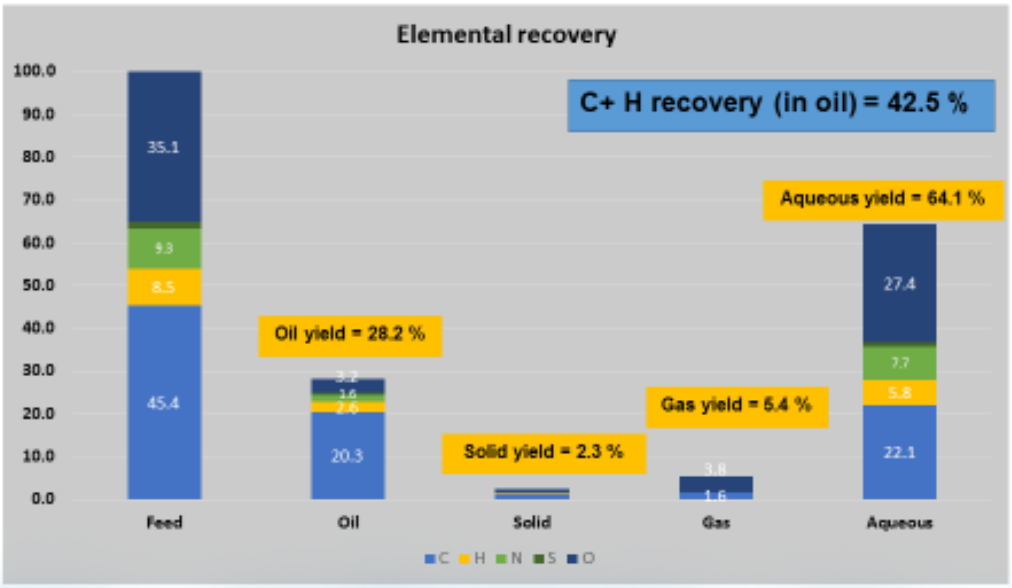

- 42.5 % of feed C+H is recovered in oil
- Significant proportion (64.2 %) of organics in feed partition into HTL aqueous

HTL of AB1 Block A slurry- Bench scale continuous run- R-Cat HTL

21

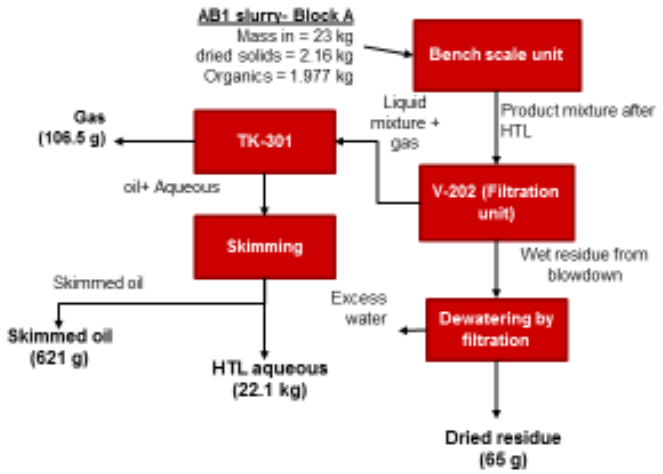

Characterization of AB1 Slurry- Block A

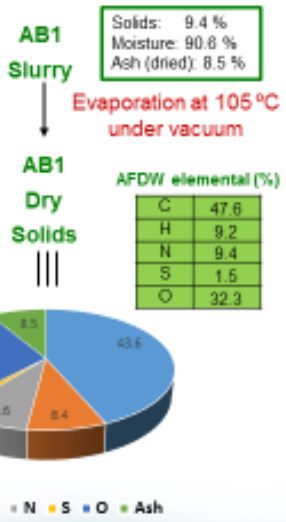

- Total of 621 g of oil was obtained with a yield of 31.4 %
- Product separation was much more easier in R-cat HTL compared to non-cat HTL

HTL of AB1 Block B slurry- Bench scale continuous run- R-cat HTL

22

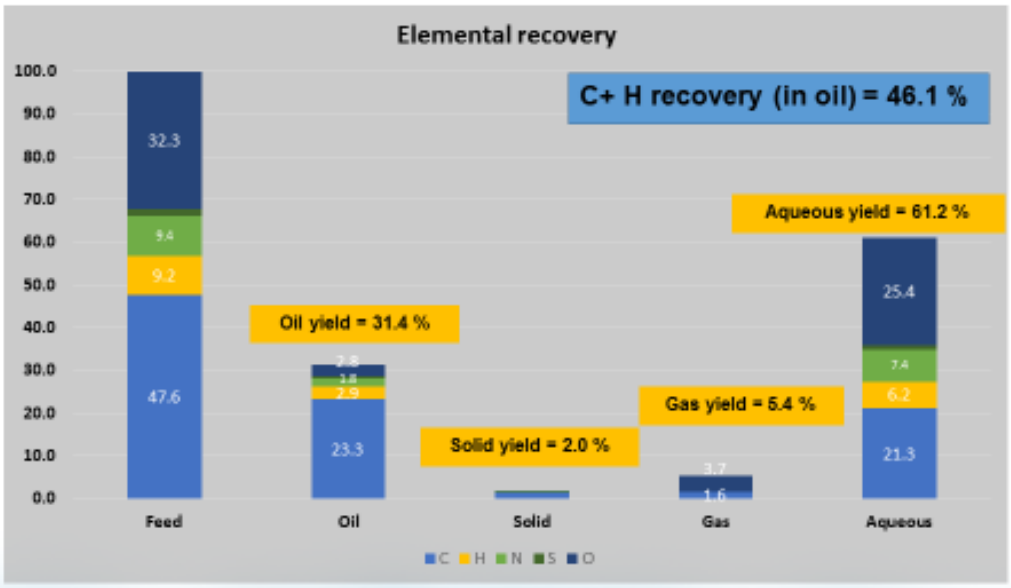

- 46.1 % of feed C+H is recovered in oil
- Significant proportion (61.2 %) of organics in feed partition into HTL aqueous

HTL of AB1 in batch and bench scale with & w/o RCAT

23

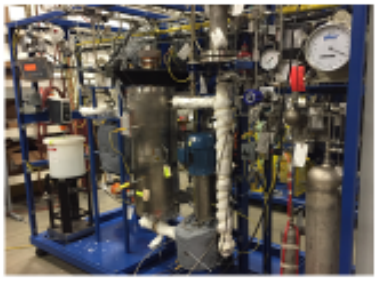

FEED	C (%)	H(%)	N (%)	S(%)	O(%)
AB1-A	45.4	8.5	9.4	1.7	35.1
AB1-B	47.6	9.2	9.4	1.5	32.3

Feed received	2018 (Block B)	2018 (Block A)	2018 (Block B)	2018 (Block A)	2018 (Block B)	2018 (Block A)
Scale	300 mL batch	300 mL batch	2L batch	2L batch	continuous	continuous
Catalyst	Nil	R-Cat	Nil	R-Cat	Nil	R-Cat
Separation method	DCM	DCM	gravity	gravity	gravity	gravity
Algal slurry (kg)	0.120	0.121	0.909	0.896	32	23
CBO yield (%)	**40.0**	**43.3**	**29.7**	**32.6**	**28.2**	**31.4**
Residue yield (%)	1.3	1.4	1.4	2	2.3	2
Gas yield (%)	5.4	5.4	5.4	5.4	5.4	5.4
Aqueous yield (%)	53.1	50	63.5	60.0	64.2	61.2
CBO- elemental characteristics						
C (%)	71.4	73.1	71.9	75.2	72.4	74.3
H (%)	8.8	8.5	9.1	9.4	9.2	9.1
N (%)	6.7	6.5	5.1	5.8	5.5	5.9
S (%)	0.9	0.9	1.4	0.5	1.4	1.7
O (%)	12.2	11	12.5	9.1	11.5	9

Appendix 3: Supporting Internal Reports

3.A. Comparison of Specific Growth Rates for Wild Type Cyanobacterium AB1 with Rates Derived from O_2 Generation Photosynthesis-Irradiance (PE) Curves (with contributions from Pacific Northwest National Laboratory)

Comparison of Specific Growth Rates for Wild Type Cyanobacterium AB1 with Rates Derived from O_2 Generation Photosynthesis-Irradiance (PE) Curves

Yanhui Yuan and Ron Chance
Algenol Biotech LLC

Ankush Katemore
School of Chemical and Biomolecular Engineering
Georgia Institute of Technology

Executive Summary

This report describes a comparison of results obtained by Pacific Northwest National Labs (PNNL) for the specific growth rate of AB1 as a function of temperature to results obtained by Algenol from O_2 evolution vs irradiance (PE) curves over a comparable temperature range. The relationship between Algenol derived photosynthetic parameters and specific growth rates is the first established on a theoretical basis. The specific growth rates derived via the Algenol Productivity Model are then compared to PNNL results. The results are in good agreement, with both data sets indicating an activation energy of about 60 kJ/mol (Q10 ~ 2). The Algenol results are consistent with all the temperature dependence being attributed to the photosaturation parameter, E_k, a result which is consistent with previous Algenol studies of AB1 and other organisms. The AB1 system is well behaved up to temperatures close to 50 °C, according to both PNNL and Algenol results. Doubling times in the 2-3 hour range are found by both PNNL and Algenol at the peak performance which occurs at about 45 °C.

Keywords: Specific growth rate, Photosynthesis irradiance curves, AB1, Temperature response, MONK, PNNL.

Introduction

Algenol supplied Pacific Northwest National Laboratories (PNNL) with our lead organism for biofuel applications (AB1) for inclusion in their DOE-funded DISCOVR (Development of Integrated Screening, Cultivar Optimization and Validation Research) project. PNNL provided Algenol with very positive feedback on the performance of AB1 in their testing protocol, including a report of their results for specific growth rate versus temperature. They also provided a second document detailing their methodology. Both documents are included as addenda to this report. Algenol generally does not measure specific growth rates. To enable comparison to the AB1 data base, we first establish the relationship between specific growth rates and the key photosynthetic parameters in the Algenol Productivity Model (E_k and α). We then describe a set of experiments measuring O_2 generation versus irradiance (PE experiments) covering a temperature range comparable to that addressed in the PNNL work. This effort was supported in part by Algenol's DOE-funded ABY2 project.

Productivity Modeling

The following discussion establishes the relationship between the Algenol-derived kinetic parameters and μ (the specific growth rate) which by definition is

$$\mu = (dC_0/dt)/C_0 \quad = P_v/C_0 \qquad (1)$$

where C_0 is the photosynthetically fixed carbon concentration (mol C/m^3), t is time (sec), and $P_v = dC_0/dt$ is the volumetric production rate. μ is a function of irradiance (E) except under saturating light conditions where P_v is replaced by P_m, the maximum rate obtained under high irradiance conditions (ignoring photoinhibition effects). This would yield the maximum specific rate, μ_m. The determination of μ or μ_m is carried out under low light absorption conditions where exponential growth is expected. Note that C_0 would contain both cellular and non-cellular (dissolved organic) components. As long as the proportionality of those components is unchanged over the time scale of the experiments, Equation (1) and the comparison below to kinetic parameters derived from PE curves are valid. In fact, because of the normalization in Equation (1) any physical property that provides a proper measure of growth (such as OD_{750nm} in most cases) can be used to determine μ.

Equation (1), under saturating light conditions ($\mu_m = P_m/C_0$), is sufficient to compare PNNL specific growth rate measurements to rates derived from Algenol's PE experiments. However, we will establish the more general relationship for arbitrary irradiance and make the connection to the photosynthetic parameters derived from the PE curves. The motivation for this approach is anticipation of an eventual comparison of the Algenol Productivity Model[1] to the PNNL productivity model[2] which employs μ as the key performance parameter for predicting outdoor performance in ponds.

Assume that PAR (Photosynthetically Active Radiation, 400 – 700 nm) irradiance (E) decays exponentially in the culture according to the Beer's Law

$$E = E_0\, e^{-kz} \qquad (2)$$

where k is the extinction coefficient (m^{-1} units), z (m) is the distance into the culture, and E_0 is the incident irradiance (μmol photons/m^2-s). k is determined as an average over the absorption spectrum in the PAR range (400 to 700 nm) and is equal to KC_0, where K is the PAR averaged absorption cross section (m^2/mol C). We have shown Equation (2) to be valid for our organisms under wide ranging conditions, making only a small (wavelength uniform) scattering correction.[1] We assume further that the photosynthetic rate per unit volume (P_v) in the culture at a point z below the surface can be described by a hyperbolic equation (the Monod equation which is similar to a Michaelis-Menten formulation)[3]

$$P_v = P_m\, E/(E_k + E) \qquad (3)$$

where P_m is the light-saturated volumetric photosynthetic rate (mol fixed carbon/m^3-s) and E_k is the half-saturation constant which describes photosaturation (μmol photons/m^2-s). This formula can be adapted to include photoinhibition effects, but we find that under most lab and outdoor conditions now employed at Algenol, those effects are small. The areal productivity (mol C/m^2-s) in a culture of depth D is derived by integrating Equation (3) over the depth (D) of the culture[1]:

$$P_a = \int_0^D P_m\, E_0\, e^{-kz}/(E_k + E_0\, e^{-kz})\, dz = (P_m/k)\, \ln((E_k + E_0)/(E_k + E_0\, e^{-kD})) \qquad (4)$$

where the z integration is performed over the limits 0 to D. In the limit when kD approaches zero (e.g. in the dilute limit), this expression reduces to:

$$P_a = P_m\, E_0 D/(E_k + E_0) \qquad (5)$$

The amount of light absorbed in a very shallow culture is kDE_0. Hence the ratio of areal production to light absorbed in a very shallow culture (the quantum yield) is:

$$P_a/kDE_0 = P_m/(k\,(E_k + E_0)) \qquad (6)$$

Now taking the limit as E_0 approaches zero, we find that the limiting quantum yield (α, reciprocal of the minimum quantum requirement) is

$$\alpha = P_m/k\ E_k \quad (7)$$

which, when multiplied by E, corresponds to the limiting areal production rate (mol carbon/m^2- sec) at low light levels.

Therefore, assuming the high irradiance limit defined as $E>>E_k$, and recognizing that $C_0 = k/K$, we have on combining Equations (1), (3), and (7)

$$\mu_m = \alpha\ E_k\ K = P_m\ K/k = P_m/C_0 \quad (8)$$

The same relationship is obtained for the exponential version of Equation (3)[3] which we will use to analyze the PE experiments. This is done because the exponential form gives a better representation of those experiments and, in particular, a better estimate of P_m which is important here for the comparison to the PNNL experiments. We accept this inconsistency in approach because the exponential formulation does not yield a simple solution for the areal rate, Equation (4). We do not expect a substantial difference in the Algenol Productivity Model with the exponential form, but have not shown that as yet.

Experiment

PNNL was supplied with AB1 by Algenol for inclusion in their DISCOVR productivity survey program. They generated a μ_m data set for AB1 covering the temperature range 4 to 47 °C. Those results are summarized in Addendum 1 with the general approach used by PNNL summarized in Addendum 2. μ measured as a function of temperature and irradiance is the key parameter in the PNNL productivity model.[2]

The oxygen PE curve measurement as executed by Algenol provides the maximum oxygen rate, P_{mO2} usually expressed on a per chlorophyll basis (μmol O_2/mg Chl.a-hr) either by direct observation or by fitting the data to a model like Michaelis-Menten. We may convert oxygen rate to carbon fixed rate with PQ (photosynthetic quotient, with PQ=1.1 molO_2/molC as a typical value and a reasonable estimate for AB1), as follows

$$P_m = P_{mO2}\ [Chl]/PQ \quad (9)$$

The initial cell concentration is commonly expressed as ash free dry weight or chlorophyll concentration and can be converted into fixed carbon concentration C_0, as

$$C_0 = [Chl]\ (C_{fixed}\ /Chl) = [DW]\ (C_{fixed}\ /DW) \quad (10)$$

The absorption cross section K, in m^2/molC can be calculated as

$$K= (Chl/\ C_{fixed})\ k/[Chl] \quad (11)$$

With Equation (8), (9) and (10) we can obtain

$$\mu_m = P_m/C_0 \quad = (Chl/\ C_{fixed})\ P_{mO2}\ /PQ \quad (12)$$

To calculate the C_0 from Dry weight in Eq. (10), we commonly used carbon content in dry weight (DWC), and dissolved organic carbon (DOC), DWC/DW is ~ 50%, and DOC/DWC ~ 30% for AB1 from previous Algenol experiment dataset[4], as

$$C_{fixed}\ /DW = (DWC + DOC)\ /DW= DWC/DW\ \ (1 + DOC/DWC) \quad (13)$$

Table 1 presents the photosynthetic parameters of strain AB1 obtained by Oxygen PE curves generated at various temperatures. Here we list the value from Webb Equation analysis, $P_{vO2} = P_{mO2}\ (1-\exp(-E/E_k))$. The P_{mO2} values from the Webb Equation analysis are more representative of the PE experiment data (better fits), but slightly smaller than those found with the Monod formulation by about 15%. The pre-culture samples are taken from indoor 1L bubbling bottles at OD_{750} = 1~ 2, which is in very active growth stage at 30 °C. The average irradiance seen by the organisms during growth (E_0/kD) was about 100 μmol photons/m^2-sec. Since acclimation in AB1 results in E_k ~ E_0/kD, roughly E_k ~100 μmol photons/m^2-s is expected and observed for the 30 °C measurement. Each sample was diluted to k = 0.1 cm^{-1} or 10 m^{-1}, and held in the dark for 3 hours at given temperature before Oxygen PE curves measurement.

Table 1: Oxygen PE curves results for AB1 at temperature 15 to 50 °C

Temperature, °C	**15**	**20**	**25**	**30**	**35**	**40**	**45**	**50**
alpha (mol O_2/mol photon)	0.05	0.10	0.12	0.11	0.11	0.08	0.08	0.06
R_0 (μmolO_2/L-min)	0.14	0.22	0.07	0.18	0.32	0.07	0.13	0
E_k (μmol photons/m^2-s)	45	34	46	81	110	192	264	246
P_{mO2} (μmolO_2/mgChl.a-hr)	96	138	226	376	509	627	850	577
P_m (μmolC/mgChl.a-hr)	87	125	206	242	463	570	773	524
Max specific growth rate from Eq. (12), 1/day	0.79	1.22	2.00	3.32	4.50	5.55	7.52	5.10
Refit E_k (μmol photons/m^2-s)	*21*	*31*	*58*	*91*	*121*	*163*	*200*	*319*
Refit P_{mO2} (μmolO_2/mgChl.a-hr)	*75*	*109*	*203*	*320*	*427*	*575*	*705*	*75*
Refit μ_m, from Eq (12), 1/day	*0.73*	*1.11*	*2.07*	*3.26*	*4.34*	*5.85*	*7.17*	*5.71*

Notes: For 20 °C to 50 °C, K= 4.66 m^2/molC and [Chl]=0.87 mgChl.a/L; for 15 °C, K= 4.5 m^2/molC and [Chl]= 0.83 mgChl.a/L. The typical ratios for AB1 are (C_{fixed} /Chl) = 2466 to 2666 μmolC/mgChl.a and (k/Chl) = 0.0115 to 0.0120 m^2/mgChl.a. Refit analysis was done by assuming the same α for all 15-45 °C, the final α = 0.100 ± 0.003 molO_2/molphoton and activation energy of E_k (or P_m, μ_m,) obtained as E_a = 59.7 kJ/mol from 15 °C to 45 °C, and E_a=56.8 kJ/mol from 20 °C to 45 °C.

Results and Discussion

In Figure 1 and Figure 2, we compare our maximum growth rate derived from oxygen PE curve measurements with PNNL DISCOVR Dataset (by *Scott Edmundson et al 2018, Addendum 1*). Figure 3 displays the Algenol PE data obtained at different temperatures from 15-50 °C. The agreement between PNNL and Algenol for μ_m is quite good from 15-45 °C (Figure 1), surprisingly good given that there was no attempt to normalize the sample preparation procedures with respect to the acclimation state of AB1. The refitting of the PE results assuming a constant α has little effect on the comparison. The Arrhenius plot results in Figure 2 are in good agreement with both data sets indicating an activation energy of about 60 kJ/mol. The downturn in μ_m as the temperature approaches 50 °C in the Algenol results is clear, and this was not seen in the PNNL results which only go up to 47 °C. As a side note, the 50 °C PE curve shows a distinctively lower α, with no apparent effect on E_k. This suggests that higher temperatures degrade the photosynthetic apparatus without substantially affecting the dark reactions represented by E_k. This observation would need confirmation with more extensive studies.

In Figure 4, we compare the current results to a compilation of maximum doubling rates (u_m/ln2) versus temperature. AB1 is clearly competitive with the best performers in this data set. The PNNL results for the final 3 or 4 points are likely to be underestimated due to the choice of 450 μE/m^2-s for irradiance which does not meet the requirement of E>>E_k. If we correct the PNNL data based on our E_k results, the PNNL results are increased for the final 3 points so that there results essentially parallel the Algenol results and the Eppley curve.

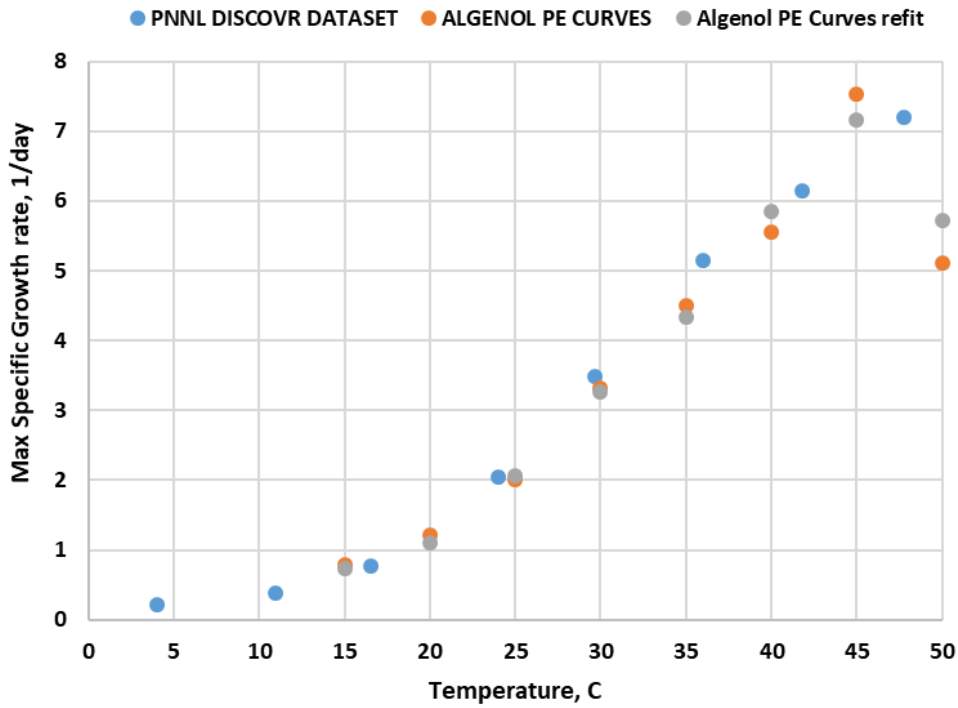

Figure 1: Maximum specific growth rate for AB1: results from PNNL based on doubling rates, direct results from Algenol PE curves, and results obtained with the assumption of a temperature independent limiting quantum yield (α).

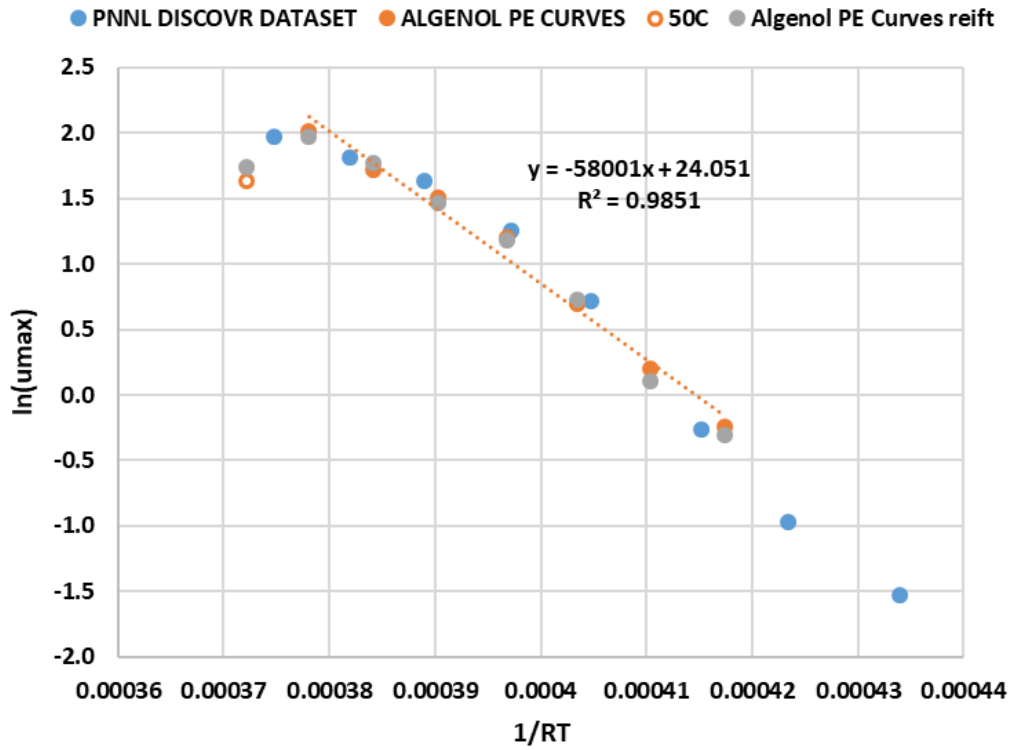

Figure 2: Arrhenius graph for ln(μ_m) vs 1/RT, activation energy is 58 ± 2 kJ/mol for AB1 from 15 to 45 °C (i.e., excluding the 50 °C point which is shown as an open circle).

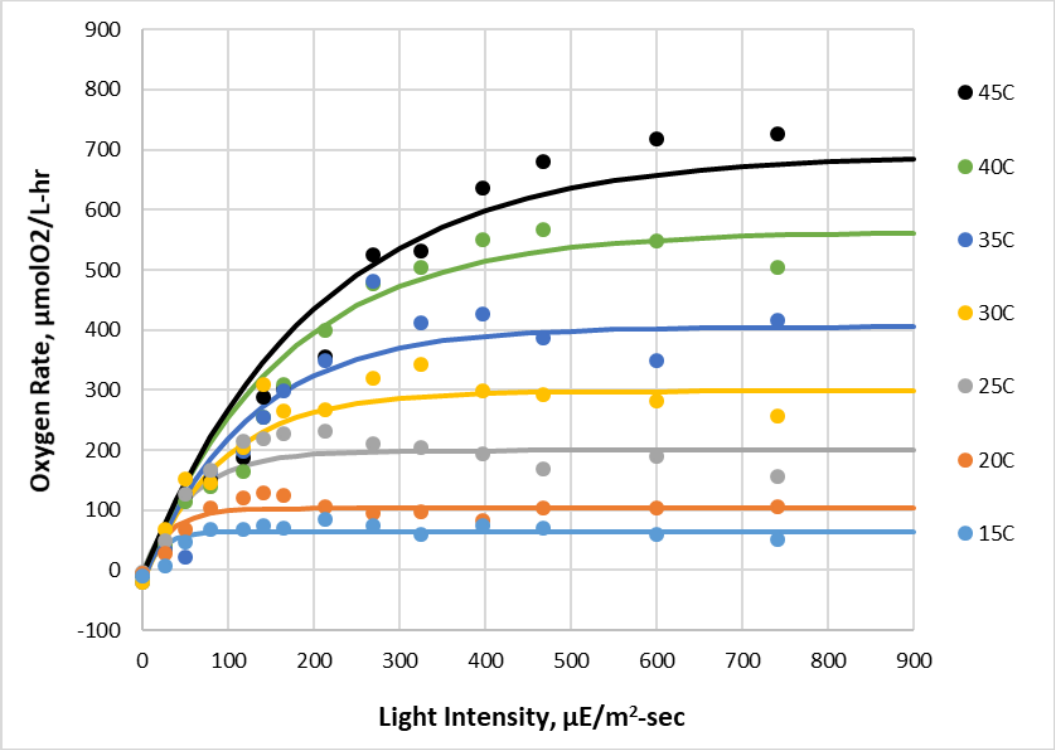

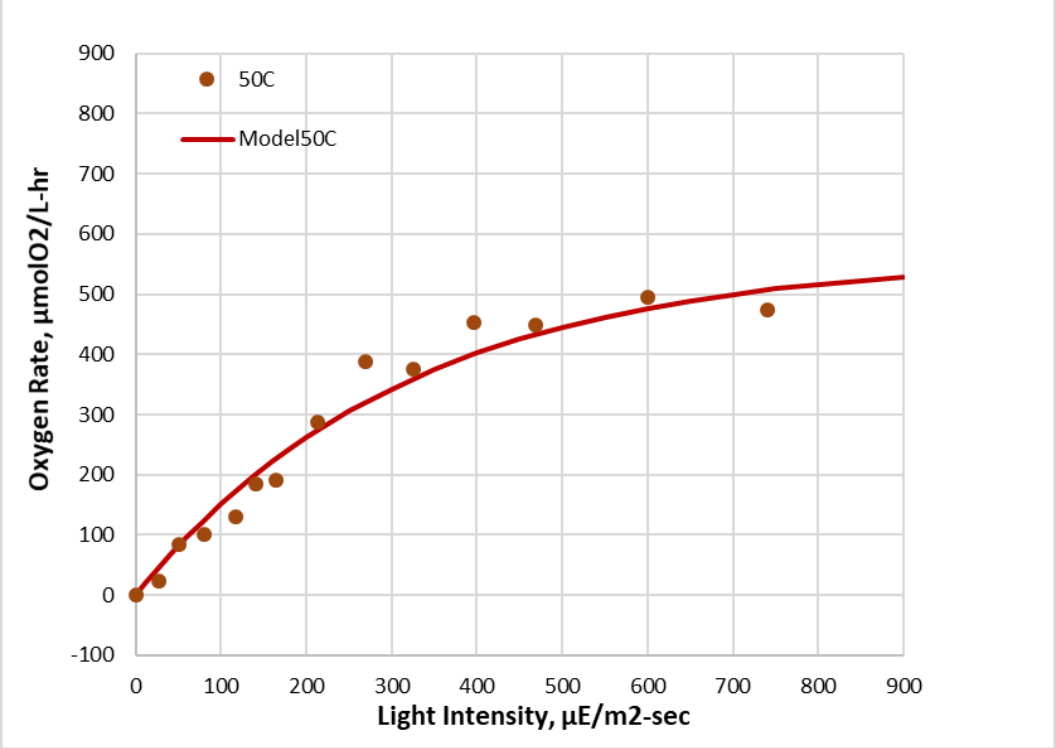

Figure 3: Top: Oxygen PE curve data and Webb model fitting, PE model parameter set as α = 0.10 mol O_2/mol photon for 15 to 45 °C, and (b) 50 °C data set, PE model parameter as α = 0.050 molO_2/mol photon, E_k = 312 µmol photons/m^2-s.

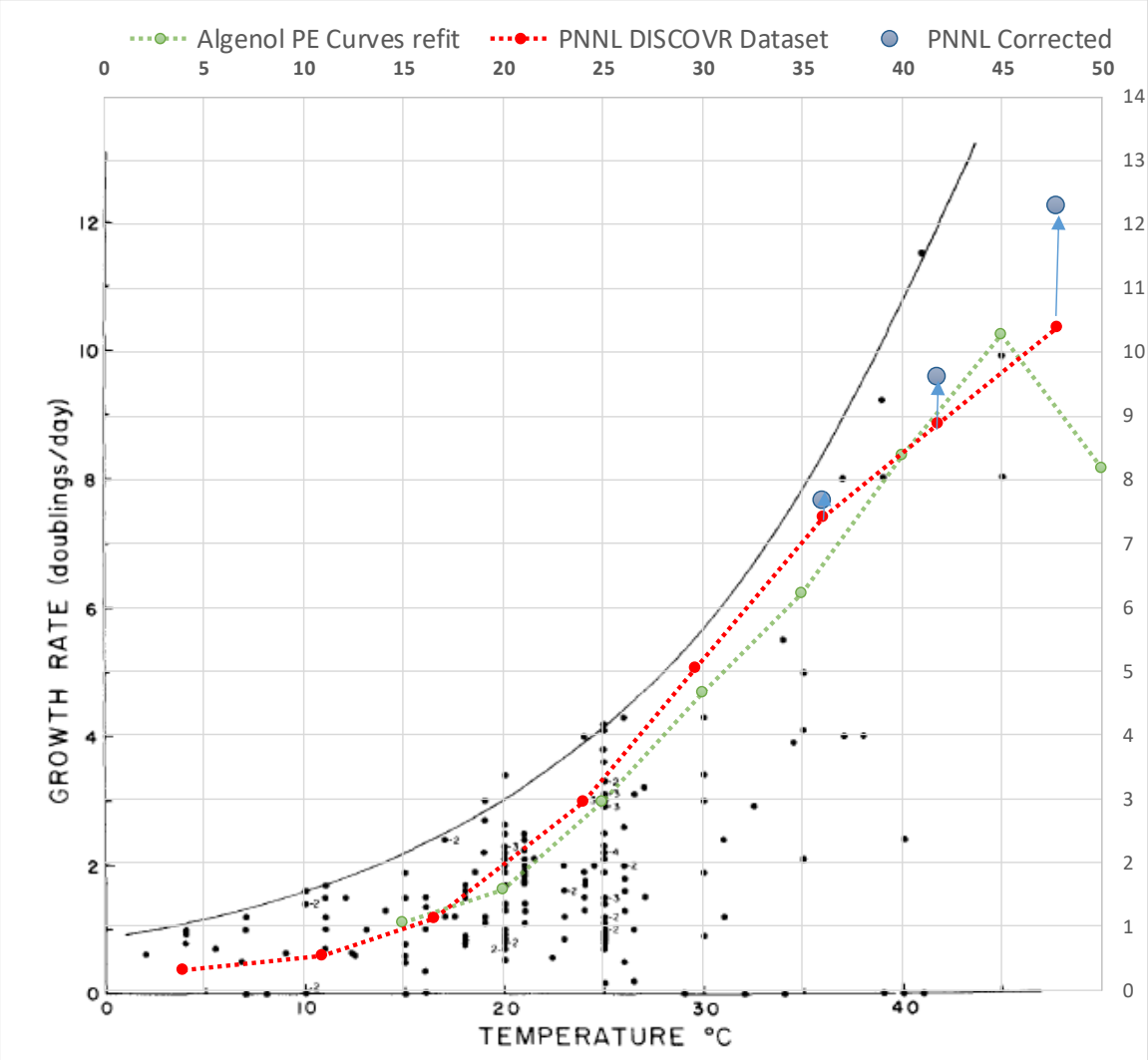

FIGURE 1.—Variation in the specific growth rate (μ) of photoautotrophic unicellular algae with temperature. Data are all for laboratory cultures. Growth rate is expressed in doublings/day. Approximately 80 of the points are from the compilation of Hoogenhout and Amesz (1965). That listing is restricted to maximum growth rates observed, largely in continuous light. The figure also includes additional data, mostly for cultures of marine phytoplankton, from the following sources: Lanskaya (1961), Eppley (1963), Castenholz (1964, 1969), Eppley and Sloan (1966), Swift and Taylor (1966), Thomas (1966), Paasche (1967, 1968), Hulburt and Guillard (1968), Jørgensen (1968), Smayda (1969), Bunt and Lee (1970), Guillard and Myklestad (1970), Ignatiades and Smayda (1970), Polikarpov and Tokareva (1970). The latter papers include about 50 strains of marine phytoplankton. The line is the growth rate predicted by Equation (1), i.e., the line of maximum expected μ. Small numbers by points indicate the number of values which fell on the point.

Figure 4. PNNL and Algenol results for growth rate, doublings/day or our $\mu_m/\ln 2$, plotted on a figure taken from R.W. Eppley, "Temperature and phytoplankton growth in the sea", *Fishery Bulletin* **70**, 1063–1085 (1972). The results show by Eppley are the maximum value observed for a particular strain plotted against the temperature for that observation. The corresponding data point for AB1 from this study would be at a little over 10 doublings/day at 45 °C. Blue dots are corrected values for PNNL data (red dots, 36 to 48 °C), with assumption of $\mu = \mu_m (1- \exp(-E_0/E_k))$, in which E_k are interpolated values from Algenol PE curve experiment data, and E_0 is PNNL incident light intensity, 450 µmol photons/m^2-s.

Summary
The underlying fundamental basis for the PNNL productivity model and the Algenol Productivity model agree well. This observation provides a solid basis for making a comparison of the predictions for the two models tested against existing experimental data.

References

[1] Y. Yuan and R. Chance, "Photobiology of ethanologenic cyanobacteria 2011-2012: Summary review and detailed description of productivity modeling in outdoor cultures", Algenol Report 482 (November 15, 2012).

[2] M. Huesemann, B. Crowe, P. Waller, A. Chavis, S. Hobbs, S. Edmundson, and M. Wigmosta, "A validated model to predict growth in outdoor pond cultures subjected to fluctuating light intensities and water temperatures", *Algal Research* **13**, 195-206 (2016).

[3] Q. Bechet, A. Shilton, and B. Guieysse, "Modeling the effect of light and temperature on algae growth: State of the art and critical assessment for productivity prediction during outdoor cultivation", *Biotechnology Advances* **31**, 1648-1663 (2013).

[4] W. Porubsky et al, "EPS Characterization: AB1:wt and AB1:1658 ", Algenol Report 660 (August 29, 2014).

Acknowledgements

We thank Scott Edmundson and Michael Huesemann for helpful discussions. This work was supported in part by the Department of Energy ABY2 program DE-EE0007690.

Addendum 1: PNNL Report on AB1 (Email, Edmundson to Chance, 10-10-2018)

Thermal and Salinity Characterization of the Industrial Wild-type Cyanobacterium "AB1" PNNL Algae DISCOVR Project

Scott Edmundson, Andrew Gutknecht, and Michael Huesemann
Pacific Northwest National Laboratory, Marine Sciences Laboratory, Sequim, WA, USA

Abstract:

The Industrial wild-type cyanobacterium "AB1" was obtained from Algenol for inclusion into the Algae DISCOVR project screening pipeline. The strain was screened for temperature (4 to 47 °C) and salinity tolerance within the standard DISCOVR screening medium (1.5 mM N and 0.9 mM P). The maximum observed specific growth rate was 6.96 ± 0.55 day^{-1} at 47.1 °C. The AB1 strain has a broad salinity tolerance, showing no significant difference in growth rate in the three salinities tested. This is a remarkably fast-growing photosynthetic organism, among the fastest tested in the DISCOVR project to date. The optimal temperature range of this organism is above the typical water temperature of an in-ground open, outdoor pond located in the continental United States (ca. 17- 35 °C). Due to the high temperature preference and the high pigmentation of this strain, cultivation in short-light path, enclosed photobioreactors may be more suitable than pond cultivation.

Summary:

The AB1 strain was received growing in a marine BG-11 medium (Instant Ocean). The strain was transferred successfully to the standard screening medium "DISCOVR" at 35 PSU (Table 1). AB1 grew in this medium without any difficulty or need for acclimation.

Temperature characterization from 4 to 47 °C was executed by measuring maximum specific growth rates (μ_{max}) on PNNL's thermal gradient incubator (TGI) under light intensities of 450 µmol photons/m^2-sec on a 12:12 photoperiod, sparging CO_2-enriched air in the DISCOVR medium. The measurement of growth rates were continued until rates stabilized, up to 6 replicates per each temperature point (Figure 1). The strain does not grow reliably below ~16 °C. The maximum observed specific growth rate was 6.96 ± 0.55 (SE, Standard Error) day^{-1} at 47.1 °C, the highest temperature tested. It is likely that the maximum tolerated temperature of this organism is much higher than 47 °C. Unfortunately, we could not adjust the gradient incubator at the time of testing due to other strains being simultaneously tested on the same thermal gradient. Further testing at higher temperatures can be accomplished in future trials, if desired.

We also tested the impact of medium salinity on the growth rate of AB1. Three salinities 5, 15, and 35 PSU, using artificial sea salts (Crystal Sea Marinemix, Marine Enterprises International, LLC.), were tested using the same N, P, and trace metal elemental sources as listed in Table 1 and 2. The salinity of the medium had no statistically significant effect on the maximum specific growth rate of AB1 at 25 °C, although there was a slight trend for lower salinities to have higher rates (*ca.* 12% greater, Figure 2).

Unlike previously characterized strains, which acclimate/adapt to the environmental conditions and reach a plateau in μ_{max}, we found that the rates of AB1 were not consistent over time when determining optimum salinity. We observed distinct periods of clustered low and high growth rates over 12 repeated sequential growth rate measurements. These growth rates appeared to correlate with the pigmentation of the cells; although no in-depth investigation was pursued. While dark, blue-green, pigmentation was exclusively observed on the thermal gradient, a lighter green pigmentation was observed over multiple sampling days on the salinity gradient. These periods with lighter pigmentation resulted in daily maximum specific growth rates around 5-6 day^{-1}, and even surpassing 7 day^{-1} on several occasions. It is not clear what caused these shifts in pigmentation and, in turn, spikes in growth rate. This may be due to the nitrogen source used in the DISCOVR medium or some other underlying metabolic factor.

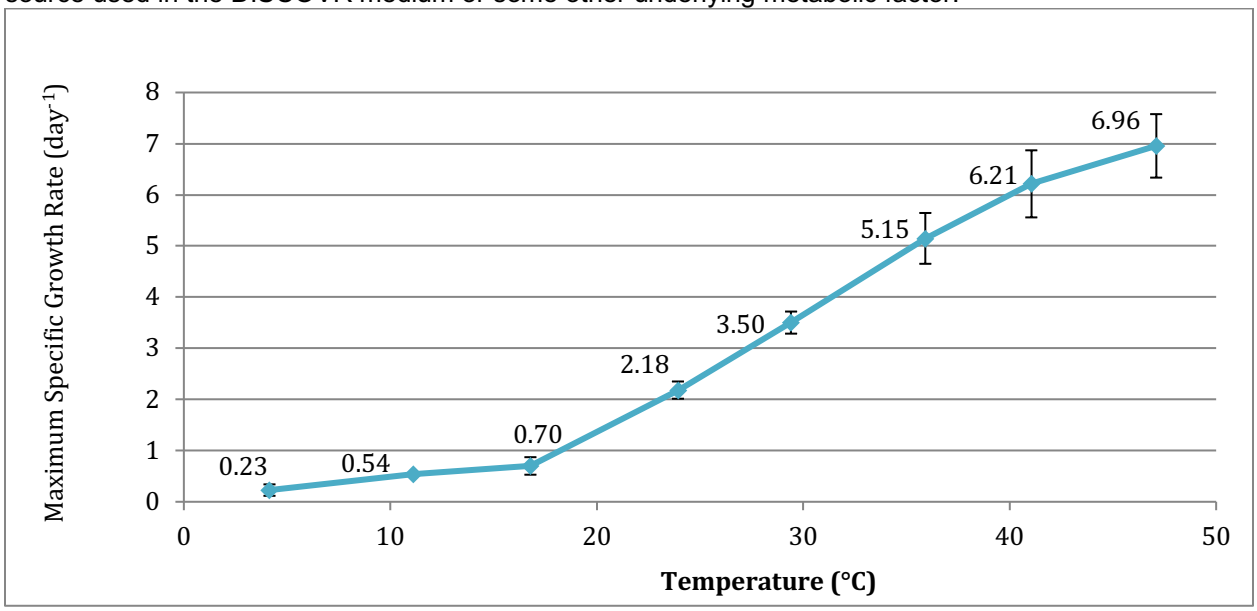

Figure 1. Maximum specific growth rates as a function of constant incubation temperature for the cyanobacterium "AB1". Error bars denote one standard error (n=6) only rates with linear regressions

above R^2=0.95 were used to plot data and report error bars. Rates at lower temperatures had fewer acceptable linear growth rates (at 4.1 C n=2 at 11.1 n=1).

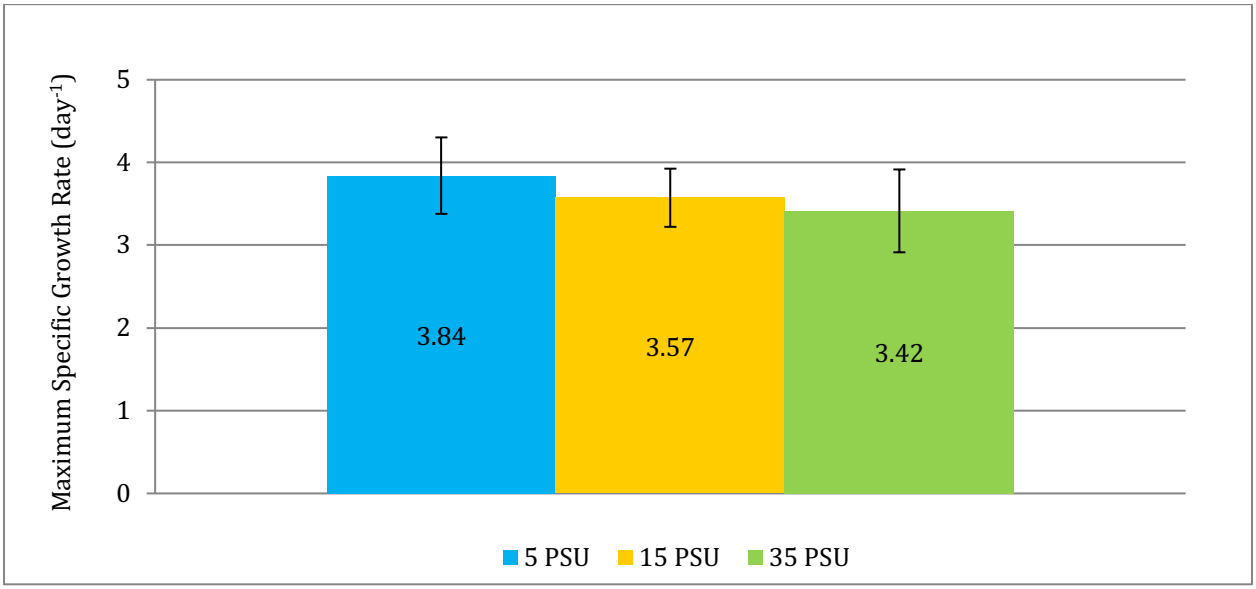

Figure 2. Maximum specific growth rates as a function of constant salinity (5, 15, and 35 PSU) for the cyanobacterium "AB1". Error bars denote one standard error (n=12).

Addendum 2: PNNL Report Describing Methods (Email, Edmundson to Chance, 10-25-18)

Thermal and Salinity Characterization of the Industrial Wild-type *Cyanobacterium* "AB1" PNNL Algae DISCOVR Project

Scott Edmundson, Andrew Gutknecht, and Michael Huesemann
Pacific Northwest National Laboratory, Marine Sciences Laboratory, Sequim, WA, USA

Supplemental Methods

Microalgal cultivation

Cyanobacterium sp. AB1, obtained from Algenol, was maintained in the DISCOVR medium (see Table 1 and Table 2 for the medium recipe) at 35 PSU salinity using artificial sea salts (Crystal Sea Marine Mix, Marine Enterprises International). Eight 125 mL (working volume of 50 mL) flasks were simultaneously inoculated with the *C.* sp. AB1 mother culture to an optical density at 750 nm (OD_{750}) of *ca.* 0.1. The eight *C.* sp. AB1 cultures were then incubated at different temperatures along a thermal gradient (4, 11, 17, 23, 29, 35, 41, and 48 °C) for 72 hours prior to growth rate measurements to acclimate to the specific temperatures of the flasks. Carbon was supplied via continuous sparging of CO_2-enriched air (0.5% v/v).

Temperature-dependent Growth

Microalgae were grown in 125 mL Erlenmeyer flasks in the custom-built TGI under neutral white (4000K) LED panels at ~450µmol $m^{-1}s^{-1}$, which was set to a 12:12 hr light:dark photoperiod. The TGI consisted of an insulated 76cm x 40cm x 10cm aluminum block on top of an Advanced Digital Shaker (VWR) set at approximately 110 rpm. Circular 2 cm deep slots in the block were machined in 3 rows of 8, allowing for incubation of up to 24 flasks at a time. Each flask was topped with a foam stopper (Jaece, identi-plugs) and sparged with a mix of humidified air and 0.5% CO_2 through a sterile 0.45 µm filter (Whatman, Polycap TF), flowing from one 24-way gas distribution manifold. A temperature gradient was established along the length of the aluminum block by a recirculating glycol/water bath set to -8°C on one end of the block and a cartridge heater set to 54.5°C on the opposite end controlled by a PID temperature controller. The temperature change between each flask along the gradient was approximately 6°C. The TGI setup is shown in Supplemental Fig. 1 and the acclimated *Cyanobacterium* sp. AB1 cultures are shown in Supplemental Fig. 2.

Growth Rates

Approximately 3 mL of culture were pipetted from each flask and absorbance was measured with a spectrophotometer (Genesys 10S UV-Vis, Thermo Scientific) at 750nm and 680nm. Optical density (OD) and pH measurements were recorded in 3-hour intervals for 5-6 hours. Maximum specific growth rate (μ_{max}) was calculated by taking the slope of the natural log-transformed OD_{750} measurements along 3 time points. Only slopes with good fit ($r^2 > 0.95$) were accepted and included in the determination of maximums specifis growth rate. Growth trials were repeated once a day at the same time to minimize variation due to timed cell division. Growth trials were continued until rates stabilized. Up to 6 growth trials were performed for each temperature, growth rates at lower temperatures were typically unreliable, and so have fewer repeated data points.

Light Attenuation

Light attenuation occurs as light becomes increasingly diffuse as it passes through a sample and is partially absorbed by the sample. In algal cultures, this attenuation results from absorption and scattering of light by algal cells in suspension and is critical to predicting the amount of light as a function of depth in an algal pond. The biomass light absorption constant, k_a, which is a value intrinsic to the sample is determined by rearranging the Beer-Lambert Law (Suh and Lee, 2003). As shown in the equation below, k_a is determined by taking the natural log of the ratio between light exiting a sample (I) and incident light entering a sample (I_o) in relation to path length (l) and absorbance at 750 nm (OD_{750}), *i.e.*:

$$k_a = -\frac{\ln\left(\frac{I}{I_o}\right)}{l * OD_{750}}$$

To measure the light attenuation constant, a cuvette holder screwed to a wooden board above a quantum sensor attached to a LICOR light meter was placed under the same LED panel used for the TGI to standardize the light source used in each experiment. k_a was measured immediately after OD_{750} had been determined at a low optical density (<0.2). Incident light (I_o) was measured with the respective culture medium as the blank. The same cuvette was filled with sample and light intensity was recorded through the sample (I) with path length (l) held constant at 1 cm. Light attenuation data collected for *Cyanobacterium* sp. AB1 are given in Supplemental Fig. 3.

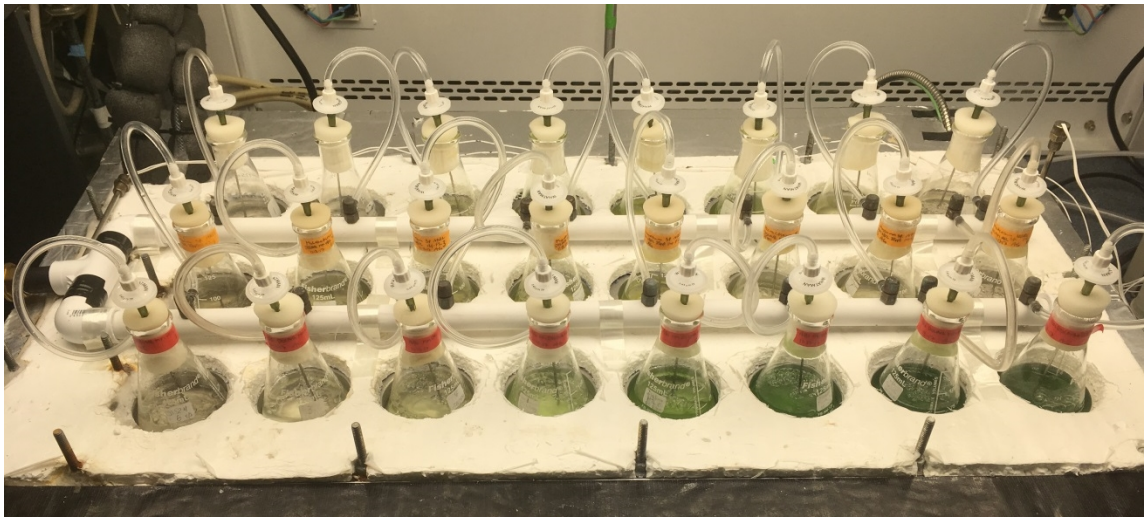

Supplemental Figure 1. TGI setup with all flasks fed CO_2:air mixture through a split manifold running along the shaker.

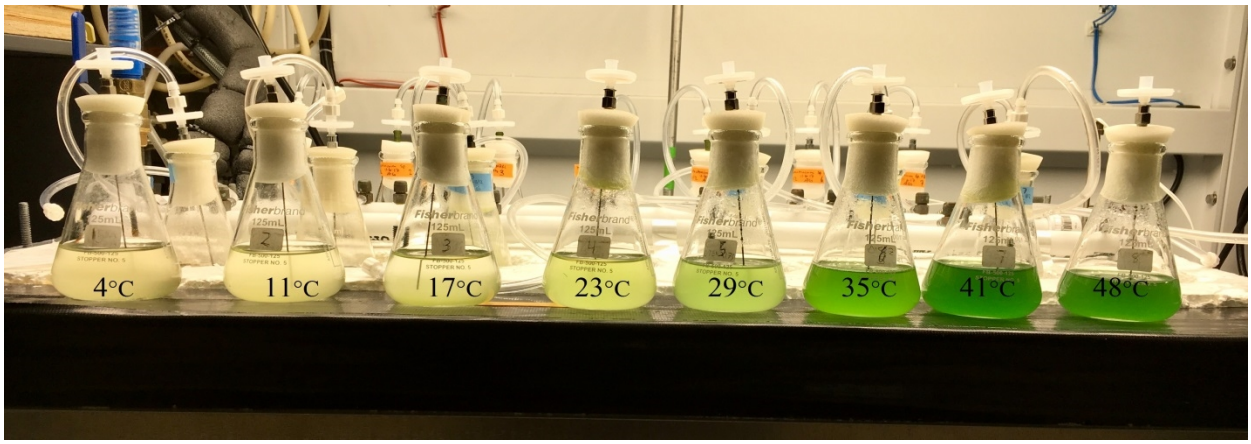

Supplemental Figure 2. Flasks of *Cyanobacterium sp.* AB1 along the TGI's temperature gradient.

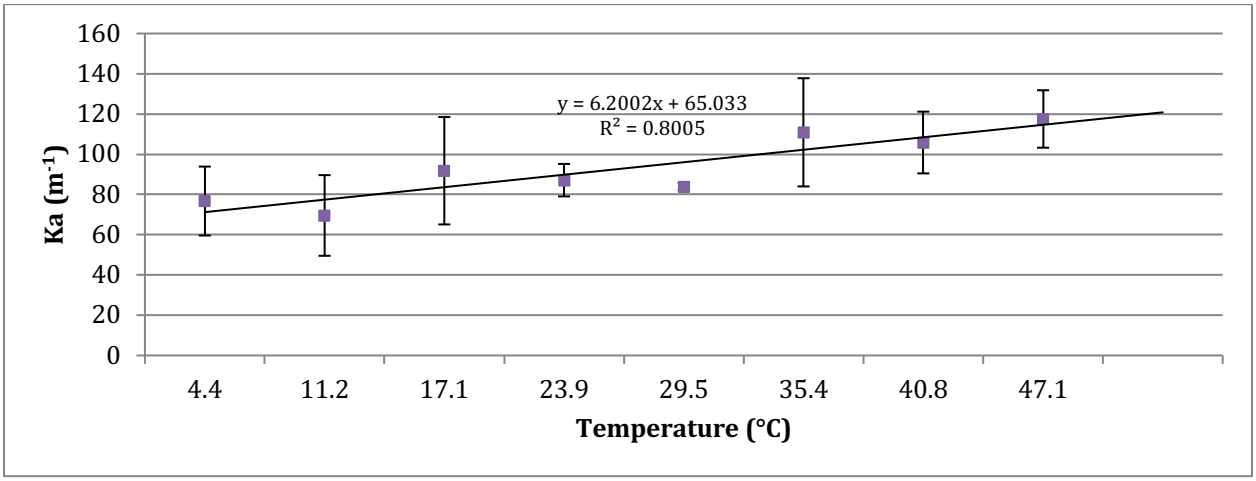

Supplemental Figure 3. k_a as a function of temperature for *Cyanobacterium sp.* AB1 with linear regression shown. Error bars denote one standard error where n=3 trials where k_a was recorded.

Table 1. DISCOVR medium components

Compound Name	Chemical Formula	Molecular weight, [g/mol]	Concentration in Final Medium (mM)
Ammonium sulfate	(NH4)2SO4	132.14	1.51
Diammonium phosphate	(NH4)2HPO4	132.02	0.09
Sodium Bicarbonate	$NaHCO_3$	84.01	3.57
Micronutrient Solution (see Table 2)	-	-	
Vitamin B_{12} solution (cyanocobalamin)	$C_{63}H_{88}CoN_{14}O_{14}P$	1355.38	3.69E-10
Crystal Sea Marinemix- Bioassay Laboratory Formula	At 35 ppt (~39.2 g/L in deionized water)		

Table 2. Micronutrient solution

Compound Name	Chemical Formula	Molecular weight, [g/mol]	Concentration in Final Medium (mM)
EDTA Disodium Salt	$Na_2EDTA{\cdot}2H_2O$	372.2	1.17E-02
Copper (II) Sulfate Pentahydrate	$CuSO_4{\cdot}5H_2O$	249.6	3.93E-05
Sodium Molybdate Dihydrate	$Na_2MoO_4{\cdot}2H_2O$	241.9	2.60E-05
Zinc Sulfate Heptahydrate	$ZnSO_4{\cdot}7H_2O$	287.4	7.65E-05
Cobalt (II) Chloride Hexahydrate	$CoCl_2{\cdot}6H_2O$	237.9	4.20E-05
Manganese (II) Chloride Tetrahydrate	$MnCl_2{\cdot}4H_2O$	197.9	9.10E-04
Iron (III) Chloride Hexahydrate	$FeCl_3{\cdot}6H_2O$	270.3	1.17E-02

References

1. Suh, I. S. and S. B. Lee. A light distribution model for an internally radiating photobioreactor. *Biotechnology & Bioengineering*. 82:180–189 (2003).